Faculty of Engineering and Science

Design, Optimization, and Control of Membrane Reactor for Water-Gas Shift Reaction

Saw Shuey Zi

This thesis is presented for the Degree of
Doctor of Philosophy
of
Curtin University

July 2017

To the best of my knowledge and belief this thesis contains no material previously published by any other person except where due acknowledgment has been made.

This thesis contains no material which has been accepted for the award of any other degree or diploma in any university.

Signature : 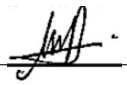

Date : 7 AUGUST 2017

"Twenty years from now you will be more disappointed by the things that you didnt do than by the ones you did do, so throw off the bowlines, sail away from safe harbor, catch the trade winds in your sails. Explore, Dream, Discover."

- Mark Twain

Acknowledgements

Firstly, I would like to express my sincere gratitude to my advisor A/Prof. Jobrun Nandong for the continuous support of my Ph.D study and related research, for his patience, motivation, and immense knowledge. His guidance helped me in all the time of research and writing of this thesis. I could not have imagined having a better advisor and mentor for my Ph.D study.

Besides my advisor, I would like to thank the rest of my thesis committee, my chairperson A/Prof. Chua Han Bing, my co-supervisor A/Prof. Zang Zhuquan, and my associate co-supervisor Dr. Ujjal K. Ghosh, for their insightful comments and encouragement, but also for the hard question which posed me to widen my research from various perspectives.

My sincere thanks also goes to Prof. Clem and Prof. Marcus, who provided me an opportunity to join Curtin University Graduate School, and who gave access to the laboratory and research facilities. Without their precious support it would not be possible to conduct this research.

I acknowledge my gratitude to the Curtin University Sarawak, Curtin Sarawak Research Institute (CSRI) and Ministry of Higher Education (MOHE) through Fundamental Research Grant Scheme (FRGS) for supporting this research study.

I thank my fellow HDR Curtin colleagues for the stimulating discussions, for the sleepless nights we were working together before deadlines, and for all the fun we have had.

I would also like to express the profound gratitude from my deep heart to my beloved parents, grandparents, and my siblings for their love and continuous support both spiritually and materially.

Finally, I would like to thank my fiancee, Chime Kho who was always there cheering me up and stood by me through the good and the bad. I dedicate this thesis to all of you.

List of Publications

Saw, Shuey Zi, Jobrun Nandong, and Ujjal K. Ghosh. 2015. Dynamic simulation of adiabatic packed bed tubular reactor for WGSR under cascade temperature control strategies-effect of secondary temperature measurement location. *In Asia Pacific Confederation of Chemical Engineering Congress 2015: APCChE 2015*, incorporating CHEMECA 2015, p. 2030. Engineers Australia.

Saw, Shuey Zi, and Jobrun Nandong. 2016. Simulation and control of water-gas shift packed bed reactor with inter-stage cooling. *In IOP Conference Series: Materials Science and Engineering* 121: 12022-12031.

Saw, Shuey Zi, and Jobrun Nandong. 2016. Optimization of Economic and Operability Performances of Water-gas Shift Membrane Reactor. *Computer Aided Chemical Engineering*, Elsevier 38: 847-852.

Saw, Shuey Zi, Jobrun Nandong, and Ujjal K. Ghosh. 2016. Comparative Study of Homogeneous and Heterogeneous Modelling of Water-Gas Shift Reaction with Macro-or Micro-kinetics. *Procedia Engineering* 148: 949-956.

Saw, Shuey Zi, Jobrun Nandong, and Ujjal K. Ghosh. 2017. Optimization of steady-state and dynamic performances of Water-Gas Shift Reaction in membrane reactor. Under reviewed *Chemical Engineering Research and Design*.

Saw, Shuey Zi, Jobrun Nandong, and Ujjal K. Ghosh. 2017. Three-loop parallel cascade control design for Water-Gas Shift Reaction in membrane reactor. Submitted to *IFAC Journal of Systems and Control*.

Saw, Shuey Zi, Jobrun Nandong, and Ujjal K. Ghosh. 2017. Simultaneous carbon capture and reuse using catalytic membrane reactor in water-gas shift reaction. Accepted to *Chemical Product and Process Modeling*.

Abstract

Over the last 100 years, rapid growth in global population coupled with industrialization have not only led to the depletion of all non-renewable energy sources, but with their uses, have also dangerously increased the levels of atmospheric greenhouse gas emissions resulting in the global warming phenomenon. The energy security crisis and global warming are now the two largest factors critically affecting political and socioeconomic stability across the world. In view of these challenges, Hydrogen Economy has emerged as a promising solution that is arguably able to alleviate both issues simultaneously as with it, the world will be able to enjoy a pollutant free and renewable energy source. The Water-Gas Shift Reaction (WGSR) is one of many methods which has been explored to achieve this Hydrogen Economy. Unfortunately, one of the key challenges in WGSR is its low performance (Hydrogen yield) in conventional reactors, which stems from the reaction being thermodynamically restricted by the nature of its chemical equilibrium. To reduce the thermodynamic restriction, extensive researches have been conducted to develop new technologies such as the proprietary membrane reactor (MR).

Although there have been several technological breakthroughs in membrane reactor to reduce WGSR thermodynamic restriction, system engineering studies related to optimal operations and robustness of the system are currently very limited. In particular, there is still a lack of research in the incorporation of process uncertainties and dynamic controllability into the process optimization especially for the Water-Gas Shift Reaction in Membrane Reactor (WGSR-MR) system. Since the effects of process uncertainties and daily operation fluctuations are known to be significant, there is a need for the development of robust control strategy for running the WGSR-MR system. The challenge in developing a robust controller for the WGSR-MR system is that, it must address a large transport delay (deadtime) in the process induced by the length of the reactor bed. The thermodynamic limitation and long deadtime problems have led to four important

research questions in this study: (1) how to design a practical WGSR-MR process system with good economic and controllability properties, (2) how to improve the system engineerings practicality of process optimization in the WGSR-MR, (3) how to quantify effects of process uncertainties on the WGSR-MR, and (4) how to improve control performance of the nonlinear WGSR-MR with a long deadtime?

In this study, the overall goal is to design, optimize and control a novel WGSR-MR system via process engineering approach. The WGSR-MR system consists of several interlinked units such as a membrane reactor, compressors and heat exchangers. To perform these tasks, a rigorous fundamental model of the WGSR-MR system was constructed and validated using literature data. In designing the WGSR-MR system, four candidates of process flowsheets were identified. Based on a detailed economic evaluation, the most economical flowsheet was selected. The chosen WGSR-MR system design was further refined via a Multi-Objective Optimization (MOO) procedure as to obtain practical values for the specified sets of design and operating parameters. The salient feature of the adopted MOO procedure is the simultaneous optimization of two conflicting performance criteria: the steady-state economic as represented by net present value (NPV) and dynamic controllability quantified in term of v-gap (control relevant) metric. Up to date, most studies on process optimization have only considered the steady-state performance criteria. For this reason, the optimized design may show a high economic potential but is difficult or even impossible to control in practice, i.e., good steady-state performance but with poor dynamic controllability property. The proposed simultaneous optimization of both the steady-state and dynamic controllability criteria shall be able to avoid such an impractical design.

One of the findings in this study showed that the proposed MOO procedure even under process uncertainties can ensure an optimal system with a positive NPV which at the same time has a good dynamic controllability property. These process uncertainties considered the fluctuations in future prices of hydrogen and electricity where Markov Chain Monte Carlo (MCMC) technique was used to identify their values. Another finding in this study supported that a triple-loop parallel cascade PID control strategy can be effectively used to control the temperatures along the WGSR-MR system. Compared to this triple-loop cascade control strategy, a single-loop PID control strategy demonstrated very sluggish disturbance rejection performance as well as poor closed-loop robustness. These poor closed-loop performance and robustness was expected from the knowledge that the WGSR-MR system has a large deadtime associated with its long membrane tubes. This suggested that the single-loop PID control was unable to

overcome the long deadtime, thus, the strategy should not be used to control the WGSR-MR system in practice.

The main contributions of the study include: (1) rigorous comparisons of several different modelling approaches, (2) a new intensified process design of WGSR-MR system with good economic and dynamic controllability performances, (3) a new simultaneous optimization methodology to address trade-off between the steady-state economic and dynamic controllability performances, and (4) a new complete design procedure for triple-loop parallel cascade PID control strategy. Significantly, the first and third contributions should enable one to design an optimal and practical WGSR-MR system in the face of process uncertainties addressing the aforementioned questions 1 to 3. Meanwhile, the fourth contribution should provide engineers with a practical way to controlling the WGSR-MR system temperature where the effective control will allow the achievements of improved safety and profitability. Poor temperature control in the WGSR-MR will lead to poor yield of hydrogen production as well as can cause rapid degradations of catalyst and membrane tubes due to hot spot temperature zone. Additionally, the presence of hot spot temperature zone can cause runaway reaction which has been responsible for several reactor explosions. In future works, the developed optimization methodology and parallel cascade control design procedure will be adapted in designing other process systems.

Contents

List of Figures

List of Tables

Chapter 1

Introduction

1.1 Background

Hydrogen (H_2) has received increased research attention because of its appealing potential as a clean energy carrier. Consequently, this has led to the conception of a hydrogen economy. Kumar et al. (2008) stated that there are several ways to produce hydrogen, but the most popular route is via the Water-Gas Shift Reaction (WGSR).

Conventionally, the WGSR has been conducted in a two-stage packed bed tubular reactor. In the first stage of an industrial-scale process unit, a high temperature water-gas shift (HT-WGS) packed bed reactor is used to exploit fast reaction kinetics but the chemical reaction equilibrium always limits the extent of conversion. Hence, the conversion in the HT-WGS stage is often fairly small and uneconomical on its own. To improve the overall conversion, the outlet stream of the HT-WGS reactor is cooled and fed to a low temperature water-gas shift (LT-WGS) packed bed reactor. At this stage, the low temperature is beneficial to exploit the chemical equilibrium, henceforth leading to a higher CO conversion overall (Georgis et al., 2014). However, the conventional two-stage WGSR process is largely dependent on the inlet temperature of the HT-WGS reactor, which often suffers from daily fluctuations. Furthermore, the hydrogen produced through this conventional approach still requires further purification in order to meet the required high purity grade of 99% (Grashoff et al., 1983). As a result of an extra separation process required, this leads to large, extra capital and production costs in hydrogen production.

In recent years, a promising new process design has been introduced to produce high purity hydrogen at a commercial scale. This new process design in-

volves integrating reaction-separation processes into a single unit. To achieve this process intensification goal, the WGSR shall be conducted in a membrane reactor with a hydrogen-selective membrane. With regard to this membrane-assisted process design, Chein et al. (2013) disclosed that the use of a membrane reactor can potentially reduce the costs of H_2 production while even enabling CO_2 capture simultaneously. This simultaneous H_2 production and CO_2 capture could increase the overall energy efficiency by 30%. Although there have been several technological breakthroughs in a membrane reactor to reduce the limitations imposed by WGSRs thermodynamic nature, system engineering studies related to the optimization and control of the new process design are currently still very limited. Most research conducted has mainly focused on a single objective optimization, such as in (Lima et al., 2012; Koc et al., 2012, 2014) and open-loop temperature control (Bequette and Mahapatra, 2010; Georgis et al., 2012, 2014). It should be noted that for a practical approach, more than one objectives have to be considered simultaneously in process optimization. On top of that, a system containing the WGSR tends to not only vary nonlinearly with operating conditions, but also to have a long transport delay due to the longer tubes used in the membrane reactor. In order to ensure practicality of the integrated system design for the WGSR, more emphasis should be made in dealing with the challenging problems in complex optimization and dynamics arising from the system.

The goal of this PhD study is to gain deeper insights into the complexity of the WGSR membrane reactor and challenges when it comes to design and operation of a WGSR membrane reactor process system. To achieve this goal, a new optimization method combining multiple objectives is proposed. In addition, a new cascade control design is developed in order to effectively control the process (hence improving operation) which is dominated by nonlinearity and long transport time-delay.

The rest of this chapter is structured as follows. Section 1.1 introduces the motivation behind this study, thus identifying the few main objectives of this dissertation. Section 1.2 presents the novelty, contributions (academic and practical), as well as the significance and benefits of this study socially and environmentally. Lastly, section 1.3 describes the flow and interconnections of the chapters that form this entire dissertation.

1.2 Motivation and Objectives

Most of the WGSR membrane reactor systems are relatively challenging to design, optimize, and control due to process variability and complexity of the membrane reactor model. Due to complicated catalytic reaction steps coupled with the transport phenomena inside the reactors involved, the dynamic behaviours of the system can prevent effective control based on the traditional single-loop feedback control structure. Until now, a limited number of studies has been conducted on process optimization and control of a WGSR membrane reactor. On top of that, most of the previous process optimization and control studies of WGSR process were developed based on a single stand-alone membrane reactor unit. In other words, other units such as compressors and heat exchangers which are part of the system in practice have often been ignored. However, it is important to note that the stand-alone unit performance and behaviour can deviate significantly from that of the process implemented industrially. In the stand-alone unit, it is difficult to estimate the interaction effects of other equipment on the membrane reactor unit. Hence, this in turn will affect the engineers ability to assess the real dynamics and controllability of the system. Obviously, the lack in the system engineering approach to study the membrane reactor system as a whole represents important research gaps, which can be explained accordingly:

a) No research has been published on the design of WGSR membrane reactor systems integrated with other equipment and with the inclusion of multiple mass-energy recycles.

b) Limited number of studies addressing the single objective optimization of the WGSR membrane reactor design. There has been no work reported on multi-objective optimization of the WGSR membrane reactor system in which both steady-state economic and dynamic controllability performances are taken into account.

c) No work has been published on multi-objective optimization under market uncertainties for the WGSR membrane reactor system.

d) Limited research has been published regarding the control design of the WGSR membrane reactor. Most of the reported control studies are related to single-input single-output control design based on the conventional single-loop feedback structure.

To address the aforementioned research gaps, it is important to have a fundamental mathematical model of the whole membrane reactor-assisted water-gas shift reaction (WGSR-MR) process system. The model shall enable one to evaluate the economic potential of the reactor system overall. A reliable model for the WGSR-MR process is a prerequisite for obtaining satisfactory results in any optimization and control study. The following model features are adopted in the process optimization and control study:

a) A one-dimensional heterogeneous reactor model with the incorporation of macrokinetic reaction (rate law) model to represent the WGSR-MR process system.

b) A shell and tube type of reactor where the catalyst pellets (Fe-Cr-O2) are packed inside the shell side. The tube walls are made of porous membrane (Pd-Ag) which is hydrogen selective. The membrane reactor is sub-divided into 10 segments of equal volume. Each segment is represented by a set of ordinary differential equations (ODEs). This division converts a set of partial differential equations (PDEs) into a relatively simpler ODEs. The conversion of PDEs into ODEs shall reduce computation time and complexity of the model simulation while maintaining the accuracy of the model prediction.

c) All physical properties such as gas density, viscosity and thermal conductivity are taken to be non-constant and are functions of the state variables.

In order to address the above mentioned four research gaps, the proposed study embarks on the following objectives:

a) To develop new industrially practical WGSR-MR process system that has the ability to process a production of 5.08 Mtonnes annually while incorporates other equipment and mass-heat recycle streams.

b) To determine the optimal operating conditions of the industrial-scale WGSR-MR system using multi-objective optimization. To ensure the optimal result is practical, the optimization considers both economic (based on net present value) and dynamic (based on v-gap metric) performances.

c) To evaluate the effect of external process uncertainties (i.e., market price and electricity cost) in the multi-objective optimization on the optimal performances of WGSR-MR system.

d) To develop some new control strategies based on the integration of parallel cascade control and multi-scale control (MSC) schemes.

1.3 Novelty, Contribution and Significance

Although there has been a number of literature reports on the WGSR membrane reactor process, the modelling, optimization, and control study of the process has not been thoroughly addressed at the system engineering level. Most of the reported work addresses the development of materials of construction for the membrane and catalysts. In regards to the optimization aspect, most of the limited research so far has focused on maximizing the production yield, which ignores the economic performance of the membrane reactor as a whole. Furthermore, the control design for the process which addresses the systems non-linearity and long transport delay has been very little mentioned in previous studies. It is worth noting that, the notable feature of this PhD study is the adoption of two conflicting objectives (economic and controllability) in the optimization process. In this case, a simultaneous optimization of the economic and dynamic controllability performances has the ability to recognize an optimal trade-off between these two objectives in the early design stage. Traditionally, a control system is designed only after the details of process design (superstructure) are decided. Once the process design is fixed, there is very little room left for improving the control performance of the system. This can lead to either high cost of implementation of control system involved or redesigning of the process if the current design is not controllable. It is also worth mentioning that, in this PhD study a new cascade control structure and design methodology that unifies the multi-scale control (MSC) schemes is developed. The control system is designed to address the current problem in dealing with some specific complex dynamic behaviours (e.g., long time-delay) in the WGSR membrane reactor system.

This research study presents its novelty in three sections: (1) process design, (2) process optimization, and (3) process control of the WGSR membrane reactor system. Firstly, in process design, a new process system is developed involving a series of other equipment and a stand-alone membrane reactor. Secondly, in process optimization, a new technique of multi-objective optimization with the incorporation of uncertainties is used to optimize the WGSR membrane reactor system for practicality. Thirdly, in process control, this study presents a novel parallel cascade control scheme that unifies multi-scale control theory which has

the ability to address process systems that exhibit non-linearity and long time-delays.

The major contributions of this research can be viewed in two aspects which are in terms of the theoretical (academic) and industrial contributions. The academic or theoretical contributions of this research are:

a) Development of new process flowsheets which incorporates membrane reactor and other equipment (i.e., heater, cooler, air compressor and heat exchanger) using a well-known chemical engineering process design procedure. These process flowsheets are simple, easy to understand and also can serve as a guideline for further WGSR process flowsheet development in the near future.

b) Development of a new multi-objective optimization methodology with the salient feature of finding an optimal trade-off between two conflicting performance criteria: the steady-state economic represented by net present value (NPV) and dynamic controllability quantified in terms of v-gap control relevant metric. This contributes to the knowledge of unifying more practical objective functions into process optimization.

c) Development of multi-objective optimization with the incorporation of external uncertainties, in order to determine the effect of uncertainties on the optimal conditions of the WGSR membrane reactor system. The addition of process uncertainties will have the ability to measure the effect of uncertainties towards the optimal conditions of the system in the near future.

d) Development of a new control strategy based on the parallel cascade control and advanced multi-scale control schemes which use a combination of 3 conventional PID controllers. The proposed triple-loop parallel cascade multi scale control scheme has the ability to minimize the adverse effects of long time-delay and nonlinearity on the closed-loop performance.

As for practical contributions, this research provides a set of knowledge, insights, and methods in modelling, optimization and control of the WGSR membrane reactor system. The analysis of the WGSR kinetics and reactor model comparison in this research study shall provide a guideline for finding a suitable pair (between kinetics model and reactor model) of WGSR kinetic-reactor models.

This study is significant for three reasons. Firstly, this study proposes new process flowsheets for the WGSR membrane reactor system. The proposed flowsheets include a membrane reactor and other equipment such as heater, cooler, air compressor, and heat exchanger. The proposed flowsheets can be readily used as a guideline in identifying the interaction of a stand-alone membrane unit with other equipment. The flowsheets presented can be implemented in a small-scale industry for hydrogen production.

Secondly, this PhD study proposes a new research direction in WGSR membrane reactor, as an intensified approach, i.e., combination of steady-state economy with dynamic controllability. This new research focus can contribute to the realization of a hydrogen economy. Moreover, with the incorporation of process uncertainties in the multi-objective optimization, the developed system is more reliable when encountering future uncertainties.

Lastly, the performance of the WGSR membrane reactor system can be improved by employing a systematic approach to its control system design. The key significance in this study is the development of an effective control system design of the WGSR membrane reactor process, which can overcome the nonlinear dynamic behaviours and also long transport delay. The development of this new control strategy can assist not only the WGSR processes, but also other process plants which have long transport delays, such as in heat exchangers, large bioreactors and distillation columns.

1.4 Dissertation Structure

Figure 1.1 shows the overview of the dissertation structure. This dissertation is outlined as follows:

Chapter 1 defines the background, motivation and objectives of this research. Also, it describes the significance and contributions towards addressing current issues and knowledge gaps relevant to this PhD study.

Chapter 2 covers the literature review on the background relevant to this PhD study. The first part covers an overview of the water-gas shift reaction process. The second part includes a critical review of the process optimization (i.e., single objective and multi-objective optimization). This is followed by the literature review of process control in WGSR membrane reactor. Lastly, this review aims to identify the existing achievements and also the research gaps relevant to this study.

Chapter 3 presents detailed fundamentals of the water-gas shift reaction membrane reactor. This chapter covers the fundamental knowledge, such as reaction mechanisms, reaction kinetics, available catalysts and membranes used in WGSR. Additionally, the detailed description of the membrane reactor mathematical model (i.e., one-dimensional, two-dimensional, three-dimensional, heterogeneous, and homogeneous) of the membrane reactor is provided in this chapter.

Chapter 4 analyzes the comparison of kinetic and reactor models used in WGSR. A conventional packed-bed tubular reactor model is used in the comparison. The simulation of all the kinetic-reactor under different combinations of reactor models and kinetic models are performed and evaluated against existing literature data. At the end of this chapter, a set of the most suitable combination of kinetic-reactor models is recommended.

Chapter 5 provides fundamental mathematical modelling of the WGSR-MR system. Here, a one-dimensional heterogeneous packed-bed tubular reactor mathematical modelling is presented. To develop a reliable and robust membrane reactor model, non-ideal gas properties are incorporated into the mathematical model. The mathematical model is validated using experimental data from literature which has a prediction accuracy of 10

Chapter 6 discusses the development of a few new process flowsheets of WGSR-MR system. The procedure of developing the flowsheets is based on the chemical engineering design handbook. The developed process flowsheets are analyzed for their detailed economic potential. The process flowsheet with the highest net present value (NPV) is chosen for the next design stage, i.e., in the parametric study. This chapter also provides the effects of parameters (i.e., retentate temperature, retentate pressure, permeate temperature, permeate pressure, concentration ratio, reactor length, reactor diameter, membrane tube diameter, and catalyst pellet size) on the NPV of the WGSR membrane reactor system. The parametric study is performed in order to identify the critical parameters for process optimization.

Chapter 7 incorporates the critical parameters identified in the previous chapter in multi-objective optimization study. This chapter also explores three different types of optimization techniques. One is based on a single-objective optimization which solely considers the economic optimization using the NPV criterion. The second type of optimization is a multi-objective optimization which simultaneously considers both economic and dynamic controllability performance criteria. While, the third is a multi-objective optimization with the incorporation of process uncertainties.

Chapter 8 proposes a new triple-loop parallel cascade control strategy where its design methodology is based on the multi-scale control scheme. The proposed control strategy is implemented into the optimized WGSR-MR flowsheet obtained in Chapter 7. This control scheme is to deal with the long transport delay problem faced by the WGSR membrane reactor system.

Chapter 9 concludes this PhD study and suggests future research opportunity related to the current study.

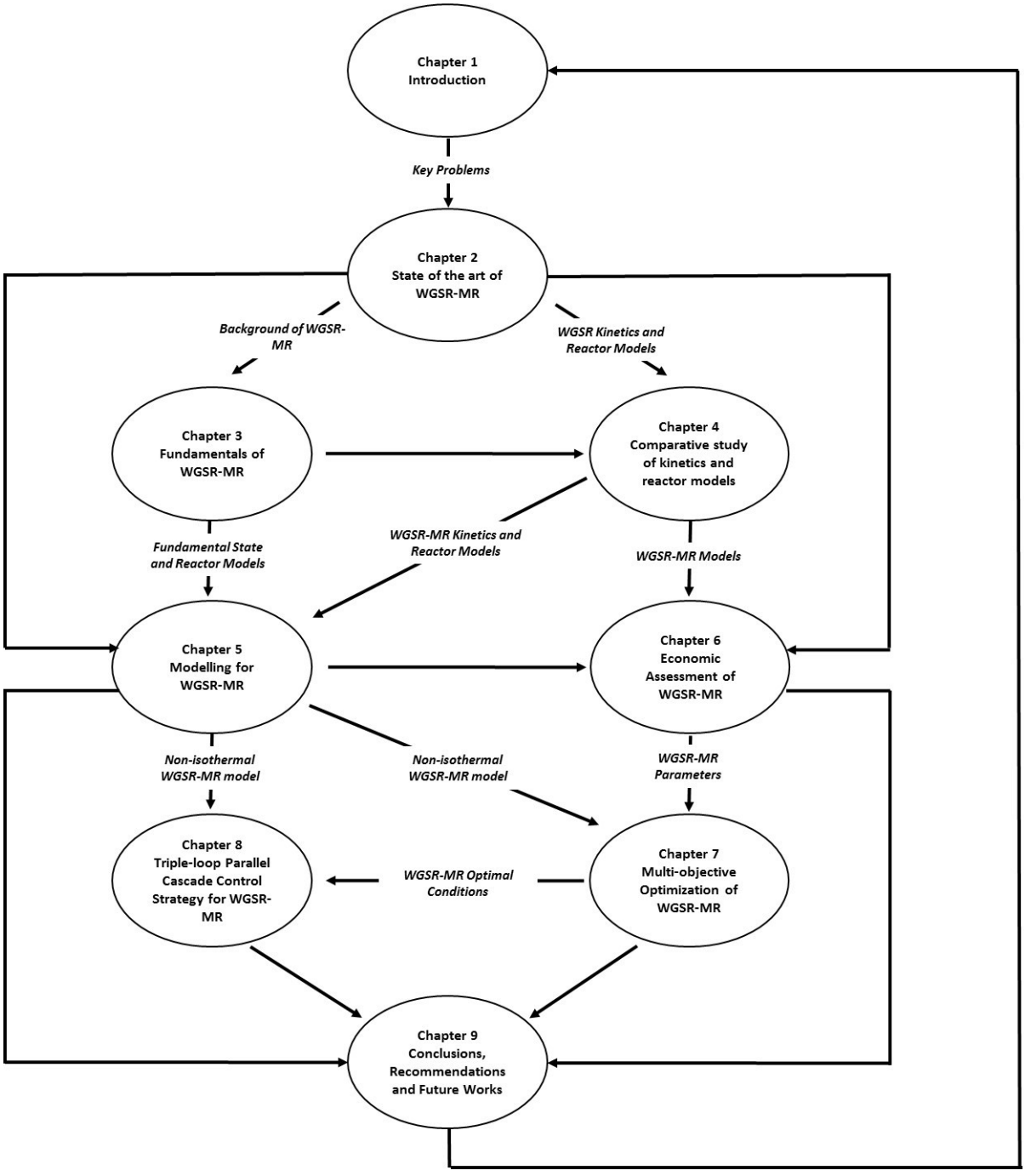

Figure 1.1: Dissertation structure overview.

Chapter 2

State of the art of WGSR-MR

2.1 Overview

This chapter introduces the background of the study of water-gas shift reaction in a membrane reactor. In this chapter, a detailed literature review will be made on existing works with the objective of establishing the knowledge in this area and thereby discussing the gaps in which this study will attempt to address.

2.2 Background

2.2.1 Hydrogen as a future energy carrier

Recently, hydrogen has received increased attention worldwide because of its potential as an energy carrier; thereby introducing the concept of a hydrogen economy (Kothari et al., 2008). Hydrogen is among the popular energy carriers due to its abundant supply as it can be retrieved from multiple renewable energy sources i.e. biomass, wastes, solar, wind, hydro or geothermal, and non-renewable sources, i.e. fossil fuels (Pen et al., 1996; Turner, 1999; Haryanto et al., 2005).

Since 2011, the world production of hydrogen has reached up to 30 trillion standard cubic feet (SCF) (Tosti et al., 2003). Interestingly, 90% of this production is generated from fossil fuels, mainly through steam reforming of natural gas or coal gasification followed by water-gas shift reactions (Sigfusson, 2007). Even with this much of supply, hydrogen only accounts for 2% of the global primary energy use (Ockwig and Nenoff, 2007), which means currently there are still lacking in the balance of supply and demand. Figure 2.1 – adapted from Bala Suresh and Yamaguchi (2015) shows the breakdown of the world consump-

tion of hydrogen and these amounts are expected to rise by 5-6% in the next five years, due to demand in the manufacturing of methanol and ammonia as well as petroleum refinery operations (hydrotreating and hydrocracking) (Bala Suresh and Yamaguchi, 2015) see Figure 2.2 – adapted from Mendes et al. (2012).

The demand for hydrogen plus the search for an alternate energy source has motivated worldwide efforts toward improving efficiency of H_2 production, whilst minimizing costs (Tanksale et al., 2010).

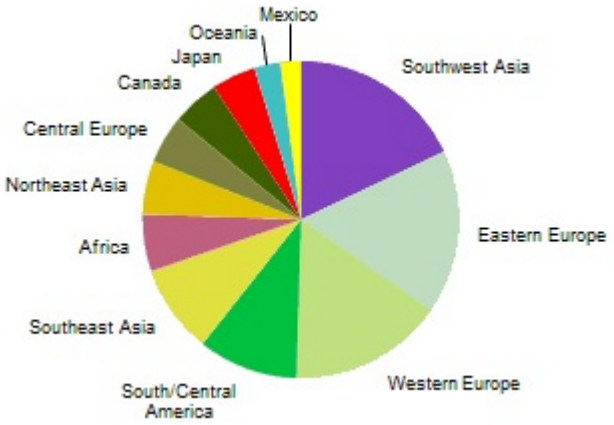

Figure 2.1: Worldwide demand of hydrogen 2014.

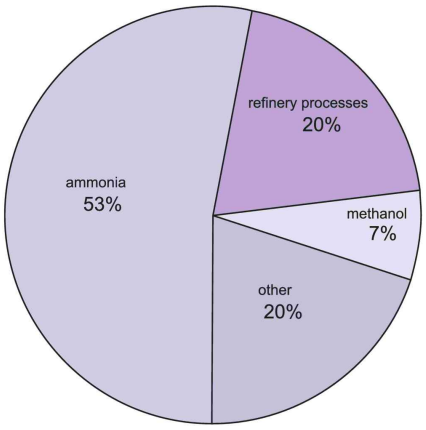

Figure 2.2: Market share of the currently produced hydrogen.

2.2.2 Water-Gas shift reaction

Water-Gas Shift Reaction (WGSR) has been one of the most common processes for hydrogen production. This process involves high-temperature reactions be-

tween $CO - H_2$ mixture and steam. The chemical reaction of WGSR is shown in Equation 2.1 (Mendes et al., 2010).

$$CO + H_2O \rightleftharpoons CO_2 + H_2 \quad \Delta H_{rx} = -41.1\, kJ/mol \tag{2.1}$$

Lund and Mond discovered the Water-Gas Shift Reaction (WGSR) in the early years of 1890s, (Mond and Langer, 1888). This reaction, however has several disadvantages. Firstly, it has an equilibrium limitation due to the nature of the reaction (i.e., reversible reaction). In essence, this reaction is more favourable at low temperature due to the nature of its exothermic reaction. However, in order to increase the rate of production, higher temperature is desirable to enable faster collisions among the reactants and achieve the activation energy required.

This two conflicting factors often complicate the design of a reactor for the WGSR. Traditionally, this reaction is conducted in a single-staged reactor whereby the reaction is conducted adiabatically. Usually, iron oxide-chromium oxide catalyst is used in the reactor. The composition of the effluent from this reactor normally consists of carbon monoxide (CO) at 2 to 4%, which approaches an equilibrium value (Lloyd et al., 1996). However, commercially the CO composition of the effluent can be further decreased by conducting the WGSR in a two adiabatic stage rather than one. The first one is at high temperature shift reactor followed by inter-stage cooling before entering a lower temperature shift reactor. The purpose of installing the inter-cooling stage is to maintain the inlet feed temperature entering the low temperature shift reactor, which is important, as high temperatures in this second reactor will damage the activities of its catalyst (Lloyd et al., 1996).

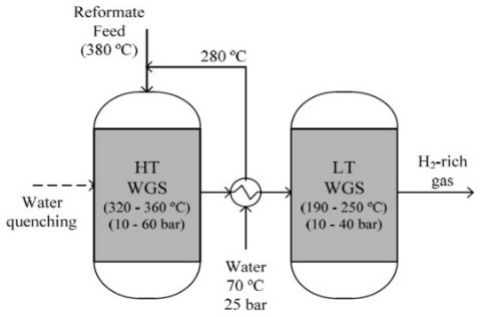

Figure 2.3: Conventional reactor design for WGSR.

Typically, with the reaction temperature of roughly around 400 - 450^0C, an outlet stream with a CO concentration between 1% and 5% can be obtained.

However, this largely depends on the performance of the high-temperature shift reactor, as well as the type of feedstock. The outlet stream is then cooled through an inter-staged cooling system, which is usually water. (Vielstich et al., 2003) − see Figure 2.3 − adapted from Mendes et al. (2010). The stream is then cooled to about 200^0C. Once the stream is cooled, it is then fed to a low-temperature shift reactor. One of the main problems arising from the low-temperature shift reactor is the volume of the reactor. Even though the WGSR thermodynamic favours lower temperatures, the reaction kinetics are often too low, resulting in a large volume of catalyst being needed to approach the high CO equilibrium conversion (Lee, 2006). This implies that if WGSR is conducted at lower temperatures, the volume of the reactor required will be much larger.

The hydrogen produced through WGSR then still requires further purification in order to meet the requirement purity grades of 99% (Grashoff et al., 1983). Purification of hydrogen can be done in several processes such as pressure swing adsorption (PSA), cryogenic distillation (CD) or even by membrane separation. It is mentioned in the work of Cheng et al. (2002), that membrane based processes are one of the most promising technologies for the production of high-purity hydrogen due to its high selectivity, permeability, and conversion.

International Union of Pure and Applied Chemistry (IUPAC) defines a membrane reactor (MR) as a device for simultaneously carrying out a reaction and separation in the same physical device (Koros et al., 1996). A membrane plays an important role not only as a separator, but also in the reaction itself − see Figure 2.4 − adapted from Lu et al. (2007). A membrane can selectively remove a product from a reversible reaction and therefore shift the equilibrium-limited reaction. This resulted in increase in reaction conversion; conversion higher than traditional reactor (TR). This has sparked a keen interest among researchers on membrane reactors (MR). They are summarized in the next few review articles (Saracco and Specchia, 1994; McLeary et al., 2006; Lu et al., 2007). Brief history of membrane reactor is reported somewhere else (Basile et al., 2008). Some other significant advantages of using membrane reactor with respect to the traditional shift reactor are outlined as follows:

- Increase in conversion for an equilibrium-limited reactions.
- Achieve better results than conventional reactor at the same operating conditions.
- Decrease in capital costs as reaction and separation are combined in one

single unit.

- Increase in hydrogen yield and purity.

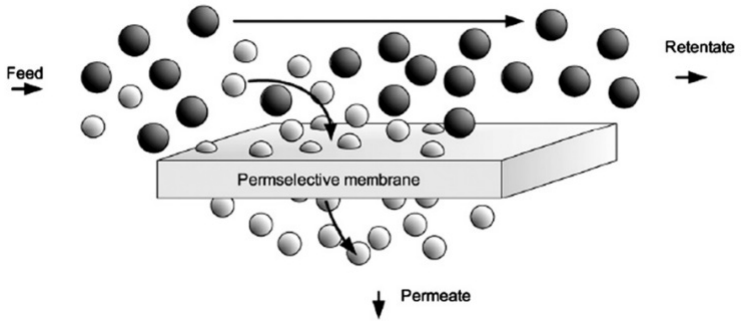

Figure 2.4: Membrane that involves in both reaction and separation process.

Process plant integrating reaction and separation units to conduct WGSR has been a promising economical hydrogen production technique. Subject to the operating conditions (such as operating pressure and temperature), the hydrogen production using a membrane reactor can become economically attractive as it can improve overall production efficiency up to 30% as compared to a traditional shift reactor (Collot, 2003). It is clear that new technologies such as the integration of membrane reactors in the process plants should be pursued in order to obtain a viable transitional step towards the hydrogen economy.

One of the objectives of this study is to develop an effective design and control strategy for a water-gas shift membrane reactor system. The study of process optimization and control toward water-gas shift membrane reactor is still fairly limited. A series of literature reviews on process optimization and control related to WGSR has been identified and research gaps are summarized at the end of this chapter. This study aims to fill the identified research gaps.

2.3 Literature Reviews

2.3.1 Process optimization related to WGSR

A fundamental of optimization is introduced briefly in this section. There are two types of optimization problems, (1) continuous and (2) discrete variables (Biegler and Grossmann, 2004). The difference between these two variables are that continuous variables are usually made up of derivative variables while discrete

variables generally are restricted to take 0-1 values only. Regardless of any of these variables, both of their optimization formulation are represented in the similar general algebraic form as shown in Equation 2.2.

$$\begin{aligned} \text{min or max} \quad J = \quad & f(x,y) \\ \text{subject to} \quad & h(x,y) = 0 \\ & g(x,y) \leq 0 \\ & x \in X, y \in \{0,1\}^m \end{aligned} \tag{2.2}$$

where function f is the objective function of the optimization such as cost or yield, function h are usually the models of the system (i.e., material and heat balances) and function g are known to be the constraints and the specification of the systems. As mentioned earlier, there are two types of variables, here in Equation 2.2, variable x refers to continuous state variables while variable y is a discrete variable with a value of 0 or 1.

There are sub-categories below these two major optimization problems. In continuous optimization, there are linear programming (LP) and non-linear programming (NLP) that fall under this optimization problem. An important distinction of NLP is whether the problem is convex and non-convex. A convex problem gives only one global optima while a non-convex problem may give multiple local optima. As for discrete optimization problem, it is classified into mixed-integer programming problem which consists of mixed-integer linear programming (MILP) and MINLP formulations. The reason is that the discrete variable takes the value of 0 or 1 which results in mixed-integer formulation. If there are no 0-1 variables, the MILP is reduced to LP or NLP depending on the linearity of the functions.

NLP and MINLP problems tend to focus more on process design. This is because design problems rely more on process development and model's prediction which requires explicit handling of performance equations resulted in non-linearity of the models. There are numerous number of applications in process design that used NLP or MINLP to formulate their optimization formulation. The same goes to WGSR membrane reactor process design. Following are some of the reviews regarding the application of LP and NLP optimization of WGSR-MR for different types of process plants.

In the work of Emun et al. (2010), the authors conducted an optimization study on WGSR in an Integrated-Gas Combined Cycle (IGCC) process. The goal of the work was to optimize the IGCC flowsheet using an old established

method of process integration coupled with a pinch analysis methodology. The pinch analysis methodology was useful in terms of optimizing the heat exchange network that is available in the whole process plant in order to save the plant operating cost. This optimization methodology, however, only targeting on the pipeline of the plant without altering any process operating conditions. Hence, this methodology is only applicable to the whole process plant flowsheet and does not take into account the details of equipment optimization.

An improvement on optimization of WGSR-MR was made in the work of Lang et al. (2011). They simulated several main units of the IGCC plant via CFD simulation and then converted the simulation into a reduced order model (ROM) using the principal component analysis (PCA). With this ROM framework, they managed to derive several units in the IGCC plant which are known to be highly non-linear into an equation-oriented simulation environment. The ROM is then used in an optimization algorithm. However, using PCA to generate ROM from CFD simulation might not be able to generate sufficient accurate model for optimization. The reason for this is that a ROM is created from linearized data obtained from the CFD simulation based on which the ROM is developed on a layer by layer of assumptions. Nonetheless, this ROM method could be quite effective when it is used in a direct simulation program that starts from scratch, for example, modelling of reactor in the MATLAB software.

In the work of Bhattacharyya et al. (2010), the author has proposed a more systematic methodology known as three-phase optimization. It is a top-down approach optimization. The first design phase is called the global design decisions which are made up by main objectives and aim of the flowsheet optimization. The first design phase is then narrowed down in the second design phase, known as local design decisions whereby major unit objectives and target are identified. Lastly, the third and final phase is the optimization of the operating condition. Upon achieving an optimal operating conditions which satisfies all the main criteria set in design phases one and two, the flowsheet is then recognized as an optimum flowsheet. The limitation of this approach is that the capital costs of the equipment are not included in the optimization calculation. Consequently, the optimal operating conditions do not guarantee the lowest capital cost as some optimal operating conditions may be located in harsh conditions whereby special fabrication and materials are needed for the equipment to function safely and smoothly.

The work of Lima et al. (2012) was the first to introduce optimization of membrane reactor incorporated in an IGCC plant. They investigated the idea

of a H_2-selective zeolite membrane for the WGSR in the IGCC plant. They discovered that a counter-current sweep gas flow lead to higher production yield than a concurrent flow. With the same model used above, they formulated a novel optimization problem to systematically determine the optimal length of the MR design. The optimization problem is solved with the objective of maximizing reactor performance (reaction conversion) while minimizing the amount of membrane surface area subjected to specific operating conditions and constraint such as pressure drop across the MR. The optimization formulation was then solved using Matlab Optimization Toolbox function *fmincon*. Note that, *fmincon* algorithm uses sequential quadratic programming method (SQL) in MATLAB software. Lima et al. (2012) successfully identified an optimum membrane area within the specific operating conditions and MR constraint. However, in this work, only one design parameter (i.e., membrane surface area) is included in the process optimization. It is interesting to point out that the robustness of the optimization can be improved with an introduction of more than one specific design and operating parameters in the optimization formulation.

In Koc et al. (2012) work, the researchers tried to identify the possibility of positive economic assessment of the MR system in IGCC plants. The authors included safety and economic feasibility in their assessment and they discover that by the implementation of MR in an IGCC plant, positive NPV of USD$ 0.71 billion and $ 0.44 billion for the cases without and with CO_2 capture can be generated over the plant lifetime of 20 years. Note that, the economic evaluation of this paper is based on commercial size membrane reactor and commercial syngas flow rate. It is worth highlighting that this paper presented an interesting economic assessment while provided valuable data and specification of a commercial sized membrane reactor.

In a separate work, Koc et al. (2012) continued their study on the economic performance of IGCC plant. In Koc et al. (2014) extended work, by studying the IGCC economic performance under uncertainty. In this work, the researchers used Monte-Carlo technique to generate the possible values for all uncertainties mentioned in the paper. In addition to this, this paper also produced a comparison of economic performance for different scenarios, such as IGCC-MR without CO_2 capture, IGCC-PBR (with traditional packed bed reactors), IGCC-MR and other technology options. It was concluded that from an environmental performance standpoint, the new MR technology option allows significant reduction of air pollutants and greenhouse gas emission in a cost-effective manner. It is worth mentioning that Koc et al. (2014) provided quite a significant insight into the

influences of calculation of operating and capital costs under several uncertainty scenarios, which can also provide general guidelines in economic performance calculation that can be used in future work for an optimization of IGCC-MR flowsheet.

In the progress of membrane reactor assisted WGSR, the focus on optimization so far has been mainly on the use of optimization based on one objective function at a time which is also known as single objective optimization (SOO). This was shown in the works of Lang et al. (2011),Bhattacharyya et al. (2010), and Lima et al. (2012), where in all these works the optimization formulation was only focusing on one objective (maximum reactant conversion). Bear in mind that for practical approach more than one objective has to be considered simultaneously. Some examples of these objectives include capital and operating costs, payback period, net present value, recovery of product, conversion of reactant, energy saving, process safety, robustness, etc. In order to achieve optimal results which are practical in industrial environments, one must combine more than one objective into the optimization formulation. This optimal approach is known as multi-objective optimization (MOO). Often, conflicts among the objectives arise due to multiple objectives in a single optimal formulation. The reason is that while achieving the optimum for one objective requires compromise on the other objectives. For an example, an increase in process operation safety resulted in increase in operational costs due to the additional cost of implementing extra process control safety equipment and thereby caused reduced in overall profit margin.

2.3.2 Multi-objective optimization in process plants

Multi-objective optimization (MOO) often results in more than one optimal solution as it has usually been tied to a non-convex problems except when the objectives are not conflicting with each other. Therefore, MOO requires specific methods that can effectively solve the optimization formulation. Till date, there are lots of methods have been developed in solving MOO problems. In general, MOO solving methods can be classified into two categories; (1) preference based methods and (2) generating methods (Rangaiah, 2009).

To current author's knowledge, there has been no literature reported of MOO problem formulation in a membrane reactor assisted in WGSR. Therefore, in this section, only selected work closely related to membrane reactor or hydrogen production plants is discussed.

Preference-based Methods

This method is sub-divided into two smaller groups, namely priori method and interactive method. In priori method, decision maker (DM) is first included at the very beginning of the objective formulation. Example of a priori method includes goal programming and lexicographic ordering. As for interactive method, the preference of DM is included in solving the problem after the first iteration. At the end of the iteration, this method is able to produce one or more Pareto-optimal solutions. Example of the interactive method includes NIMBUS and a trade-off method (Rangaiah, 2009).

In the work of Chakraborty and Linninger (2002), the authors proposed a new methodology for plant-wide waste management that consists of two stage synthesis algorithm followed by rigorous optimization. In this work, goal programming method is used to find all Pareto-optimal solutions that gave best process economics with minimum environmental impact. In an extension work Chakraborty and Linninger (2003), the authors used the same methodology as in previous work with the addition of uncertainties. A linear mathematical model was used to estimate the uncertain parameter variation that affects plant cost and environmental impact. In this work, Chakraborty and Linninger (2003) suggested a practical approach to open-ended flowsheet problems that deal with uncertainty.

In the most recent work Nixon (2016), non-linear goal programming to optimize the design parameters of an anaerobic digestion (AD) system was used. The objectives of the optimization were to minimize the cost of electricity while maximizes the energy potential and mass reduction. The author demonstrated that this optimization is a promising option for AD design.

This preference based methods are suitable for optimization problems where DM understood well each of the objective functions and able to identify the interdependency of the multiple objectives or the range of the feasible objective values. This method requires a lot of experience and great knowledge from the decision makers.

Generating Methods

The solutions generated from this method usually end up with one or more Pareto-optimal solutions. If there is more than one Pareto-optimal solutions, then an introduction to the role of decision maker (DM) is made. The DM role is entrusted with the task to choose one of the Pareto-optimal solutions based on conditions that are not included in the MOO problem formulation. There are

three sub-categories in this generating method: (1) no-preference methods (i.e., global criterion), (2) posteriori methods using multi-objective approach (i.e., simulated annealing, genetic algorithm), and (3) posteriori methods using scalarization approach (i.e., ϵ-constraint method, weighted method) (Sharma and Rangaiah, 2013).

Yu et al. (2007) performed MOO for methane steam reforming in a porous ceramic membrane reactor. They applied non-dominated sorting genetic algorithm (NSGA) in solving the optimization problems. The authors formulated two MOO optimization problems, (1) maximization of hydrogen production rate and recovery, and (2) maximization of hydrogen rate while minimize the sweep gas flow rate or membrane surface area. The Pareto-optimal solutions obtained served as the guidance for future decision makers.

In the work of Quddus et al. (2010), the same MOO formulation presented in Yu et al. (2007) was used to study in the optimization of a porous ceramic membrane reactor for an oxidation coupling methane. Quddus et al. (2010) modified the algorithm of NSGA with an addition of jumping genes into the algorithm. In this work, the researchers discovered a significant improvement in performances in terms of selectivity and yields when two objectives optimization problems were optimized instantaneous.

Cheng et al. (2008), developed a triple-objective optimization for catalytic membrane reactors. The authors too used NSGA technique to optimize the multi-objective optimization formulation for alcohol synthesis and for hydrogen generation. The results presented in this work showed two distinctive features. An optimal solution of randomly scattered and an optimal solution of a straight linear line. The researchers discovered that for both systems, the membrane area and membrane thickness plays an important role in the optimal solutions. Cheng and his co-workers believed that MOO provides more information on the correlation between different objective functions and optimal solutions.

Montazer-Rahmati and Binaee (2010), too employed NSGA technique to perform multi-objective optimization in simultaneous maximization of steam flow rate and hydrogen production rate of an existing hydrogen plant. The hydrogen plant consists of steam reformer, shift converters, absorber and a methanator. For the design configuration considered in this study, several sets of Pareto-optimal operating conditions were obtained.

Recently, Shahhosseini et al. (2016) proposed the application of elitist non-dominated sorting genetic algorithm (NSGA-II) in simultaneous maximization of methane conversion, and hydrogen and carbon monoxide selectivity. The Pareto

optimal obtained was further selected using decision making methods such as LINMAP, TOPSIS, Shannon's entropy and Fuzzy Bellman-Zadeh.

All the above-mentioned works are in the category of posteriori methods using multi-objective approach. The approaches in this category are highly complex as compared to the category of posteriori methods using scalarization approach. There are two major approaches in the classical scalarization method, namely the ϵ-constraint method and weighted sum method.

In the work of Salcedo et al. (2012), an ϵ-constraint method is used to solve a multi-objective mixed-integer nonlinear programming model (MINLP). The MOO considered simultaneous minimization of environmental impact and cost of the desalination plants. With environmental performance quantified using life cycle assessment and the cost performance calculated by operational costs. The results obtained by the authors showed that the optimal approach is able to lead a significant environmental savings at a small increment in cost.

In the work of Vlysidis et al. (2011), a MOO problem was formulated to maximize the profit while minimizes the environmental impact of the overall process. The MOO was solved using the ϵ-constraint method of optimizing the cycle time of the batch fermentation and the water flow rate. These two parameters were chosen as they have a significant effect on the economics of the biorefinery process. This method is often preferred to solve MOO when the constraint on one of the objective function is identified.

The ϵ-constraints method creates a single objective model in which only one of the objective function is optimized while the other remaining functions become the constraints of the model (Donoso and Fabregat, 2016). The method has an advantage of solving non-convex MOO problems. The drawback of this method is that one must understand the MOO formulation well and that the values of the ϵ-constraints.

The weighted sum method is first introduced by Zadeh (1963). Since the beginning, this method has been mentioned prominently in literature. The reason of this is because this method provides the simplest approach in solving MOO problems. This method can effectively scalarized a MOO problem formulation in forming a SOO by multiplying each objective with a user supplied weight.

In the work of Aslan (2008), weighted sum method was used to solve for a multi-objective optimization in a multi-gravity separator. The problem was formulated to maximize the concentration grade and recovery of the separator. Two equal weights have been assigned to each objective as it was assumed to be equally important. The optimization results showed considerable improvement in both

the quality characteristics. The results obtained from the multi-objective optimization showed better grade and recovery compared to the initial (unoptimized) value of the grade and recovery.

Mitsos et al. (2008), developed an integer linear program formulation for an automatic method to reduce the kinetic model. In this work, the researchers incorporated the weighted sum methodology into the linear program formulation to estimate the parameters for the reduced kinetic models. In this study, an equal weight percentage was given to the parameters according to their importance. Based on the multi-objective optimization developments, the reduced kinetic models have the same prediction accuracy as the initial (unreduced) kinetic models with significant reduction in computational time.

Albrecht et al. (2010) addressed the challenges faced in designing batch processes using multi-objective optimization. The work presented a modified version of the multi-stage framework for a continuous assessment of the batch process design. Three main objectives are used in the MOO formulation (i.e., cost, cumulative energy demand and hazard). Although, there was more than two objectives function, the weight percentage was divided equally among the objectives. This modified framework has been successfully implemented in a production process for 4-(2-methoxyethyl) -phenol.

Yunqiang et al. (2011), presented a novel approach for modelling and optimization for a hydrogen network in refineries. In this multi-objective optimization, the authors used weighted sum methodology for the MOO formulation of minimizing operating and investment cost simultaneously. The proposed method took into account constraints such as pressure, purity, payback period and so on. The applicability of the approach was tested in a real case study.

Although the weighted sum method has been widely used in solving MOO problems, researchers were more focused on the distribution of the weightage between each objectives especially for optimization of more than two objectives. Yoon and Hwang (1995) developed a rating method to identify the percentage of weight for each objective. The most important objective was given a more significant percentage of weight compared to a less important objective. Saaty (2003) developed an eigenvalue method for determining weights using a pairwise comparison between objective functions. The author is able to obtain a comparison matrix in the formed of eigenvalues which is then used as the weights.

Due to many literatures concerning the weight distribution, Marler and Arora (2010) proposed a method that can identify the fundamental of the weighted sum preferences. They too introduced a set of guidelines in choosing and developing

the percentage of the weights specifically for more than two objectives function. To date, this method is still widely used in process application. Mohseni-Bonab et al. (2015) used weighted sum method in combination with Monte Carlo simulation to optimize the reactor power dispatch considering load uncertainties. This method was also seen in the work of Majidi et al. (2017), where it was used to solve minimization of CO_2 emission and total cost of the hybrid system.

2.3.3 Integrated design and control optimization

In multi-objective optimization, one can choose multiple objective functions as to achieve optimum values that is able to satisfy all the objectives. However, one requires deep understanding of the interaction among each objective in order to determine a suitable combination objectives to form a multi-objective function optimization (Kookos and Perkins, 2001). As such, in process plant industries, the common perception is that process design is dominated by steady-state economic performances (e.g., profit, total annual costs and net present value). However, many researchers have recognized the conflicts and competitions between economic and controllability of chemical processes (Seferlis and Georgiadis, 2004). Unfortunately, in most cases there is always a trade-off between economic profitability with process controllability. Therefore, it is important to find the optimal balance between these two aspects, especially in process plant design stage. Traditionally, control system is designed only after the details of process design are decided. Once the process design is fixed, there is little room left for improving the control performance and this has always led to either high cost of implementation of control systems or redesigning of the process. Recognizing the interaction between process design and control, an integrated approach in which the combination of these two objectives into a multi-objective optimization is very much desired.

Some of the researchers such as the authors of Luyben (1994) had employed a multi-objective function for incorporating economic objectives (i.e., capital and operating costs) and controllability measures (i.e., relative gain array (RGA)). They used generalized benders decomposition (GBD) algorithm Geoffrion (1972) to solve the MINLP objective formulation. The trend was then followed by Chacon-Mondragon and Himmelblau (1996), as they proposed a bi-objective optimization which includes costs and flexibility of the process. Similarly, Alhammadi and Romagnoli (2004) proposed an optimization framework whereby the combination of economic, controllability and environmental measures to form a

single multi-objective function. The combination of economic and controllability in a single optimization is recognized as a more practical method compared to other integration of process design and control, but simultaneous optimization of economic and controllability posed a tough challenge and high complexity (Sharifzadeh, 2013). Therefore, systematic approach to solve this optimization is highly encouraged.

Even though multi-objective optimization is able to generate optimum values, these optimizations are still subjected to uncertainty. A large number of problems, including production planning, finance and engineering design require decisions be made in the presence of uncertainty. There are lots of uncertainties, for instance, prices of fuels, the cost of electricity and demand for chemical products (Ahmed and Garcia, 2003; Li et al., 2012). With the presence of uncertainties, process optimization becomes even more challenging. As such Beale (1955), Bellman and Kalaba (1965), and Dantzig (1955) had focused their research in developing algorithms to solve optimization that involves uncertainties.

2.3.4 Optimization with uncertainties

Two types of uncertainties:

a) Endogenous uncertainty − sources of uncertainty can be either related to the process or the final product such as the process operating conditions or the properties of the intermediates being processed, and

b) Exogenous uncertainty − externally given by the environment, such as product demand or raw material and finished product prices and availabilities (Martín and Martínez, 2015).

Uncertainty can negatively or positively impact the proper operation and market success in any new or modified product. It can also have a significant impact on how easy or difficult to incorporate modifications in future generations of existing products. Figure 2.5 − adapted from Goel and Grossmann (2006) shows the different types of sources within these two categories of uncertainty.

The demand and supply of hydrogen fluctuate as time. The fluctuation caused changes in economic situation (Gebreslassie et al., 2012; Michalek et al., 2011; Guillén-Gosálbez and Grossmann, 2009). Hence, hydrogen production process industries are usually susceptible to exogenous uncertainties.

There are two types of modelling uncertainties:

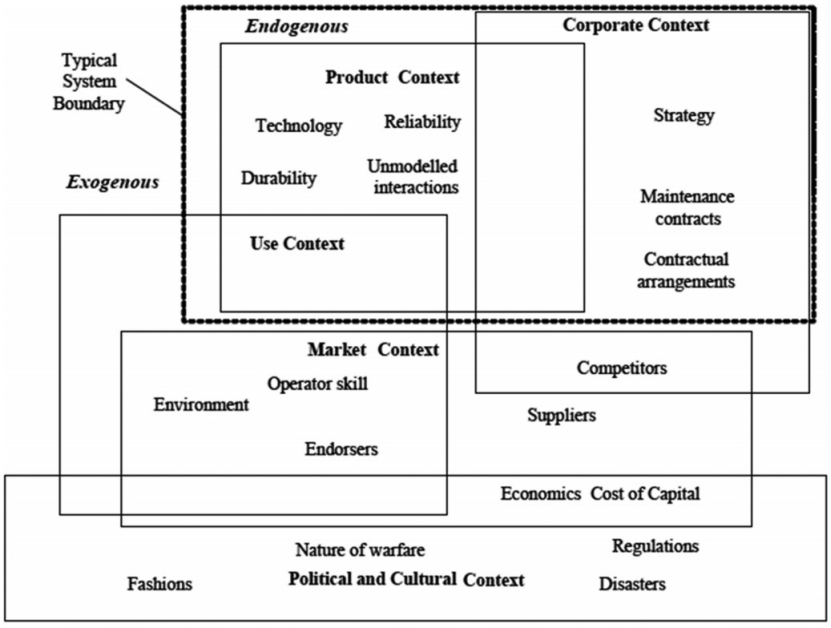

Figure 2.5: Different sources of uncertainties.

a) Deterministic model − assumes a certainty in all aspects. Examples of deterministic models are linear programming model, and economic order quantity model.

b) Stochastic or probabilistic model − calculate the likelihood of the uncertain parameters. Some more common stochastic models are queueing models, Monte Carlo, and Markov chains (Maybeck, 1982).

Note that most models really should be stochastic or probabilistic rather than deterministic, as a stochastic model generates more reliable data compared to the deterministic model (Lazo et al., 2003).

Stochastic programming models are large-scale optimization problems that are used to facilitate decision-making under uncertainty. Optimization algorithms for such problems require the evaluation of the expected future costs of current decisions, often referred to as the recourse function. In practice, this calculation is computationally difficult as it requires the evaluation of a multidimensional integral whose integrand is an optimization problem (Parpas et al., 2015). Many algorithms approximate the value of the recourse function using quadrature rules (Pennanen and Koivu, 2005) or Monte Carlo (MC) methods (Shapiro et al., 2014; Birge and Louveaux, 2011). MC methods are particularly appealing for this purpose because they are easy to implement and remain computationally

tractable when the recourse function depends on multiple random variables.

Koc et al. (2012) is the first to propose the element of uncertainties in a hydrogen production process plant that incorporate a membrane reactor. The authors extended their work with the inclusion of more uncertainties (Koc et al., 2014). In both the works, the authors used Monte Carlo algorithm to simulate the element of uncertainties. It was observed in these papers that, even with a large number of uncertainties presented, MC algorithm was capable of calculating the likelihood for each uncertain parameter. This suggested that the MC algorithm is effective as it is able to handle large amount of process uncertainties.

MC algorithm consists of numerous probabilistic models to generate several sets of probability data. These sets of data are then used to generate the expected outcomes. For instance a simpler probabilistic model is known to be Markov Chain. A Markov Chain is commonly used to obtain a desired probability distribution. This model is well known as it is capable of modelling time dependent random variable. The combination of this model and Monte Carlo simulation formed a special technique, namely Markov Chain Monte Carlo (MCMC).

MCMC method has been widely used since its establishment. The introduction of this method can be found in the work of Metropolis et al. (1953), Geman and Geman (1984), Gelfand and Smith (1990) and Hastings (1970). This method has become well known as a powerful computational tool for analysis of complex statistical problems. Even though this method has the ability to predict numbers or values based on probabilistic simulation, a number of uncertainties faced in every design of a process plant are immeasurable. One is not able to detect all the uncertainties during the design stage of a process plant being exogenous or endogenous. Thus, there is a need of implementing process control in a process plant. Process control can ensure a safe operation of the process plants, even the process plants are subjected to uncertainties, due to its robustness in handling perturbations as well as plants uncertainties.

2.3.5 Control strategy in membrane reactor technology

To date, there has been a very little study conducted at the direction of control strategy development for membrane reactors. Several works had been conducted on the development of control strategies for a whole IGCC process plant. For an example, Bequette and Mahapatra (2010) used ASPENTECH software to perform steady-state and dynamic simulations of an IGCC power plant. Furthermore, few techniques were used to assess the steady-state and dynamic operability

of the power plant such as linear system analysis under various plant operating conditions. A model predictive control (MPC) strategy was developed to improve the dynamic operation of the power plant. Due to high maintenance cost of implementation of MPC, this control strategy is not as popular as other control strategies, for example, fuzzy logic control and Linear-quadratic-Gaussian control (Camacho and Alba, 2013).

Lima et al. (2013) developed a nonlinear model predictive control for the same process plant used by Bequette and Mahapatra (2010). They have successfully developed a centralized nonlinear MPC strategy using a collocation based algorithm to control power generation according to the demand. This strategy has been successfully implemented to address several scenarios that consider power load transitions (setpoint tracking) and variability in slurry feed compositions (disturbance rejection). The closed-loop simulation results showed that power control can be attained without violating process constraints. Nevertheless, Lima et al. (2013) did not evaluate the closed loop performance in terms of robustness against uncertainty which is important as the IGCC-MR model is subject to uncertainty (e.g., parametric errors and structural mismatch) that will affect the control performance.

As mentioned before, due to the exothermic nature of WGSR and this reaction is usually conducted in a non-isothermal packed bed membrane reactor, the temperature will rise along the membrane reactor. Without a proper control strategy, the hot spot temperature might reach the catalyst deactivation temperature and cause reduction in the yield of hydrogen. Georgis et al. (2012) proposed to use three different controller outputs to control the hot spot temperature of an exothermic tubular packed bed reactor. Because all the three different controller outputs failed to regulate the temperature profiles, Georgis and his co-workers incorporated nonlinear controller into the control system. It showed that the controller can suppress perturbation due to the modelling errors. However, it can be observed that the controller was unable to reduce large spikes, which was caused by the proportional-integral (PI) controller. Bear in mind that, a high spike in controller output has been one of the reasons causing malfunction of the controller unit.

Georgis et al. (2014) intended to further improve the control strategy. The authors used multiple cooling zone to first regulate the reactor temperature and proposed a control strategy using the flow rate of the cooling fluid. The same nonlinear controller as in the previous paper Georgis et al. (2012) was used, this time a better temperature control can be achieved by implementing the cooling

zone. But the paper did not address the limitation of the spike induced by the controller. Furthermore, complex reactions such as the WGSR, a single-loop controller is hardly effective for controlling the reactor hotspot temperature due to the presence of significant transport delay because of the reactor length.

2.3.6 Cascade control strategy in process plants

In the presence of a large transport delay due to reactor length, a cascade control strategy employing a secondary measurement located somewhere along the reactor is recommended to improve the disturbance rejection performance. In other words, the secondary controller is used to reject incoming disturbances in advance before the main controlled variable is seriously upset i.e., the hot spot or effluent temperature. It should be noted that, the secondary controller (known as the slave controller) has to react faster to the disturbance than the primary (master) controller. The benefits of the cascade control strategy are reported in many process control textbooks, e.g., see (Seborg et al., 2006; Ogunnaike and Ray, 1994). This control strategy has been implemented and tested on packed bed reactor and the results showed that with the implementation of this control strategy, the performance of the reactor can be significantly improved Saw et al. (2015).

Cascade control is one of the widely used advanced control strategies in the process industries. As a cascade control has the ability to control complex and highly nonlinear process systems (Luyben, 1989). Note that, the higher the nonlinearity of the processes corresponds to the unpredictability of the process responses. Cascade control effectively reduces the effect of possible disturbances as well as improving the dynamic performance of the closed loop system. A general cascade system consists of two control loops, one loop (secondary, inner or slave) nested in the other (primary, outer or master) loop (Santosh and Chidambaram, 2016).

There are two types of cascade control known as series cascade and parallel cascade. In series cascade control structure, the manipulated variable affects one controlled variable, which then affects a second controlled variable. While in parallel cascade control, the manipulated variable affects both the controlled variables (Luyben and Luyben, 1997). It should be noted that they are two different control strategies and therefore cannot be directly compared as to which one is the more effective. Each cascade system should be compared only with its non-cascade equivalent. However, one can say parallel cascade has an advantage

of requiring minimum process data to formulate the controller tuning.

To formulate series cascade control tunings, one required to run at least twice the process simulation. Example:

a) First process simulation − to obtain a slave controller tuning,

b) Based on the results obtained from the first tuning, a second process simulation is run − to obtain the master controller tuning.

An addition of the inner loops for the series cascade control systems results in an addition run of process simulations. On the other hand, a parallel cascade controller tuning is able to form multiple process transfer functions with one time process simulation data. For a clear comparison, a series and parallel cascade in terms of block diagram are shown in Figure 2.6 - 2.7 respectively.

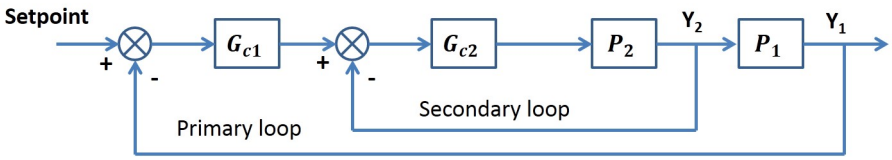

Figure 2.6: Series cascade control - two loops.

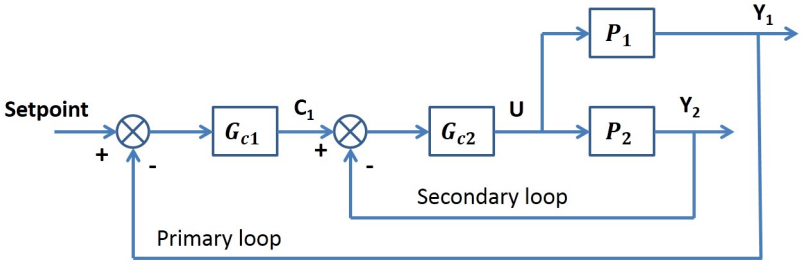

Figure 2.7: Parallel cascade control - two loops.

Parallel cascade was first introduced in the work of Luyben (1973). In parallel cascade control, the secondary loop plays an important role in both disturbance rejection and reduction of the nonlinearity possessed in the manipulated variable (Seborg et al., 2010). Generally, a parallel cascade control is used when the innermost loop can effectively reduce the disturbance before entering the outermost loop. Furthermore, the parallel cascade control is also appropriate when the outermost loop has a long process delay. Despite clear benefits of the parallel cascade control and its wide-spread use in process industries, the design on the parallel cascade control systems has attracted relatively little research.

Yu (1988) analyzed and designed a conventional controller for a parallel cascade control structure. Yu designed a perfect disturbance-rejection controller for the secondary loop while the primary controller served as the servo controller. From this work, it was discovered there was an interaction between the primary and secondary loops and hence, Yu proposed a new measurement γ to improve the parallel cascade control. To address the interaction problem, the author Brambilla and Semino (1992) introduced a nonlinear filter in the cascade control. The nonlinear filter is able to partially separate the dynamics of the loops. In addition, the nonlinear filter has a stabilizing effect on the cascade structure which results in reducing the tuning difficulties. Brambilla et al. (1994), then proposed some non-dimensional parameters to address the choices which are required to design parallel cascade controllers for multi-component distillation columns with dual control.

Chidambaram (1993) extended the application of parallel cascade control to a continuous stirred tank bioreactor. The parallel cascade control strategy is then expanded to a process applications by "reverse engineering" the functions of the baroreceptor reflex–the biological control system that regulates arterial blood pressure (Pottmann et al., 1996). A parallel control structure for process applications is then developed by re-parameterizing the controllers in the biologically derived architecture. The results from this work showed the superior performance and failure tolerance that can be achieved with the parallel control strategy compared to cascade control and single-input, single-output control techniques.

Parallel cascade control has shown impressive results in terms of disturbance rejection and this has encouraged researchers to focus in the area of developing a better controller tuning for the parallel cascade control. Lee et al. (2006) proposed an analytical method to tune the PID controllers for a parallel cascade control. The analytical tuning rules were derived from an internal model control (IMC) procedure and this proposed method took into the consideration of the interaction between the primary and secondary control loops. Rao et al. (2009) applied parallel cascade control onto a process with delay. They incorporated a delay compensator in the primary loop while the secondary loop controller was designed using IMC method. Significant improvement in the closed loop performances was obtained with the delay compensator over that of a conventional parallel cascade control system.

Yin et al. (2011) proposed a modified IMC tuning in cascade control. The controller tuning took into account both set-point tracking and disturbance re-

jection. As in a conventional cascade system, set-point tracking response and load disturbance response in the secondary loop possessed great influenced in the primary controller loop. With the implementation of two degrees of freedoms, the performance of the controllers is adjustable. In the work of Padhan and Majhi (2012a), a modified Smith predictor was used to address the process time delay. They found out that the proposed scheme produced better results compared to existing conventional parallel cascade control methods.

Padhan and Majhi (2012b) then proposed a new parallel cascade control scheme for unstable processes with time delay. They designed the secondary loop using an IMC tuning approach while the primary loop was designed based on a PID controller with lead/lag filter. The results presented by the authors showed improvement in the disturbance rejection performances. Raja and Ali (2015) developed a better version of cascade control for time delayed integrating process models. The proposed parallel cascade control structure has three controllers: a stabilizing (P) controller, a primary (PI) controller and secondary (PID) controller. They obtained a better performance in disturbance rejection compared to the previous work (Padhan and Majhi, 2012b).

Santosh and Chidambaram (2016) introduce a simple method to design parallel cascade controllers for open loop unstable processes. The tuning consider a proportional (P) controller for the innermost loop while a proportional-integral (PI) controller for the outermost loop. The results showed improvement for both servo and regulatory problems in comparison to Padhan and Majhi (2012a) work. Raja and Ali (2017) proposed a modified parallel cascade control structure (PCCS) with Smith predictor for open loop unstable and integrating process models. They used RouthHurwitz stability criterion and internal model control approach in their tuning approach. The results yields improved and robust closed-loop performance in first and second order integrating models plus time delay.

However, most of the literature focused on developing a parallel cascade control for stable/unstable first order plus dead time (FOPDT) model. Nandong and Zang (2014c) proposed a novel scheme named Multi-Scale Control (MSC) scheme. They incorporated this scheme into the tuning a PID controller and they discovered that this newly tuned formula was applicable for both FOPDT and even second order plus zero (SOPZ) model. The numerical study showed improved performance over an IMC approach for a parallel cascade process.

The basic idea of the MSC is to decompose a complex plant P into a sum of its basic modes, which are first- or second-order systems with real coefficients.

Through this decomposition, it is easier to design several sub-controllers where each is based on a specific mode than to design an overall controller directly. Additionally, the conventional controller design approach can be very difficult to apply especially towards a high-order system with complicated dynamics. The plant decomposition is represented as follows:

$$P(s) = m_0 + m_1 + m_2 + ... + m_n \tag{2.3}$$

where m_i, $i = 0, 1, 2,..., n$ indicates the basic modes. The outermost mode is the slowest mode in the system and is represented by m_0, meanwhile m_i, $i = 1, 2,..., n$ are known as the inner layer modes. The modes are arranged in the order of increasing speed of responses towards a manipulated variable changes.

The sub-controllers for all the individual plant decomposition are capable of enhancing the cooperation among the different modes. In this case, a two-layer MSC scheme assuming the plant system of the primary loop can be decomposed into a sum of two modes only. In Figure 8.1, K_1 denotes the sub-controllers for the innermost loop W, while the controller K_0 controls the outermost loop P.

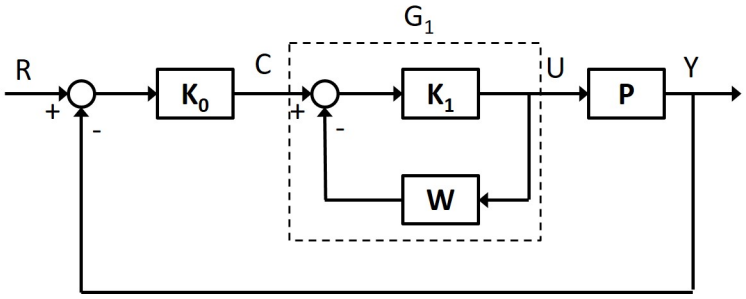

Figure 2.8: Block diagram of a two-layer MSC scheme.

In Figure 8.1, the closed-loop inner layer transfer function is expressed as follows:

$$G_1(s) = \frac{K_1(s)}{1 + K_1(s)W_1(s)} \tag{2.4}$$

where, the overall multi-scale controller is:

$$K_{msc}(s) = K_0(s)G_1(s) \tag{2.5}$$

The MSC scheme gives better performance when dealing with complicated process plants, especially process plants that is in high order. This is because MSC strategy is able to decompose a high order process plant into a low order

transfer function (i.e., not more than second order). This indirectly results in easier controller design and thus, a better performance and robustness of the controller tuning.

2.3.7 Research gaps

The following research gaps can be identified from the literature review:

a) System engineering study (optimal operations and robustness) remains inadequate in the water-gas shift reaction process with the incorporation of membrane reactor.

b) There is a lack of research in the consideration of process uncertainties into process optimization, especially in the scope of membrane technology − due to relatively new technology.

c) There is the need for robust controller tuning strategy in addressing large transport delay processes − specifically in WGSR-MR due to the length of the reactor.

In the first research gap, there have been a few researchers started to focus on the optimization of the WGSR membrane reactor. However, to date only single objective optimization (SOO) (i.e., maximization of conversion or yield) of the membrane reactor has been performed. It has been discussed that SOO approach lacks of practicality. Hence, the need of multi-objective optimization (MOO).

In addition, in a design stage of a process plant, it is very likely for the WGSR-MR design to have process uncertainties (i.e., exogenous or/and endogenous). With these uncertainties, there will be a caused-effect towards the optimization. Thus, care needs to be taken during process optimization. However, it is impossible to address all uncertainties for a process plant. Hence, there is the need of process control implementation to ensure the safety of the process plant. A good control scheme is crucial for safe and reliable operation of any chemical process. Most of the researchers focused on open-loop control of the membrane reactor. Single-input single-output (SISO) controller is still inadequate to effectively control a large transport delay process.

In this work:

a) To address the practicality of the optimal approach. A multi-objective optimization that incorporates two objectives function:

i) steady-state economic performance − net present value (NPV)

ii) dynamic controllability − v-gap metric

The reason of adopting these two objectives function is that, if the optimization is done without incorporating the controllability, there is a possibility of that the design will be difficult to control and operate. A MOO formulation using the weighted sum method can be employed to optimize these two objectives function simultaneously. This is because of the computationally effective and easy implementation of this method. Equal percentage of weight is assigned denoting that the equal importance of the two performance criteria.

b) To integrate uncertainties in the process optimization. Here, only exogenous uncertainties are taken into account:

i) hydrogen selling cost

ii) electricity cost

Electricity is being considered due to large usage in the whole process. Changes in the cost of electricity might pose a large threat in the operational expenditure. Since the late 80s, the electricity industry has sustained important adjustments worldwide (Dyner et al., 2003). As for the hydrogen selling cost, it is included due to the fluctuation of market demand. According to U.S. Department of Energy's standard model for small-scale distributed hydrogen production, the price of hydrogen differs due to various different productions of hydrogen (Steward et al., 2009). Markov Chain Monte Carlo (MCMC) algorithm is employed to generate the future probability values of these two uncertainties. As this method is relatively simple, computationally effective and commonly used in simulating a small number of uncertainties.

c) To develop a robust control strategy for large transport delay process specifically in WGSR-MR. To address large transport delay, cascade control is commonly employed. There are two categories of cascade control:

i) series cascade control

ii) parallel cascade control

Note that, to date only two/double-loop cascade control has been developed to address this problem. However, the robustness of the control strategy based on a double-loop cascade control towards a large processing delay is still ineffective. Therefore, this study aims to develop an effective methodology using parallel cascade control. It should be noted that, an effective and robust control for the optimized reactor system (as an overall) is a crucial factor to ensure a safe and reliable operation of the system.

2.4 Summary

In summary:

- To date, only single objective optimization (SOO) approach has been applied in the optimization of membrane reactor performance (i.e., maximized reactant conversion or hydrogen production yield). The idea of single objective optimization is impractical in reality.

- Uncertainties are bound to exist at any stages of process development. To date, there is still lack of works related to the incorporation of uncertainties into process optimization especially in WGSR-MR.

- In control related to WGSR-MR, only single-input single-output (SISO) controller strategy has been implemented to address the temperature control of the membrane reactor. WGSR-MR is subjected to large transport delay due to the length of the membrane reactor. Currently, only a two/double-loop cascade control has been developed to address this problem. However, this strategy is still ineffective.

- To address the impracticality of previous optimization approach, a multi-objective optimization (MOO) is adopted to optimize the WGSR-MR. Two objectives can be simultaneously considered in the optimization problem formulation. There are steady-state economic (represented by net present value) and dynamic controllability (represented by v-gap metric). This is a novel optimization approach as there has been no work mentioned about the MOO approach in the optimization of WGSR-MR. The main characteristic of this approach is to find the trade-off in economic performance without sacrificing the dynamic performance of the WGSR-MR.

- To address the uncertainties, Markov Chain Monte Carlo algorithm can be used to calculate the likelihood values of the uncertainties.
- To address the problems related to the control of large transport delay, a triple-loop parallel cascade control can be developed. Triple-loop parallel cascade control can be more robust and effective compared to double-loop parallel cascade control. As the addition of an inner loop, effectively suppressed the disturbance before it significantly upset the primary/master controller loop. Furthermore, the development of a triple-loop parallel cascade control has yet been explored.
- To achieve the aforementioned goals successfully, a fundamental knowledge of water-gas shift reaction membrane reactor is required. These knowledge aids in the modelling, optimization and control of this process system. Thus, an in-depth fundamental of WGSR-MR will be presented in the next chapter.

Chapter 3

Fundamentals of WGSR-MR

3.1 Overview

Fundamental knowledge of water-gas shift reaction membrane reactor (WGSR-MR) served as a foundation in this present study. This chapter presents an in-depth understanding of water-gas shift reaction and membrane-assisted reactors. The features of water-gas shift reaction to be presented in the chapter include:

a) Reaction mechanisms of WGSR − Langmuir-Hinshelwood and Regenerative mechanisms.

b) Reaction kinetics of WGSR − microkinetic and macrokinetic mechanisms.

c) Present catalysts in WGSR − low-temperature and high-temperature catalysts.

d) Present membranes in WGSR − microporous and dense metal membranes.

The core detailed of membrane-assisted reactors presented are:

a) Types of membrane-assisted reactors − packed-bed and multi-tube membrane reactors.

b) Fundamental state models − one-dimensional, two-dimensional, and three-dimensional state models.

c) Reactor models − heterogeneous and homogeneous reactor models.

The information about this chapter can serve as future references and a guideline to be used in the later section of the present study.

3.2 Reaction Mechanisms of WGSR

There are seven consecutive steps describing the rate of reaction for all heterogeneous reactions that involved a catalyst (Froment and Bischoff, 1979). These rates of reaction may include the effects of transport process rates as well as intrinsic reaction rates. A mechanism of an irreversible reaction from a reactant to form a product is illustrated in Figure 3.1 − adapted from Froment and Bischoff (1979).

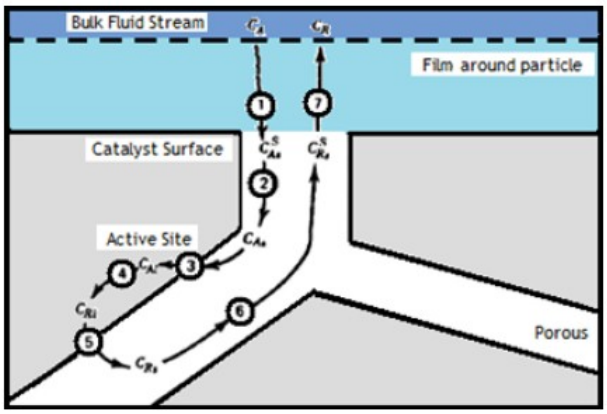

Figure 3.1: Steps involved in reactions on solid catalyst.

In the mechanisms presented in Figure 3.1, there is a total of seven reaction steps (Bond, 1987):

1. The diffusion of reactants from the bulk fluid onto catalyst surface.
2. The diffusion of the reactant from catalyst surface to the active site of the catalyst pore.
3. Adsorption of reactant on the active site of the catalyst pore.
4. The reactant will undergo chemical changes.
5. Product is formed and desorption of the product from the active catalyst pore.
6. Diffusion of the product to the catalyst surface.
7. Diffusion of product from catalyst surface to bulk fluid.

Although there are only four species (i.e., CO, H_2O, CO_2 and H_2) in WGSR, researchers are yet to come to a full agreement concerning the reaction mechanism (Mendes et al., 2010). The two most commonly discussed mechanisms are Langmuir-Hinshelwood (LH) and Regenerative (Redox) mechanisms. Few researchers such as Rhodes and his co-workers Rhodes et al. (1995) suggested that low-temperature WGSR favours Langmuir-Hinshelwood mechanism while high-temperature WGSR favours Redox mechanism.

An example of a LH mechanism for WGSR is expressed in Equations 3.1 to 3.5. This mechanism considers steps that involved:

a) The adsorption of reactants (i.e., CO and H_2O) onto the catalyst surface to form intermediate.

b) Instantaneous chemical reaction of reactants to products, and the desorption of the products.

Note that, the slowest step is the rate determining step (Equation 3.3) (Ayastuy et al., 2005).

$$CO_{(g)} + Z \rightleftharpoons CO_{(ads)} - Z \tag{3.1}$$

$$H_2O_{(g)} + Z \rightleftharpoons H_2O_{(ads)} - Z \tag{3.2}$$

$$CO_{(ads)} - Z + H_2O_{(ads)} - Z \rightleftharpoons CO_{2(ads)} - Z + H_{2(ads)} - Z \tag{3.3}$$

$$CO_{2(ads)} - Z \rightleftharpoons CO_{2(g)} + Z \tag{3.4}$$

$$H_{2(ads)} - Z \rightleftharpoons H_{2(g)} + Z \tag{3.5}$$

The equation rate for this LH mechanism is given as follows:

$$-r_{CO} = \frac{k\left(P_{CO}P_{H_2O} - \frac{P_{CO_2}P_{H_2}}{K_p}\right)}{\left(1 + K_{CO}P_{CO} + K_{H_2O}P_{H_2O} + K_{CO_2}P_{CO_2} + K_{H_2}P_{H2}\right)^2} \tag{3.6}$$

where k is the rate of forward reaction, K_p is the equilibrium constant, K_i is the equilibrium adsorption constant for species i and P_i is the corresponding partial pressure.

As long as there is a cyclic reduction-oxidation reactions occurs on the catalyst surface, it is considered as Redox mechanism (Rhodes et al., 1995). In this mechanism, water (H_2O) is reduced on the catalyst surface to produce hydrogen while the carbon monoxide (CO) is oxidized (Choi and Stenger, 2003). This mechanism is represented by Equations 3.7 - 3.8

$$H_2O + s \rightleftharpoons H_2 + O.s \tag{3.7}$$

$$CO + O.s \rightleftharpoons CO_2 + s \tag{3.8}$$

If the rate determining steps is Equation 3.8, then the rate equation derived from this model is Ayastuy et al. (2005):

$$-r_{CO} = \frac{k\left(P_{H_2O} - \frac{P_{CO_2}P_{H_2}}{P_{CO}K_p}\right)}{1 + \frac{K_{CO_2}P_{CO_2}}{P_{CO}}} \tag{3.9}$$

All the parameters from each equation can be obtained using the rate data of CO obtained experimentally. Hence, for simplification, an empirical Power-Law (PL) rate equation (Equation 3.10) is used.

3.3 Reaction Kinetics of WGSR

The kinetic models are often developed as to provide the simplest way to represent a chemical reaction for engineers to design an appropriate size of the reactor involved. Fundamentally, the kinetic expressions (models) can be relegated into two main categories:

a) Microkinetic models − based on the detailed information about all the elementary (intermediate) steps that comprise an entire chemical reaction. This model explores the detailed mechanisms that occur during the course of a reaction.

b) Macrokinetic models − predicated on authentic experimental data and are customarily represented in terms of Arrhenius or Power-law expression.

A study by Fishtik and Datta (2002) showed that the elementary steps comprising the WGSR conducted on the Cu (111) catalyst and ascertained that there is a total of 13 elementary steps involved. From these 13 elementary steps, a total of 17 possible reaction routes has been proposed for the WGSR. Interestingly,

there are only three reaction routes that are deemed to govern the entire reaction and this finding led them to the identification of three ascendant elementary steps in the reaction. This study was then further elongated by Callaghan et al. (2003); they discovered that there is a total of 70 possible reaction routes predicated based on their newly integrated fourth elementary steps onto the previously mentioned 13 elementary steps. Interestingly, they too managed to stream down these four steps into three elementary steps based on the highest likelihood of a reaction to occur. However, these three elementary steps are different from those previously proposed steps by Fishtik and Datta (2002). Callaghan et al. (2003) had established a latest rate of reaction based on their findings. As both microkinetic studies proposed different rates of reaction on the same Cu (111) catalyst, this has led to the perplexity and questions of the precision of the rate of reaction by these different microkinetic models.

Macrokinetic models provide more facile and computationally lighter way to predict the rate of a reaction without the detailed erudition of the complex elementary steps involved. Most of the simulation and control studies of WGSR are typically used on this type of model. Apart from the power law type of kinetic expression, other complicated kinetic expressions have additionally been developed to represent the WGSR kinetic. For example, Podolski and Kim (1974) made a comprehensive study of the existing power law models and concluded through their experimental data that it is paramount to produce a more extensive model − addition temperature and pressure dependent variables. In Newsome (1980), the author developed a model that is capable of prognosticating the reaction rate in the presence of H_2S (hydrogen sulfide) gas. While in Park et al. (2009), the authors carried out a high-temperature reaction on diverse catalyst compositions and derived two rate equations. As for Keiski et al. (1996), they provided an expression for the high-temperature shift reaction for some specific types of catalyst. Note that, most of the available catalysts have macrokinetic models to represent their own rate of reaction. However, one of the disadvantages of the macrokinetic models is that they are restricted to specific categorical catalysts under limited operating conditions.

Both of these macrokinetic and microkinetic models are widely used in process simulation to represent the kinetics of the WGSR. However, presently there has been no rigorous comparison being done between microkinetic and macroeconomic models based on the same type of catalyst pellet. This comparison can establish a better understanding on which model has better accuracy in terms of predicting the trajectory of the catalyst behaviour. In the present study, the pre-

cision of these both kinetic models is compared and analyzed in the next chapter. This is to provide a basic knowledge for a better decision making in choosing a suitable model for the modelling of WGSR-MR in this study.

3.4 Catalysts in WGSR

Catalyst development in WGSR can be distinctively divided into two categories: (1) high temperature and (2) low temperature catalyst. Note that WGSR thermodynamically favours lower temperature, but kinetically favours higher temperature. For a lower temperature WGSR which is roughly around 200-350°C, the most suitable type of catalyst is copper-based catalysts. Copper-based catalysts are much durable at lower temperature and has better catalytic activity comparable to others. The copper-based catalysts are able to achieve exit CO concentration of 0.1 to 0.3%. Hence, copper-based catalysts are normally known as Low Temperature (LT) shift catalysts. Meanwhile, the Iron-based catalysts are known as High Temperature (HT) shift catalysts due to its operating temperature in the range of 400 - 500°C.

Both high-temperature and low-temperature catalysts are available commercially. Different compositions of the catalyst yield different characteristics of the specific catalysts. Therefore, active research is still carried out to develop better catalysts i.e., better conversion, high stability and sustainability of the catalysts for WGSR.

3.4.1 High-temperature shift catalysts

High-temperature (HT) catalyst are commonly known as *ferrochrome* (Fe) catalysts because most of HT catalysts are iron-based catalysts (Rhodes et al., 1995). The earliest industrial available heterogeneous catalysts for WGSR are the Fe-based catalysts. The Fe-based catalysts are usually accompanied by Cr oxide (Cr_2O_3). This is because Cr_2O_3 is a structural promoter, it has the ability to prevent the occurrences of sintering and loss of Fe oxide surface area. Thus, leading to the improvement in the catalysts stability and activity of Fe catalysts (Rase, 2000). However, the addition of Cr oxide (Cr_2O_3) will cause environmental and health problems due to Cr hexavalent characteristic (Smith et al., 2010).

The different catalyst promoter will contribute to interesting effect on the chemical and structural properties of the catalysts. This has sparked up the interest among researchers to research on the catalyst promoter for iron-based

catalysts. Among the other researchers, Topsøe and Boudart (1973) and Gonzalez et al. (1986) suggested that with the addition of other cations as the metal promoters might improve the catalyst activity. As metal promoted catalysts formed a new metal lattice of that had different electronic properties compared to the unpromoted catalysts (Mendes et al., 2010). In the work of Topsøe and Boudart (1973) and Gonzalez et al. (1986), it was found that Cu as the metal promoters into Fe-Cr catalyst had the ability to increase in selectivity and catalytic activity. Increment in catalytic activity results in a reduction of energy costs. Hence this discovery has led in lowering the operating costs for WGSR.

Rhodes et al. (2002) studied the metal promotion for $FeCr$ catalysts. They tested few metal promoters such as copper (Cu), mercury (Hg), silver (Ag), boron (B), barium (Ba) and lead (Pb) onto $FeCr$ catalysts. They observed that through the addition of the few metals (i.e. Hg, Ag, or Ba) coupled with Cu metal showed higher catalytic activity at temperatures of 350 and 440°C. More recently, Natesakhawat et al. (2006) studied the effect of adding another metal promoter such as manganese-oxide (MnO), copper-oxide (CuO), cobalt-oxide (CoO) and zinc-oxide (ZnO) on the Fe-Cr catalysts. They uncovered that Co- and Cu oxides showed an optimistic increase in the catalytic activity.

Costa et al. (2002) used thorium (Th) instead of Cr in a Cu-doped Fe-based catalysts for the HT WGS reactor. Thorium possessed the attribute in an increasing surface area which resulted in high activity and this made thorium a potentially promising catalyst to replace the conventional $FeCr$. However, the activity rates are still lower than Cr metal promoters. Various studies have shown that the promotion by Cu, Co and Th on the Fe catalyst is promising. Due to potential environmental and health problems of Cr metal as mentioned above, plenty of efforts are being made in the development of new Cr-free metal promoters. Unfortunately, the replacement of chromium promoters by other less toxic component, so far, has not been commercially successful.

3.4.2 Low-temperature shift catalysts

Cu-based catalysts are conventionally categorized as low-temperature (LT) shift catalysts. Several Cu formulations have been utilized in the LT-WGSR (Lloyd et al., 1996). Extensive research has been conducted on LT catalysts as in the case of HT catalyst where most of the works are on the amendment of reduced sintering, catalytic activity, and stability of the LT catalysts. As for the thermal stability, however, is still poor compared to that of HT catalyst. One of the

other drawbacks is that Cu were vulnerable to thermal sintering. This is due to surface migration resulted in a reduction in catalysts lifespan. Researchers had made major advances in achieving enhanced stability in the Cu catalysts exhaustive the prelude of additive components that act as structural spacers and hence decrementing the aggregation of Cu crystallites. Even so, the operating temperature of Cu-based catalysts are still restricted to below 300°C (Twigg and Spencer, 2001).

The most widely used metal promoters for LT WGS catalyst are aluminium oxide (AlO), copper oxide (CuO), and zinc oxide (ZnO). Apart from being structural promoters, ZnO and AlO are additionally known for their chemical promoters, albeit this point remains controversial. Yurieva and Minyukova (1985) and Kanai et al. (1994) observed an increment in the catalytic activity when ZnO is integrated to the Cu-predicated catalyst. This is because ZnO has high synergetic effects that accountable for better covalence between the different oxidation states of Cu in the metal lattice. Through the work of Ginés et al. (1995), the WGS catalyst activity is ameliorated by incorporating Al_2O_3 into the binary Cu/ZnO to become ternary $Cu/ZnO/Al_2O_3$ mixture. It revealed that the alumina is a factor contributing to the formation of hydrotalcite phase, which leads to an improvement in catalyst performance.

In order to further enhance the catalytic activity of Cu-based catalyst, a reduction treatment at temperatures between 180 and 260°C has to be performed. This reduction treatment is customarily performed before the startup of the LT-WGS reactor (Lee, 2006). During this process, temperature controller of the catalyst bed has to be employed due to the possibility of catalyst degeneration and exothermic nature of the reaction(s) involved. To contravene the temperature complication, several researchers such as Gottschalk and Hutchings (1989),Yeragi et al. (2006), and Tanaka et al. (2003) used Cu-Mn oxide as it exhibits excellent activity and heat stability as compared to the conventional Cu-predicated materials.

3.4.3 Recent advancement of WGSR catalysts

Even though Fe-Cr catalyst formulations have the advantages in term of being cheap and stable, there is a major drawback of these catalysts which is the fact that this catalyst formulation have the potential of causing health and environmental issues. As for Cu-based formulations, although these catalysts can only be operated within a limited temperature range due to sintering issue. They are

Table 3.1: Comparison performance of catalysts reported for WGSR

	Fe-Cr	*Cu-ZnO-*Al_2O_3	*Co*	*Au*	*Pt*
Temperature	320-450°C; HT	<200°C; LT	> 350°C; HT	<320°C; HT	200-500°C; LT/HT
Deactivation	Minimal	No deactivation for 2 - 4 years	Prone to sintering and support over-reduction		Negligible for 800 hours
Activity level	High	Higher than *Fe-CrO*	Higher than *Fe-Cr*	High at LT; more active than *Pt*	High with absence of methanation
Pre-treatment	Controlled reduction of activation		-		-
Promoters employed	*Cu*, *Co*, *Mn*, *Zn*, *B*, *Ba*, *Pb*, *Hg* and *Ag*	*MnO* for better structural and chemical stability	Pot carbonate		-
New variants	*Cr* free with *Al*, *Mn*, *Ga*, *Cu*, *Co*	*Cu-*CeO_2		Nano *Au* (5 nm) on TiO_2, α-Fe_2O_3, Co_3O_4 or CeO_2	*Pt-*Al_2O_3 and *Pt-*CeO_2; monolithic supports
Special advantages	Commercially tried for coal, naphtha and natural gas based *CO*		Provides highly pure H_2	Formulated by M/s. John Mathey	Significant reactor volume reduction
Disadvantages	Hexavalent *Cr* leaching	Lower thermal stability; and structural sensitivity	Increased methane and decreased H_2 yield	Formation of surface carbonates/formates	Formate formation

susceptible to poisoning, although they still possessed good activity with even below temperature of 200°C (Twigg and Spencer, 2001). However, one of the disadvantages of Cu-based materials are the need for activation before the operation and this process usually takes long time. Hence, many researchers have focused on introducing a new catalyst formulation which has higher catalytic activity, stability towards poisoning, improved stability, fast startup or even better with no requirement for exceptional pre-treatments (Ghenciu, 2002).

Presently, a sulfur-tolerant Co-predicated catalyst has been found by few researchers (Farrauto et al., 2003; Hutchings et al., 1992; Lund, 1996). Co-predicated catalyst has low activity at a temperature between 200 and 300°C which makes it quite useless for LT application (Farrauto et al., 2003). However, this catalyst material shows better catalytic activity than the standard commercial $FeCr$-oxide HT WGS catalyst (Hutchings et al., 1992). However, there is still one major disadvantage of this catalyst utility as it caused an increment in by-product methane production while decreasing the production of H_2.

Recently, two advance materials, Au- and Pt-based catalysts have gained much attention of the researchers as they are described to have surmounted many limitations. The Au- and Pt-based catalysts are observed to have high catalytic activity and stability due to its nano-sized. This characteristic has made these two materials favourable candidates as a metal promoter to other catalysts. Despite the poor chemisorption ability toward reactant molecules such as O_2 and H_2 and its low catalytic behaviour of Au, the authors of Haruta et al. (1989) still researched on Au catalyst. They, however, observed opposite trend as abovementioned, they observed high catalytic activity for the CO oxidation reaction utilizing catalysts containing Au particles more minuscule than 5 nm, deposited on different metal oxides (e.g. TiO_2, α-Fe_2O_3, Co_3O_4). Due to the more minute particle size of Au, the metallic character is reduced. Hence the mobility of surface atoms reduced, resulting in more atoms come into contact with the support (Bond and Thompson, 1999). As for Pt-based catalyst, detected activity, and stability are higher compared to Au-predicated materials. Lund (1996) observed higher durability, activity, and absence of methanation activity over a range of temperatures 200-500°C. Furthermore, the authors of Jacobs et al. (2003) too observed that this catalyst was highly durable with no activity decay for more than 800 hours over a wide range of temperatures at high space velocities.

Even though Au and Pt based catalysts show promising catalytic activity, the cost of purchasing these catalysts is high. Table 3.1 − adapted from Babita et al. (2011) illustrates the comparative performance between reported catalysts

for the WGSR in a concise manner. As the main purpose of this research work is not to develop new types of catalysts for the WGSR. Thus, a commercial industrial catalyst is used in this present study. Fe-based catalyst is considered due to its cheaper price compared to Au and Pt based catalysts. Although the performance of Fe-based catalyst is not on par with Au and Pt-based catalysts, this problem can be solved by doping the ternary material onto Fe-Cr-based shift catalyst. The effect in the doping of ternary material has been proven by Qi and Flytzani-Stephanopoulos (2004).

Nevertheless, in this study, the PL rate of reaction is use because the design and optimization of an industrial reactor requires high computational effort which can be facilitated by the used of this simpler rate equation (San Shwe et al., 2009). In addition, the main purpose of this research work is not to determine the mechanism of WGSR, therefore PL rate of reaction is used for practical design and simulation study. Together with the chosen Fe-Cr-based shift catalyst, the power law of this catalyst is as follows:

$$-r_{CO} = kP_{CO}^{a}P_{H_2O}^{b}P_{CO_2}^{c}P_{H_2}^{d}(1-\beta) \tag{3.10}$$

The parameters a, b, c, d, and the kinetic rate constants for this power-law kinetics are as follows (San Shwe et al., 2009), for temperature range 450°C - 600 °C.

$$\begin{aligned} a &= 0.9 \pm 0.041 \\ b &= 0.31 \pm 0.056 \\ c &= -0.156 \pm 0.078 \\ d &= -0.05 \pm 0.006 \end{aligned} \tag{3.11}$$

$$k = 10^{0.659 \pm 0.0125} \exp\left(\frac{-88 \pm 2.18}{RT}\right) \tag{3.12}$$

3.5 Membranes in WGSR

Membranes can be arranged into four classes:

a) Polymeric membranes.

b) Porous membranes.

c) Dense metal membranes.

d) Proton conducting membranes.

The determination of types of membrane to be utilized as a part of membrane reactor relies on upon a couple of criteria, for example, partition selectivity, film lifetime, physical and substance organizations at certain working conditions and in particular, the cost.

3.5.1 Microporous membranes

Microporous membrane refers to a type of membrane with pore diameters smaller than 2 nm. There are two types of microporous membrane which are crystalline (zeolites and metal-organic framework (MOF)) and amorphous (silica and carbon). Zeolites are microporous crystalline aluminosilicates with uniform molecular pore size (Gallucci et al., 2013). This well-defined pore size contributes to the unique properties and chemical stability of zeolite. Extensive studies are still ongoing in order to further improve zeolites membrane, especially in terms of hydrogen permeation and selectivity. Lai and Gavalas (2000) developed a ZSM-5 zeolite membrane which gave H_2 permeance of 1.2×10^{-7} mol m^{-2} s^{-1} Pa^{-1}. Meanwhile Welk et al. (2004) used the same membrane and observed that the H_2 purity increased from 76% to more than 98% in a single pass module. Recently, Zhang et al. (2012) developed a MFI zeolite membrane and has noted a H_2 permeance of 2.82×10^{-7} mol m^{-2} s^{-1} Pa^{-1}.

As for the structure of metal-organic framework (MOF), it is a microporous crystalline hybrid materials that consist of cationic oxide/metal cation clusters that are linked by organic molecules. Due to the interesting tailorability of pore size combined with tunable sorption behaviour, MOF type of membrane said to have the possibilities to solve the industrial problems related to long-term stability, regeneration and ease of maintenance (Gascon and Kapteijn, 2010). MOF membranes are less energy intensive to synthesize and are mechanically less stiff and brittle compared to zeolites catalysts (Tan and Cheetham, 2011; Shah et al., 2012). Furthermore, a subfamily of MOF membranes called the zeolitic imidazolate frameworks (ZIFs) are expected to be promising candidates for gas separation, thanks to their high thermal and chemical stabilities in combination with their small pores (Shah et al., 2012). However, some studies showed otherwise. Li et al. (2010) conducted test on ZIF-7 membrane and obtained permeance of 4.55×10^{-8} mol m^{-2} s^{-1} Pa^{-1} which is lower than the zeolite membrane permeance. Nevertheless, it was discovered by McCarthy et al. (2010) that ZIF-8 membrane showed H_2 permeance of 1.73×10^{-7} mol m^{-2} s^{-1} Pa^{-1}.

One of the most important representatives of amorphous microporous membranes is silica membrane, as it is easily prepared as super or even ultra microporous thin layers compared to other metal oxides. Even so, silica membrane has a huge disadvantage on preparation of the membranes. The preparation of a silica membrane requires substantial capital investment and well controlled conditions and this has made their industrial applications become less attractive. On the other hand, carbon membranes show a bright future for hydrogen separation due to their excellent separation and resistance against thermal and chemical degradations (Koros and Mahajan, 2000; Ismail and David, 2001). Owing to their small pores, carbon molecular sieve (CMS) membranes possess high selectivity for gas mixture separation especially those that contain small gas species. According to Hosseini and Chung (2009), they reported that the carbon membranes H_2 permeability is 7.98 - 23.94 $\times$ 10^{-6} cm^3 cm cm^{-2} s^{-1} Pa^{-1}. Similarly, Grainger and Hägg (2007) reported that a CMS permeability to be 1.47 $\times$ 10^{-4} cm^3 cm cm^{-2} s^{-1} Pa^{-1}. Because of its high permeability, Media and Process Technology, Inc has been commercializing CSM composite membranes (Sedigh et al. (2000); Abdollahi et al. (2010)).

Bear in mind that, different types of membrane materials exhibit distinct characteristic, operating conditions, disadvantages and installation costs. Table 3.2 − adapted from Gallucci et al. (2013) shows a comparison of membrane types for hydrogen separation. It can be seen that some membranes offer better characteristics than the others, especially carbon type of membranes; however, each has its own limitations.

3.5.2 Dense metal membranes

Dense metal membranes are commonly used to obtain high purity hydrogen. The standard mechanism of hydrogen permeation through the dense metal membranes is illustrated in Figure 3.2 − adapted from Yun and Oyama (2011). This mechanism is known to follow a solution diffusion mechanism. As such, the gas which is at the high pressure side of the membrane dissolved and diffused through the membrane towards the low pressure side. The separation, however, is based on the differences in the diffusion rates of the mixture components in the membrane and the sorption characteristics (Rautenbach and Albrecht, 1989). The solution diffusion model can also be expressed mathematically in terms of Henrys law (solubility) and Ficks law (diffusion) which then leads to the flux (J) of the permeating species (Baker, 2001):

Table 3.2: Comparison of membrane types for hydrogen separation

Membrane type	**Polymeric**	**Microporous ceramic**	**Porous carbon**	**Dense metallic**	**Proton conducting dense ceramic**
Materials	Polymers: polyimide, cellulose acetate, polysulfone, etc.	Silica, alumina, zirconia, titania, zeolites, metal-organic frameworks (MOF)	Carbon	Palladium alloys	Perovskites (mainly $SrCeO_{3-\delta}$)
Temperature (°C)	<100	200-600	500-900	300-700	600-900
H_2 selectivity	Low	5-139	4-20	>1000	>1000
H_2 flux (10^{-3} mol m^{-2} s^{-1}) at $\Delta P = 1$ bar	Low	60-300	10-200	60-300	6-80
Transport mechanism	Solution diffusion	Molecular sieving	Surface diffusion, molecular sieving	Solution diffusion	Solution diffusion
Stability issues	Swelling, compaction, mechanical strength	Stability in H_2O	Brittle, oxidizing	Phase transition (causes embrittlement)	Stability in CO_2
Poisoning issues	HCl, SO_x, CO		Strong adsorbing vapors, organics	H_2S, HCl, CO	H_2S
Cost	Low	Low	Low	Moderate	Low

$$J = \frac{D_f.S_g.\Delta p}{\delta} = \frac{Pe_{mem}.\Delta p}{\delta} \tag{3.13}$$

where D_f is the diffusion coefficient of the species in the membrane (kinetic term), S_g is the gas solubility (a thermodynamic term), Δp is the pressure difference between the high and low pressure side, δ is the membrane thickness, and Pe_{mem} is the so-called membrane permeability coefficient.

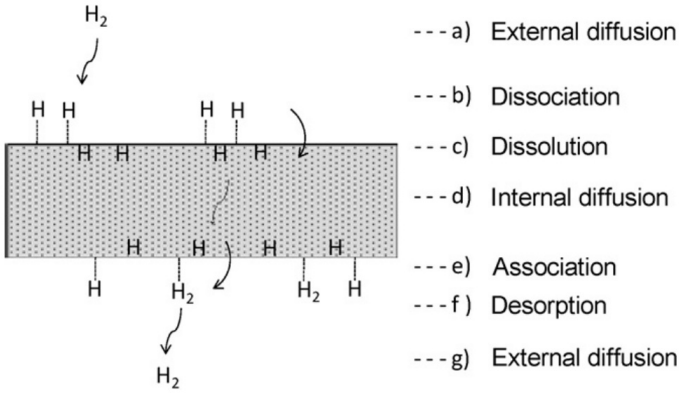

Figure 3.2: Schematic diagram of hydrogen permeation mechanism.

In the early of the 1970s, palladium (Pd) and Pd alloy were one of the early types of dense metal materials for hydrogen production (Holleck, 1970; Grashoff et al., 1983; Buxbaum, 1993). However, pure Pd membranes are not famous due to its association with the hydrogen embrittlement phenomenon. Severe lattice strains are observed, which in this case cause the Pd membrane becoming brittle when the operating temperature is below 300°C and a pressure of below 2MPa (Hsieh, 1991).

Another main problem is that these membranes are susceptible to experiencing the Pd surface poisoning which can become significant especially for thin metal membranes, by H_2O (Li et al., 2000), carbon monoxide (Amandusson et al., 2000), sulfur compounds (Edlund and Pledger, 1994), chlorine, carbon, etc. To avert the surface poisoning and hydrogen embrittlement as well as to reducing membrane cost, Pd can be grinded into fine grains that can be used in nanometer sized (Pacheco Tanaka et al., 2006) or it can be alloyed with other metallic elements such as Ag, Cu, Fe, Ni and Pt (Bryden and Ying, 2002; Uemiya et al., 2007; Qiao et al., 2010).

Interestingly, it has been discovered that there is a group of metals traditionally known as refractory metals such as vanadium (V), niobium (Nb) and tantalum (Ta), which at lower temperatures, have higher permeability compared

to palladium. Furthermore, these metals have better tolerance towards high temperature and are much cheaper. However, by using only these pure metals to produce membrane would only result in poor quality of membrane (high embrittlement). Nevertheless, by alloying these metals onto palladium forming metal-metal matrix membranes, the surface barriers are removed (non-embrittlement) and hydrogen permeation follows the trend shown in Figure 3.3 – adapted from Basile et al. (2008).

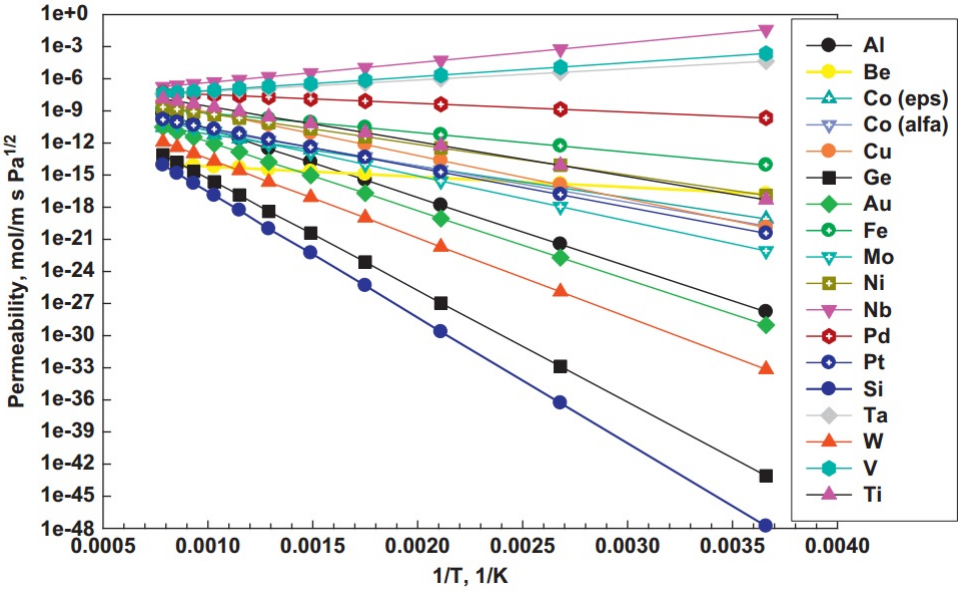

Figure 3.3: Hydrogen permeability through several metals alloy.

In this study, a $Pd - Ag$ membrane is used to simulate the WGSR due to the fact that this membrane has high affinity in separating and strong capability in producing pure hydrogen (Mendes et al., 2010). Through application of the Sieverts law, the hydrogen flux of this membrane is expressed as Mendes et al. (2010):

$$J_{H_2} = \frac{Pe_{mem}}{\delta}\left[\left(p_{H_2}^{retentate}\right)^n - \left(p_{H_2}^{permeate}\right)^n\right] \tag{3.14}$$

where $p_{H_2}^{retentate}$ stands for retentate hydrogen partial pressure, $p_{H_2}^{permeate}$ for permeate hydrogen partial pressure, δ stands for membrane thickness and $n = 0.5$. The relation of the permeability with the temperature is described by the Arrhenius law, as shown in Equation 3.15:

$$Pe = Pe^0 exp\left(\frac{-E_a}{RT}\right) \tag{3.15}$$

where E_a represents the activation energy and Pe^0 represents the pre-exponential factor. The hydrogen flux through the membrane increases when the thickness decreases. The same tendency is obtained with the increase in temperature, because the process is thermally activated.

3.6 Membrane-Assisted Reactors for WGSR

The author Gryaznov et al. (1970) was the first to propose the application of membrane reactors for dehydrogenation reactions. He discovered the removal of hydrogen using a thick membrane on a reversible reaction. Through the removal of the hydrogen, he too discovered the shift of the equilibrium reaction towards the product. With this discovery, researchers then worked towards developing different types of membrane reactors for hydrogen production. There are several types of membrane geometries such as tubular (i.e., capillaries, tubes and hollow fibers), planar, spiral wound, and plate and frame. The most commonly used geometries for gas separation are tubular and planer. Tubular membranes are usually used for medium to large-industrial scale while planar membranes are often used in laboratory studies. Tubular membranes are the most preferred option due to their larger surface area to volume ratio which induced in higher permeation.

3.6.1 Packed-bed membrane reactor (PBMR)

The packed-bed membrane reactor configuration is the first and the most studied configurations for hydrogen production. This is because the geometry of this reactor results in reduction in complication of complex fluid dynamics as compared to fluidized bed. Furthermore, the majority of the former work has been carried out in packed-bed membrane reactors (PBMR) due to ease in obtaining fabricated materials commercially.

There are two configurations for the tubular packed bed membrane reactor:

a) Catalyst pellets packed in membrane tube (Figure 3.4 − adapted from Gallucci et al. (2013)).

b) Catalyst pellets packed in shell of the reactor (Figure 3.5 − adapted from Gallucci et al. (2013)).

Packed bed reactor configuration has been adopted in many hydrogen production process. Gallucci et al. (2006) and Matsumura and Tong (2008), proposed

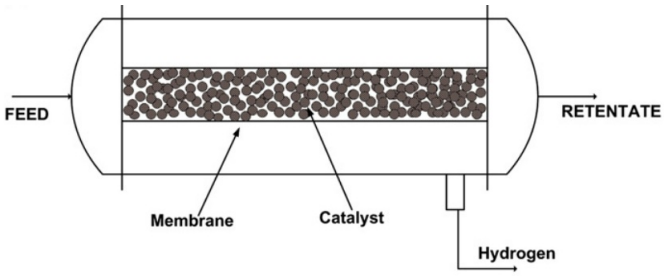

Figure 3.4: MR catalyst in tube configuration.

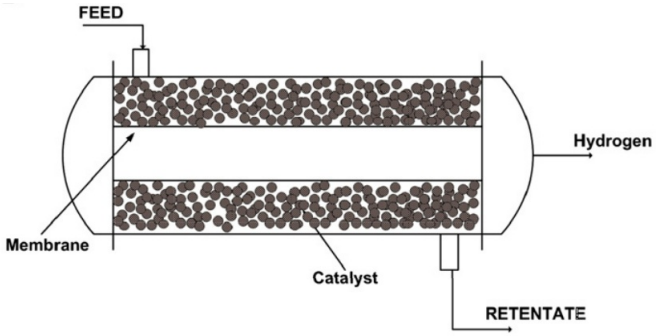

Figure 3.5: MR catalyst in shell configuration.

this reactor configuration into methane-steam reforming for hydrogen production. They discovered that membrane reactor offers a better conversion as compared to traditional shirt reactors. Other authors such as Kikuchi et al. (2003) and Tosti et al. (2009) used this membrane reactor configuration for their studies of alcohol reforming in hydrogen production.

To increase the hydrogen percentage of recovery, first an increase in membrane surface area is required. In order to increase the membrane area without increasing the volume of the reactor, Buxbaum (2002), has patented an example of multi-tube configuration membrane housing − see Figure 3.6 − adapted from Gallucci et al. (2013). This configuration is introduced to increase the ratio of membrane area to the volume of the packed-bed reactor. This configuration is being tested by the authors Tosti et al. (2008) in an experiment of ethanol steam reforming. They discovered that with this configuration, almost complete recovery of the hydrogen is obtained.

Here, in this study a packed bed membrane reactor configuration is used as it more stable and commonly used in process industries. In this study, this configuration adapted the multi-tubular tube membrane reactor geometry due to its high percentage of recovery and space saving concepts.

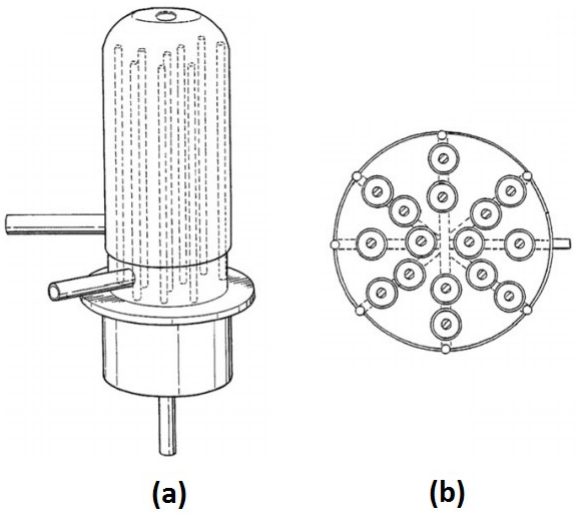

Figure 3.6: Membrane configurations (a) membrane housing and (b) multi-tube membrane reactor.

3.7 Reactor Modelling for PBMR in WGSR

The approaches to reactor modelling of the WGSR can be categorized into 6 different types: (1) fundamental state model (i.e., one-dimensional - Model 1A, 1B and 1C, two-dimensional - Model 2A, 2B and 2C, and three-dimensional - Model 3A, 3B and 3C) and (2) different reactor modelling approaches (i.e., homogeneous modelling approaches - Model 1A, 2A and 3A, homogeneous modelling approaches with transfer limitation - Model 1B, 2B and 3B, and heterogeneous modelling approaches - Model 1C, 2C and 3C). Detailed explanation can be found in Table 3.3.

3.7.1 State models

Water-gas shift membrane reactor has been extensively studied, through both experimental and numerical simulations. In the numerical simulation, models are acclimated to predict a reactor performance and this is essential as it provides an insight behaviour of the reactor. Ergo, to simulate a membrane reactor that mimics reality, a highly precise model is required. There are three types of state models that are able to represent a membrane reactor mathematically: one-dimensional (1D), two-dimensional (2D) and three-dimensional (3D) state models. A 1D model only considers the membrane reactor performance variation in an axial direction while a 2D model considers changes in reactor performance

across both axial and radial directions. As for a 3D model, it takes into account the same changes as a 2D model, but with an extra transition in the angular direction.

In literature, most of the simulation work use steady-state, one dimensional (1D) models (Shoko et al., 2006; Tanksale et al., 2010; Vitart et al., 2008). This model is most commonly used in modelling of membrane reactor due to the fact that they are mathematically simple and easy to solve. Researchers have used this model to predict the reactor behaviour based on a few assumptions. One of the major assumptions is that the diameter of the membrane reactor tube is small and therefore, the flow dispersion in radial direction can be neglected.

In Piemonte et al. (2010) paper, a different MR configuration was investigated using a 1D pseudo-homogeneous model which has been validated with WGSR industrial data reported in the open literature. This paper shares similar assumptions as in Brunetti et al. (2007) work, where only plug flow will occur in retentate and permeate streams because the streams flow through a very thin annulus, and therefore the dispersion and radial profiles can be neglected or assumed to be very small compared with the axial profiles. As for Huang et al. (2005) work and Battersby et al. (2010), they too used 1D non-isothermal model to simulate the membrane reactor behaviours. Their assumptions were pretty similar to the former literature where they mentioned that there was no temperature variation in the radial direction inside a hollow fiber membrane due to its small dimension and there is no axial mixing as well (i.e., perfect mixing). Additionally, in Adrover et al. (2009a) and Gosiewski et al. (2010) too used 1D mathematical model to describe the WGSR in the MR. Both of these papers share the same assumptions which is to neglect all of the effects in radial directions.

On the other hand, Marín et al. (2012) mentioned that membrane reactors with a large diameter present a non-negligible variation in the radial axis because of the permeation of hydrogen and the heat transfer through the membrane. For this reason, the use of 1D models is rather questionable, as they can under- or over-predict the catalyst conversion which has been proven to be true in this work. Therefore, 2D models are more appropriate to represent the behaviour of a large diameter membrane reactor as it has the capability to capture both the axial and the radial profiles inside the reactor. The use of this model is rare in literature due to the need of more sophisticated software tools to solve a set of partial differential equations. Some recent research employed 2D models which consider both axial and radial concentration gradients (Mendes et al., 2010; McLellan et al., 2005; Williams, 2002).

Unlike the 1D models, fewer researchers have used 2D models to predict the reactor performance; for example, in the work of Chein et al. (2013), the models consisted of the governing equations for both partial derivatives for axial and radial directions. This model was applied together with boundary conditions and simulated using computational fluid dynamic (CFD) software to obtain the reactor temperature profile. This paper shows that using the 2D model, the behaviour of the reactor can be described reliably compared to 1D model. Using the 2D model it can be shown that the hotspot developed not only in the axial but also radial directions of the reactor. While in the work of Markatos et al. (2005), the performance of the membrane reactor was assessed against the effects of mass and heat dispersion. A 2D model was applied and this paper concluded that heat and mass dispersion effects were too significant to be neglected. Hence the 2D model were much more convincing in predicting the membrane reactor module's behaviour. Similarly Chiappetta et al. (2008) too used a 2D model in simulating the steady state operation of a membrane reactor for WGSR. They showed that there were variation of heat and mass balance in both axial and radial profiles, which suggested the need of the 2D model in accurately predicting the reactor performance.

Oyama et al. (2012) developed both 1D and 2D models for methane steam reforming reactors. Both of the models fitted well with the experimental data, but at high pressure the 2D model predicted better than the 1D model. This was because the 2D model was able to foresee a decline in hydrogen partial pressures which led to lower methane conversion as the driving force of hydrogen permeation was low. Francesconi et al. (2007) used a 1D model to compare with a 2D model considering temperature and mass gradients in both the radial and axial directions of the reactor tube. They found that discrepancies were slight due to radial changes, and that the 1D model could produce satisfactory results for steady-state considerations. Through comparison between 2D models and the 1D models, 2D models have proven to be more accurate in terms of predicting the reactor performance provided that the diameter of the membrane reactor tube is larger (i.e., diameter of membrane reactor tube ¿20% of the diameter of membrane reactor) and it is operated at high operating pressure of 50 bar and above. The accuracy of the results were clearly demonstrated by a few other studies such as (Markatos et al., 2005; Chiappetta et al., 2008; Basile et al., 2003). However, some researchers have argued that 2D was still inadequate in investigating the reactor performance as the profiles in the angular direction have not been taken into account. This led to the extension of the two to the three-dimensional

(3D) model. A high complexity often results from the use of 3D reactor models which attempted to capture reactor behaviours in the axial, radial and angular directions. To use a 3D model would require more highly advance computer programming tools to simulate the membrane reactor.

Due to modelling complexity, relatively little work has been reported on the use of 3D models to predict the reactor performance where one of the works was done by Iyoha et al. (2007). In this work, a 3D model was used to simulate the reactor for experimental validation purposes using a software named COMSOL to model the reactor performance. The same 3D model was used by Chein et al. (2014). Meanwhile, in the work of Smith et al. (2011), a 3D model was simulated using CFD software, where the flow pattern around the reactor was generated. In their study, they showed that due to the reactor shape that was highly symmetrical, hence there were no changes in the reactor profile in the angular direction. Therefore, the use of 3D model to produce more accurate results was not justified unless in the case of highly non-symmetrical reactors.

In the present study, a 1D state model is used for modelling the water-gas shift reaction membrane reactor. This is motivated by the realization that multi-tube membrane reactor configuration has multiple small membrane reactor tube. These small membrane reactor tubes possess negligible changes in terms of radial direction. Hence, a 1D model is sufficient to predict the behaviour of the membrane reactor. Furthermore, a 1D model is computationally effective and easy compared to a 2D and a highly complex 3D. There is no reason to use a 3D model as this model is applicable only for a non-symmetrical membrane reactor.

3.7.2 Reactor models

Note that, in general, there are two types of reactor modelling approaches: (1) homogeneous, and (2) heterogeneous modelling. The homogeneous reactor model describes a pseudo-homogeneous reaction occurring in the reactor solid phase which is assumed to be in equilibrium with the gaseous phase. This modelling approach is illustrated by Adrover et al. (2009b), in which a pseudo-homogeneous 1D model was used to describe the steady-state operation of the MR. Meanwhile, for heterogeneous reactor modelling, it is an approach where the two phases (solid and gaseous) are explicitly considered in the reactor modelling. In the work of Adams and Barton (2009), a heterogeneous reactor modelling was developed for a packed bed tubular reactor and the model validation showed good agreement with experimental data.

It should be noted that, as for homogeneous reactor modelling, Marín et al. (2012) has questioned its credibility as a way to produce rigorous predictions of the performance of the membrane reactor. It is argued that by ignoring the solid catalyst phase might lead to the negligence of heat and mass transfer limitation experienced by the catalyst pellets. As mentioned in Lloyd et al. (1996), catalysts are made up of numerous pores which limited the transfers reactant and heat. The reason is that the uneven surface of catalyst pores resulted in longer time span for the reactant to travel in and out of the pores. Hence, Marín et al. (2012) made an improvement on the homogeneous reactor modelling by incorporating a correction term, namely Thiele modulus to take into account the transfer limitation problems. They developed a 2D rigorous reactor model, which considered both axial and radial profiles. This model includes the normal momentum, mass, and energy differential equations with a nested mass transfer limitation within the porous catalyst. Unlike some other previous 2D models, the model of Marín et al. (2012) includes the Thiele modulus term. Note that, the model was then compared with a simplified model which has often been used in previous study reported in the literature. It is worth highlighting that, the comparative simulation results using several models showed that by neglecting the effect of mass transfer within the catalysts and also momentum balances, the predicted results from the models will tend to produce over-prediction on the conversion of the reactant CO. As an implication, the models neglecting the heat-mass transfer limitations will lead to misinterpretation of the behaviour of the membrane reactor. This argument is supported through the validation work of Sanz et al. (2015).

Table 3.3: Model classification sections

	1-Dimensional	**Major ref.**
Homogeneous model	Without heat and mass transfer limitation - Model 1A	Adrover et al. (2009a); Gosiewski et al. (2010)
	With heat and mass transfer limitation - Model 1B	-
Heterogeneous model	Model 1C	Adams and Barton (2009)

	2-Dimensional	**Major ref.**
Homogeneous model	Without heat and mass transfer limitation - Model 2A	Mendes et al. (2010); Basile et al. (2003)
	With heat and mass transfer limitation - Model 2B	Marín et al. (2012)
Heterogeneous model	Model 2C	-

	3-Dimensional	**Major ref.**
Homogeneous model	Without heat and mass transfer limitation - Model 3A	Iyoha et al. (2007); Chein et al. (2014); Smith et al. (2011)
	With heat and mass transfer limitation - Model 3B	-
Heterogeneous model	Model 3C	-

Unlike in the homogeneous reaction approach, in heterogeneous reaction approach both fluid and solid phases are included in the reactor model; the reactor

is divided into two different phases. In this case, the mass-energy balance equations are explicitly written for both solid catalyst and gas phases. In Adams and Barton (2009), the heterogeneous reaction approach was used to model the shift reactor. It was discovered that by separately modelling the solid and gas phases, there was no need for including the mass-heat transfer limitation correction factor (i.e., Thiele modulus) into the kinetic expression.

It should be noted that heterogeneous and homogeneous have different reactor modelling approach. While homogeneous is pseudo-homogeneous approach with either transfer limitation factor and heterogeneous is separation of solid and fluid phases modelling approach. These two modelling fundamentally differ from one another while the comparative accuracy of predicting the trajectory of the membrane reactor between these two reactor models are still unknown. Thus, the comparative study of these two reactor modelling approaches will be analyzed in the next chapter. The comparison and analysis reported in the next chapter served as the guideline of choosing the most appropriate kinetic and reactor modelling approach to be used for the later section of this study.

3.8 Summary

This chapter summarize a few important points:

- There are two types of reaction kinetics: (1) microkinetic - generated based on step-by-step reaction fundamentals and (2) macrokinetic - generated based on experimental data. The accuracy of these two kinetics models has not yet been analyzed.

- There have been numerous development in the types of catalysts and membrane modules used in water-gas shift reaction. A thorough investigation of all types of catalysts and membranes has been identified. A ternary doped high-temperature catalyst Fe_2O_3Cr and $Pd-Ag$ membrane are chosen to be used in this study.

- Packed bed tubular membrane reactor with multi-tube configuration is chosen as the membrane reactor configuration of this study due to its space saving concepts while able to achieve a higher percentage of recovery.

- There are three different state model classification: (1) one-dimensional, (2) two-dimensional and (3) three-dimensional models. From literature,

3D model possessed a high complexity, however, this 3D model is only applicable for the asymmetrical shift reactor. As for 2D and 1D models, 2D model is applicable when there is a significant change in radial direction. In this study, a 1D model is used as the reactor configuration is made up of numerous small tubes and hence radial profile changes are insignificant. In addition, 1D model is computational effective with the reduction in the complexity of the reactor model.

- There are three different reactor modelling approaches: (1) homogeneous reactor approach, (2) homogeneous with transfer limitation reactor approach and (3) heterogeneous reactor approach. These three approaches have not yet been compared and analyzed on their accuracy of predicting a membrane reactor behaviour.

- The comparison and analysis of different kinetic models and membrane reactor models will be presented in the next chapter.

Chapter 4

Kinetics and Reactors Modelling of Water-Gas Shift Reaction

4.1 Overview

This chapter presents a simulation study on water-gas shift reaction's (WGSR) kinetic models as well as the modelling approaches of the packed-bed tubular reactor (PBTR). There are two different types of models often used to represent WGSR kinetics: (1) macro-kinetics and (2) micro-kinetics models. The PBTR models can be divided into homogeneous or heterogeneous types. There is ample literature regarding the use of different models for the WGSR reactor simulation and design. However, there is currently no guideline in choosing the most suitable combination of kinetic and reactor models. Answering this question is the main objective of this chapter. Several major kinds of kinetic-reactor combination are compared based on the same Cu (111) catalyst to predict the CO conversion of the shift reactor. The predictions are then compared against reported experimental data to test the model accuracy. At the end of this chapter, it is discovered that there are three kinetic-reactor models that are the most recommended: (1) microkinetic with homogeneous reactor model, (2) macrokinetic with Thiele modulus homogeneous reactor model, and (3) macrokinetic with heterogeneous reactor model. The comparison among these different models shall provide a better understanding on the selection of suitable kinetic-reactor model for designing a PBTR. The rest of this chapter is structured as follows. Section 4.2 describes the background of each kinetics and reactor models. Section 4.3 explains in detailed the macro- and micro-kinetics models using Cu(111) catalyst. Meanwhile, section 4.4 covers detailed mathematical equations of packed-bed reactor models

(i.e., homo- and heterogeneous), while section 4.5 defines the boundary conditions for each model. Based on the mathematical models provided in section 4.3, 4.4 and 4.5, section 4.6 and 4.7 explore the comparison between each kinetics-reactor models pair. Lastly, section 4.8 concludes the important findings in this chapter.

4.2 Introduction of WGSR Kinetics and Reactor Models

To simulate the WGSR process, a reliable model representing the system is required. This WGSR model consists of two components: (1) kinetics model, and (2) reactor model. The kinetics model represents the chemical reaction process at the molecular (micro-scale) level. Meanwhile, the reactor model represents a set of energy and mass balance equations which describe the entire process at the macro-scale level. It is important to note that the accuracy of the given WGSR system model depends on the choice of which kinetics and reactor models are adopted.

There are different types of kinetics and reactor models used in the simulation of WGSR systems. Figure 4.1 illustrates the classification for the kinetics and reactor models used in the design, optimization and simulation studies of the WGSR systems.

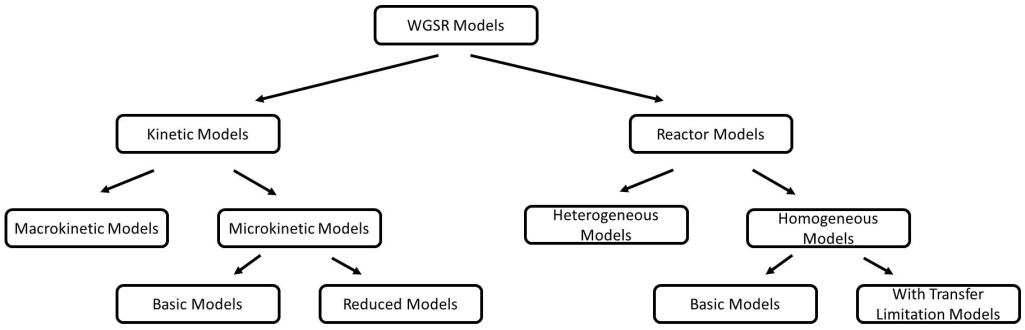

Figure 4.1: Classification of kinetics and reactor modelling for WGSR.

4.2.1 Reaction kinetic modelling

To design a reactor for the WGSR, it is important to have a good estimation of the reaction rate, which is often predicted from a model representing the reaction kinetics. It is important to note that, the accuracy of a model representing the

reaction kinetics is very important for reliable design, optimization and control studies. The kinetic models are often developed as to provide the simplest way to represent the chemical reaction but should be sufficiently accurate in order to help design the reactor involved. Fundamentally, the kinetic expressions (models) can be classified into two main categories: (1) micro-kinetic and (2) macro-kinetic models. The micro-kinetic model is constructed based on the detailed information about all of the elementary (intermediate) steps that comprise the entire chemical reaction. This model explores the detailed mechanisms that occur during the course of the reaction.

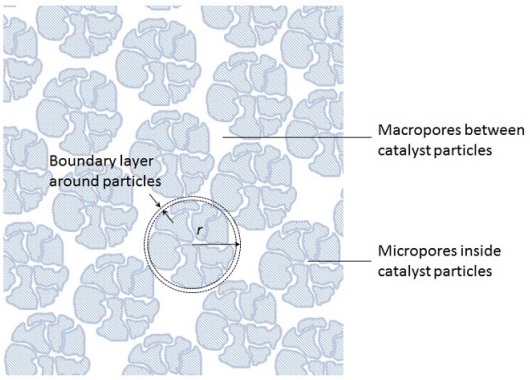

Figure 4.2: Reaction took place at the boundary layer assumed in macrokinetic model.

In contrast to micro-kinetic models, the macro-kinetic models are built based on the experimental data and typically in the form of the Arrhenius or Power-law expression. These macro-kinetic models provide an easy and computationally lighter way to predict the rate of reaction without the detailed knowledge of the complex elementary steps involved. Most of the simulation and control studies of WGSR are based on this type of model, i.e., to understand the reactor macroscopic behaviour. For convenient applications, most of the available catalysts for the WGSR have their own macro-kinetic models. However, a disadvantage of the macro-kinetic models is that they are limited to specific catalysts and narrow operating conditions. To date, there are several unresolved questions concerning which kinetic mechanisms and types of kinetic models are most appropriate for WGSR reactor design and simulation. In particular, a rigorous comparison between the macro- and micro-kinetics for different types of catalysts remains unavailable. Such a limited comparative study is partly due to the lack of experimental data to build micro-kinetics models. The differences between these two kinetic models can be easily explained through the boundary layers shown in

Figure 4.2 and 4.3 – adapted from Dixon (2014). For a micro-kinetics model, the boundary of reaction is taken to be on the surface of the catalyst pellets which ignores the micropores within the pellets. On the contrary, a micro-kinetics model considers reaction boundary inside the micropores within the pellets and all the mass transfer and reaction steps involved. Thus, a micro-kinetic model tends to be a lot more complicated than a macro-kinetic model. Consequently, a reactor model based on the micro-kinetic will involve a lot more of differential-algebraic equations (DAEs) than the one based on the macro-kinetic model, i.e., heavy computation is required when micro-kinetic model is used.

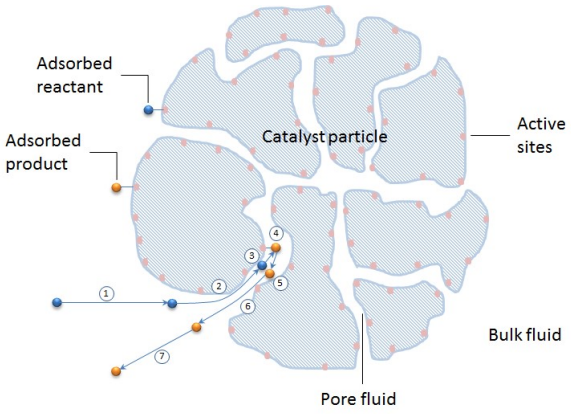

Figure 4.3: Actual reaction took place in a solid catalyst pellet.

4.2.2 Reactor modelling

So far, the behaviour of WGSR in a packed bed tubular reactor (PBTR) has been extensively studied, both via experimental and numerical simulation methods. In the numerical simulation study, the choice of kinetic models used to predict the reaction rate is very important in order to provide an insight into the true behaviour of the reactor. Therefore, to simulate the PBTR that closely mimics reality, a highly accurate model is required. There are two types of modelling approaches for the reactor involved: (1) homogeneous reactor modelling, and (2) heterogeneous reactor modelling; refer to Table 3.3 in Section 3.7.2. The homogeneous modelling assumes that a pseudo-homogeneous reaction occur in the reactor in which the solid phase is in equilibrium with the gaseous phase. As for the heterogeneous reactor modelling, the two phases (solid and gaseous) are explicitly taken into account in the reactor modelling.

With respect to the homogeneous reactor modelling, Marín et al. (2012) ques-

tioned that this modelling approach can lead to poor prediction of the performance of WGSR reactors. The reason for this is that the approach neglects heat and mass transfer limitations within a catalyst pellet. As mentioned by Twigg and Twigg (1989), catalyst pellets are made up of numerous pores within which the reaction takes place. The pores can pose substantial limitations on the transfer of reactants into and products out of the pores as well as heat transfer via convection. These limitations in turn reduce the reaction kinetics, hence lowering the reactor performance overall. In view of such limitations, Marín et al. (2012) proposed an improvement on the homogeneous reactor modelling by introducing a correction factor known as the Thiele modulus to take into account the limiting effects of heat-mass transfer on reaction kinetics.

Unlike in the homogeneous modelling approach, in the heterogeneous modelling approach both fluid and solid phases are explicitly considered in the reactor model. Based on this approach, a reactor model is divided into two different phases. In this case, the mass-energy balance equations are explicitly written for both solid catalyst and gas phases. In Adams and Barton (2009), the heterogeneous reactor modelling was used to model a water-gas shift reactor. It was discovered that by separately modelling the solid and gas phases, there was no need for including the mass-heat transfer limitation correction factor (i.e., Thiele modulus) into the kinetic expression.

To date, it is interesting to point out that the simulation studies based on the heterogeneous reaction model have solely relied upon the macro-kinetic models to represent the WGSR kinetics. Till date, there has been no literature report on the incorporation of a micro-kinetic model in a heterogeneous reactor model. Such study has not been conducted due to the complexity of the system of equations which arise from the micro-kinetics model. Furthermore, there is yet a comparison between the homogeneous and heterogeneous modelling approaches for the WGSR in a PBTR.

4.3 Water-Gas Shift Reaction Modelling

4.3.1 WGSR microkinetic models

There are two types of microkinetic models. One is the original version of microkinetic model discovered by Fishtik and Datta (2002) while the other is the modified version, namely reduced microkinetic model developed by Callaghan et al. (2003). According to Callaghan et al. (2003), there are 17 elementary steps

that involve in the WGSR. Table 4.1 − adapted from Callaghan et al. (2003) shows the microkinetic model for the WGSR on Cu (111) catalyst.

Table 4.1: Microkinetic model for WGSR in Cu(111)

	$\overrightarrow{E_j}$	$\overrightarrow{A_j}$	**Elementary reactions**	$\overleftarrow{E_j}$	$\overleftarrow{A_j}$	ΔH	
s_1:	0	10^6	$H_2O + S \rightleftharpoons H_2OS$	13.6	10^{14}	-13.6	a,b
s_2:	0	10^6	$CO + S \rightleftharpoons COS$	12.0	10^{14}	-12.0	a,b
s_3:	5.3	4×10^{12}	$CO_2S \rightleftharpoons CO_2 + S$	0	10^6	5.3	a,b
s_4:	15.3	10^{13}	$HS + HS \rightleftharpoons H_2S + S$	12.8	10^{13}	2.5	a
s_5:	5.5	6×10^{12}	$H_2S \rightleftharpoons H_2 + S$	0	10^6	5.5	a,b
s_6:	25.4	10^{13}	$H_2OS + S \rightleftharpoons OHS + HS$	1.6	10^{13}	23.8	a
s_7:	10.7	10^{13}	$COS + OS \rightleftharpoons CO_2S + S$	28.0	10^{13}	-17.3	a
s_8:	0	10^{13}	$COS + OHS \rightleftharpoons HCOOS + S$	20.4	10^{13}	-20.4	a
s_9:	15.5	10^{13}	$OHS + S \rightleftharpoons OS + HS$	20.7	10^{13}	-5.2	a
s_{10}:	0	10^{13}	$COS + OHS \rightleftharpoons CO_2S + HS$	22.5	10^{13}	-22.5	a
s_{11}:	1.4	10^{13}	$HCOOS + S \rightleftharpoons CO_2S + HS$	3.5	10^{13}	-2.1	a
s_{12}:	4.0	10^{13}	$HCOOS + OS \rightleftharpoons CO_2S + OHS$	0.9	10^{13}	3.1	a
s_{13}:	29.0	10^{13}	$H_2OS + OS \rightleftharpoons 2OHS$	0	10^{13}	29.0	a
s_{14}:	26.3	10^{13}	$H_2OS + HS \rightleftharpoons OHS + H_2S$	0	10^{13}	26.3	a
s_{15}:	1.3	10^{13}	$OHS + HS \rightleftharpoons OH + H_2S$	4.0	10^{13}	-2.7	a
s_{16}:	0.9	10^{13}	$HCOOS + OHS \rightleftharpoons CO_2S + H_2OS$	26.8	10^{13}	-25.9	a
s_{17}:	14.6	10^{13}	$HCOOS + HS \rightleftharpoons CO_2S + H_2S$	14.2	10^{13}	0.4	a

a - activation energies in kcal/mol estimated according to Nakamura et al. (1990) and the results coincide with estimation made by Ovesen et al. (1996): b - pre-exponential factors with unit of $Pa_{-1}s_{-1}$ adjusted to fit overall reactions given by Satterfield (1991)

Note that, for the reaction scheme shown in Table 4.1, 4 extra elementary steps (i.e. s_{14}, s_{15}, s_{16} and s_{17}) were added to the 13 elementary steps found by Fishtik and Datta (2002). These more comprehensive elementary steps are employed in the establishment of reaction routes (RRs) introduced by Fishtik and Datta (2002). Continuing from the work of Fishtik and Datta (2002), Callaghan et al. (2003) managed to identify 70 overall RRs for the WGSR on Cu (111) whereby the complete list of these overall RRs can be found in Campbell and Daube (1987). They then managed to reduce the overall RRs to only 3 dominant reaction routes whereby the dominant RRs are found by identifying the rate determining steps of the overall RRs. However, these 3 dominant routes are different from those mentioned by Fishtik and Datta (2002). For further clarification of both authors, Fishtik and Datta (2002) and Callaghan et al. (2003), the dominant RRs are presented in this section.

Firstly, consider the 3 dominant RRs obtained by Fishtik and Datta (2002). The sum of these 3 dominant RRs fluxes determines an overall rate of reaction, r. In Fishtik and Datta (2002) work, the 3 dominant RRs are s_8, s_9 and s_{10} and thereby the overall rate of reaction, r is given as follows:

$$r_8 = \frac{\overrightarrow{k_6}\overrightarrow{k_8}K_1K_2P_{H_2O}P_{CO}\theta_0^2}{\frac{\left(\overrightarrow{k_6}/K_6\right)P_{H_2}^{1/2}}{(K_4K_5)^{1/2}} + \overrightarrow{k_9} + \left(\overrightarrow{k_8}\overrightarrow{k_{10}}\right)K_2P_{CO}} \times \left(1 - \frac{P_{CO_2}P_{H_2}}{KP_{H_2O}P_{CO}}\right) \tag{4.1}$$

$$r_9 = \frac{\overrightarrow{k_6}\overrightarrow{k_9}K_1 P_{H_2O}\theta_0^2}{\frac{\left(\overrightarrow{k_6}/K_6\right)P_{H_2}^{1/2}}{(K_4K_5)^{1/2}} + \overrightarrow{k_9} + \left(\overrightarrow{k_8}\overrightarrow{k_{10}}\right)K_2 P_{CO}} \times \left(1 - \frac{P_{CO_2}P_{H_2}}{K P_{H_2O}P_{CO}}\right) \tag{4.2}$$

$$r_{10} = \frac{\overrightarrow{k_6}\overrightarrow{k_{10}}K_1 K_2 P_{H_2O}P_{CO}\theta_0^2}{\frac{\left(\overrightarrow{k_6}/K_6\right)P_{H_2}^{1/2}}{(K_4K_5)^{1/2}} + \overrightarrow{k_9} + \left(\overrightarrow{k_8}\overrightarrow{k_{10}}\right)K_2 P_{CO}} \times \left(1 - \frac{P_{CO_2}P_{H_2}}{K P_{H_2O}P_{CO}}\right) \tag{4.3}$$

Meanwhile, Callaghan et al. (2003) suggested that the 3 dominant RRs are s_8, s_{10} and s_{15} which are slightly different from those proposed by Fishtik and Datta (2002). Equations 4.4 - 4.6 show the 3 dominant RRs proposed by Callaghan et al. (2003).

$$r_8 = \frac{\overrightarrow{k_6}\overrightarrow{k_8}K_1 K_2 P_{H_2O}P_{CO}\theta_0^2}{\frac{\left((\overrightarrow{k_6}/K_6)+\overrightarrow{k_{15}}\right)P_{H_2}^{1/2}}{(K_4K_5)^{1/2}} + \overrightarrow{k_9} + \left(\overrightarrow{k_8}\overrightarrow{k_{10}}\right)K_2 P_{CO}} \times \left(1 - \frac{P_{CO_2}P_{H_2}}{K P_{H_2O}P_{CO}}\right) \tag{4.4}$$

$$r_{10} = \frac{\overrightarrow{k_6}\overrightarrow{k_{10}}K_1 K_2 P_{H_2O}P_{CO}\theta_0^2}{\frac{\left((\overrightarrow{k_6}/K_6)+\overrightarrow{k_{15}}\right)P_{H_2}^{1/2}}{(K_4K_5)^{1/2}} + \overrightarrow{k_9} + \left(\overrightarrow{k_8}\overrightarrow{k_{10}}\right)K_2 P_{CO}} \times \left(1 - \frac{P_{CO_2}P_{H_2}}{K P_{H_2O}P_{CO}}\right) \tag{4.5}$$

$$r_{15} = \frac{\overrightarrow{k_6}\overrightarrow{k_{15}}K_1 (K_4K_5)^{1/2} P_{H_2O}P_{H_2}^{1/2}\theta_0^2}{\frac{\left((\overrightarrow{k_6}/K_6)+\overrightarrow{k_{15}}\right)P_{H_2}^{1/2}}{(K_4K_5)^{1/2}} + \overrightarrow{k_9} + \left(\overrightarrow{k_8}\overrightarrow{k_{10}}\right)K_2 P_{CO}} \times \left(1 - \frac{P_{CO_2}P_{H_2}}{K P_{H_2O}P_{CO}}\right) \tag{4.6}$$

Both of the proposed RRs share the same constant K which denotes the equilibrium constant of WGSR. Meanwhile, θ_0 the surface coverage given by

$$\theta_0 = \frac{1}{K_1 P_{H_2O} + K_2 P_{CO} + (K_4K_5)^{-1/2}P_{H_2}^{1/2}} \tag{4.7}$$

Through the summation of fluxes, the overall rate of reaction, r_f based on the Fishtik and Datta (2002) is

$$r_f = \frac{\overrightarrow{k_6}K_1 P_{H_2O}\theta_0^2\left[\overrightarrow{k_9} + \left(\overrightarrow{k_8}\overrightarrow{k_{10}}\right)K_2 P_{CO}\right]}{\frac{\left(\overrightarrow{k_6}/K_6\right)P_{H_2O}^{1/2}}{(K_4K_5)^{1/2}} + \overrightarrow{k_9} + \left(\overrightarrow{k_8} + \overrightarrow{k_{10}}\right)K_2 P_{CO}} \times \left(1 - \frac{P_{CO_2}P_{H_2}}{K P_{H_2O}P_{CO}}\right) \tag{4.8}$$

As for Callaghan et al. (2003), the overall rate of reaction, r_c is expressed in the form of

$$r_c = \frac{\overrightarrow{k_6} K_1 P_{H_2O} \theta_0^2 \left[\left(\overrightarrow{k_8} + \overrightarrow{k_{10}} \right) K_2 P_{CO} + \overrightarrow{k_{15}} (K_4 K_5)^{-1/2} P_{H_2}^{1/2} \right]}{\frac{\left(\overrightarrow{k_6}/K_6 + \overrightarrow{k_{15}} \right) P_{H_2O}^{1/2}}{(K_4 K_5)^{1/2}} + \left(\overrightarrow{k_8} + \overrightarrow{k_{10}} \right) K_2 P_{CO}} \times \left(1 - \frac{P_{CO_2} P_{H_2}}{K P_{H_2O} P_{CO}} \right) \tag{4.9}$$

It can be seen that, the difference between equations 4.8 and 4.9 lies in the availability of $\overrightarrow{k_9}$ and $\overrightarrow{k_{15}}$. This dissimilarity is due to the different rate determining steps obtained by the two above-mentioned groups of researchers.

4.3.2 WGSR macrokinetic model

So far, only one power law kinetic model has been published on the Cu (111) catalyst. Campbell and Daube (1987) established the kinetics of WGSR on a clean Cu (111) single-crystal surface through a series of experiments. It was identified that the reaction activation energy is 17 kcal/mole and reaction orders in terms of H_2O and CO pressures are 0 and 0.5 - 1.0 respectively. The power law kinetics model for this catalyst is

$$r_m = A exp \left(\frac{E_a}{RT} \right) P_{H_2O}^0 P_{CO}^{0.5-1.0} \tag{4.10}$$

where A denotes a kinetic constant parameter, E_a the activation energy, R the gas constant, T the temperature and P the pressure of the specific component.

4.4 Packed Bed Reactor Models

The assumptions made in the packed bed tubular reactor (PBTR) modelling are:

a) Only the axial temperature change is taken into account.

b) The radial temperature change is neglected due to the fact that the diameter of the reactor is small and adiabatic (no heat loss from the surface of the reactor); see Aboudheir et al. (2006).

c) The momentum conservation equation is disregarded in this model because the bed height is quite small to create a significant amount of pressure drop, i.e., see Shahrokhi and Baghmisheh (2005).

d) Gas properties, the permeance and kinetics are assumed to be in non-isothermal conditions, which means that they depend upon temperature change.

e) Plug flow is assumed as it is often the preferred flow behaviour considered in industries.

f) Only low temperature shift Cu (111) catalyst is used in this case study due to the lack of kinetics data for other types of catalysts.

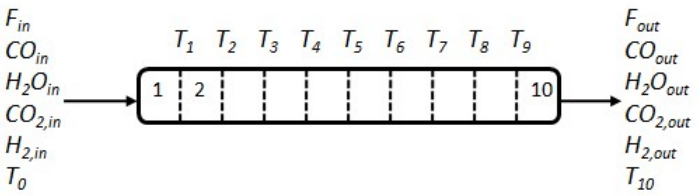

Figure 4.4: Division of the packed bed tubular reactor into 10 sub-sections.

For computational simplicity, the tubular reactor is divided into 10 equal segments of volume (see Figure 4.4). The reactor is sub-divided into 10 equal volume where each segment is represented by a set of ODEs. This reduces a set of partial differential equations (PDEs) into a relatively simpler ordinary differential equations (ODEs). The conversion of PDEs into ODEs reduces computational time and complexity of the model simulation while maintaining the accuracy of the model. As illustrate in Figure 4.5, it is sufficient to just sub-divide the reactor length into 10 sub-sections since this already leads to an acceptably small error (less than 10%) in the model prediction. In other words, further increase in the number of sub-divisions will not lead to significance improvement in the prediction accuracy. The dimension of the PBTR system used in this study is scaled to 1 (one) meter in length, which is based on the pilot-scale membrane reactor commercialized by Tokyo Gas Company Ltd. Mori (2005). For the PBTR modelling, it is assumed that the Cu (111) catalyst is used with property as reported in Campbell and Daube (1987).

The output data from each sub-section of the PBTR are calculated using the fundamental model described in the following section. Two modelling approaches are compared in the simulation study: (1) homogeneous model and (2) heterogeneous model. The details of these two models are presented in the following sections.

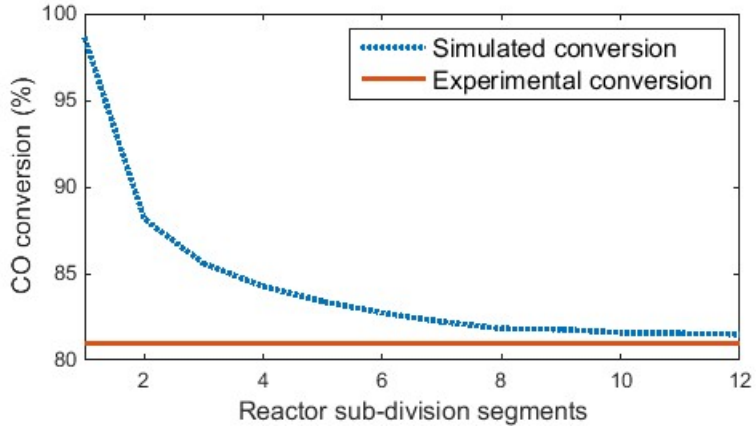

Figure 4.5: Model conversion prediction for different numbers of reactor segments.

4.4.1 Homogeneous modelling

For the development of a homogeneous reactor model, both of the solid catalyst and gas phases are lumped into one single phase (pseudo-homogeneous) to reduce the model complexity. Consequently, this reduced complexity will lead to a lower computational time when using the model in simulation. Based on the homogeneous modelling approach, two sub-types of reactor models can be formed (see classification shown in Figure 4.1):

a) A reaction model which includes the heat and mass transfer limitations in the catalyst pellets, i.e., known as Model 1B in this study.

b) The reactor model which totally ignores the heat-mass transfer limitation effects - refer as Model 1A.

The term η_{gl} in the mass and energy balance equations represents a corrective term to account for the presence of mass-heat transfer limitations as shown in equations 4.11 - 4.12.

For the gas phase, the species mass balance:

$$\epsilon V \frac{dC_{i,j}}{dt} = F(C_{i,j-1} - C_{i,j}) \pm r_{A,j} W \eta_{gl} \qquad j = 1, 2...n \tag{4.11}$$

For the solid phase, the heat balance:

$$(1-\epsilon) V \rho_s C_{p,s} \frac{dT_{s,j}}{dt} = -r_{A,j} W \Delta H_r x \eta_{gl} - UA(T_{s,j} - T_{f,j}) \tag{4.12}$$

In the gas phase, the heat balance:

$$\epsilon V \rho_f C_{p,f} \frac{dT_{f,j}}{dt} = F C_{p,f} \rho_f (T_{f,j-1} - T_{f,j}) + UA(T_{s,j} - T_j) \tag{4.13}$$

Here, ϵ denotes the bed voidage factor, V (m^3) the sub-section volume of the reactor, $C_{i,j}$ (mol/m^3) the molar concentration of component i at the j^{th} sub-section, F (m^3/hr) the feed flow rate, W (g) the weight of catalyst in the reactor sub-section, ρ_s and ρ_f (kg/m^3) the density of catalyst and fluid respectively, $C_{p,s}$ and $C_{p,f}$ (kJ/kg.K) the specific heat capacity of catalyst and fluid, T_s (K) the catalyst temperature, T_f (K) the fluid temperature, $\Delta H_r x$ (kJ/mol) the heat of reaction, U (kJ/hr.m^2.K) the convective overall heat transfer coefficient, A (m^2) the heat transfer area and η_{gl} is the global effectiveness factor. In equation 4.11, the $\pm$ sign indicates either species consumption or generation; for CO and H_2O (reactants) the sign is minus and vice versa for the products.

Note that, the global effectiveness factor is neglected in the homogeneous modelling, i.e., the heat-mass transfer limitations are ignored. The basic global effectiveness factor is often used to take into account the mass transfer resistances occurring in the internal and external of catalyst particles. In the global effectiveness calculation, the effective diffusion coefficient used is approximated by Knudsen diffusion in accordance with the physical properties of the gaseous compounds and textural properties of the catalyst. Meanwhile, the mass transfer resistance external of the catalyst particles is modelled by using the mass transfer coefficient for transport in packed-bed. Note that, the internal mass transfer resistance within catalyst particles is modelled based on the generalized Thiele modulus. The internal effectiveness factor (generalized Thiele modulus) is used to model the contribution of the mass transfer resistance inside the porous catalyst particles. The expression of the internal effectiveness factor is suitable for a catalyst in the form of pellets. The expression used in the reaction model should fit the reversible power-law type kinetic equation. The internal effectiveness factor, generalized Thiele modulus and global effectiveness factor are expressed in equations 4.14, 4.15, and 4.18 respectively:

$$\eta_{int} = \frac{1}{\phi}\left(\frac{1}{tanh(3\phi)} - \frac{1}{3\phi}\right) \tag{4.14}$$

$$\phi = \frac{(d_p/4)\rho_s r_{A,j}}{[2D_{ep}\rho_s \int_{C_{ieq}}^{C_i} r_{A,j} dC_i]^{\frac{1}{2}}} \tag{4.15}$$

$$D_{ep} = \frac{d_{pore}\epsilon_{int}}{\tau}\frac{4}{3}\sqrt{\frac{RT}{2\pi M}} \tag{4.16}$$

$$a_s K_G = \frac{6D_{CO_m}}{d_p^2}(2 + 1.1Re^{0.60}Sc^{0.33}) \tag{4.17}$$

$$\eta_{gl} = \frac{1}{\frac{1}{\eta_{int}} + \frac{\rho_s}{a_s K_G}\left(\frac{\partial r_{A,j}}{\partial C_{CO}}\right)} \tag{4.18}$$

where ϕ denotes the generalized Thiele modulus, d_p (m) is the diameter of the catalyst particle, D_{ep} is the pore effective diffusion coefficient, $a_s K_G$ denotes the mass transfer coefficient, d_{pore} (m) is the diameter particle pore size, ϵ_{int} is the internal porosity, τ is the tortuosity, M (kg/mol) is molar weight, D_{CO_m} (m^2/s) is molecular diffusion of CO in the reaction mixture, Re is Reynolds number and Sc is Schmidt number.

4.4.2 Heterogeneous modelling

Based on the heterogeneous modelling approach, one type of reactor models is developed - see Model 1C. The mass and energy balance equations used are shown in the following sections.

Gas phase species balance

For the bulk gas phase outside of the catalyst, the dynamic species mass balances are given as Adams and Barton (2009):

$$\epsilon V \frac{dC_{i,j}}{dt} = F_{in} C_{i,j-1} - F_{out} C_{i,j} + \nu_i k_{c,i} a V \Delta C_{i,j} \tag{4.19}$$

where F_{in} and F_{out} (m^3/hr) denotes the volumetric flow rate of the feed inlet and outlet respectively. V (m^3) is the sub-division volume of reactor, ϵ the bed voidage factor, ν_i the stoichiometric coefficient of species i (-1 for reactant and +1 for product), C_i (mol/m^3) is the molar concentration of species i at the j^{th} sub-section, a (m^2/m^3) the total catalyst external surface area per unit volume, $k_{c,i}$ is the mass transfer coefficient between the catalysts surface and the bulk gas phase for species i and t (hr) is time.

Here, $\Delta Ci, j$ (mol/m^3) is the concentration difference between the catalyst surface and the gas bulk phase defined as follows:

$$\Delta C_{i,j} = C_{i,j,surf} - C_{i,j} \tag{4.20}$$

where $C_{c,i,surf}$ is the concentration of species i at the catalyst surface.

Gas phase energy balance

In the gas phase, the energy balance equation is given as:

$$\begin{aligned}((1-\epsilon)\rho_s C_{p,s}V + \epsilon\rho_g C_{p,g}V)\frac{dT_{r,j}}{dt} =& F_{in}C_{p,g,in}\rho_g T_{r,j-1} \\ &- F_{out}C_{p,g,out}\rho_g T_{r,j} \\ &+ h_f aV(T_{c,surf,j} - T_{r,j}) \\ &+ a_v \sum_{i=1}^{N_s} k_{c,i}(H_{c,i,surf} - Hi) \\ &\times (C_{c,i,surf,j} - C_{i,j})\end{aligned} \tag{4.21}$$

where ρ_s (kg/m^3) is the catalyst bulk density, $C_{p,s}$ and $C_{p,g}$ (kJ/kg.K) are the specific heat capacity for solid catalyst and gas phase respectively, h_f (W/m^2.K) is the heat transfer coefficient between the the catalyst surface and bulk gas phase, $k_{c,i}$ (m/hr) is the mass transfer coefficient for species i between the catalyst surface and the bulk gas phase, $T_{c,surf,j}$ (K) is the catalyst temperature at the surface and $T_{r,j}$ (K) is the retentate temperature at j^{th} section. $H_{c,i,surf}$ and H_i (kJ/mol) are the enthalpies at the catalyst surface and for the species i in the bulk gas respectively defined as follows:

$$H_{c,i} = \Delta H^f_{298} + \int_{298}^{T} C_{p,i}(T)dT \tag{4.22}$$

where H_{298} is the heat of formation for each species i. The heats of formation of CO, H_2O and CO_2 are -110.5, -241.9, and -393.5 kJ/mol, respectively (Rankin, 2009). The heat of formation of H_2 is zero by definition. The enthalpies are added into the equation to include the entropy changes of the transfer medium.

Catalyst phase species balance

The species mass balances for the catalyst phase are modelled as a homogeneous mixture of two phases:

a) Solid catalyst phase.

b) Gas in the pores.

It is assumed that the reaction takes place in the catalyst pores only and therefore, the reaction in the solid catalyst is negligible. The species concentrations inside

the catalyst pores are modelled as a function of catalyst radius, r. The diameter, d_p of solid catalyst is typically in a range of 1-3 mm and pores, d_{pore} in a range of 7-9 μm. Due to the small size of pores, it is assumed that only diffusion dominates the internal mass transfer where the resistances via convection and pressure difference terms are assumed to be negligible. Hence, the dynamic mass balance of species i inside the catalyst pores is defined as:

$$\frac{dC_{c,i,j}}{dt} = \frac{1}{r^2}\frac{\partial}{\partial r}\left(D_{i,m}r^2\frac{\partial C_{c,i,j}}{\partial r}\right) + r_i \tag{4.23}$$

where r (m) denotes the spherical coordinates of the catalyst pellet radius and $D_{i,m}$ (m/hr) is the effective gas diffusivity of species i in the mixture.

Equation 4.23 representing the species concentration includes changes over both time and radius of the catalyst pellet. In order to determine the need of considering both changes in the reactor model, a simulation study is carried out to evaluate the dynamic inside the catalyst pellet. The equation is solved using the *pde* solver in $Matlab$ 2013b software.

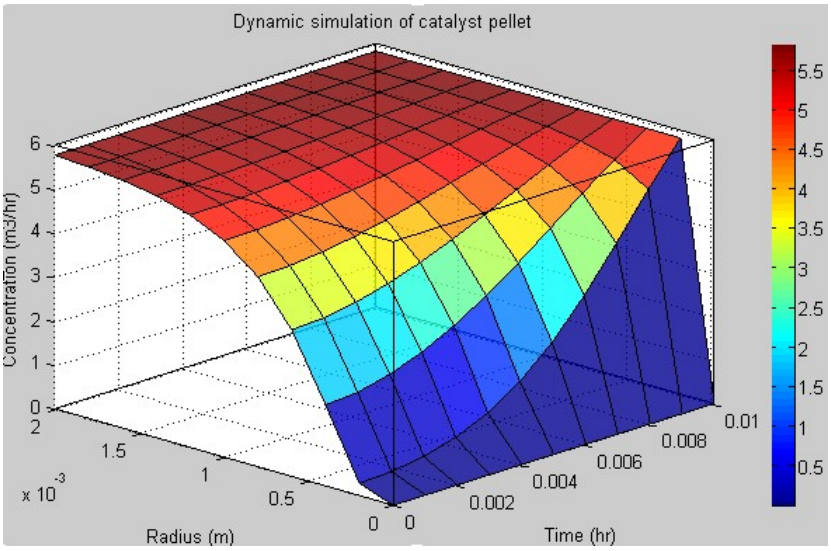

Figure 4.6: Dynamic simulation of catalyst pellet

As shown in Figure 4.6, the rate of reaction reaches a steady-state value at time t = 0.01 hour which is equivalent to 36 sec. This result implies that there is a negligible lag of time for the reaction taking place inside the catalyst. Since the reaction dynamic is very fast compared with the dynamic of reactor overall, it should be acceptable to ignore the temporal distribution in the catalyst pellets, i..e to assume $dc_i/dt = 0$. Therefore, the pseudo-steady state condition can be

assumed for the change of concentration over time in the catalyst pellet. With this assumption, equation 4.23 is now re-written in the following form:

$$\frac{d}{dr}\left(D_{i,m}r^2\frac{dC_{c,i,j}}{dr}\right) = -r_i r^2 \tag{4.24}$$

By solving the double differentiation of equation 4.24, the surface concentration of the catalyst pellet can be obtained and then used in equation 4.20.

Catalyst phase energy balance

Through an energy balance in equation 4.21, the temperature changes occurring inside the catalyst pellet can be predicted. In this energy balance, it is assumed that the temperature of the solid catalyst at radius r is the same as the gas phase in the pores at radius r. Due to the small pellet size, it is also assumed that the thermal conductivity of the catalyst is constant throughout the radius r. Therefore, the energy balance for the solid phase in a catalyst pellet becomes:

$$\frac{dT_{cat,j}}{dt} = \frac{1}{r}\frac{\partial}{\partial r}\left(\frac{2\lambda_{cat}T_{cat,j} + \theta D_{i,m}\frac{\partial C_{c,i,j}}{\partial r}C_{p,i} + \lambda_{cat}r\frac{\partial T_{cat,j}}{\partial r}}{(1-\theta)\rho_{cat}C_{p,cat} + \theta\sum_i^{N_s} C_{p,i}C_{c,i,j}}\right) \tag{4.25}$$

where $T_{cat,j}$ (K) denoted the temperature of the catalyst at j^{th} section, λ_{cat} (W/m) is thermal conductivity of the catalyst pellet including pores effect, $C_{p,i}$ (kJ/mol) is the heat capacity of i in catalyst pores, θ is the percentage volume of catalyst occupied by the pores and ρ_{cat} (kg/m^3) is the bulk density of the solid catalyst.

Equation 4.25 is solved using the same technique as that used for solving equation 4.23. It is found that the results obtained are identical. Therefore, the catalyst pellet temperature can be assumed to be in pseudo-steady state. Hence, equation 4.25 can be simplified to:

$$\frac{d}{dr}\left(\frac{2\lambda_{cat}T_{cat,j} + \theta D_{i,m}\frac{\partial C_{c,i,j}}{\partial r}C_{p,i} + \lambda_{cat}r\frac{\partial T_{cat,j}}{\partial r}}{(1-\theta)\rho_{cat}C_{p,cat} + \theta\sum_i^{N_s} C_{p,i}C_{c,i,j}}\right) = 0 \tag{4.26}$$

By using the *ode* solver in *Matlab* software to solve equation 4.26, the temperature at the catalyst surface can be determined and this value is used in the gas phase energy balance as shown in equation 4.21.

4.5 Boundary Conditions

Both the homogeneous and heterogeneous reactor models described in the previous sections used the same boundary conditions.

4.5.1 Gas phase boundary conditions

The boundary conditions for the gas phase at the inlet of the reactor ($j = 0$) are given as:

$$T_{r,j} = T_{in} \tag{4.27}$$

$$C_{i,j} = C_{in} \tag{4.28}$$

where T_{in} (K) is the inlet temperature of the gas before entering the PBTR and C_{in} (mol/hr) is the initial inlet concentration at the starting of the PBTR.

4.5.2 Catalyst phase boundary conditions

Note that, the boundary condition for catalyst pellet is only used in the heterogeneous model. For a catalyst pellet, it is assumed that the boundary conditions at the centre ($r = 0$) at any point of j^{th} section of the reactor is given by:

$$\frac{dC_{c,i,j}}{dz}(z, r = 0) = 0 \tag{4.29}$$

$$\frac{dT_{cat,j}}{dz}(z, r = 0) = 0 \tag{4.30}$$

As for the boundary conditions at the surface of the catalyst pellet ($r = R$), where $R = 0.5D_{cat}$, the flux conditions are assumed to be:

$$k_{c,i}(C_{c,i,j}(z, r = R) - C_{i,j}(z)) = -D_{i,m}\frac{\partial C_{c,i,j}}{\partial r}(z, r = R) \tag{4.31}$$

$$
\begin{aligned}
h_f(T_{cat,j}(z, r = R) - T_{r,j}(z)) + \sum_{i}^{N_s} H_i(z) & \\
\times k_{c,i}(C_{c,i,j}(z, r = R) - C_{i,j}(z)) = & -\lambda_{cat} \frac{\partial T_{cat,j}}{\partial r}(z, r = R) \\
& - \sum_{i}^{N_s} H_{c,i}(z, r = R) \\
& \times D_{i,m} \frac{\partial C_{c,i,j}}{\partial r}(z, r = R)
\end{aligned}
\tag{4.32}
$$

Equations 4.29 - 4.32 are the boundary conditions required in order to correctly simulate the behaviour of the PBTR. All the mentioned boundary conditions are obtained from Adams and Barton (2009).

4.6 Analysis of WGSR Kinetic Modelling

In this section, comparative predictions of the CO conversion via the different types of macro- and micro-kinetic models are evaluated. These kinetic models are simulated based on the homogeneous PBTR reactor model, i.e., Model 1A (Table 3.3 in Section 3.7.2) is used to conduct the comparison for different kinetic models. Figure 4.7 shows the CO conversion results based on the simulation study at different inlet temperatures. The percentage of CO conversion is calculated as follows

$$
CO \text{ conversion} = \left(\frac{F_{in} C_{i,in} - F_{out} C_{i,out}}{F_{in} C_{i,in}} \right) \times 100\% \tag{4.33}
$$

where the $C_{i,in}$ and $C_{i,out}$ denote the inlet and outlet concentrations of CO.

The inlet temperature used in this simulation ranges from 573 to 673 K. Note that, the availability of experimental data for Cu (111) catalyst in the literature is within this range. Figure 4.7 shows the predicted CO conversions by the 3 different WGSR kinetic models (micro-kinetics, reduced micro-kinetics and macro-kinetics) and the experimental conversion. For a fair comparison, the percentage error from the experimental data from Campbell and Daube (1987) is used to determine the accuracy of the model predictions. The percentage error is calculated as follows:

$$
\text{Absolute error } \% = \left\| \frac{(predicted\, value\, - experimental\, value)}{experimental\, value} \right\| \tag{4.34}
$$

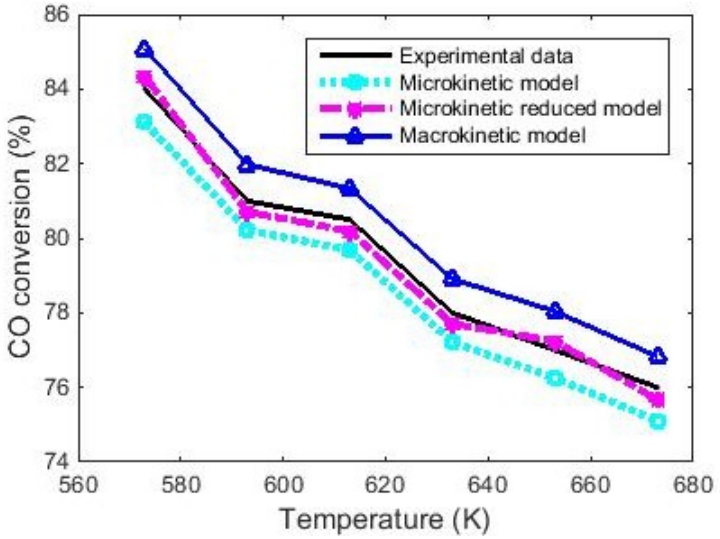

Figure 4.7: Comparison on CO conversion for 3 different kinetic models based on Model 1A.

The absolute error shows that the macro-kinetic model gives the highest percentage error, which suggests the presence of significant mass-heat transfer limitations reported in some literature, e.g., see Marín et al. (2012); Adams and Barton (2009). The macro-kinetics model tends to give over-prediction of the experimental data. According to Twigg and Twigg (1989), the solid catalyst contains small pores that contribute to the diffusion limitation resulting in mass transfer limitation.

The original micro-kinetic model developed by Fishtik and Datta (2002) gives lower percentage errors than the macro-kinetic model. This better accuracy is expected because the micro-kinetic model takes into account the transfer limitation within the catalyst pellets. However, the percentage error shown is larger than the reduced micro-kinetics model developed by Callaghan et al. (2003). Even though similar approach was used to determine the rate of reaction, Callaghan and his co-workers took into account improved detailed reaction mechanism that occurred on Cu (111) catalyst. The rate of reaction model developed by Callaghan et al. (2003) shows little deviation (i.e., the average percentage error is about 3%) from the real experimental data. It can be concluded that the reduced micro-kinetic model should be used in modelling of the WGSR reactor as it leads to accurate model prediction. However, the micro-kinetic model is only limited to certain types of catalyst as research in this particular direction has not yet progressed well. One reason for this lack of progress is due to high complexity and tedious

experimental work needed to obtain a set of micro-kinetic data for a single type of catalyst. Thus, the macro-kinetic model incorporating mass-heat transfer limitation is recommended in designing a reactor because it is easily obtained for many kinds of catalysts available. The mass-heat transfer limitation term can be estimated through the simple calculation using equation 4.18.

4.7 Analysis of PBTR Reactor Modelling

In this section, comparative predictions are performed for 6 different types of reactor models based on the homogeneous and heterogeneous modelling types - refer to Table 3.3. Simulation is done assuming the same type of catalyst within the same range of operating conditions as in the Section 4.6. Figure 4.8 illustrates the comparative results for the 6 different reactor models.

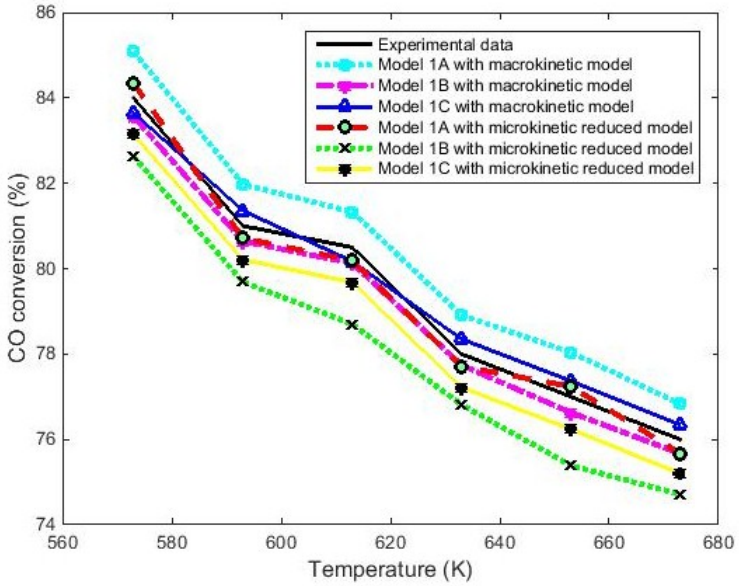

Figure 4.8: Comparison of 3 different types of reactor modelling on macro- and micro-kinetic modelling.

Obviously, 3 of the 6 reactor models show good predictions of the experimental data as shown in Figure 4.8. For a clearer comparison, the same percentage error in equation 4.34 is used. Here, we mainly focus on comparing between homogeneous and heterogeneous reactor models. For the same macro-kinetic model used in the homogeneous and heterogeneous models, it can be seen that the Model 1C gives lower percentage error than that of the Models 1A and 1B.

However, the percentage difference is less than 1% with respect to the Model 1B. This means that with the incorporation of the transfer limitation (Thiele modulus correction factor), the relatively simple homogeneous model can provide reliable prediction as that of the more complex heterogeneous model. When heat and mass transfer limitations are introduced into the macro-kinetic model as proposed by Marín et al. (2012), the results show a large decrease in the prediction error. The incorporation of mass transfer limitation into the macro-kinetic model leads to a decrease in the prediction error of the homogeneous reactor model to within 2.5% error margin from the experimental data.

Contrary to the idealized macro-kinetics, the use of reduced micro-kinetics in homogeneous reactor model (Model 1A) gives the least amounts of prediction errors. When the reduced micro-kinetics model is incorporated into the homogeneous Model 1B and heterogeneous Model 1C, both reactor models give under-predicted values of the reactor CO conversion. This is because of both Models 1B and 1C have already taken into account the mass transfer limitation factor into the model calculations.

It is interesting to point out that, the reduced micro-kinetics model represents the most accurate kinetics for the WGSR. Such an improved accuracy is a result of the activation energy and collision factor for each step of elementary reaction was taken into account when developing this micro-kinetics model for Cu (111) catalyst. Therefore, when using the reduced micro-kinetics model, there is no need to include the transfer limitation correction factor as in the macro-kinetics case. As a conclusion, either the macro-kinetics with the transfer limitation or the reduced micro-kinetics model can give an accurate prediction based on whichever modelling approach (heterogeneous or heterogeneous) is adopted. Of course, for minimum computational effort, it is recommended to adopt homogeneous reactor modelling approach in which the macro-kinetics model is coupled with the mass transfer limitation factor. This approach is very flexible as the kinetic data on many catalysts are available in for the micro-kinetic models.

4.8 Summary

This chapter is summarized as follows:

- Understanding of different types of reaction kinetics and reactor modelling approaches is crucial to developing a reliable model of the WGSR system.
- The WGSR kinetics can be represented in the forms of: (1) macrokinetic

and (2) microkinetic. Meanwhile, the reactor modelling approaches can be broadly divided into:

a) Homogeneous - both the solid catalyst and gas phases are lumped into one single phase (pseudo-homogeneous).

b) Heterogeneous - two different phases are considered, i.e., solid catalyst and gaseous phases.

- The most effective and reliable reactor models are:

a) Model 1A with reduced microkinetic model - less computational effort (i.e., less ODEs) and the mass and heat transfer limitation is taken into account via the microkinetic model.

b) Model 1B with macrokinetics model - takes into account of mass transfer limitation via Thiele modulus. Ease in computational effort due to less complex model.

c) Model 1C with macrokinetics model - takes into account mass and heat transfer limitation via two phases simulation (i.e., solid and gaseous phases). Less computational effort due to simple macrokinetic model.

In view that very limited info on limitation of microkinetic model for most catalysts, it is recommended to use macrokinetics model in WGSR system modelling.

- The work reported in this chapter has been published in Procedia Engineering 2016. [1]

[1] Comparative Study of Homogeneous and Heterogeneous Modelling of Water-Gas Shift Reaction with Macro-or Micro-kinetics. *Procedia Engineering* 148: 949-956.

Chapter 5

Modelling of Water-Gas Shift Reaction Membrane Reactor (WGSR-MR)

5.1 Overview

This chapter provides detailed modelling of the heterogeneous membrane reactor - Model 1C previously encountered in Chapter 4. This model is adopted in this further study due to its high accuracy and consistency in predicting reactor behaviour. Since the structure of the membrane reactor consists of a number of small tubes, this results in the temperature and concentration changes in radial direction being insignificant compared to those in axial direction. In this chapter, a one-dimensional (1D) model is proposed for the membrane reactor modelling based on non-ideal conditions where gas properties (e.g., density, viscosity and thermal conductivity), membrane permeance and reaction kinetics are dependent on pressure and temperature changes. In a membrane reactor, the operating pressure and temperature vary along the reactor. Thus, it is impractical for the above-mentioned properties to be assumed constant along the membrane reactor. The incorporation of these non-ideal properties in the model has made the model prediction more robust. It is discovered that the model developed in this study has a very comparable accuracy with a 2D model. The rest of this chapter is organized as follows. Section 5.2 and 5.3 discuss in detailed of the modelling assumptions that govern this model and the solid/catalyst and gas phase mass-energy balance equations respectively. Meanwhile, section 5.4 covers the model validation of the developed 1D heterogeneous membrane reactor model.

5.2 Membrane Reactor Modelling

Heterogeneous reactor modelling takes into account both solid and gaseous phase changes directly without the need of incorporating the correction factor for the heat-mass transfer limitation (Thiele modulus). Furthermore, the macrokinetic model is used in this modelling because of data is readily available for this kinetics.

5.2.1 Model assumptions

The assumptions used in modelling the membrane reactor are given as follows:

a) A membrane reactor with multiple small tubes where the catalyst pellets are packed outside the tubes, i.e., in the shell side; see Figure 5.2.

b) The surface of the tube wall is made up of a thin layered membrane.

c) Sweep gas is allowed to flow inside the tube side to reduce the H_2 partial pressure. H_2 sweep gas is used to enhance the purity of hydrogen produced without the aid of an external purification.

d) Only the axial temperature change is taken into account. Radial temperature change is neglected because the diameter of the membrane reactor is small and adiabatic (no heat loss from the surface of the reactor) (Aboudheir et al., 2006); see Figure 5.1.

e) Gas properties, membrane permeance and reaction kinetics are assumed to depend on temperature and/or pressure.

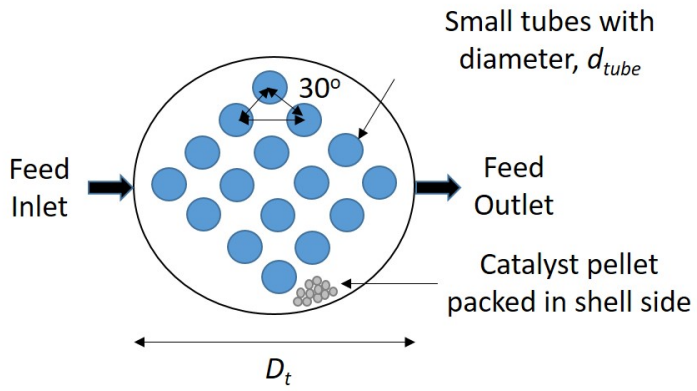

Figure 5.1: Cross-sectional diagram of the packed bed tubular membrane reactor.

All the assumptions are made based on few literature studies; see Morpeth et al. (2015), Battersby et al. (2010), and Augustine et al. (2011) with the exception of temperature dependence properties. In most reported works, the membrane reactor modelling is based on ideal conditions. In this study, however, all of the properties of gas, membrane and kinetics are simulated based on non-ideal conditions, hence they are dependent on pressure and temperature changes. For an example, the density of gas can fluctuates up to 10 times within the studied ranges of pressure and temperature (Francesconi et al., 2007). In the membrane reactor, the operating pressure and temperature vary along the reactor. Thus, properties such as density of gas should not be assumed constant along the membrane reactor. Similar to the modelling of packed bed reactor in Chapter 4, the membrane reactor is sub-divided into 10 equal volume where each segment is represented by a set of ODEs.

5.3 Membrane Reactor Mass-Energy Balance Equations

5.3.1 Gas phase model equations

Gas phase species balances

For the feed or retentate gas phase outside the catalyst pellets (i.e., inside the tubes), the species mass balances are given as Fogler (1999).

$$\begin{aligned} \epsilon V_j \frac{dC_{i,j}}{dt} =& F_{in}C_{i,j-1} - F_{out}C_{i,j} \\ &+ \nu_i k_{c,i,j} a V \Delta C_{i,j} - Q_{i,j} \qquad j = 1, 2...n \end{aligned} \tag{5.1}$$

where F_{in} and F_{out} (m^3/hr) represents the volumetric flow rates of the feed inlet and outlet respectively. V_j (m^3) the volume of the sub-division reactor at the j^{th} sub-segment − see Figure 5.2, ϵ the bed voidage factor, ν_i the stoichiometric coefficient of species i (-1 for CO and H_2O and +1 for CO_2 and H_2), $C_{i,j}$ (mol/m^3) the molar concentration of species i at the j^{th} sub-segment, a (m^2/m^3) the total catalyst surface area per unit volume, $k_{c,i,j}$ the mass transfer coefficient between the catalyst surface and the bulk gas phase and t (hr) the time of the reaction.

Here, $\Delta C_{i,j}$ (mol/m^3) represents the concentration difference between the catalyst surface and the gas bulk phase, defined as:

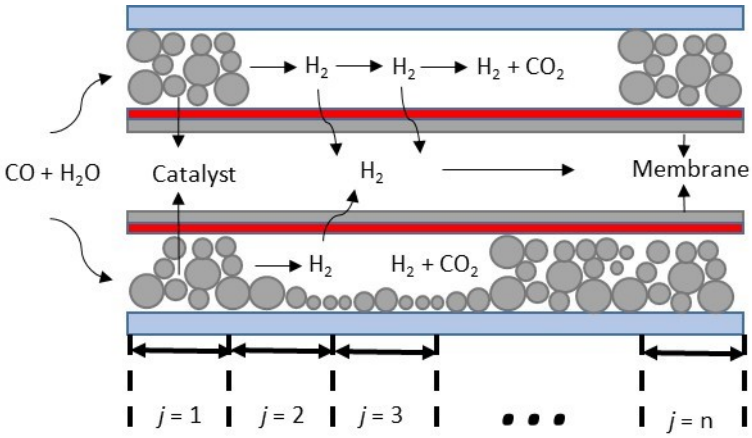

Figure 5.2: Small cross-section of membrane reactor.

$$\Delta C_{i,j} = C_{i,j,surf} - C_{i,j} \tag{5.2}$$

where $C_{i,j,surf}$ is the concentration of species i at the catalyst surface. The parameters of a_v and ϵ are both estimated using equations 5.3 and 5.4 respectively:

$$a_v = 6(1-\epsilon)/D_{cat} \tag{5.3}$$

$$\epsilon = 0.38 + 0.073\left(1 - \frac{(D_{rct}/D_{cat} - 2)^2}{(D_{rct}/D_{cat})^2}\right) \tag{5.4}$$

where D_{cat} (m) is the diameter of catalyst pellet and D_{rct} (m) is the diameter of reactor (shell diameter).

The permeate (inside the tubes) side, the species mass balances are as follow:

$$V_{p,j}\frac{dC_{i,p,j}}{dt} = F_{p,in}C_{i,p,j-1} - F_{p,out}C_{i,p,j} + Q_{i,j} \tag{5.5}$$

where $F_{p,in}$ and $F_{p,out}$ (m^3/hr) denotes the volumetric flow rates of the sweep gas inlet and outlet respectively. $V_{p,j}$ (m^3) the sub-division volume of permeate at the j^{th} sub-section, $C_{i,p,j}$ (mol/m^3) the molar concentration of species i in permeate at the j^{th} sub-section, and $Q_{i,j}$ (mol/hr) the molar flow rate in the permeate side at the j^{th} sub-section. $Q_{i,j}$ is defined as:

$$Q_{i,j} = A_{surf}V_p\frac{Q_m}{\delta_m}exp\left(\frac{-E_d}{RT_{r,j}}\right)\left(P_{r,j}^{0.5} - P_{p,j}^{0.5}\right) \tag{5.6}$$

where, A_{surf} (m^2) is the sub-division surface area of the membrane, δ_m (m) is the thickness of the membrane, E_d (J/mol) is the activation energy for diffusion through membrane, Q_m (mol/m.hr.$Pa^{0.5}$) is the permeance of component i, R (J/mol.K) is the gas constant, $T_{r,j}$ (K) is the retentate temperature while $P_{r,j}$ and $P_{p,j}$ (Pa) are the retentate and permeate pressure, respectively. All the parameter values are obtained from Koc et al. (2012).

Gas phase momentum balance

The dynamic momentum balance for the gas phase is as in Wilkes (2006):

$$\frac{dP_j}{dz} = \frac{G^2}{\rho_g D_{cat}} \frac{1-\epsilon}{\epsilon^3} \left(1.75 + 4.2 \frac{1-\epsilon}{Re^{1/6}}\right) \tag{5.7}$$

where P_j (Pa) is the pressure drop at j^{th} section (Note that this pressure drop equation applies to both permeate and retentate). Here, ρ_g (kg/m^3) is the density of air and Re is dimensionless Reynolds number. G (m/hr) is the molar flux given as:

$$G = \frac{4F_0}{\pi D_{rct}^2 \epsilon} \tag{5.8}$$

where F_0 (m^3/hr) represents total feed flow rate for the retentate side and total sweep gas flow rate for the permeate side.

Gas phase energy balance

In the gas phase, the energy balance equation on the retentate side is expressed as follows:

$$\begin{aligned}((1-\epsilon)\rho_s C_{p,s} V + \epsilon \rho_g C_{p,g} V)\frac{dT_{r,j}}{dt} =& F_{in} C_{p,g,in} \rho_g T_{r,j-1} \\ &- F_{out} C_{p,g,out} \rho_g T_{r,j} \\ &- Q_{i,j} MW_i C_{p,i} (T_{r,j} - T_{p,j}) \\ &- U_0 A_{surf} (T_{r,j} - T_{p,j}) \\ &+ h_f a V (T_{r,j,surf} - T_{r,j}) \\ &+ a_v \sum_{i=1}^{N_s} k_{c,i,j} (H_{i,j,surf} - H_{i,j}) \\ &\times (C_{i,j,surf} - C_{i,j})\end{aligned} \tag{5.9}$$

where ρ_s (kg/m^3) represents the catalyst bulk density, $C_{p,s}$ and $C_{p,g}$ (kJ/kg.K) the specific heat capacity for solid catalyst and gas phase respectively, U_0 (W/m^2.K) the heat transfer coefficient between membrane wall and bulk gas phase in permeate and retentate, MW_i (g/gmol) the average molecular weight of the permeate species, h_f (W/m^2.K) the heat transfer coefficient between the catalyst surface and bulk gas phase in retentate, $T_{r,j,surf}$ (K) the catalyst temperature at the surface and $T_{r,j}$ (K) represents the retentate temperature at j^{th} section. Here, $H_{i,j,surf}$ and $H_{i,j}$ (kJ/mol) are the enthalpies at the catalyst surface and bulk gas of species i respectively. The enthalpies are added into the equation to include the entropy changes of the transfer medium. $H_{i,j}$ is defined as:

$$H_{i,j} = \Delta H^f_{298} + \int_{298}^{T_{r,j}} C_{p,i}(T)dT + \Delta H_v \tag{5.10}$$

where ΔH^f_{298} and ΔH_v (kJ/mol) are the heat of formation and heat of vaporization for each species i, respectively. Note that, the heat of vaporization term is only applicable for species that undergoes phase change during reaction. The heats of formation of CO, H_2O and CO_2 are -110.5, -241.9, and -393.5 kJ/mol, respectively (Lide, 2009). The heat of formation of H_2 is zero by definition.

On the permeate side, the energy balance is given by:

$$\begin{aligned}\rho_p C_{p,p} V_p \left(\frac{dT_{p,j}}{dt}\right) =& F_{p,in} C_{p,p,in} \rho_{p,in} T_{p,in,j-1} \\ &- F_{p,out} C_{p,p,out} \rho_{p,out} T_{p,j} \\ &+ Q_{i,j} MW_i C_{p,i} (T_{r,j} - T_{p,j}) \\ &+ U_0 A_{surf} (T_{r,j} - T_{p,j})\end{aligned} \tag{5.11}$$

where $\rho_{p,in}$ and $\rho_{p,out}$ (kg/m^3) are the density of permeate flow rates in the inlet and outlet respectively, $C_{p,p,in}$ and $C_{p,p,out}$ (kJ/kg.K) are the specific heat capacities for the inlet and outlet of permeate side respectively and $T_{p,j}$ (K) is the permeate temperature at j^{th} section.

Gas phase boundary conditions

For retentate side, the inlet boundary conditions ($j = 0$) are given as:

$$T_{r,j} = T_{in} \tag{5.12}$$

$$C_{i,j} = C_{i,in} \tag{5.13}$$

$$P_{r,j} = P_{r,in} \tag{5.14}$$

and for permeate side:

$$T_{p,j} = T_{p,in} \tag{5.15}$$

$$C_{i,p,j} = C_{i,p,in} \tag{5.16}$$

$$P_{p,j} = P_{p,in} \tag{5.17}$$

where, T_{in} (K) is the inlet retentate temperature of the gas before entering the MR, $C_{i,in}$ (mol/hr) is the initial inlet retentate concentration at the starting of the MR and $P_{r,in}$ (Pa) is the initial retentate pressure in MR. Meanwhile, $T_{p,in}$ (K), $C_{i,p,in}$ (mol/hr) and $P_{p,in}$ (Pa) are the initial permeate temperature, concentration and pressure respectively.

5.3.2 Solid phase mass-energy balance equations

Solid/catalyst phase species balances

The species mass balances for the catalyst phase are modelled as a homogeneous mixture of two phases: (1) the solid catalyst phase and (2) the gas in the pores. It is assumed that, the reaction takes place inside the catalyst pores only and the degradation of the solid catalyst is negligible. Detailed explanation of the species mass balance can be found in Chapter 4 - refer to Section 4.4.2. The species concentrations inside the catalyst pores are modelled as a function of catalyst radius, r. The dynamic mass balance of a species i inside the catalyst pores is given as:

$$\frac{d}{dr}\left(D_{i,m} r^2 \frac{dC_{c,i,j}}{dr}\right) = -r_i r^2 \tag{5.18}$$

By solving the double differentiation in equation 5.18, the surface concentration of the catalyst pellet can be calculated and used in the equation 5.2.

Solid/catalyst phase energy balance

The temperature change occurring inside the catalyst pellet can be modelled by using catalyst energy balance. The detailed description of the catalyst energy

balance can be found in Chapter 4, Section 4.4.2. Due to the small pellet size, it is also assumed that the thermal conductivity of the catalyst is constant throughout the radius r. Therefore, the energy balance for the solidphase in a catalyst pellet becomes:

$$\frac{d}{dr}\left(\frac{2\lambda_{cat}T_{cat}+\theta D_{i,m}\frac{\partial C_{c,i,j}}{\partial r}C_{p,i}+\lambda_{cat}r\frac{\partial T_{cat,j}}{\partial r}}{(1-\theta)\rho_{cat}C_{p,cat}+\theta\sum_{i}^{N_s}C_{p,i}C_{c,i,j}}\right)=0 \tag{5.19}$$

By using *ode* solver in $Matlab$ software to solve equation 5.19, the temperature of the catalyst surface is obtained. This value is transferred to the reactor model shown in the equation 5.9.

Solid/catalyst phase boundary conditions

Note that, the boundary condition for catalyst pellet is only used in the heterogeneous model. For a catalyst pellet, it is assumed that the boundary conditions at the centre ($r = 0$) at any point of j^{th} section of the reactor is given by:

$$\frac{dC_{i,j}}{dz}(z, r=0)=0 \tag{5.20}$$

$$\frac{dT_{cat,j}}{dz}(z, r=0)=0 \tag{5.21}$$

As for the boundary conditions at the surface of the catalyst pellet ($r = R$), where $R = 0.5D_{cat}$, the flux conditions are assumed to be:

$$k_{c,i,j}(C_{i,j}(z, r=R)-C_{i,j}(z))=-D_{i,m}\frac{\partial C_{i,j}}{\partial r}(z, r=R) \tag{5.22}$$

$$\begin{aligned} h_f(T_{cat,j}(z, r=R)-T_{r,j}(z))+\sum_{i}^{N_s}H_i(z) & \\ \times k_{c,i,j}(C_{i,j}(z, r=R)-C_{i,j}(z))= & -\lambda_{cat}\frac{\partial T_{cat,j}}{\partial r}(z, r=R) \\ & -\sum_{i}^{N_s}H_{i,j}(z, r=R) \\ & \times D_{i,m}\frac{\partial C_{i,j}}{\partial r}(z, r=R) \end{aligned} \tag{5.23}$$

Equations 5.20 - 5.23 are the boundary conditions required in order to correctly predict the behaviour of the membrane reactor (MR). Without proper boundary conditions, there is a possibility of over-prediction in the calculated

performance of MR. All the aforementioned boundary conditions are obtained from Adams and Barton (2009).

5.3.3 Other correlations equations

In order to develop a model that is applicable to wide ranges of pressures and temperatures, most of the physical properties and transfer coefficients should not be assumed constant values, especially in the bulk gas phase of the reactor as gas properties are highly dependent on temperature. Therefore, some gas property correlations are included to model the non-ideal conditions.

Density of gases

The density of gas depends on pressure and temperature due to the effect arising from an interaction between gas particles. Therefore, to precisely predict the non-ideal gas density, an equation of state is used. The equation of state can be applied to either vapour-liquid or supercritical phenomena. Many equations of state have been proposed in the literature which can be categorized into either an empirical, or semi-empirical or theoretical type. Some comprehensive reviews on the equations of state can be found in the works of Martin (1979), Gubbins et al. (1983),Economou and Donohue (1996), Wei and Sadus (2000), and Sengers et al. (2000).

In this research, the Peng-Robinson equation of state is used, since it can produce a relatively accurate, non-iterative and computationally efficient correlation for high-pressure fluid mixtures (Harstad et al., 1997). Furthermore, it has been found to be more effective in calculating density for carbon-based molecules (Zhao and Olesik, 1999). In a general state equation, the pressure (P_g) is related to the temperature (T), ideal gas constant (R) and molar volume (V) via:

$$P_g = \frac{RT}{V-b} - \frac{a(T)}{V^2 + 2bV - b^2} \tag{5.24}$$

Equation 5.24 has two pure component parameters a and b. The parameter a represents a measure of the attractive forces between the molecules, and b is related to the size of the molecules. Peng and Robinson (1976) redefined $a(T)$ as:

$$a(T) = (1 + \kappa(1 - \sqrt{T}_{cr}))^2 a_c \tag{5.25}$$

$$a_c = 0.45724 \frac{R^2 T_{cr}^2}{P_{cr}} \tag{5.26}$$

$$b = 0.07780\frac{RT_{cr}}{P_{cr}} \tag{5.27}$$

and κ is a dimensionless parameter such that

$$\kappa = 0.37464 + 1.54226\omega - 0.26992\omega^2, \qquad if\omega \leq 0.49 \tag{5.28}$$

$$\kappa = 0.379642 + 1.48503\omega - 0.164423\omega^2 + 0.016666\omega^3, \qquad otherwise \tag{5.29}$$

where ω is the acentric factor, T_{cr} (K) is the critical temperature and P_{cr} (Pa) is the critical pressure. All the values needed for each gaseous component can be obtained from Poling et al. (2001).

It is important to note that the equations 5.24 - 5.26, are only applicable to pure component parameters. This is not appropriate in the present research whereby there is interaction between different molecules. Consequently, some mixing rules are required to calculate the mixing component parameters of a and b.

The parameters of Peng-Robinson equation for the mixture of N simple fluids where the molar percent of the i^{th} component is y_i defined by mixing rules:

$$a_{c,m} = \sum_{i=1}^{N}\sum_{I=1}^{N} y_i y_I a_{c,iI} \tag{5.30}$$

$$b_m = \sum_{i=1}^{N} y_i b_i \tag{5.31}$$

Here b_i is calculated from equation 5.27 based on the pure component species i, y_i is the mole fraction of species i, y_I represents the mole fraction of species I. Species $i \neq I$, for example, if species i is CO then species I is any other species (H_2O, CO_2, H_2). Meanwhile a_{iI} is expressed through empirically determined binary interaction coefficient δ_{iI} characterizing the binary mixture of components i and I:

$$a_{c,iI} = (1 - \delta_{iI})\sqrt{a_{c,i}a_{c,I}} \tag{5.32}$$

where a_i and a_I can be obtained using Equation 5.26. Some δ_{iI} are tabulated (e.g. Table 4.2 in Pedersen et al. (2014)). For values which are not tabulated, the formula of Chueh and Prausnitz (1967) could be used:

$$1 - \delta_{iI} = \left[\frac{2V_{cr,i}^{\frac{1}{6}} V_{cr,I}^{\frac{1}{6}}}{V_{cr,i}^{\frac{1}{3}} + V_{cr,I}^{\frac{1}{3}}} \right] \tag{5.33}$$

where V_{cr} (m^3) is the critical volume for pure component i and component I. All the required values for the density calculation are tabulated in Table A.1 in Appendix A. By solving equations 5.30 - 5.33, the binary mixture parameters $a_{c,m}$ and b_m can be obtained and then substituted into the respective terms ($a(T)$ and b) in equation 5.24 to calculate the real gas density.

Equation 5.24 can be rearranged to form:

$$Z^3 + (B-1)Z^2 + (A - 2B - 3B^2)Z + (B^3 + B^2 - AB) = 0 \tag{5.34}$$

where

$$A = \frac{a(T)P}{R^2T^2} \tag{5.35}$$

$$B = \frac{bP}{RT} \tag{5.36}$$

By using *fsolve* function in *Matlab* software to solve equation 5.34, the compressibility factor, Z can be obtained. Upon obtaining Z, the density of the gas can be calculated from equation 5.37.

$$Z = \frac{P}{\rho RT} \tag{5.37}$$

Binary diffusivity

Inside the catalyst pores, it has been known that the bulk diffusivity is affected by the shape, size and nature of the pores. The effective binary gas diffusivity inside a pore can be approximated by:

$$D_{eff,iI} = D_{iI}\theta/\tau \tag{5.38}$$

where $D_{eff,iI}$ is the effective diffusivity of two species, i and I. For example, if species i is H_2O then species I will be either CO, CO_2 or H_2. Meanwhile, τ is the tortuosity of the catalyst pore, which is an approximate measure of how the wall interaction slow down the diffusion inside the catalyst and D_{ij} is the binary gas diffusivity for a pair of components i and I. The corresponding data and calculation for each pair of components are tabulated in Table A.2 in Appendix A.

Diffusion in a multispecies mixture is often complex and most of the correlations involved are often unavailable. Fortunately, the gas diffusion can be approximated by Green et al. (2008).

$$D_{i,m} = \frac{1 - y_i}{\sum_{j \neq i}^{N} y_I / D_{eff,iI}} \tag{5.39}$$

where $D_{i,m}$ is the effective diffusivity of the species i in the mixture, and y_I is the mole fraction of the species I.

Specific heat capacities

The heat capacity of gas is often a function of temperature. Hence, it is not advisable to assume a constant value of heat capacity. The specific heat capacity of gas phase is calculated as a function of temperature:

$$C_{p,i} = A_{cp} + B_{cp}T + C_{cp}T^2 + D_{cp}/T^2 \tag{5.40}$$

where A_{cp}, B_{cp}, C_{cp} and D_{cp} are the gas phase heat capacity constants for selected species. The values for these constants are shown in Table A.3 in Appendix A.

As for the mixture of gases, the specific heat capacity is taken to be the molar average of individual heat capacity:

$$C_{p,g} = \sum_{i=1}^{N} y_i C_{p,i} \tag{5.41}$$

Gas phase viscosity

Viscosity describes a fluid's internal resistance to flow and may be thought of as a measure of fluid friction. All real fluids (except superfluids) have some resistances to stress leading to viscous fluids (Brush, 1962). Upon raising of temperature, the viscosity of gas increases. In addition, viscosity has a direct effect on the pressure drop as shown in equation 5.7. Hence, it is not recommended to use average or constant value for the gas viscosity. The gas viscosity for each species is calculated by:

$$\mu_i = \frac{A_{vis}T^{B_{vis}}}{1 + (C_{vis}/T) + (D_{vis}/T^2)} \tag{5.42}$$

where A_{vis}, B_{vis}, C_{vis} and D_{vis} are the gas phase viscosity constants for selected species i. The values for these constants are shown in Table A.4 in Appendix A.

The viscosity of the mixture of gases is estimated by Francesconi et al. (2007):

$$\mu = \sum_{i=1}^{N} \frac{y_i \mu_i}{\sum_{I=1}^{N} y_I \sqrt{MW_I/MW_i}} \tag{5.43}$$

where μ (N.s/m^2) is the mixture viscosity, μ_i (N.s/m^2) is the viscosity of species i, and MW_i and MW_I is the molecular weight of species i and I.

Thermal conductivity of the gas phase

The calculation of the thermal conductivity is given as:

$$\lambda' = \sum_{i=1}^{N} \frac{y_i \lambda_i}{\sum_{I=1}^{N} y_I A_{iI}} \tag{5.44}$$

where λ_i (kcal/h.m.K) is the gas phase thermal conductivity for species i where the calculation is shown in equation 5.45. Notice that A_{iI} is the binary interaction parameters which can be calculated by using the Sutherlands model:

$$\lambda_i = \frac{A_{lam} T^{B_{lam}}}{1 + (C_{lam}/T) + (D_{lam}/T^2)} \tag{5.45}$$

where A_{lam}, B_{lam}, C_{lam} and D_{lam} are the gas phase thermal conductivity constants for selected species i, respectively. The values for these constants are shown in Table A.5 in Appendix A.

$$A_{iI} = \frac{1}{4} \left[1 + \left[\frac{\mu_i}{\mu_I} \left(\frac{MW_I}{MW_i} \right)^{\frac{3}{4}} \frac{1 + \frac{S_i}{T}}{1 + \frac{S_I}{T}} \right]^{\frac{1}{2}} \right]^2 \frac{\left(1 + \frac{S_{iI}}{T}\right)}{\left(1 + \frac{S_i}{T}\right)} \tag{5.46}$$

where S_i and S_I is the Sutherland constants for species i and I. Except for the hydrogen, deuterium, and helium which have fixed values of Sutherland constants given by Lindsay and Bromley (1950), the Sutherland constants of other pure gases are taken as:

$$S_i = 1.5 T_B \tag{5.47}$$

where T_B (K) is the boiling point of species i at one atmospheric pressure. This assumption creates an error of 20% in the Sutherland constant but this only affects the calculated mixture conductivity by 1%. Hence the simplification is justified.

For the collision of unlike molecules, the Sutherland constant S_{iI} may be taken as the geometric mean in all cases except for the case where one of the molecules has a strong dipole moment. In the latter case, the procedure proposed by Gruss and Schmick (1928) is followed where geometric mean is multiplied by 0.733. Thus,

$$S_{iI} = \sqrt{S_i S_I} \tag{5.48}$$

otherwise, when one constituent has strong polarity, then

$$S_{iI} = 0.733\sqrt{S_i S_I} \tag{5.49}$$

This latter equation 5.49 is used for a mixture containing steam or ammonia.

The thermal conductivity is also often given as a function of pressure. For the thermal conductivity estimation, Stiel and Thodos (1964) had established the approximate analytical expressions for the bulk mixture at above atmospheric pressure, given as:

$$(\lambda_{cat} - \lambda')\Gamma Z_{cm}^5 = 1.22 \times 10^{-2}[\exp(0.535\rho_{cr}) - 1] \qquad \text{if}\, \rho_{cr} < 0.5 \tag{5.50}$$

$$(\lambda_{cat} - \lambda')\Gamma Z_{cm}^5 = 1.14 \times 10^{-2}[\exp(0.67\rho_{cr}) - 1.069] \qquad \text{if}\, 0.5 \leq \rho_{cr} < 2.0 \tag{5.51}$$

$$(\lambda_{cat} - \lambda')\Gamma Z_{cm}^5 = 2.60 \times 10^{-3}[\exp(1.155\rho_{cr}) + 2.016] \qquad \text{if}\, 2.0 \leq \rho_{cr} < 2.8 \tag{5.52}$$

where λ_{cat} (W/m.K) is the bulk mixture thermal conductivity at above atmospheric pressure, Z_{cm} is the mixture critical compressiblility, ρ_{cr} is the reduced density and Γ (m.K/W) is the reduced, inverse thermal conductivity.

$$Z_{cm} = 0.291 - \omega_m \tag{5.53}$$

where ω_m is the mixture acentric factor and can be obtained via:

$$\omega_m = \sum_{i=1}^{N} \omega_i \tag{5.54}$$

where ω_i is the acentric factor of an individual species i which the values can be obtained in Table A.1 in Appendix A.

Meanwhile, the reduced pressure is given as follows:

$$\rho_{cr} = \frac{\rho}{\rho_c} = \frac{V_c}{V} \tag{5.55}$$

where ρ (kg/m^3) is the bulk gas mixture density, ρ_c (kg/m^3) is the critical pressure of bulk gas, V (m^3) is the volume of the gas and V_c (m^3) is the critical volume of gas.

The reduced thermal conductivity relation was developed by Roy and Thodos (1968), and Roy and Thodos (1970) and it is expressed as

$$\Gamma = 210 \left(\frac{T_{crm} MW_m}{P_{crm}^4} \right)^{\frac{1}{6}} \tag{5.56}$$

where T_{crm} (K) is the mixture gases critical temperature, MW_m (mol/g) is the mixture molecular weight and P_{crm} (bars) is the mixture critical pressure. The following equations are required in equation 5.56.

$$MW_m = \sum_{i=1}^{N} y_i MW_i \tag{5.57}$$

$$T_{crm} = \frac{\sum_{i=1}^{N} \sum_{I=1}^{N} y_i y_I V_{ciI} T_{ciI}}{V_{crm}} \tag{5.58}$$

where T_{ciI} (K) and V_{ciI} (m^3) are critical temperature and critical volume of species i and I respectively. The V_{crm} (m^3) is the mixture critical volume.

$$V_{ciI} = \frac{\left[\left(V_{ci}^{1/3} + V_{cI}^{1/3} \right) \right]^3}{8} \tag{5.59}$$

$$T_{ciI} = (T_{ci} T_{cI})^{1/2} \tag{5.60}$$

where V_{ci}, V_{cI}, T_{ci} and T_{cI} are the critical volumes and critical temperatures of each species i and I individually. As for the mixture critical volume,

$$V_{crm} = \sum_{i=1}^{N} \sum_{I=1}^{N} y_i y_I C_{iI} \tag{5.61}$$

The mixture critical pressure is represent by:

$$P_{crm} = \frac{Z_{cm} R T_{crm}}{V_{crm}} \tag{5.62}$$

Mass transfer coefficient

The mass transfer coefficient between the bulk gas phase and the catalyst surface can be estimated using the relation in Poling et al. (2001):

$$k_{c,i,j} = 0.357 \left(\frac{\rho MW_m D_{i,m}}{\mu} \right)^{2/3} \left(\frac{G}{\rho MW_m \epsilon_b} \right) \left(\frac{\mu}{D_{cat} G} \right)^{0.359} \tag{5.63}$$

Heat transfer coefficient

The temperatures of both reaction (retentate) and sweep gas (permeate) sides are affected by the heat of reaction in addition to both conductive and convective heat transfer across the membrane. The overall heat transfer coefficient U_0, is derived via the series of resistance method to include all the heat transfer mentioned above (Pabby et al., 2015).

$$\begin{aligned} \frac{1}{U_0} =& \frac{1}{h^{Shell}} + \frac{OD^{Tube}}{2k^{Mem}} \ln \left(\frac{OD^{Tube}}{ID^{Tube} + 2\delta^{Supp}} \right) \\ &+ \frac{OD^{Tube}}{2k^{Supp}} \ln \left(\frac{ID^{Tube} + 2\delta^{Supp}}{ID^{Tube}} \right) \\ &+ \frac{OD^{Tube}}{ID^{Tube}} \frac{1}{h^{Tube}} \end{aligned} \tag{5.64}$$

where the outer areas are used as a reference for the shell and tube side. The thermal conductivity of porous support k^{Supp} is calculated as follow

$$k^{Supp} = (1 - \epsilon_{Supp}) k_s + \epsilon k_{Mix}^{Perm} \tag{5.65}$$

where k_s (J/(s.m.K)) and k_{Mix}^{Perm} (J/(s.m.K)) are the thermal conductivity of the tube material and of the gaseous mixture in the tube (permeate) side respectively. For a packed bed reactor, the heat transfer coefficient between the fluid in the bed and the walls (membrane on one side and external wall on the other) is calculated as in Markatos et al. (2005):

$$h^{Shell} = \frac{5 k_{Mix}^{Ret}}{d_p} Re_p^{0.365} \tag{5.66}$$

where

$$Re_p = \frac{\rho v d_p}{\mu} \tag{5.67}$$

where v (m/s) is velocity of gas in shell side and Re_p is the dimensionless Reynolds number. As for the tube side heat transfer coefficient, the following correlations are used (refer Markatos et al. (2005)):

$$h^{Tube} = 1.86 \frac{k_{Mix}^{Perm}}{D_{Eq}} \left(\frac{D_{Eq}}{l^{Mem}} RePr \right)^{1/3} \tag{5.68}$$

$$h^{Tube} = 0.027 \frac{k_{Mix}^{Perm}}{D_{Eq}} Re^{0.8} Pr^{1/3} \tag{5.69}$$

where D_{Eq} (m) is equivalent diameter and Pr is dimensionless Prandtl number. Equation 5.68 is only applicable to laminar flow while equation 5.69 is applicable to turbulent flow. For flow in a circular pipe, when $Re > 4000$, the flow is considered to be turbulent flow.

5.4 Model Validations

The model developed in this study is validated by using two cases. It should be noted that, the model validation is based on experimental data from the literature for WGSR in a membrane reactor where Pd-based membrane was used.

5.4.1 Case study 1: Data and specifications

All the data and specifications are obtained from Sanz et al. (2015). The data from this literature is chosen because in this study, the type of membrane reactor used is similar to the one reported in the literature. Furthermore, the membrane quality prepared by the aforementioned researchers showed good stability with no carbon deposition. Please note that, the carbon deposition can induce interference in membrane and promote catalyst decomposition. Tables 5.1 and 5.2 summarize the specifications used in the studied.

Table 5.1: Operating conditions and parameter values for case study 1

Parameters	**Values**
Feed inlet composition (flow rate percentage)	
Carbon monoxide (CO)	0.09
Steam (H_2O)	0.09
Carbon dioxide (CO_2)	0.12
Hydrogen (H_2)	0.7
Inlet specification (retentate)	
Inlet flow rate (m^3/h)	0.0178
Inlet temperature (K)	573.15 - 673.15
Inlet pressure (bar)	2
Inlet specification (permeate)	
Sweep gas flow rate (m^3/h)	0
Reactor dimension	
Bed length (m)	0.07
Tube external radius (m)	0.0129
Tube internal radius (m)	0.009

Table 5.2: Operating conditions and parameter values for case study 1 (continued)

Parameters	**Values**
Catalyst specification	
Catalyst pellet diameter (m)	0.006
Density of catalyst (kg/m^3)	1960
Catalyst reaction rate ($mol/s.kg_{cat}$)	$r_i = exp\left(8.22 - \frac{8008}{T}\right) C_{CO}^{0.54} C_{H_2O}^{0.1} \left(1 - \frac{C_{CO_2} C_{H_2}}{K_{eq} C_{CO} C_{H_2O}}\right)$
Membrane specification	
Type of membrane	Pd-composite membrane
Membrane thickness	10.2 μm
Membrane permeability	$3.96 \times 10^{-4} exp\left(-3.19 - \frac{2803}{T}\right)$

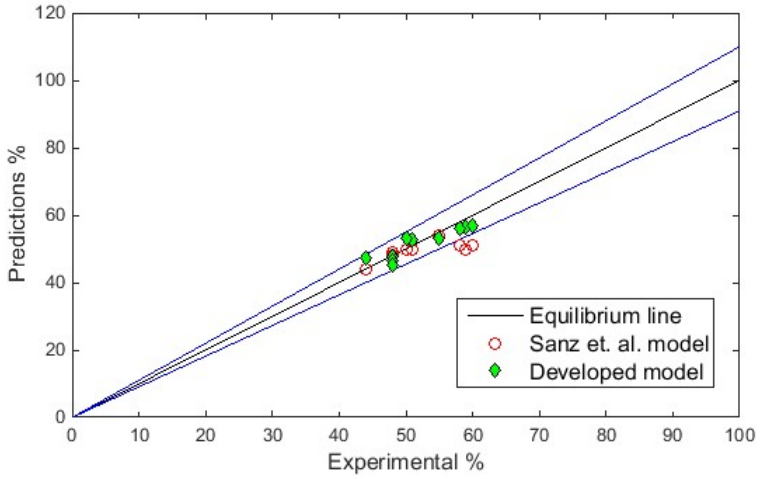

Figure 5.3: Model validation for case study 1: parity plots.

5.4.2 Case study 1: Results and discussion

In order to evaluate the validation results, Figure 5.3 shows the comparison between experimental and the simulated CO conversions. Note that, the discrepancies between experiments and simulations are in the range of $\pm$ 10% as shown by the blue line in Figure 5.3. The developed 1D heterogeneous model has slightly better accuracy compared to the model used in Sanz et al. (2015) (i.e., homogeneous reactor model). Based on the comparison done in Chapter 4, a heterogeneous reactor model has a better reactor prediction than a homogeneous reactor without heat-mass transfer limitation model.

5.4.3 Case study 2: Data and specifications

In the second model validation, the specifications are obtained from the work of Morpeth et al. (2015). This work is chosen for model validation as the experimental data published in the paper contains CO conversion data for different lengths of membrane reactor. Besides that, the membrane reactor configuration used in the aforementioned work is similar to the configuration used in this study. In addition, the above researchers conducted the experiments in an adiabatic condition that is the same as condition adopted in this study. Tables 5.3 and **??** provide all reactor design and operational specifications.

Table 5.3: Parameter values used in case study 2

Parameters	**Values**
Feed inlet composition (molar fraction)	
Carbon monoxide (CO)	0.645
Steam (H_2O)	0
Carbon dioxide (CO_2)	0.025
Hydrogen (H_2)	0.33
Inlet specification (retentate)	
Syngas flowrate (L/min)	4
Inlet temperature (°C)	350
Inlet pressure (bar)	15
Inlet specification (permeate)	
Sweep gas flow rate (m^3/h)	4
Sweep gas temperature (°C)	349.3
Sweep gas pressure (bar)	1 - 8
Reactor dimension	
Bed length (m)	0.02 - 0.78
Bed radius (m)	0.0127
Tube radius (m)	0.004975
Catalyst pellet diameter (m)	0.00216
Density of catalyst (kg/m^3)	2100
Catalyst reaction rate ($mol/s.g_{cat}$)	$r_i = 10^{0.659} exp\left(\frac{-88000}{RT}\right) P_{CO}^{0.9} P_{H_2O}^{0.31} P_{CO_2}^{-0.156} P_{H_2}^{-0.05} \left(1 - \frac{P_{CO_2} P_{H_2}}{K_{eq} P_{CO} P_{H_2O}}\right)$
Membrane specification	
Type of membrane	Pd-Ag23 wt% membrane
Membrane thickness	0.1 mm
Membrane permeability	$2.783 \times 10^{-3} exp\left(\frac{-22028}{RT}\right)$

5.4.4 Case study 2: Results and discussion

Due to some differences in model assumptions, only eleven experimental data are extracted and used for validation in this study. Morpeth et al. (2015) used a two-dimensional (2D) model for the simulation in their work, while in this study one-dimensional (1D) model is used.

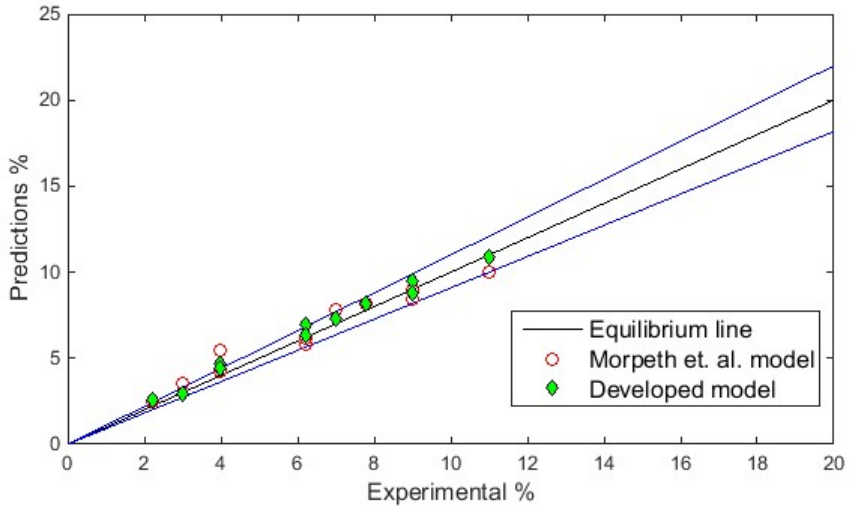

Figure 5.4: Model validation: parity plot of conversion data corresponding to literature experimental data.

Based on the Figure 5.4, it can be concluded that the 1D model developed in this study has very comparable accuracy with the 2D model developed by Morpeth et al. (2015). Both of these models have the accuracy within ± 10% deviation − blue line in Figure 5.4. Following this model validation, the 1D heterogeneous model in this study is considered reliable for simulation and control studies. It should be note that, the developed 1D model will be used in the latter section of this study.

5.5 Summary

In recent years, a number of research works have been reported on the production of hydrogen via WGSR in membrane reactors. It has been argued that the use of membrane reactor can increase hydrogen production yield because it has the capability of addressing the equilibrium limitation. This capability has resulted in the focus on developing mathematical model in order to gain better understanding of the reactor.

- A 1D heterogeneous reactor model with salient features where all properties are taken as functions of temperature and pressure, also known as non-ideal properties, has been developed. The reason for this improvement is that the pressure and temperature vary along the membrane reactor. Thus, all property values vary across the reactor.

- For simplicity and computational efficiency, the multi-tubular reactor is divided into 10 segments of equal volume. Each segment is represented by a set of ODEs. The conversion of PDEs into ODEs reduces computational time and complexity of the model simulation, while maintaining the accuracy of the model prediction.

- The 1D model has a very comparable accuracy with a 2D model of Morpeth et al. (2015). It should be noted that, the 1D model in this study has the advantage of computational efficiency over the more complex 2D model.

- It is important to note that, a computational efficiency reactor model which has both the accuracy and robustness is efficient, especially for the usage in optimization and control development stages. The validated 1D model in this chapter will be used in the subsequent parts of the study as reported in Chapters 6 - 8.

- The model presented in this chapter has been used in paper published in Computer Aided Chemical Engineering 2016. [1]

[1]Optimization of Economic and Operability Performances of Water-gas Shift Membrane Reactor. *Computer Aided Chemical Engineering*, Elsevier 38: 847-852.

Chapter 6

Economic Assessment of WGSR-MR

6.1 Overview

The heterogeneous one-dimensional membrane reactor model developed in Chapter 5 is adopted for the simulation study in this chapter. In this chapter, a few new process flowsheet designs of water-gas shift reaction in a membrane reactor (WGSR-MR) system are developed. For practicality, all process flowsheets involved include several other units in addition to the membrane reactor. The other units involved in the flowsheets are compressors and heat exchangers. Compared with most of the previous studies which focused only on the membrane reactor unit, the present study is more rigorous and practical as it addresses several interlinked units with both mass and energy recycles. Note that, these proposed flowsheets can serve as a basic guideline for the development of WGSR-MR systems. Each of the total four WGSR-MR flowsheets are evaluated on detailed economic assessment. An economic assessment of the process flowsheets of WGSR-MR system is performed via the net present value (NPV) as the economic criterion. The NPV of these flowsheets is calculated by taking into account the detailed calculations of capital and production costs. The highest NPV flowsheet is then used for future parametric economic assessment. The reason for conducting the parametric economic assessment is to identify the critical parameters affecting the flowsheets. It is important to note that, the use of these critical parameters is able to reduce the computational effort in the optimization process. The rest of this chapter is laid down as follows. Section 6.2 discusses on the designs of WGSR-MR process system flowsheets coupled with detailed economic calculation of capital

and production costs on each process flowsheet. This section identifies the main process flowsheet (highest NPV) to be used in the rest of the study. Meanwhile, section 6.3 covers the results and discussion of the parametric economic assessment. It is concluded in this section that retentate temperature, permeate and retentate pressures have significant effects on the NPV of the system under study.

6.2 WSGR-MR Network System Design

Process synthesis and development of a flowsheet usually has been carried out in a sequence of hierarchical steps. The most common design hierarchy in chemical engineering process design is known as an onion diagram (Towler and Sinnott, 2012). Note that, the reality of process development in the industry is usually more complicated than the theoretical onion diagram design. Therefore, a new approach is suggested by Towler and Sinnott (2012), which combined Douglas hierarchy (Douglas, 1988), and onion diagram. Figure 6.1 adopted from Towler and Sinnott (2012) shows the procedure used in this study to develop the candidate flowsheets. These flowsheets are evaluated based on their economic performance in order to choose the most economical flowsheet. Next, the most economical process flowsheet will be used in parametric study. Finally, the chosen process flowsheet will be used in process optimization and process control development.

6.2.1 WGSR-MR process flowsheet

Four different process flowsheets for WGSR-MR system have been developed following the procedure shown in Figure 6.1. Please note that, the scope of this study is limited to these four configurations. Bear in mind that, in reality the configurations of WGSR-MR systems are not limited to only these four flowsheets. Some of the steps in Figure 6.1 have been combined due to membrane reactor unit. For example, reaction and separation procedure are now combined into one single step. However, the overall process flowchart for the WGSR-MR system design is still based on the fundamental procedure. Figure 6.2 shows four different process flowsheets of WGSR-MR system.

Figure 6.2 (a) shows a possibility of recycling both permeate side sweep gas and also retentate product, which contains un-reacted CO and H_2O. The reason a heater is placed at the inlet of the membrane reactor is to heat up the incoming water to the same temperature as the feed syngas. A cooler is used to reduce the temperature of the inlet permeate. Both of the recycled streams experience

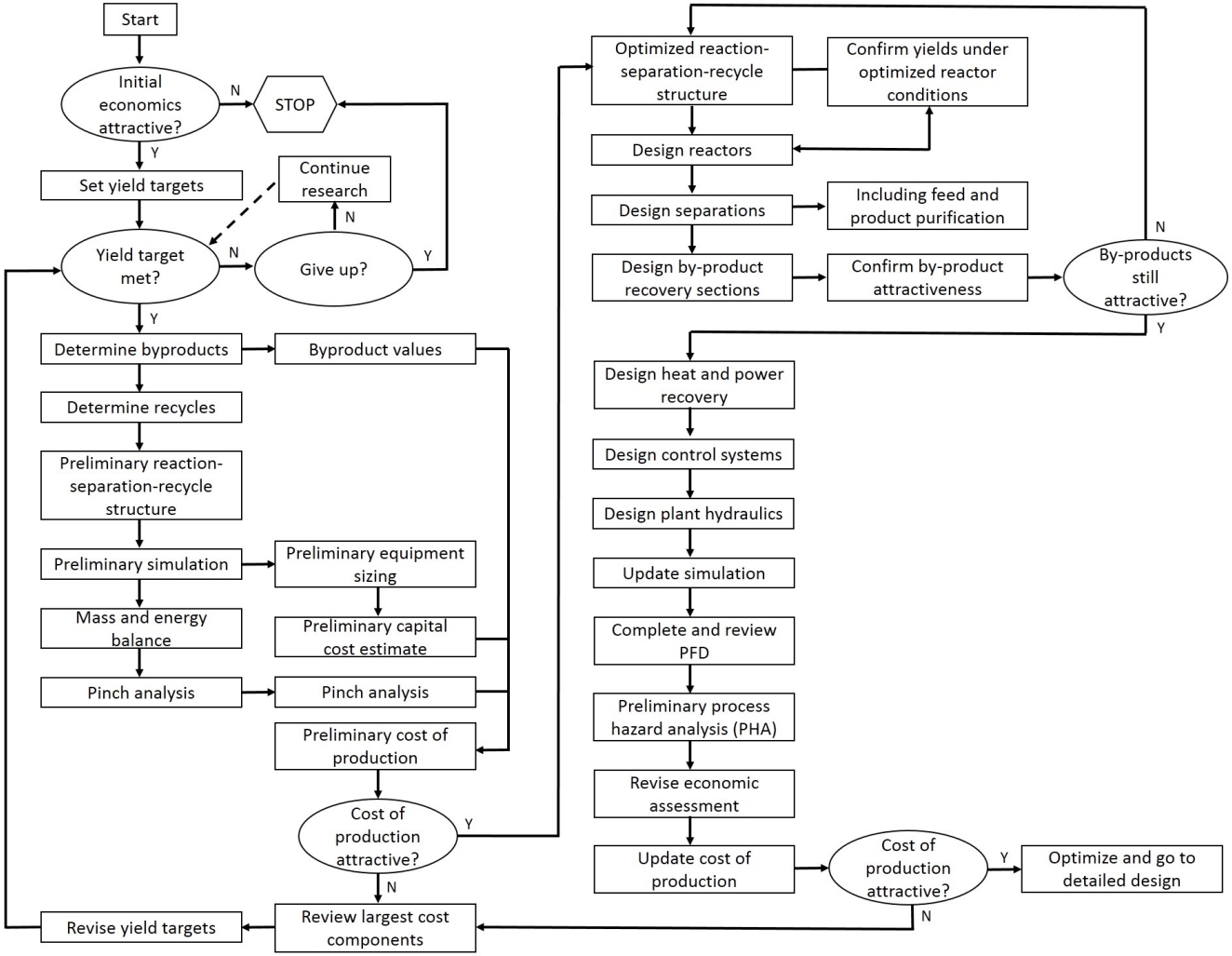

Figure 6.1: Procedure for process synthesis.

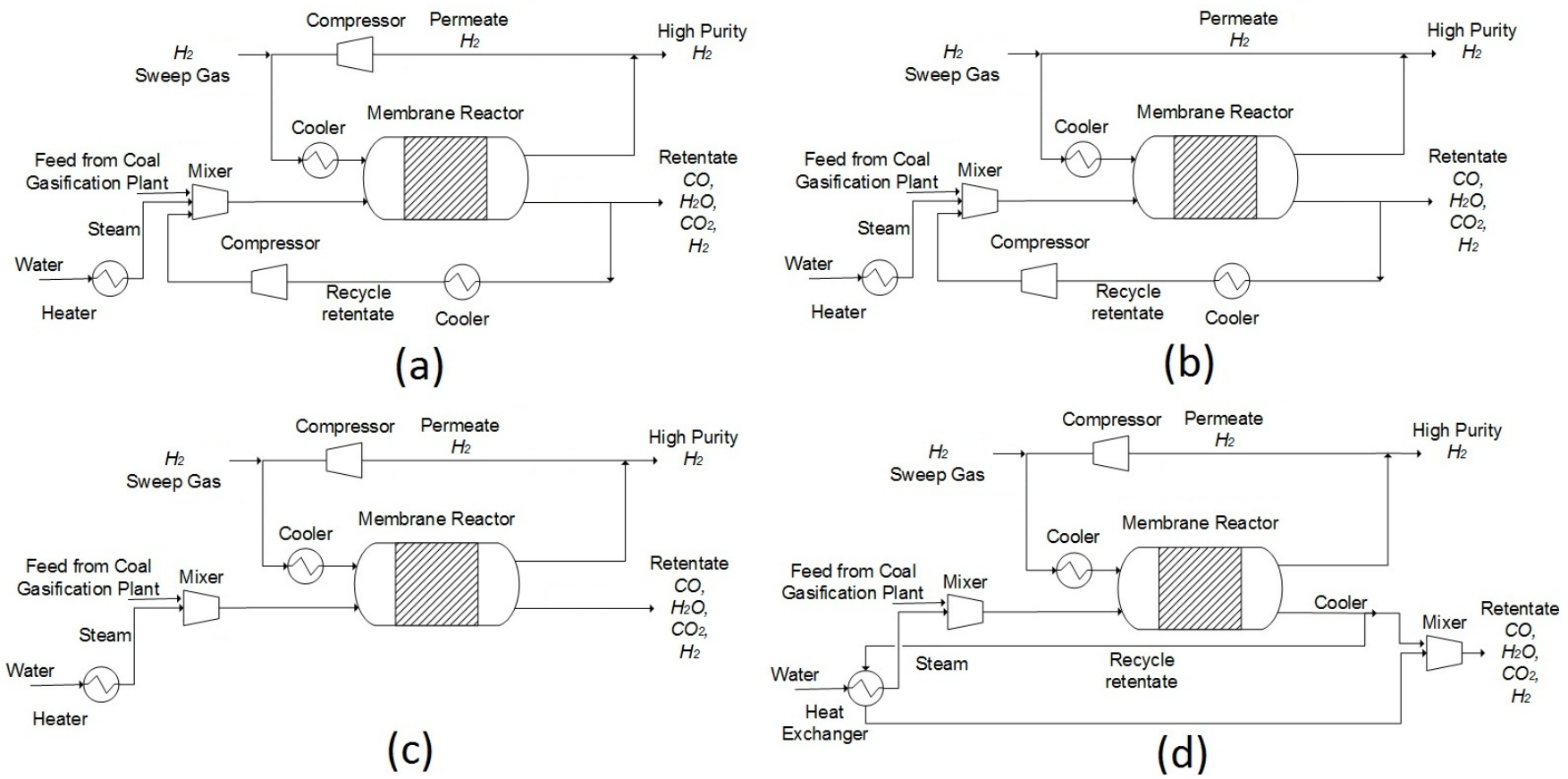

Figure 6.2: Four possible process flowsheets for WGSR-MR systems design.

temperature increases due to exothermic reaction and air compression. As for Figure 6.2 (b), this flowsheet is similar to process flowsheet shown in Figure 6.2 (a) except for the non-existence of air compressor in the permeate side.

In Figure 6.2 (c), only permeate stream is recycled back to act as permeate sweep gas. The outlet of the retentate stream is stored in a storage tank for further usage. The idea is to explore the possibility of cost saving without the addition of air compressor at the recycled retentate stream which can be seen in the flowsheets in Figure 6.2 (a) and (b). Figure 6.2 (d) has similar configuration to the design in Figure 6.2 (c) but with slight amendment in the inlet of MR. A heat exchanger is used to replace the heater in Figure 6.2 (a), (b), and (c). Due to the exothermic nature of the process, the high temperature effluent exiting the reactor acts as a heating utility in the heat exchanger.

6.2.2 Carbon capture and storage

Note that, the exit retentate stream from the membrane reactor in all the process flowsheets contain high percentage of CO_2. Hence, a proper strategy of carbon capture is needed to minimize the emission of CO_2 which have impact both socially and environmentally. Emission of carbon dioxide (CO_2) has become a major concern of society because it contributes to increase in the greenhouse gas level. So, CO_2 contributes to the risk of climate change. In 2006, the emissions of CO_2 from industry and petroleum refineries, directly and indirectly, reached 11 Gt CO_2. This has accounted for about 40% of total global emissions (Kuramochi et al., 2012). To address this issue, CO_2 capture and storage (CCS) has been recognized as a promising opportunity to reduce CO_2 emissions. Thus, CCS can mitigate global climate change together with other efforts in implementing and discovery of energy efficient technologies, renewable energies and nuclear power.

In a post-conversion capture, CO_2 is separated from the waste gas stream only after the conversion of carbon source to CO_2. This option has been applied in various industries through different post-conversion capture methods, such as absorption by chemical solvents, adsorption by solid sorbents, membranes and cryogenic separation and pressure or vacuum swing adsorption (Cuéllar-Franca and Azapagic, 2015).

Meanwhile, a pre-conversion capture involves separation of CO_2 which is produced as an undesired intermediate by-product of a conversion process. Pre-conversion capture has been mainly applied in an integrated gasification combined cycle (IGCC) power plant where CO_2 must be separated from hydrogen.

The separation technology includes absorption by physical and chemical solvents as well as by porous organic framework membranes (Cuéllar-Franca and Azapagic, 2015).

Lastly, the oxy-fuel combustion requires the combustion process in which the fossil fuel is burnt with pure or enriched oxygen. This option is expensive since it requires separation of a pure source of oxygen from air.

The CO_2 removed from the industry or utility plants is later compressed and shipped or pipelined to be stored in secure reservoirs, such as stored in underground, ocean and as a mineral carbonate (Kuramochi et al., 2012). To date, instead of CO_2 storage, the CO_2 captured can be reused as commercial products either directly in the food industry and enhanced oil recovery (EOR) or conversion into chemicals or fuels (Cuéllar-Franca and Azapagic, 2015). Recently, microalgae cultivation has been adopted as a mean to capture CO_2. The cultivated microalgae can be used for the production of biofuels.

Due to the diversity of processes in industries, various separation technologies have been developed to ensure compatibility with the need of an industrial process. Among the different types of separation technologies, chemical absorption is the most matured and preferable capture technology but it is considered moderately economical and efficient compared with some new commercially available technologies (Kuramochi et al., 2012). Currently, separation by membranes has become more attractive although most membranes are still in the development phase (Kentish et al., 2008; Kanniche and Bouallou, 2007). Membrane systems are now being explored mainly because they offer fundamental engineering and economic advantages in terms of flexibility, reliability, modularity and generally lower, or, at least, comparable requirement of energy intensity with that of the conventional absorption. Several studies have focused on the use of a membrane reactor employing a H_2 selective membrane with the incorporation of dry methanation reaction technology for the carbon capture and reuse purposes. While carbon capture, storage and reuse are not in the scope of this study, it is nevertheless important to have some detailed understanding of this proposed technology; see Appendix B.

6.2.3 Economic evaluation

A detailed economic evaluation is carried out on each of the four WGSR-MR flowsheets. Capital investment and total product costs are included in the detailed economic evaluation. The aim of this study is to choose the most economical

Table 6.1: The specifications for economic evaluation of an industrial-scale membrane reactor

Parameters specifications	**Values**
Total inlet flow rate to the MR (mol/s)	9575.2
Feed composition (%)	CO:17.25, CO_2:9, H_2:22, H_2O:51.75
Retentate temperature (^{0}C)	350
Permeate temperature (^{0}C)	450
Retentate pressure (atm)	40
Permeate pressure (atm)	7
Sweep gas to feed flow rate ratio	0.1
Concentration of H_2O to CO ratio	3.0
Length of membrane reactor (m)	9.525
Diameter of membrane reactor (m)	1.25
Diameter of membrane reactor tube (mm)	20
Diameter of catalyst particle (mm)	6
Catalyst kinetics	$r_{CO} = kP^a_{CO}P^b_{H_2O}P^c_{CO_2}P^d_{H_2}(1-\beta)$ $k = 10^{0.659\pm0.0125}\exp\left(\frac{-88\pm2.18}{RT}\right)$ $a = 0.9 \pm 0.041$ $b = 0.31 \pm 0.056$ $c = -0.156 \pm 0.078$ $d = -0.05 \pm 0.006$
Membrane permeance (m^3/[m^2.h.atm$^{0.5}$])	38.94

(highest NPV) process flowsheet. After the most economical flowsheet is identified, the optimization and control studies will be conducted on the flowsheet.

Please note that all of the flowsheets are simulated based on the conditions of an industrial-scale load specifications given in Table 6.1. Some of the process specifications are obtained from the work of (Koc et al., 2014).

Table 6.2 shows the detailed breakdowns of capital cost calculation while Table 6.3 shows the detailed breakdowns of production cost calculation for the four process flowsheets in Figure 6.2. The costs are calculated and recorded in $USD millions.

Methods used for estimating other costs such as purchased equipment, raw material and utilities are discussed in Appendix C. All data for the purchased cost is obtained from Turton et al. (2012). Since this data was obtained from a survey

Table 6.2: Capital costs for all process flowsheets (values in $USD millions)

Capital Costs	**Figure 6.2 (a)**	**Figure 6.2 (b)**	**Figure 6.2 (c)**	**Figure 6.2 (d)**
I. Direct costs				
A. Equipment + installation + instrumentation + piping + electrical + insulation + painting				
1. Purchased equipment				
a. WGS membrane reactor	55.8	55.8	55.8	55.8
b. Compressor(s)	2.31	2.31	2.31	2.31
c. Heater(s)/Cooler(s)/Heat exchanger(s)	6.14	5.72	5.72	0.59
Total purchased equipment	64.2	63.8	63.8	58.7
2. Installation (40 % of total purchased equipment)	25.7	25.5	25.5	23.5
3. Instrumentation and controls, installed (18 % of total purchased equipment)	11.6	11.5	11.5	10.6
4. Piping, installed (45 % of total purchased equipment)	28.9	28.7	28.7	26.4
5. Electrical, installed (25 % of total purchased equipment)	16.1	15.9	15.9	14.7
B. Buildings, process and auxiliary (20 % of total purchased equipment)	12.8	12.8	12.8	11.7
C. Service facilities and yard improvements (40 % of total purchased equipment)	25.7	25.5	25.5	23.5
D. Land (4 % of total purchased equipment)	2.57	2.55	2.55	2.35
Total direct costs	187.5	186.3	186.3	171.3
II. Indirect costs				
A. Engineering and supervision (17.5 % of total direct cost)	32.8	32.6	32.6	30.0
B. Construction expense and supervision (18 % of total direct cost)	33.7	33.5	33.5	30.8
C. Contingency (10 % of fixed capital investment)	28.2	28.0	28.0	25.8
Total indirect costs	94.7	94.1	94.1	86.6
III. Fixed capital investment = I + II	282.3	280.4	280.4	257.9
IV. Working capital (15 % of total capital investment)	49.8	49.5	49.5	45.5
V. Total capital investment = III + IV	332.1	329.9	329.9	303.4

Note: The cost proportions/ranges shown are commonly used for estimation of total capital investment (Koc et al., 2014).

Table 6.3: Production cost for all process flowsheets (values in $USD millions)

Production Costs	**Figure 6.2 (a)**	**Figure 6.2 (b)**	**Figure 6.2 (c)**	**Figure 6.2 (d)**
I. Manufacturing cost = A + B				
A. Direct production costs				
1. Raw materials				
a. Water	42.4	42.3	44.6	44.6
2. Operating labor (15 % of total product cost)	53.7	53.5	54.1	52.7
3. Direct supervisory and clerical labour (17.5 % of operating labour)	9.39	9.37	9.47	9.22
4. Utilities = electricity + steam + cooling water				
a. Electricity	77.9	77.9	77.9	77.9
b. Steam	0.016	0.016	0.016	0
c. Cooling water	0.21	0.11	0.11	0.11
5. Maintenance				
a. WGS catalyst (=catalyst cost/catalyst lifetime)	0.2	0.2	0.2	0.2
b. Membrane replacement (=membrane cost/membrane lifetime)	15.8	15.8	15.8	15.8
6. Laboratory charges (15 % of operating labour)	8.05	8.03	8.12	7.90
7. Patents and loyalties (3 % of total product cost)	10.7	10.7	10.8	10.5
B. Fixed charges				
1. Depreciation (10 % of fixed capital investment)	28.2	28.0	28.0	25.8
2. Local taxes (4 % of fixed capital investment)	11.3	11.2	11.2	10.3
3. Insurance (0.7 % of fixed capital investment)	1.98	1.96	1.96	1.81
Total manufacturing cost	259.8	259.2	262.3	256.8
II. General expenses = administrative + distribution & selling + R&D costs				
A. Administrative costs (4 % of total product cost)	14.3	14.3	14.4	14.1
B. Distribution & selling costs (11 % of total product cost)	39.4	39.3	39.7	38.6
C. R & D costs (5 % of total product cost)	17.9	17.8	18.0	17.6
D. Financing (8 % of total capital investment)	26.6	26.4	26.4	24.3
Total general expenses	98.1	97.8	98.6	94.5
III. Total production cost = I + II	357.9	356.9	360.8	351.3

Note: The cost proportions/ranges shown are commonly used for the estimation of total product cost (Koc et al., 2014).

of equipment manufacturers in 2001, so an average value of Chemical Engineering Plant Cost Index (CEPCI) of 397 is used. It is better to use the composite indices published for various industries in the trade journals. The choice of the index to use is based upon industrial types. For a general construction, the Engineering News Record (ENR) Index is the most recommended. This index may be found weekly in Engineering News Record. An engineer in the petroleum or petrochemical business might find the Nelson Farrar (NF) Index to be the most suitable. This index is published in the first issue each month of the Oil and Gas Journal quarterly. In the chemical process industries, either the Chemical Engineering (CE) or the Marshall Swift Index (M&S) is recommended. These indicators can be found in Chemical Engineering under Economic Indicators. Although these latter two indexes have different bases, both of them give similar results (Towler and Sinnott, 2012). As a rule of thumb, cost indexes are accurate over a 4 to 5 year period at best (Lozowski, 2012). In this study, CE index of year 2013 is used as it is the most current CE index that is publicly available (Bailey, 2014).

In order to determine the best flowsheet, NPV economic criterion is used in this study. Note that, other economic measures such as payback period and return of investment (ROI) are not able to capture the time dependence of cash flows during the project lifetime. The timing of cash flows is very important as not all the capital must be financed immediately. In this study, the NPV-model relies on the standard calculation on the difference between gross present value (GPV) of future net cash flows and the initial total capital investment (TCI) as shown in equation 6.1 (Benninga et al., 2010):

$$\mathrm{NPV} = \mathrm{GPV} - \mathrm{TCI} \tag{6.1}$$

where GPV is defined as the sum of the discounted stream of net cash flows over the WGSR-MR system lifetime (Turton et al., 2008):

$$\mathrm{GPV} = \sum_{n=1}^{n=t} \frac{\mathrm{CF}_n}{(1+i)^n} \tag{6.2}$$

where CF_n is the cash flow after tax in year n, t is the project life in years and i represents the nominal discount rate. A fixed value of 16% of nominal discount rate is used in this study, i.e., based on the most likely value for a process syngas plant (Ma et al., 2015).

The net present value is always less than the total future worth of the project because of the discounting of future cash flows. The NPV is a strong function of

the interest rate used and the time period of study. Note that, NPV_{10} denotes the NPV over a 10-year period. Among the four process flowsheets, the one in Figure 6.2 (d) shows the highest NPV as shown in Table 6.4. This is due to the fact that, with a heat exchanger installation instead of a heater, the cost can be reduced. Consequently, this process flowsheet shows a better NPV at the baseline conditions compared to other flowsheets. Thus, this process flowsheet will be adopted for the process optimization study in the next section, i.e., the parametric study.

Table 6.4: NPVs for the four process flowsheets

Economic assessment	**Figure 6.2 (a)**	**Figure 6.2 (b)**	**Figure 6.2 (c)**	**Figure 6.2 (d)**
Total capital investment (TCI)	332.1	329.9	329.9	303.4
Gross present value (GPV)	-127.6	-126.6	-130.5	-121.0
Net present value (NPV_{10})	-608.8	-604.5	-613.0	-565.7

Note: All units are in $USD millions. The time period used in this study is 10 years.

6.3 Parametric Study On Economic Performance of WGSR-MR

Several researchers studied the effects of operating and design parameters on the membrane reactor performance criteria, i.e., percentage conversion and hydrogen recovery. Note that in this study, the effects of parameters on the economic performance of WGSR-MR are evaluated. The study aims to identify the parameters that have significant effects on the economic performance, i.e., NPV of the whole system. It is interesting to point out that, even if a parameter has positive effect on membrane reactor performance (e.g., percentage conversion) it does not necessarily has the same effect on the NPV of the process plant. This is because the change in that particular parameter might induce extra costs in terms of capital and/or production costs. To resolve potential conflicts among different parameters, this parametric study identify the lower and upper limits on the operating conditions of the whole process system. Identifying these constraints are important as to provide the boundary conditions during the process optimization. In the process optimization, the parameters which are deemed having strong effects on the economic performance will be used as the decision variables.

In this study the parameter under study are categorized into operating parameters and design parameters.

Operating parameters for the WGSR-MR include:

a) Pressure of retentate and permeate.

b) Temperature of retentate and permeate.

c) Sweep gas to feed flow rate ratio.

d) Steam to CO concentration ratio.

The design parameters for the WGSR-MR include:

a) Reactor length and diameter - increase in length and diameter increase the CO conversion but it will also increase the capital cost.

b) Tube diameter - Smaller tube diameter leads to larger number of tubes and in return gives higher permeability but can cause high pressure drop.

c) Diameter of catalyst pellet - large pellet size leads to reduced pressure drop but increases in the mass-heat transfer resistances. Increase in mass-heat transfer resistance can reduce the overall reaction kinetics.

Previously, some studies were conducted to identify the parameters affecting the performance of membrane reactor. However the effects of these parameters on the NPV of the WGSR-MR system are still unknown. It is important to note that in this parametric study, the effect of these parameters are plotted against the normalized (index) length of the membrane reactor (MR). Index length is a dimensionless number where it is normalized by:

$$\text{Index length} = \frac{L_j}{L_t} \tag{6.3}$$

where L_j (m) is the j^{th} sub-division length of the reactor and L_t (m) is the total length of the reactor which is 9.525m.

6.3.1 Effect of retentate temperature

Due to the exothermic nature of the WGSR, a high inlet temperature might result in the exit reactor temperature exceeding a threshold limit above which the catalyst starts to deactivate seriously. Violating the limit of the high temperature

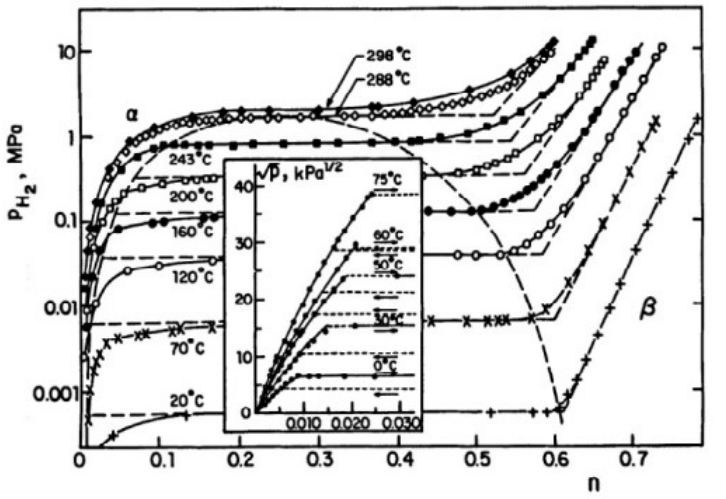

Figure 6.3: Equilibrium solubility isotherms of PdH_n for bulk Pd at different temperatures (inset figure: low pressure region).

can damage both the catalyst and Pd-based membrane tubes. Furthermore, a runaway reaction might happen and cause reactor explosion in the process plant. A runaway reaction is the term used to describe a phenomenon where the reaction temperature increases rapidly without bound (unstable behaviour), i.e., when the temperature passes the point where the heat generation is larger than heat removal. This runaway reaction can cause reactor explosion or serious damage to the reactor involved.

Note that, Pd-based membranes have a minimum and maximum working temperatures. For a pure Pd-based membrane, the working temperature should be higher than 300^0C to avoid the nucleation of β-hydride from the α-phase (Basile et al., 2011) − see Figure 6.3 adopted from (Koc, 2012). The nucleation of β-hydride can cause severe lattice strain and results in the embrittlement of membrane which in turn leads to loss in membrane selectivity. However, for a Pd-alloy such as $Pd-Ag$, $Pd-Cu$ and $Pd-Au$ membranes, the critical temperature for the $\alpha-\beta$ phase transition is below 300^0C. The maximum temperature of these membrane can go up to 900 ^{0}C (Basile et al., 2011).

As shown in Figure 6.4, the adiabatic membrane reactor model is simulated using a retentate inlet temperature in the range of 250 to 450^0C. Note that, as the inlet temperature increases, so also the NPV - this trend is due to faster reaction kinetics at higher temperature. Also, it can be seen that for a given inlet temperature, the NPV increases with the length of the reactor - increase in length leads to increase in the CO conversion to H_2. The question now is that,

how high could the inlet retentate temperature be before one expect damages to the catalyst and membrane material? To answer this question, one needs to examine the exit reactor temperature corresponding to a given inlet retentate temperature. By simulation, it is found that the maximum inlet temperature is up to 450^0C as increasing above this temperature will lead to violation of the maximum working temperature of the membrane. Based on the studies by some researchers, e.g., (Adrover et al., 2009a; Chein et al., 2013; Morpeth et al., 2015; Caravella et al., 2016; Fernandez et al., 2016; Adrover et al., 2016), the higher the inlet temperature the better the conversion - this is confirmed in the simulation study mentioned above. Note that, a higher conversion is accompanied by increase in production cost and capital cost, i.e., increase in equipment sizing. Thus, the effect of this parameter (positive or negative) on the NPV of this WGSR-MR system should be investigated.

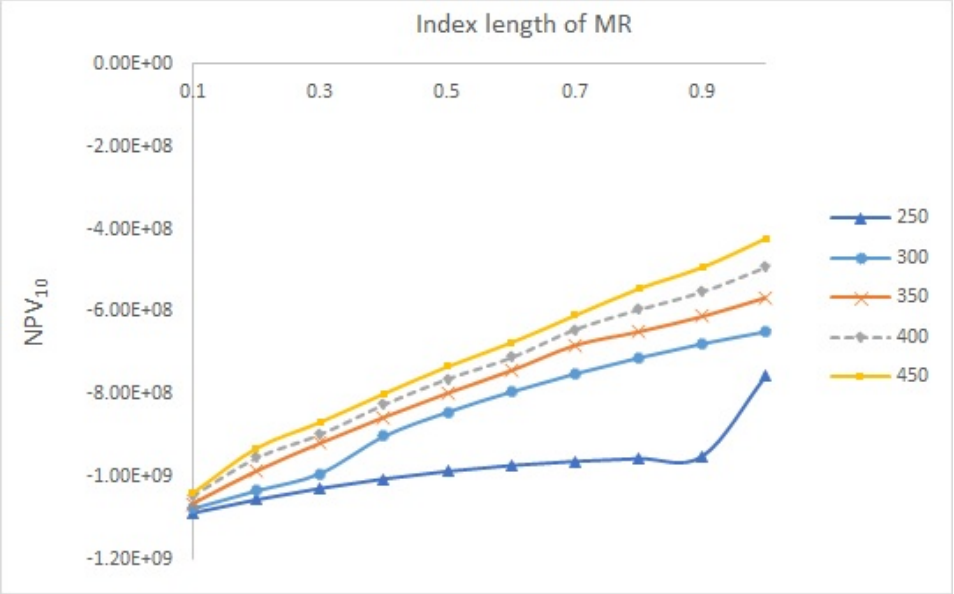

Figure 6.4: Effect of inlet temperature on NPV.

Note that, the negative NPV presented in this parametric study is due to the NPV value of the chosen flowsheet. In the current situation, negative NPV is due to a high production cost. As illustrated in Figure 6.4, when the operating inlet retentate temperature is close to 250^0C, the NPV of this system shows lower values due to low reaction kinetics limitation. Through simulation, it is found that the minimum working temperature of the shift catalyst should be about 300^0C. Notice that (Figure 6.4), there is a steep increase in the NPV for this feed temperature at the reactor index length of 0.9.

For higher (above 250^0C) inlet retentate temperature, a steady increment of NPV along the reactor length is observed. From the parametric study of the WGSR-MR system, one can conclude that higher reaction temperature can produce higher profit margin. This is shown by an increase of 33.75% in NPV (calculated at x = 0.1) when the inlet temperature increases from 250 to 450^0C. However, high inlet temperature may lead to a possibility of accident due to run away reaction. Thus, an optimum inlet temperature considering both profit margin and process safety must be identified for this process - this will be done via optimization of the system in the next chapter.

Effect of permeate temperature

The economic performance of the WGSR-MR system is also evaluated under a wide range of permeate temperature (350 - 550^0C). In the simulation to investigate the effects of permeate temperature, the inlet retentate temperature is fixed at 350^0C and the specifications in Table 6.1 are used. The range of permeate temperature is varied within lower and upper bounds of the membrane working temperature, i.e., see Section 6.3.1.

According to equation 5.9, the rate of change of retentate temperature is a function of permeate temperature. The decrease in permeate temperature suggests a decline of retentate temperature due to enhanced process heat transfer from the retentate to permeate side. Since the WGSR is by nature an exothermic reaction, the decrease in reaction temperature shall result in the reduction of rate of reaction. Hence, lowering the inlet permeate temperature will reduce the hydrogen production.

From the simulation study, it is discovered that the change in permeate temperature has insignificant effect on the cost of the WGSR-MR system − see Figure 6.5. Although the result implies that this parameter has little influence on the cost margin of this system, the interactive effects of permeate temperature with other parameters could be significant. Hence, it is still worth investigating the interactive effects. The rise of permeate temperature from 350 - 550^0C shows slight increment of NPV (3.1%) due to the increment of hydrogen production. However, the elevation of the production is little compared to the overall cost.

6.3.2 Effect of retentate pressure

In the WGSR-MR, other than the reaction temperature, parameters such as the retentate and permeate pressure can be used to enhance the hydrogen recovery

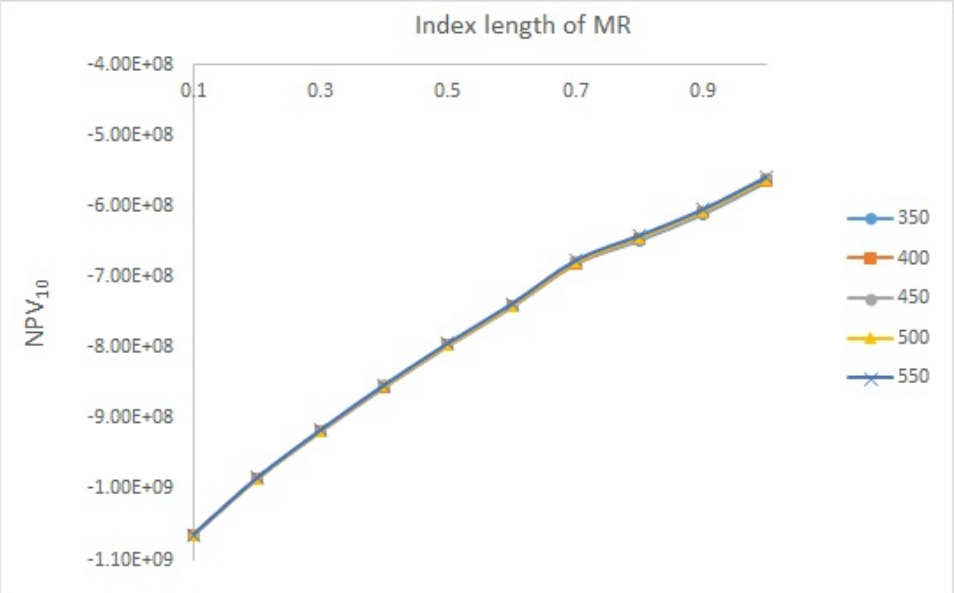

Figure 6.5: Effect of inlet permeate temperature on NPV.

level. According to Sieverts law - see equation 5.6, the trans-membrane pressure plays an important role in determining the permeability of hydrogen through the membrane. Unlike in the traditional packed bed reactors, the retentate side pressure has a powerful effect on the hydrogen recovery. As reported in the work of Boutikos and Nikolakis (2010) and Morpeth et al. (2015) a large difference in retentate and permeate pressures shall induce high hydrogen permeability.

In this study, the WGSR-MR system model is evaluated under a reaction side pressure range of 30-50 atms. The highest retentate pressure is limited to 50 atms as higher than this causes difficulty in membrane reactor fabrication (Mendes et al., 2010).

Referring to Figure 6.6, there is an increase of 37.5% in NPV when the pressure increase from 30 to 50 atms. This is due to the increase in the driving force for the hydrogen permeation by raising the reaction pressure. This leads to an enhancement of the hydrogen flux through the membrane, i.e., increase in hydrogen recovery. Hence, increasing the growth in profit margin. It is interesting to note that, the NPV of the system can be increased dramatically by using higher reaction pressure. Unfortunately, a drawback is that the higher pressure used will demand a greater amount of work by the compressor, which may lead to an unacceptably high electricity cost. Despite higher reaction pressure can give larger profit margin, one needs to be careful not to use excessively high reaction pressure which can trigger potential hazards such as, membrane tube

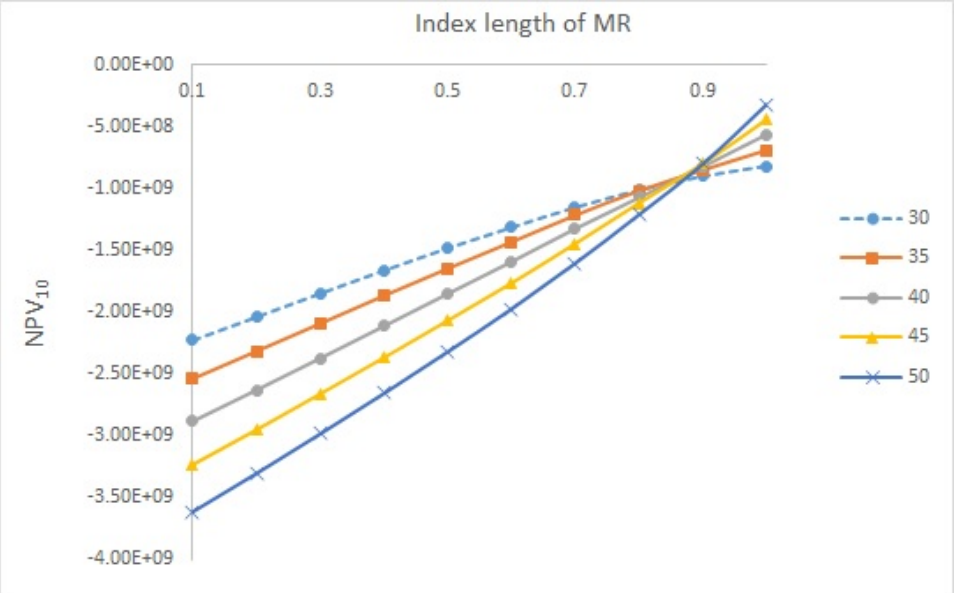

Figure 6.6: Effect of inlet retentate pressure on NPV.

cracking and difficulties in process control. Thus, an optimum retentate pressure that considers trade-offs between both cost and safety of the plant should be optimized.

6.3.3 Effect of permeate pressure

As mentioned earlier in the Section 6.3.2, partial pressure difference between retentate and permeate is responsible for the enhancement of hydrogen recovery and CO percentage conversion. The partial pressure of the trans-membrane can be increased via several ways, such as by increasing the retentate side pressure and decreasing the permeate side pressure. Another way is to reduce the permeate side pressure via the sweep gas in permeate side. An extra separation unit is needed at the end of the permeate side if other than hydrogen is used as the sweep gas (i.e., nitrogen or argon gas). In this study, hydrogen gas is used as the sweep gas in order to obtain high purity hydrogen without additional separation units. It is assumed that there is no reverse diffusivity of hydrogen to retentate side due to a steep gradient difference across the membrane walls.

According to previous works such as in (Koc et al., 2011; Marín et al., 2012; Hla et al., 2015), it has been observed that by reducing the permeation pressure, it is possible to achieve a higher hydrogen yield. In this study, a permeate pressure in the range of 5-9 atms is applied in order to investigate the effect of this parameter

on the NPV of the WGSR-MR system. The lowest permeation pressure is set to be 5 atms since a pressure lower than this can result in an exit pressure below the atmospheric pressure (1 atm). Consequently if this happens, special materials are needed to construct the membrane reactor that operates at pressure lower than 1 atm. Hence, extra costs will be incurred due to the use of some specific materials.

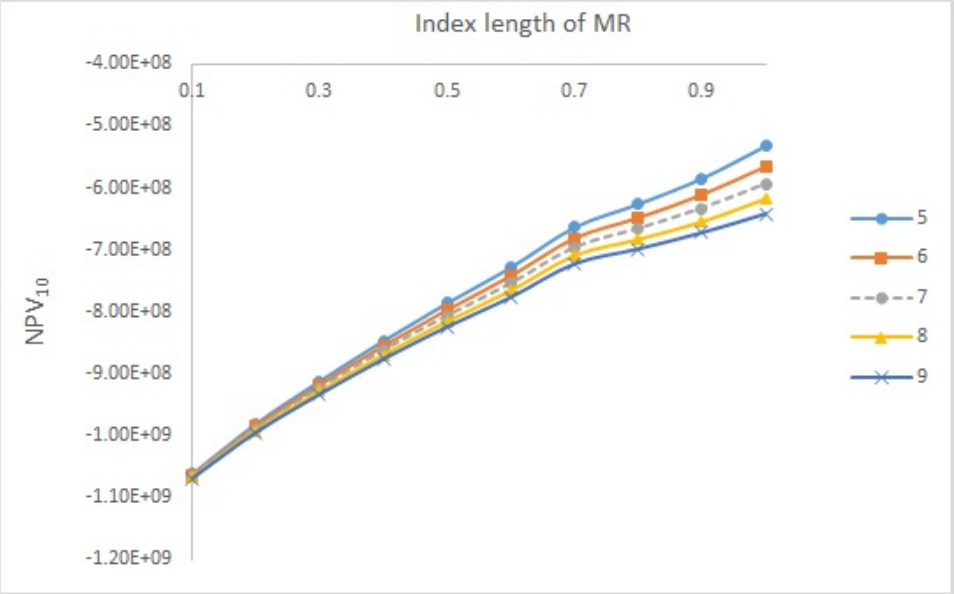

Figure 6.7: Effect of inlet permeate pressure on NPV.

It can be observed that decrease in permeate pressure leads to higher NPV values - depicted in Figure 6.7. A low permeate pressure produces higher profit margin, for example, an increase of 19.2% in NPV when the permeate pressure decreases from 9 atms to 5 atms. This is due to two reasons, (1) higher hydrogen yield due to larger trans-membrane pressure (increase in revenue) and (2) lower compressor power requirement and hence lowering electricity cost (decrease in operational cost). Although lower permeate pressure results in better hydrogen recovery, it can cause some operational hazard such as the collapse of the membrane tube. Thus, an optimum permeate pressure has to be considered for safety reason.

6.3.4 Effect of sweep gas to feed flow rate ratio

Sweep gas is used to decrease the permeation side partial pressure so to increase the flow of hydrogen from reaction side to permeate side. The sweep gas flow rate

promotes turbulence in membrane reactor tube which in turn reduce the partial pressure in the membrane tube. Cornaglia et al. (2013) found that an increase in sweep gas flow rate leads to slight improvement in hydrogen permeation due to the reduction of partial pressure in the permeate side. The benefit of using sweep gas was confirmed in Dong et al. (2015) where similar trend was observed in higher permeation flux due to sweep gas flow rate. However, Mendes et al. (2010) discovered that an increase in sweep gas to a certain value can lead to a small temperature decrease on the outer surface of membrane, which leads to the decrement of the H_2 permeability (Arrhenius law).

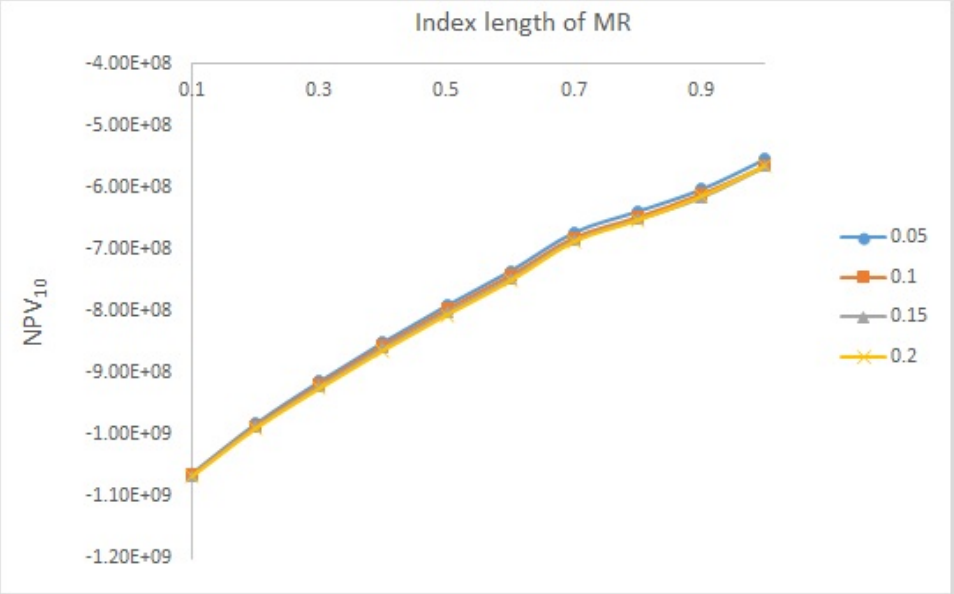

Figure 6.8: Effect of sweep gas to feed flow rate ratio on NPV.

The effect of sweep gas to feed flow rate ratio on the NPV for a range of 0.05 to 0.2 is explored. Larger sweep gas flow rate induces great pressure drop and causes process hazard (cracking in membrane tube and sintering in membrane). Thus, the maximum limit of the ratio is set to be 0.2. As illustrated in Figure 6.8, as the ratio increases from 0.05 to 0.2, the NPV decreases by 3.8%. Although bigger ratio leads to increase in hydrogen recovery, it also causes increase in electricity consumption by compressor. The gain in profit margin generated by hydrogen production is lower than the production costs due to increase in capital and operating costs. Thus, smaller ratio of sweep gas is preferred.

6.3.5 Effect of steam to CO concentration ratio

Excess steam is always fed to the membrane reactor to enhance the reaction as well as to regulate the reaction temperature. The rise of temperature due to heat generated can easily cause the exit reactor temperature to be higher than 900^0C. An efficient way to control the reaction temperature is by controlling the excess steam in the feed. Although increase in excess steam tends to produce lower reaction temperature, it has a negative impact on hydrogen recovery. Based on the studies conducted by (Chen et al., 2017; Baloyi et al., 2016; Basile et al., 2015; Chein et al., 2013), it was observed that an increase in steam to CO (S/C) ratio decreases the hydrogen permeability. The reason for this is the inhibiting nature of excess steam on the permeation through the membrane. At lower S/C ratio, the partial pressure of steam is low and leads to increase in partial pressure of H_2. As a result, H_2 permeation rate is enhanced, thereby, higher hydrogen yield is achieved.

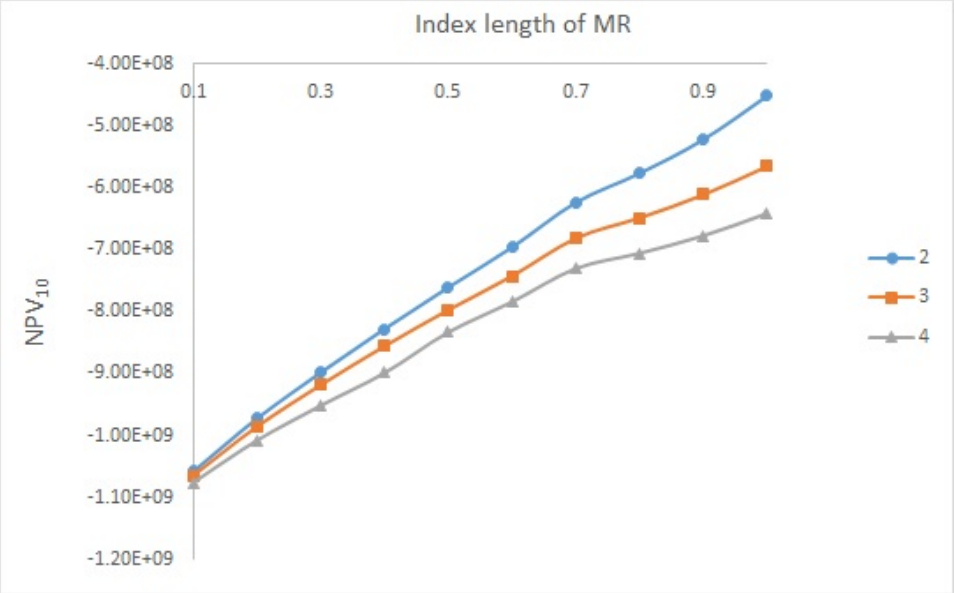

Figure 6.9: Effect of H_2O to CO concentration ratio on NPV.

It is interesting to study the impact of H_2O to CO ratio on the WGSR-MR system. The result obtained is plotted in Figure 6.9. It is observed that an increase of NPV by 30.8% can be achieved by decreasing the S/C ratio from 4 to 2. Furthermore, the decrease in S/C ratio is equivalent to a reduction of total cost due to lower raw material and equipment costs. Although lower S/C ratio is beneficial in terms of reducing cost of the system, too low steam injection can lead

to reverse shift of the equilibrium. A reverse shift can only happen in a reversible reaction. When the concentration of the product is higher than the concentration of reactant, a reverse shift of equilibrium occurs. Thus, an optimum S/C ratio is needed to ensure smooth and safe operation of the system.

6.3.6 Membrane reactor length

In a non-isothermal membrane reactor, the reaction temperature throughout the membrane reactor is critically affecting the safety of the whole process. Excessively high temperature can lead to runaway reaction, membrane thermal cracking and catalyst deactivation. Note that, in an adiabatic membrane reactor, the temperature progressively rises along the reactor. Additionally, increase in membrane reactor brings increment in conversion and hydrogen production. This trend has been observed in previous studies of (Uemiya et al., 1991; Ma and Lund, 2003; Barbieri et al., 2005; Ghasemzadeh et al., 2016).

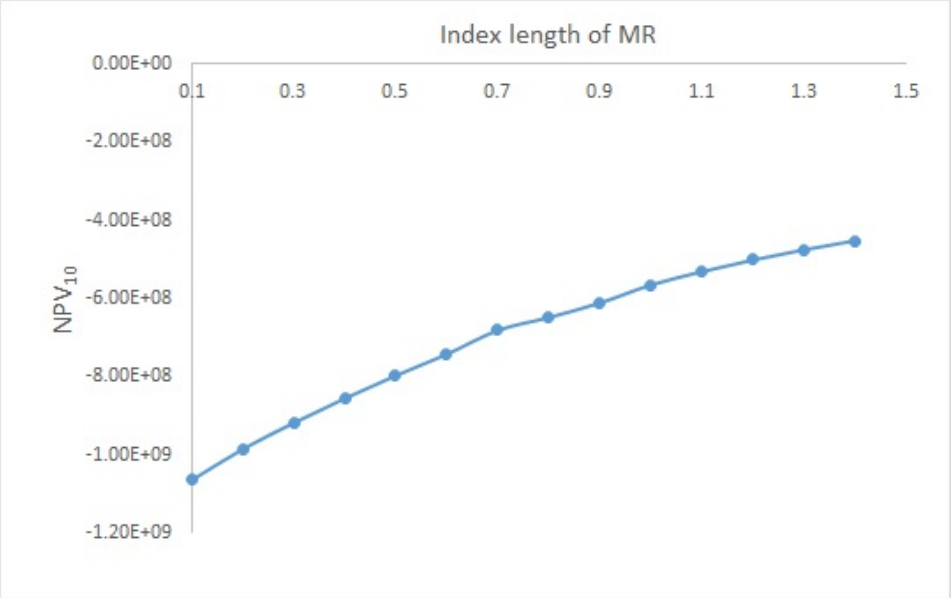

Figure 6.10: Effect of membrane reactor length on NPV.

Similar trend as in the works of (Barbieri et al., 2005; Ghasemzadeh et al., 2016) is observed as depicted in Figure 6.10. With 40% increase in membrane reactor length, an increase of 27.6% in the NPV can be attained. Even though the increment in membrane reactor length will increase capital cost (due to larger membrane surface area and equipment costs), the production of hydrogen shows a steeper increment compared with the rise of capital cost. Note that, longer

membrane reactor gives higher NPV but this can lead to some process hazards. Longer membrane reactor means a longer process reaction time. This leads to substantial transport delay as the reactor gets longer. Transport delay can cause difficulty in controlling the process when subjected to disturbances. Furthermore, longer reactor results in larger pressure drop which causes membrane tube cracking and other process difficulties. Hence, an optimum reactor length should be considered for this WGSR-MR system design.

6.3.7 Membrane reactor shell diameter

In this study, the membrane reactor is designed as a shell and tube reactor - analogous to heat exchanger shell-and-tube design. The size of the membrane reactor shell plays an important role as the size determines the number of membrane tubes. A larger number of membrane tubes increases hydrogen recovery due to larger surface area of membrane. However, larger membrane surface area leads to higher membrane reactor purchased cost. It is important to note that, a larger diameter of membrane reactor can be susceptible to the presence of temperature hot-spot in the membrane reactor due to inefficiency of process heat transfer from the reaction side to the permeate side.

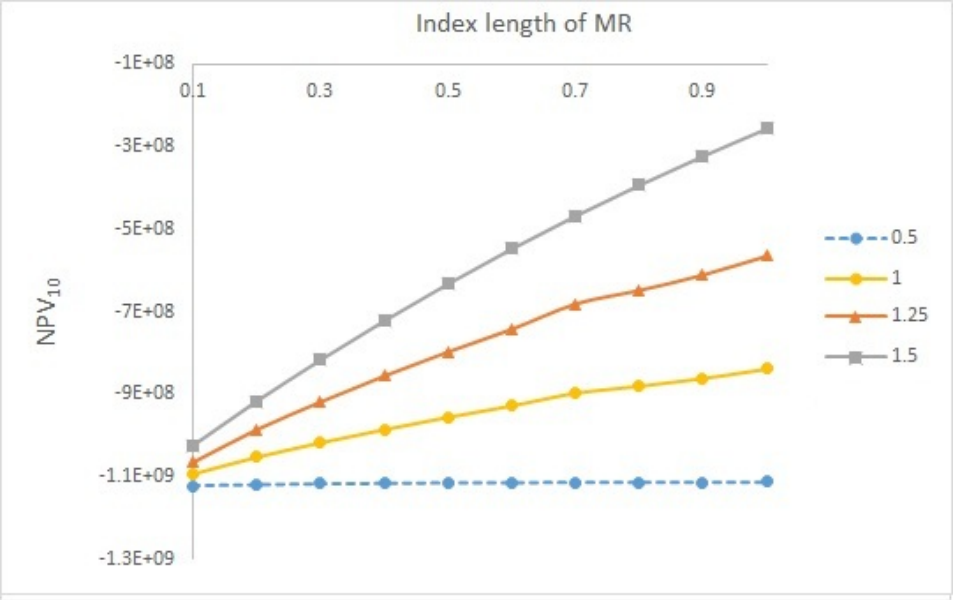

Figure 6.11: Effect of diameter of membrane reactor on NPV.

As shown in Figure 6.11, NPV increases as the reactor diameter increases in the range of 0.5 to 1.5 m. An increase of 74.5% in NPV is noted with the increase

from minimum to maximum of the reactor diameter. Even with the large amount of increase in NPV, a safe and preferably optimum reactor diameter is still needed for this WGSR-MR system.

6.3.8 Membrane reactor tube diameter

To the best of our knowledge so far, there has been no work published on the effect of membrane reactor tube diameter on the WGSR-MR performance. Hence, it is interesting to investigate the effect of membrane reactor tube diameter on the NPV of WGSR-MR system. Bear in mind that, the total surface area of the membrane depends on the tube diameter and number of tubes. Larger number of tubes give higher hydrogen permeability - bigger membrane surface area. On the other hand, small diameter of membrane reactor tube can cause large pressure drop and contributes to process hazard in the system.

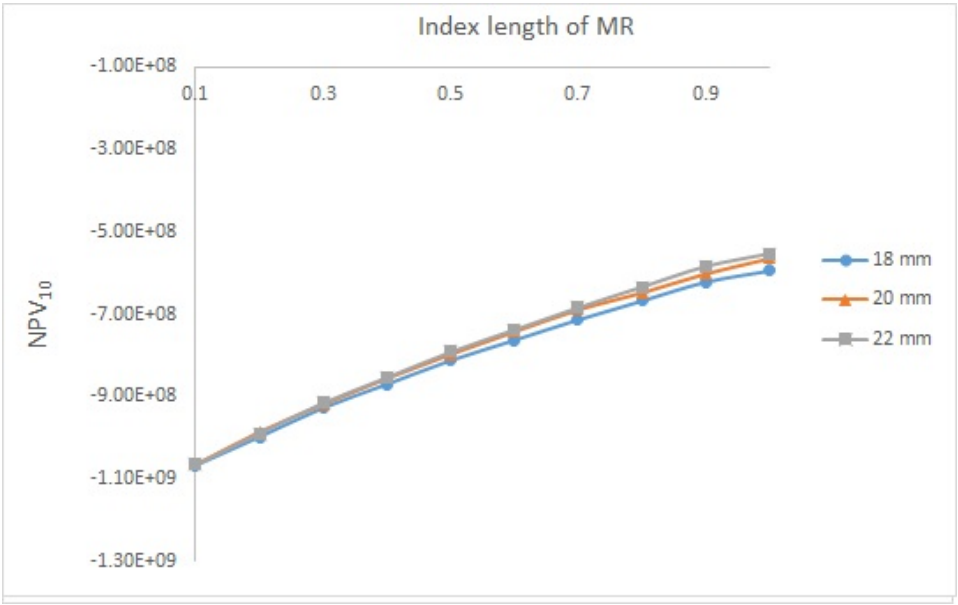

Figure 6.12: Effect of membrane reactor tube diameter on NPV.

In this simulation, the tube diameter is obtained from the commercially available tube sizes. From Figure 6.12, membrane tube diameter has insignificant effect on the NPV of the system. It is observed that large membrane tube diameter presents higher amount of NPV - increase of 3.1% when tube diameter increases from 18 to 22 mm. The slight increment of NPV as with the increase of tube diameter is due to difference in pressure drop. A bigger tube diameter has lower pressure drop compared to a smaller tube diameter. Thus, a smaller tube

diameter leads to cost increment. However, the difference in the cost increment is tiny.

6.3.9 Catalyst pellet diameter

This parameter has been scarcely explored by researchers which could be partly due to limitation of catalyst pellet sizes available commercially. The change in catalyst pellet size affects pressure drop in the retentate side - see equation 5.7. The pressure drop calculation is a function of $\frac{1}{d_{cat}}$, where d_{cat} refers to diameter of the catalyst pellet. Thus, a small catalyst pellet size has the ability to induce large pressure drop.

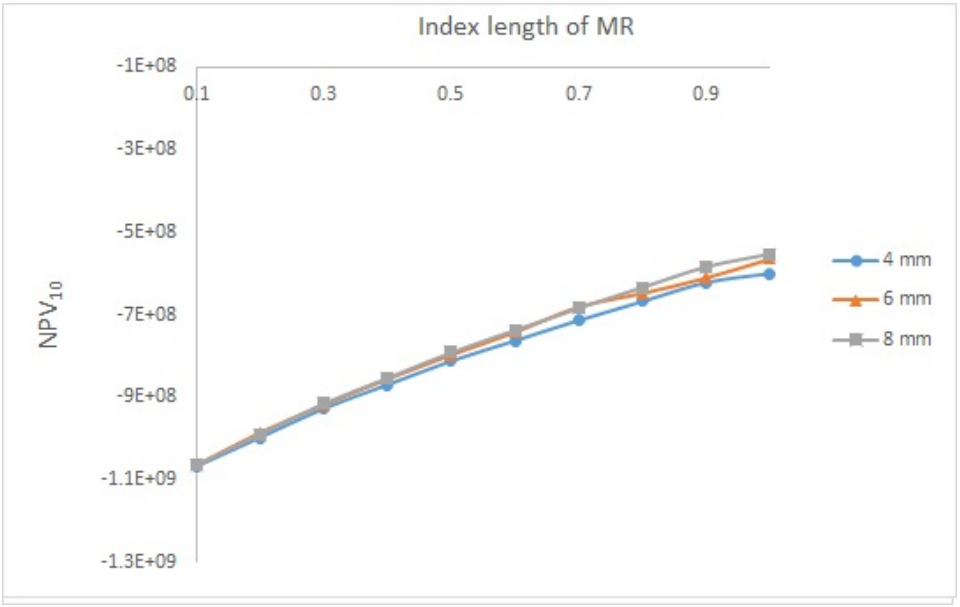

Figure 6.13: Effect of catalyst pellet size on NPV.

In this study, a set of commercial catalyst pellet sizes which are limited to a range of 4 - 8 mm (Koc et al., 2014) is used. It is interesting to note that, larger pellet size results in higher NPV as depicted in Figure 6.13. An increase of 3.6% in NPV is observed with the increment of pellet size from 4 to 8 mm. The reason of this NPV increment is due to the decrease in capital (decreased in amount of catalyst purchased) and production (decreased in electricity) costs.

6.3.10 Discussion of parameter effects

Based on the overall economic assessment of all the parameters mentioned above, it can be concluded that retentate temperature, permeate pressure and retentate

pressure have significant effects on the NPV of the system under study. In order to identify which parameters should be included in the next process optimization, a percentage change of NPV is used. The percentage change of NPV is calculated based on the maximum and minimum NPV obtained over the range of a given parameter as given in equation 6.4:

$$\text{NPV}_\text{N} \text{ percentage change} = \frac{NPV_{N,max} - NPV_{N,min}}{NPV_{N,max}} \times 100 \tag{6.4}$$

where $NPV_{N,min}$ and $NPV_{N,max}$ represent the minimum and maximum of the NPV for a parameter N. Meanwhile, the percentage change of the parameter is given by

$$N \text{ percentage change} = \frac{N_{max} - N_{min}}{N_{max}} \times 100 \tag{6.5}$$

where N_{min} and N_{max} represent the minimum and maximum bounds of the parameter N.

Table 6.5: Percentage change of NPV based on each parameter range

Parameter, N	N Percentage Change (%)	NPV Percentage Change (%)
Retentate temperature	44.44	33.75
Permeate temperature	36.36	3.10
Retentate pressure	40.00	37.50
Permeate pressure	44.44	19.20
Steam to feed flow rate ratio	75.00	3.80
H_2O to CO concentration ratio	50.00	30.80
Membrane reactor length	40.00	27.60
Membrane reactor diameter	66.67	74.50
Membrane tube diameter	18.18	3.10
Catalyst pellet diameter	50.00	3.60

Note: All percentage changed are calculated based on Equation 6.4 and 6.5.

The percentage changes are tabulated in Table 6.5. In this study, the parameter that has/have a NPV percentage contribution of less than 3.5% will not be included in the next process optimization, i.e., the parameter effect is considered insignificant which in this case are the permeate temperature and membrane tube diameter. It is supported by the previous studies of Adrover et al. (2009a); Baloyi et al. (2016) that the permeate temperature and membrane tube diameter had insignificant effect towards the membrane reactor performance.

6.4 Summary

To date, works reported on WGSR-MR mainly focused on a stand-alone unit of a membrane reactor. However, it is important to note that a stand-alone unit's performance and behaviour are impractical at an industrial-scale. In a stand-alone unit, it is difficult to grasp the interaction of other equipment towards the performance of the membrane reactor unit. This chapter can be summarized as follows:

- Four new process flowsheets of WGSR-MR system have been developed using the chemical engineering process design procedure.
- To further understand each pros and cons of the process flowsheets, a detailed economic evaluation based on net present values (NPV) is performed on each flowsheet.
- It is discovered by comparing the developed flowsheets, the candidate with a heat exchanger yield the highest NPV.
- Parametric study on the economic performance of WGSR-MR system is conducted to choose the important parameters to be used in the optimization process. The scrutinizing approach of the parametric study aids in the computational efficiency of the process optimization.
- With regard to the parameter effect on NPV, if it varies less than 3.5% then the parameter is considered insignificant and will not be considered as a decision variable in the next chapter of process optimization.
- It should be noted that, the interaction among these parameters which causes nonlinear behavior of membrane reactor performance (i.e., NPV of the system). Therefore, it is important that the parameter interaction are to be considered in the process optimization.
- The work in this chapter has been published in Computer Aided Chemical Engineering 2016. [1]
- The subsection of carbon capture in this chapter has been accepted for publication in Chemical Product and Process Modeling 2017. [2]

[1] Optimization of Economic and Operability Performances of Water-gas Shift Membrane Reactor. *Computer Aided Chemical Engineering*, Elsevier 38: 847-852.

[2] Simultaneous carbon capture and reuse using catalytic membrane reactor in water-gas shift reaction. Submitted to *Chemical Product and Process Modeling*.

Chapter 7

Multi-objective Optimization of Steady-state and Dynamic Performances of WGSR-MR

7.1 Overview

This chapter presents a new methodology for optimization of a WGSR-MR system design based on the significant parameters that has been identified in the previous chapter. Two optimization formulations are adopted: (a) single-objective optimization using net present value (NPV) as a steady-state performance criterion, and (b) multi-objective optimization considering both steady-state and process controllability performances. The process controllability performance is quantified using v-gap metric whose value indicates whether a given design is easily controllable or not. The market uncertainties for hydrogen and electricity prices are forecasted using Markov-Chain Monte Carlo (MCMC) simulation. Given a time frame of 10 years and syngas throughput of 5.8 Mtonnes annually, the results of this study show that: (a) single-objective optimization (SOO) leads to the NPV of USD 857 millions, (b) multi-objective optimization (MOO) assuming no market uncertainty yields NPV of USD 513 millions, and (c) multi-objective optimization in the presence of market uncertainties gives NPV of USD 471 millions. Although the single-objective optimization leads to a larger NPV than that of the multi-objective optimization, the reactor will be very difficult to control under the optimal design conditions given by the former method. Noteworthy, simultaneous optimization of steady-state and dynamic controllability criteria can avoid plant design with poor controllability but at a price of lower NPV. The

rest of this chapter is organized as follows. Section 7.2 discusses briefly on the basic concepts and equations of the main terms (i.e., operability, uncertainty and MCMC) used in this chapter. Section 7.3 presents a step-by-step optimization methodology with the incorporation of the uncertainties. Meanwhile, section 7.4 covers the results and discussion of the three above-mentioned optimization objectives (i.e., SOO and MOO with/without uncertainties).

7.2 Preliminaries

7.2.1 Dynamic operability

In the work of (Vinnicombe, 2000), the authors introduced a new metric known as v-gap metric on the space of multivariable linear time-invariant systems. V-gap measures the metric between two systems P_0 and P_1. The v-gap values lie in between 0 and 1. A small value (relative to 1) implies that any controller that stabilizes P_0 will likely stabilize P_1, moreover, the closed-loop gains of the two closed-loop systems will be similar. A v-gap of 0 implies that P_0 equals P_1, and a value of 1 implies that the plants are far apart. The numerical calculation of v-gap is as shown in equation 7.1 - 7.2 below

$$\arcsin b(P_1.K_1) \geq \arcsin b(P_0.K_0) - \arcsin \delta(P_0.P_1) - \arcsin \delta(K_0.K_1) \qquad (7.1)$$

where

$$b(P_i, K_i) = \left\| \begin{bmatrix} I \\ K_i \end{bmatrix} (I - P_i K_i)^{-1} \begin{bmatrix} P_i & I \end{bmatrix} \right\|, \quad \text{for} \quad i = 1, 2...n \qquad (7.2)$$

whereby n is the number of perturbed plants, while K_0 and K_1 are controllers designed based on P_0 and P_1 respectively. The interpretation of this result is that, if a nominal plant P_0 is stabilized by controller K_0 with 'stability margin' $b(P_0, K_0)$, then the stability margin when P_0 is perturbed to P_1 and K_0 is perturbed to K_1 is degraded by no more than equation 7.1. The idea of using v-gap is to determine the extent of difficulty of controlling a given plant design under certain conditions. If the v-gap metric of a certain plant operation lies within the b_{opt} of the control system, one can easily control the plant operation. Especially for a nonlinear system such as WGSR-MR, the extent of nonlinearity can be measured by the v-gap metric. It is desired to have a small v-gap values when

the nonlinear system is perturbed, which implies weak nonlinearity, hence easy to control. In this respects, it is crucial to find a set of key design and operating conditions that contribute to weak nonlinearity for a given perturbation, i.e., due to uncertainties.

7.2.2 Uncertainties

There are two types of uncertainties: the endogenous category which relates to the process operating conditions, and exogenous category related to the external environments such as product demand and prices (Martín and Martínez, 2015). Uncertainty can negatively or positively affect the proper operation and market success in any new or modified product.

In the present work, the focus is to consider market uncertainties (exogenous) influence on the NPV calculation. Please note that, the endogeneous uncertainties due to variations in the operating conditions are addressed via the v-gap metric, i.e., the dynamic performance measure. In any given industry such as hydrogen production, the lifetime of the product follows certain trends and subjected to market demand. Therefore, market uncertainties such as selling price of hydrogen and cost of electricity have to be taken into account in the optimization. These two market uncertainties are being considered because of two reasons. Firstly, the large usage of electricity means that changes in the cost of electricity impose great impact on the operational expenditure. Secondly, the selling price of hydrogen is subject to fluctuation due to varying market demand. According to U.S. Department of Energy's standard model for small-scale distributed hydrogen production, the price of hydrogen depends on various different production of hydrogen (Steward et al., 2009). With these uncertainties, it is hard to justify whether a given plant is still able to generate positive NPV if it is to experience these market uncertainties. Hence, by incorporating uncertainties into the optimization of the plant design, one could expect a more convincing solution in the face of changing market environments.

7.2.3 Markov-Chain monte carlo

Markov-Chain Monte Carlo (MCMC) simulation is to find $P(y|x)$ with given $\pi(x)$. Note that, $P(y|x)$ denotes the uncertainty value while $\pi(x)$ means probability data. MCMC algorithm generates a number of possible solutions, hence in order to generate one unique solution Metropolis-Hasting algorithm is generally used.

$$\pi(x)P(y|x) = \pi(y)P(x|y) \text{ for all } x, y \ \in \ \Omega \tag{7.3}$$

where a Markov chain ($x, y \in \Omega$) is a discrete time stochastic process.

$$P(y|x) = Q(y|x)\ \alpha(y|x) \quad \text{x} \neq \text{y} \tag{7.4}$$

$$\alpha(y|x) = r(x,y)\ \pi(y)\ Q(x|y)\ \leq 1 \tag{7.5}$$

where $Q(y|x)$ is a proposal kernel and $\alpha(y|x) \in [0, 1]$ is an acceptance probability. Meanwhile, $r(x, y)$ is equivalent to the minimum of the two proposed kernel.

Thus,

$$\alpha(y|x) = min\left\{1, \frac{\pi(y)Q(x|y)}{\pi(x)Q(y|x)}\right\} \tag{7.6}$$

Hence, through equation 7.4 - 7.6, a value of uncertainty can be estimated.

7.3 Optimization Methodology

A newly developed algorithm for multi-objective optimization (MOO) with uncertainties is presented in this section. Following are the steps used to construct the optimization formulation.

Step 1: Specify performance measures. For a given process flowsheet, specify a row vector of performance measures $\Psi = [\psi_1, \psi_2 \ ... \ \psi_P]$, i.e., P number of criteria such as the NPV, profit, v-gap, relative gain array, etc. $\Psi \in R^P$.

In this study,

$$\Psi = [\psi_1,\ \psi_2] \tag{7.7}$$

where ψ_1 = NPV and ψ_2 = v-gap of this system. These criteria are used to measure the performances of the WGSR-MR system.

Step 2: Selection of decision variables U_I. From the given process flowsheet and model, select the decision variables which consist of operating and design parameters. The selection can be made based on prior knowledge obtained from the literature. Assume that $U_I \in R^r$ is a row vector with a total r number of operating and design parameters.

$$U_I = [u_1,\ u_2,\ u_3 \ ... \ u_r] \tag{7.8}$$

where in this study a total of eight parameters are selected as the decision variables for the process optimization. The selection of these parameters are based on

each of their economic performance presented in previous chapter - see Chapter 6.

Step 3: Determination of constrains. All constraints imposed on the selected decision variables as well as other constraints must be identified and their values specified. It is assumed that the decision variables are bounded as follows

$$U_{I,min} < U_I < U_{I,max} \tag{7.9}$$

where $U_{I,min}$ and $U_{I,max}$ denote the lower and upper limits on U_I respectively.

Step 4: Selection of baseline condition. The baseline or nominal condition represents the nominal values of operating and design parameters selected in Step 1. The baseline condition can be selected based on the prior knowledge obtained from previous study or literature reports. Alternatively, if one has a process model corresponding to the desired flowsheet, numerical or simulation study can be first conducted in order to determine a viable baseline condition. Note that, Table 6.1 presented the proposed nominal condition for this study.

Step 5: Design of experiment (DOE). Based on the number of decision variables, conduct DOE to determine the number of experimental or simulation runs. These strategies were originally developed for the model fitting of physical experiments, but can also be applied to numerical experiments. The objective of DOE is the selection of the points where the response should be evaluated. Most of the criteria for optimal design of experiments are associated with the mathematical model of the process. Generally, these mathematical models are polynomials with an unknown structure, so the corresponding experiments are designed only for every particular problem. The choice of the design of experiments can have a large influence on the accuracy of the approximation and the cost of constructing the response surface.

A detailed description of the design of experiments theory can be found in Box and Draper (1987), Montgomery and Myers (1995), and Montgomery (2008). Schoofs et al. (1987) reviewed the application of experimental design to structural optimization, Ferro-Luzzi et al. (1996) discussed the use of several designs for response surface methodology and multidisciplinary design optimization and Simpson et al. (1997) presented a complete review of the use of statistics in design.

A factorial design is a strategy in which the decision variables, U_I are varied together, instead of one at a time. The allowable range is then identified in between the lower and upper bounds of each variables as explained in Step 3. If each of the variables is defined at only the lower and upper bounds (two levels),

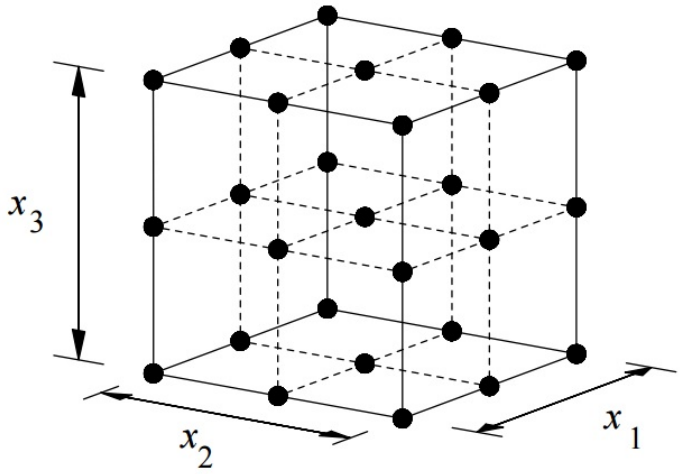

Figure 7.1: A 3^3 full factorial design.

the experimental design is called 2^N fractional factorial. However, if the midpoints are included, the design is called 3^N full factorial as illustrated in Figure 7.1

If a full factorial design is applied, then the total number of runs will be $3^r + 1$, which includes the baseline condition (Box and Draper, 1987); the number of perturbed simulation runs around the baseline condition is 3^r. It should be noted that, full factorial design typically is used for five or fewer variables. Other design method such as fractional factorial design are useful as to reduce the number of runs compared to full factorial.

Step 6: Magnitude of input perturbations. Select the magnitude of perturbation of each decision variable. The magnitude of perturbation must be reasonably large but must not violate any constraint imposed on that particular variable specified in Step 3. Thus, prior knowledge of all the constraints involved in the process design is crucial.

In this study, the magnitude of input perturbations for the decision variables U_I are given in Table 7.1. The magnitude of perturbation is determined based on each decision variable r constraint in WGSR-MR system.

Step 7: Formation of dataset, X. Based on Steps 5 and 6, by using the process model a series of simulation runs is conducted, i.e., $3^r + 1$ number of runs. For each simulation run, calculate the performance measures.

Then, a dataset,

$$X \in R^{(3^r+1)\times(r+P)} \tag{7.10}$$

Table 7.1: Real values and coded factor level of input perturbation

Variables	Level (-1)	Level (0)	Level (1)
Retentate Temperature (^{0}C)	252	350	448
Retentate Pressure (bar)	30.8	40.0	49.2
Permeate Pressure (bar)	5.005	6.500	7.995
Sweep gas to feed flowrate ratio	0.050	0.125	0.175
Concentration of H_2O to CO ratio	2.1	3.0	3.9
MR length (m)	5.715	9.525	13.350
MR diameter (m)	1.00	1.25	1.50
Catalyst pellet diameter (m)	0.004	0.006	0.008

Note: The maximum and minimum level of the real values for each parameters is set as closed as possible to the boundary constraints.

which 3^r+1 represents the number of rows of full factorial plus baseline condition and $r+P$ represents the number of columns. It is assumed that all specified performance measures are included in the dataset.

Step 8: Identification of main parameters. The principal component analysis (PCA) is applied to the dataset X in order to identify the main decision (i.e., from the sets of operating and design parameters) variables from the sets of U_I, which have dominant effects on the specified performance measures. With respect to a given performance measure ψ_k, the corresponding set of main parameters or inputs $U_k^d = \{u_{k,1}, u_{k,2}, ...u_{k,m}\}$ is identified from the set of all inputs $U_I = \{u_1, u_2, ...u_r\}$ using the PCA. The set of main variables is a subset of the set of all decision variables ($U_k^d \subset U_I$ where $m \leq r$)

Step 9: Construction of Response Surface Models (RSMs). For a specified performance measure, develop a RSM to capture the effects of main parameters U_k^d on the performance measure ψ_k:

$$\psi_k(U_k^d) = \alpha_{k0} + \sum_{j=1}^{m} \alpha_{k1,j} u_j + \sum_{i=1}^{m-1} \sum_{j=i+1}^{m} \alpha_{k2,i,j} u_i u_j + \epsilon_k \tag{7.11}$$

where the first term, α_{k0} is a constant term, while the second term, $\alpha_{k1,j}$ are coefficients for linear expressions followed by the third term, $\alpha_{k2,i,j}$ are coefficients for an interactive expressions and the last term, ϵ_k represents a corrective error.

Step 10: Optimization formulation. Two types of optimization formula-

tions: (1) Single Objective (SOO), and (2) Multiple Objectives (MOO).

For a given ψ_k, the SOO is written as follows

$$\begin{aligned} J_k^* = & \max_{U_k^d} \quad \psi_k(U_k^d) \\ & \text{subject to} \quad U_{k,ll}^d \ < \ U_k^d \ < \ U_{k,ul}^d \end{aligned} \tag{7.12}$$

where the $U_{k,ll}^d$ and $U_{k,ul}^d$ denote the lower and upper limits on U_k^d. The solution to the SOO will be $U_k^d = U_k^{d*}$ giving an optimum value of the objective function equal to J_k^*.

Meanwhile, for the MOO formulation with P number of performance measures

$$\begin{aligned} J_{moo}^* = & \max_{U_{moo}^d} \quad w_1\psi_1(U_1^d) + w_2\psi_2(U_2^d) + ...w_P\psi_P(U_P^d) \\ & \text{subject to} \quad U_{moo,min}^d \ < \ U_{moo}^d \ < \ U_{moo,max}^d \end{aligned} \tag{7.13}$$

The set of main variables for the optimization is given by the unification of all the sets of main decision variables

$$U_{moo}^d \ = \ U_1^d \ \sqcup \ U_2^d \ \sqcup \ ... \ U_P^d \tag{7.14}$$

and an equal weightage coefficients are given for each objective functions for representation of equal importance. Note that, the summation of the weightage coefficients must fulfil:

$$w_1 \ = \ w_2 \ = \ ... \ w_i, \quad \forall_i = \{1, 2, ...P\} \tag{7.15}$$

$$\sum_{i=1}^{P} w_i = 1 \tag{7.16}$$

The solutions to the MOO will be $U_{moo}^d = U_{moo}^{d*}$ giving an optimum value of the objective functions equal to J_{moo}^*.

Step 11: Solving optimization. The optimization problem (SOO or MOO) is solved using the Matlab Optimization toolbox in *Matlab 2014* using *fmincon* solver.

Remark 7.1: In the present study, there are two performance measures: $\psi_1 =$ NPV and $\psi_2 =$ v-gap. The performance measure consists of two parts: linear and interactive terms of the main parameter effects. Here, $\alpha_{k0}, \alpha_{k1,j}$ and $\alpha_{k2,i,j}$ are coefficients while ϵ_k denotes the fitting error. The size of the coefficients represent the magnitudes of effects of the corresponding parameters or interactive parameters on ψ_k. Thus, the influences of the parameters on ψ_k can be quantified and

ranked via the analysis of the RSM coefficients. The single-parameter terms or interactive parameter terms with small coefficient magnitudes compared with the maximum magnitude of coefficient will be discarded from the overall optimization in Step 11.

A short summary of the optimization methodology is illustrated in Figure **??**

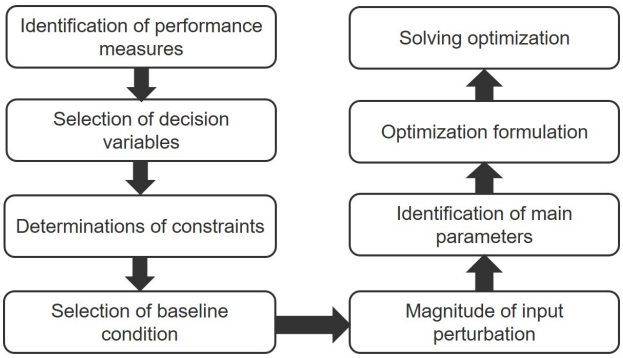

Figure 7.2: Summary of the process of multi-objective optimization.

7.4 Results and Discussion

7.4.1 Single objective optimization - Economic analysis

Bear in mind that, the objective for this optimization formulation is to maximize NPV of the WGSR-MR system design. Following the step 8 in the methodology, identification of main parameters or decision variables is conducted via PCA. This leads to identification of the main variables that affect the values of NPV. Figure 7.3 - 7.5 show the PCA results for the combination of 8 parameters (i.e., 3 design parameters and 5 operating parameters).

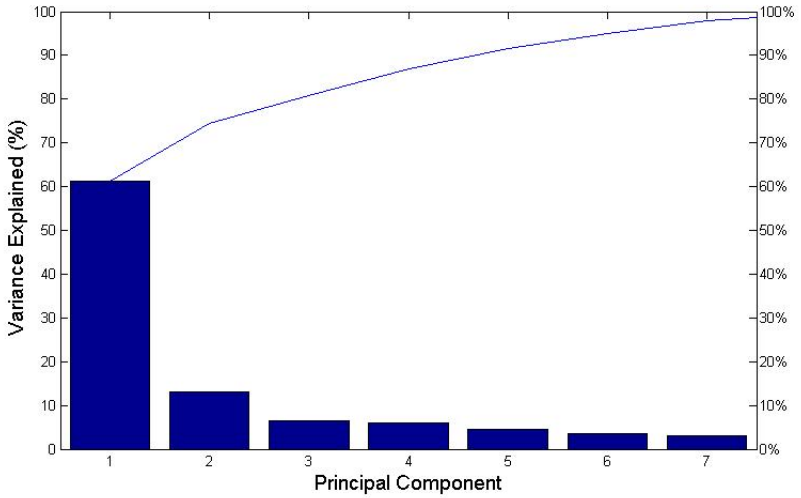

Figure 7.3: Pareto plot based on PCA analysis towards both operating and design parameters.

Figure 7.3 provides the detailed pareto plot whereby the plot shows that three major components required for selecting the critical parameters that affect the NPV of this system. Figure 7.4 shows the critical parameters that affect NPV based on major components 1 and 2, while Figure 7.5 shows the other critical parameters that has similar effect on NPV but is based on major components 1 and 3. These two plots are shown instead of a 3-dimensional figure for ease of understanding and clarity of the critical parameters.

By combining both Figure 7.4 and Figure 7.5, one can see that NPV is directly correlated with all 8 parameters (these parameters either on the same quadrant as NPV or opposite quadrant, i.e., 2 & 4 quadrants in Figure 7.4 and 1 & 3 quadrants in Figure 7.5). However, only few parameters have large impact on NPV (based on their individual scores - see Figure 7.4 and 7.5). These parameters are retentate temperature, retentate pressure, permeate pressure and H_2O to CO concentration ratio. While the other 4 parameters have relatively less influences on NPV. Nevertheless, all 8 parameters are still used in the optimization due to their substantial effects on NPV. Furthermore, a RSM is constructed in this study to validate the results obtained by PCA. Also the RSM will be used later in the optimization.

Optimization SOO-1 is done based on SOO formulation explained in equation 7.12 which considers α_{k0} and $\alpha_{k1,j}$ only. While Optimization SOO-2 is based on equation 7.12 which takes into account both linear and interactive terms, $\alpha_{k0}, \alpha_{k1,j}$ and $\alpha_{k2,i,j}$. Table 7.2 shows the optimization result based on these two different

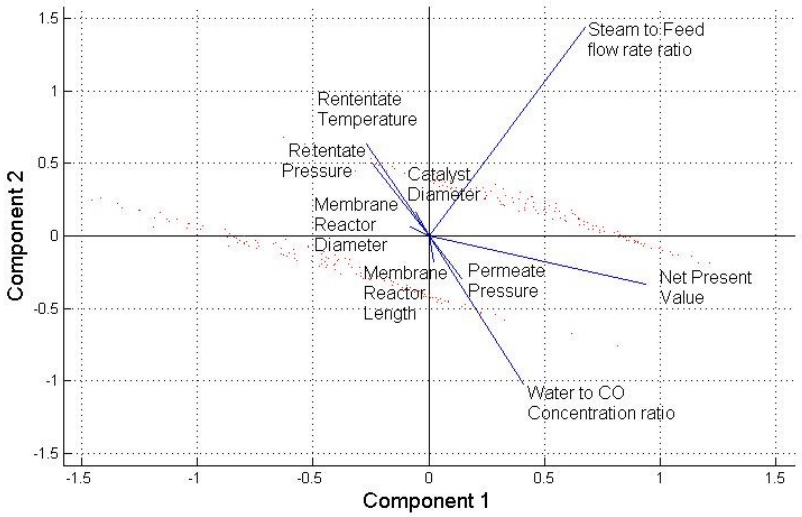

Figure 7.4: PCA analysis based on principal components 1 and 2.

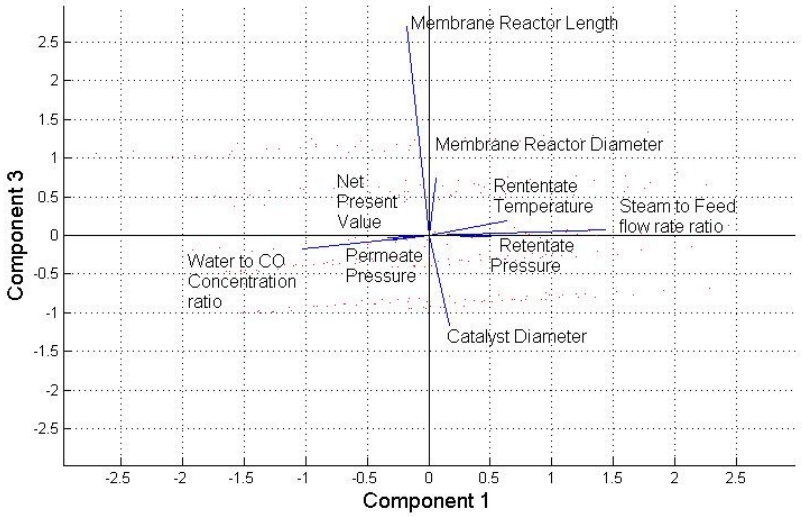

Figure 7.5: PCA analysis based on principal components 1 and 3.

optimization.

Table 7.2: Optimization results for both operating and design parameters based on economic performance

Variables	Optimization SOO-1	Optimization SOO-2
Membrane reactor length (m)	5.715	9.525
Membrane reactor diameter (m)	1.00	1.25
Catalyst pellet diameter (m)	0.004	0.008
H_2O to CO concentration ratio	4.0	2.0
Steam to feed flow rate ratio	0.05	0.05
Retentate temperature (K)	250	450
Retentate pressure (bar)	30.0	50.0
Permeate pressure (bar)	8.0	5.0
Net present value	**-8.17 $\times$ 10^8**	**8.57 $\times$ 10^8**
v-gap metric	**0.174**	**0.512**

Note: Net present value (NPV) is in $USD. This optimization only consider NPV and not v-gap metric.

Based on the optimization results in Table 7.2, it is obvious that parameters interaction plays an important part in optimization especially if it involves large number of parameters. The effect of parameters interaction is not as significant if the number of individual parameters is small. When the number of individual parameters increases, the number of parameters interaction will increase exponentially. Hence, while some of the parameters interaction terms maybe insignificant, other terms may have significant impact on NPV. In view of such behaviours of parameter interactions, one should not neglect the effect of combined parameters effects when there are more than four parameters under study. On top of that, the results shown in Table 7.2, prove that the four main parameters mentioned in PCA results have more significant effects on NPV (i.e., higher percentage changes).

The result obtained through optimization SOO-2 clearly shows that the maximum NPV is achieved at the constraints of every operating parameters. However for design parameters, the highest NPV is achieved somewhere near the middle of the constraint window such as, near the middle between the upper and lower limits of membrane reactor length and membrane reactor diameter - see Table

7.1. In order to prove the validity of this result, a RSM plot for the membrane reactor length and diameter versus NPV is generated.

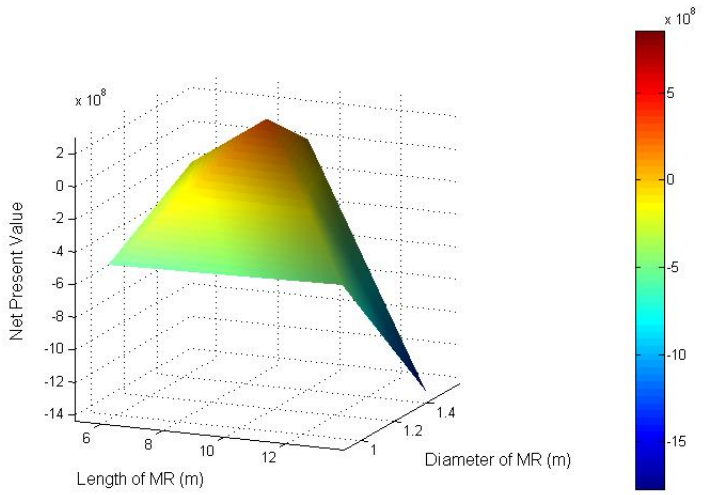

Figure 7.6: Effect of MR length and diameter towards NPV.

Figure 7.6, shows the effects of MR length and diameter on NPV. It shows that the highest peak of NPV is located near the middle of these two parameters. Hence, the results obtained in Table 7.2 is verified.

7.4.2 Multi-objective optimization - Economic and controllability

One of the main reason to combine both economic and dynamic operability into optimization, J^*_{moo}, is to determine an optimal balance between economic and dynamic operability. The optimization objective serves to maximize NPV while to ensure the system can be controlled effectively. In some cases where the optimization objective is to achieve optimum NPV value, the resulting design can be very difficult to control, i.e., poor controllability.

Figure 7.7 below illustrate the idea of b_{opt} (red coloured circle) and the importance of v-gap metric in identifying the robust plant operating conditions. If the worst v-gap either coming from upper or lower perturbation is greater than b_{opt}, it means that the system will behave as highly non-linear when encountering the disturbances. However, if even the worst case v-gap is within the area of b_{opt} as shown in Figure 7.7 (b), we can say for sure that the process system is still well-behaved when subjected to disturbances.

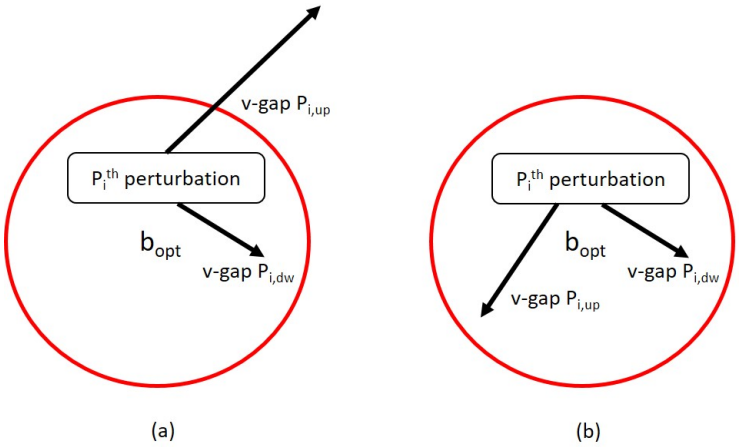

Figure 7.7: Example of b_{opt} and v-gap metric.

Based on the MOO optimization formulation stated in equation 7.13, the optimization result is tabulated in Table 7.3. Here, Optimization MOO-1 is based on MOO formulation without considering market uncertainties. The percentage deviation provided in this table represents the percentage difference between MOO-1 optimization as compared to SOO-2.

Table 7.3: Multi-objective optimization results

Variables	Optimization MOO-1	Percentage Deviation (%)
Membrane reactor length (m)	9.525	0.0
Membrane reactor diameter (m)	1.25	0.0
Catalyst pellet diameter (m)	0.008	0.0
H_2O to CO concentration ratio	2.1	5.0
Steam to feed flow rate ratio	0.05	0.0
Retentate temperature (K)	430	-4.4
Retentate pressure (bar)	45	-10.0
Permeate pressure (bar)	6.5	30.0
Net present value	**5.13×10^8**	**-40.1**
v-gap	**0.277**	**-45.9**

Note: Net present value (NPV) is in $USD.

In this study, the v-gap is calculated by assuming single-input single-output (SISO) controller is employed where the manipulated variable is the retentate feed flow rate. The retentate feed flow rate is assumed to fluctuate within ± 30% of its

baseline design value. This retentate feed flow varies in response to daily influence of product demand, hence the system has to be able to handle large disturbances while maintaining the safety and its performance (good controllability and high NPV). An upper and lower perturbation limits are applied to the perturbed condition, P_i. This results in two new conditions, $P_{i,up}$ and $P_{i,dw}$. Both these conditions are then used to calculate the linearized models which are used to compute v-gap values with respect to P_i and the largest value (worst case) is taken into account for the MOO optimization. Therefore, there is $2 \times (r + 1)$ v-gap values obtained including the one at the baseline condition. Note that, this is the simplest way to estimate the difficulty of controlling the system at a given operating condition. A more rigorous way would require more perturbations (with more than one inputs) around a given perturbed conditions.

Notice from Table 7.3, the SOO-2 based on NPV alone leads to a large v-gap value which implies the system is difficult to control when operated at the optimal condition. On the contrary, in the optimization MOO-1 where both NPV and controllability (v-gap) are simultaneously optimized, the v-gap is reduced by about 46% implying better controllability performance at the corresponding optimal conditions. Larger v-gap implies highly nonlinear dynamic response between the perturbed and base systems. Hence, this leads to difficulty in controlling the system dynamics. Therefore, a smaller v-gap value is often considered to guarantee both stability and good dynamic performance. However, the improvement on the process controllability comes with a penalty, i.e., the NPV value is reduced from USD 857 millions to USD 513 millions, equivalent to about 40% drop in NPV value with respect to that obtained via SOO-2.

7.4.3 Multi-objective Optimization with uncertainties

As mentioned in section 4, step 7 optimization includes the uncertainties factor. Here, by incorporation of $P(y|x)$ into equation 7.13 yields the following optimization formulation shown in equation 7.17.

$$\begin{aligned} J^*_{moo,un} = \max_{U^d_{moo,un}} \quad & w_1\psi_1(U^d_1) + w_2\psi_2(U^d_2) + ...w_P\psi_P(U^d_P) \\ \text{subject to} \quad & U^d_{moo,min} < U^d_{moo} < U^d_{moo,max} \\ & Pro_z(y|x) \end{aligned} \tag{7.17}$$

Whereby, Pro_z is the probability of z uncertainties. The value of uncertainty is obtained using MCMC technique. Figure 7.8 shows the distribution with the high-

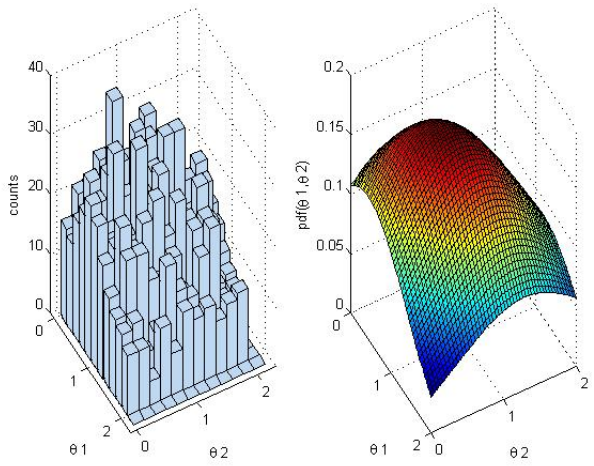

Figure 7.9: Electric cost computed by MCMC.

est probability of hydrogen selling price. The value computed through MCMC simulation is $ USD 3.7552/ kg of hydrogen. Figure 7.9 illustrates the highest probability of electrical cost is $ USD 16.31 cents/ kWh. These two obtained values are then embedded into the multi-objective optimization to calculate a new optimal values of the operating and design parameters.

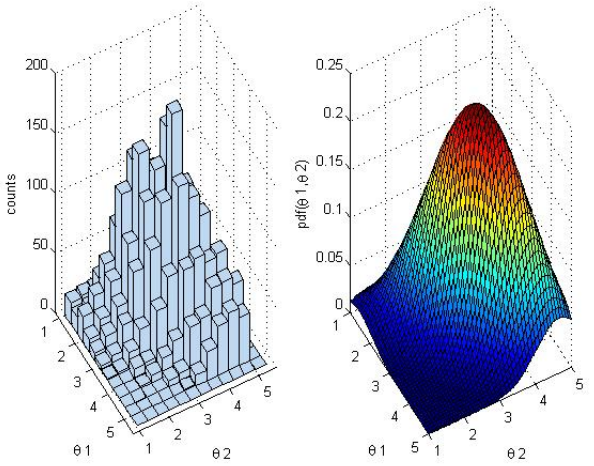

Figure 7.8: Hydrogen selling price computed by MCMC.

The results obtained from optimization with uncertainty through Optimization MOO-2 are shown in Table 7.4. The percentage deviation shows the deviation of MOO-2 (optimization with uncertainties) as compared to MOO-1 (without

Table 7.4: Multi-objective optimization results with uncertainty

Variables	Optimization MOO-2	Percentage Deviation (%)
Membrane reactor length (m)	9.525	0.0
Membrane reactor diameter (m)	1.25	0.0
Catalyst pellet diameter (m)	0.008	0.0
H_2O to CO concentration ratio	2.1	0.0
Steam to feed flow rate ratio	0.05	0.0
Retentate temperature (K)	430	0.0
Retentate pressure (bar)	43.5	-3.3
Permeate pressure (bar)	7.0	7.7
Net present value	$\mathbf{4.71 \times 10^8}$	**-8.2**
v-gap	**0.253**	**-8.7**

Note: Net present value (NPV) is in $ USD.

market uncertainties). It is shown that with the incorporation of uncertainty values, there is a slight change in the values especially on the retentate pressure and permeate pressure. The change in pressure caused by high consumption of electricity to run the compressor. Previously the electricity cost used in MOO-1 is USD 10.60 cents/ kWh and USD 2.00/ kg for hydrogen selling price. Through MCMC simulation the newly generated selling price of hydrogen increase by 88% while the electricity cost increase by 54%. Even though hydrogen selling price has higher percentage increase than electricity cost, the optimization results show a decreased value in NPV. This can be expected since to generate one kg/h of hydrogen, it requires 43 kWh of electricity. Therefore, even with small increment in electricity cost, it will have significant impact on the NPV of this system. However, the decrease in the NPV value due to market uncertainties is less than 10% where the change in controllability in terms of v-gap value is small. It is interesting to point out that, the main reason for the hydrogen price to increase is the expected increase in demand of hydrogen as predicted by U.S Energy Outlook 2016 (Outlook et al., 2016). Hence, with expected increment in hydrogen selling price, it is possible to compensate for the rise of the electricity cost, which in turn implies that a positive NPV value remains attainable via the reliable MOO approach.

Although in this study exogenous process uncertainties are considered in the process optimization, there are still other process uncertainties in this design and

optimization stage of the WGSR-MR system. It is quite impossible to address all the uncertainties at one go, thus, the system may subject to lesser uncertainties. These process uncertainties are able to negatively or positively affect the performance of this system. Therefore, in order to safe guard this process system, process control is inevitable. Note that, in the next chapter a robust process control will be developed and used to control the performance of the WGSR-MR system under process uncertainties and daily perturbations.

7.5 Summary

In this chapter, the key points are summarized as follows:

- A new optimization methodology for WGSR-MR system is presented. The salient feature of the methodology is to reduce a large set of decision variables (design and operating parameters) into a smaller sub-set of dominant or critical variables, which strongly correlate with a given performance measure.

- An important contribution on the multi-objective optimization is the combination of optimization which considers net-present value as its economic parameter and v-gap metric as the dynamic controllability parameter. This optimization takes into account an optimal trade-off between the conflicting parameters.

- By making early consideration of process controllability in the design, one can avoid poor plant design that has control difficulties. Poor controllability imposes a serious threat to operational safety are difficult to operate and control.

- Process control plays an important role in process safety of an operation. Hence, in the next chapter, a robust process control scheme is developed for this WGSR-MR system for a smooth and safe process operation even under perturbations and uncertainties.

- The work in this chapter is under reviewed by Chemical Engineering Research and Design 2017. [1]

[1]Optimization of steady-state and dynamic performances of Water-Gas Shift Reaction in membrane reactor. Submitted to *Chemical Engineering Research and Design.*

Chapter 8

Triple-loop Parallel Cascade Control Strategy for WGSR-MR

8.1 Overview

Conducting water-gas shift reaction (WGSR) for hydrogen production and CO_2 capture via a membrane reactor (MR) represents a promising approach to improve energy security and greenhouse gas emission. This WGSR-MR system combines both reaction and separation in one unit capable of removing the equilibrium kinetic limitations inherent in the WGSR while producing high purity hydrogen. The WGSR-MR system possesses high-order dynamics and a large transport delay, which shall impose substantial challenges to control design but the issues remain scarcely addressed in the literature. This chapter advocates the use of a triple-loop parallel cascade control scheme to regulate the temperatures inside the membrane reactor. Regulating the exit temperature is important to prevent catalyst deactivation due to overheating and to maintain the hydrogen yield in the presence of disturbances. Rigorous stability analyses based on the classical Routh-Hurwitz criteria and the recent Multi-scale Control (MSC) scheme are performed as to construct stabilizing regions for the tertiary, secondary and primary P/P/PIDF controllers. Considering the identified stabilizing regions, a generalized procedure for tuning the parallel cascade control scheme is proposed. An extensive numerical study based on the WGSR-MR system is carried out to evaluate the effectiveness of the control scheme. The rest of this chapter is organized as follows. Section 8.2 explains in brief the preliminary of multi-scale control scheme. This is followed by section 8.3 which presents the development of the controller design starting from the innermost (slave controller) to the outermost

(master controller). This section establishes tuning rules for each controller loop (i.e., controller gain, integral, derivative, and lead-lag filter). Meanwhile, section 8.4 presents a general tuning procedure to tune the triple-loop cascade control scheme. Lastly, section 8.5 covers the application of the developed triple-loop parallel cascade scheme in the WGSR-MR system. This section identifies the robustness of the control scheme based on the performance of the controller under disturbance rejection, setpoint tracking and modelling uncertainties.

8.2 Preliminary

8.2.1 Multi-Scale control scheme

The multi-scale control (MSC) scheme is introduced by Nandong and Zang (2014a). The basic idea of the MSC is to decompose a complex plant P into a sum of its basic modes, which will be either first- or second-order systems with real coefficients. Through this decomposition, it is easier to design several sub-controllers where each is based on a specific mode than to design an overall controller directly. Plus, the conventional controller design approach can be very difficult to apply especially to a high-order system with complicated dynamics. The plant decomposition is represented as follows:

$$P(s) = m_0 + m_1 + m_2 + ... + m_n \tag{8.1}$$

where m_i, $i = 0, 1, 2,..., n$ indicates the basic modes. The outermost mode is the slowest mode in the system and is represented by m_0, meanwhile m_i, $i = 1, 2,..., n$ are known as the inner layer modes. The modes are arranged in the order of increasing speed of responses towards a manipulated variable change.

The sub-controllers for all the individual plant modes combined in such a way capable of enhancing the cooperation among the different modes. In this case, a two-layer MSC scheme assuming the plant system (e.g., the primary process) can be decomposed into a sum of two modes only. In Figure 8.1, K_1 denotes the sub-controller for the innermost loop, $W = m_1$ indicates the multi-scale predictor and K_0 the sub-controller for the outermost m_0.

In Figure 8.1, the closed-loop inner layer transfer function is expressed as follows

$$G_1(s) = \frac{K_1(s)}{1 + K_1(s)W_1(s)} \tag{8.2}$$

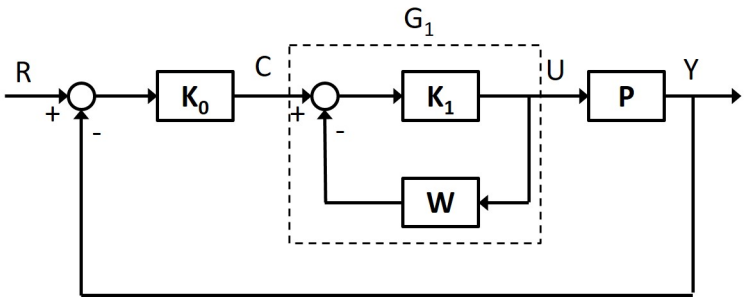

Figure 8.1: Block diagram of a two-layer MSC scheme.

The overall multi-scale controller can be obtained as follows

$$K_{msc}(s) = K_0(s)G_1(s) \tag{8.3}$$

8.3 Fundamental of Triple-loop Parallel Cascade Scheme

In the triple-loop parallel cascade control strategy there are three controllers to be designed. The order of controller design is from the innermost loop to the outermost loop where the design takes place in sequence. Figure 8.2 shows the generalized block diagram for the proposed triple-loop parallel cascade control strategy. As illustrated in Figure 8.2, the first (slave) controller loop is usually the fastest responding loop in the system and should be the closest to the disturbance sources. For simplicity, a Proportional (P) controller with gain Kc_3 is used for the first loop. Once the P controller has been obtained, the second P controller with gain Kc_2 and the third PIDF controller with gain Kc_1 are then tuned in sequence.

For controller tuning purposes, the primary, secondary, and tertiary transfer functions are represented by a first-order plus deadtime (FOPDT) model given by

$$P_i(s) = \frac{Y_i(s)}{U(s)} = \frac{K_{pi}\exp(-\theta_i s)}{\tau_{pi}s + 1} \ , \ i \ = \ 1, 2, 3 \tag{8.4}$$

where K_{pi}, τ_{pi} and θ_i denote the process gain, time constant, and deadtime for the i^{th} process respectively.

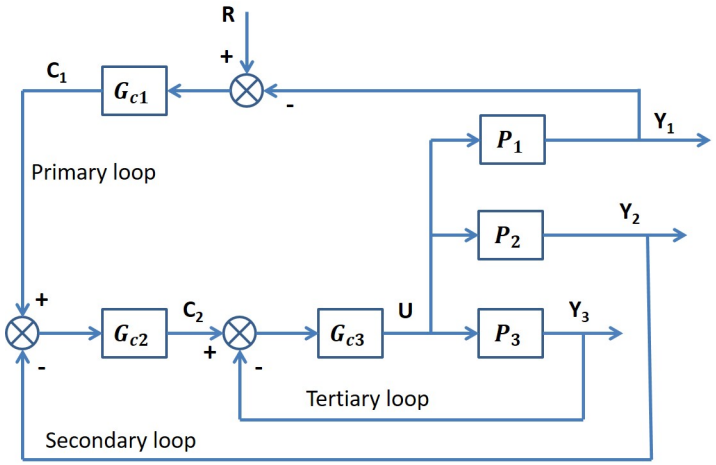

Figure 8.2: General structure of three loops parallel cascade control.

8.3.1 Tertiary controller design

For the innermost loop, a Proportional (P) controller is selected where, $G_{c3} = K_{c3}$. In this study, the controller tuning relations will be established once the stability region is found. Once the stability region is obtained, regardless of the tuning parameter value, as long as the values fall within the stability region, it can be guaranteed that the controller tuning will be stable. To find a stability region corresponding to the P controller, the necessary criterion of Routh stability is first apply.

The tertiary closed-loop characteristic equation is $1 + G_{c3}P_3 = 0$. By using first order Pade formula to approximate the deadtime term in P_3, i.e., $\exp(-\theta_3 s) \simeq \frac{1-0.5\theta_3 s}{1+0.5\theta_3 s}$, the closed-loop characteristic equation becomes

$$1 + K_{c3}\frac{K_{p3}(1 - 0.5\theta_3 s)}{(1 + 0.5\theta_3 s)(\tau_{p3}s + 1)} = 0 \tag{8.5}$$

By expanding (8.5),

$$0.5\tau_{p3}\theta_3 s^2 + (0.5\theta_3 + \tau_{p3} - 0.5K_3\theta_3)s + 1 + K_3 = 0 \tag{8.6}$$

where the loop gain $K_3 = K_{c3}K_{p3}$. From (8.6), in order to achieve necessary criterion of stability, all the coefficients of (8.6) have to be greater than 0. As a result, the stability region for G_{c3} can be derived as follows.

Note that, the coefficient of s^2 is always greater than zero as τ_{p3} and θ_3 are always positive. Based on the coefficient of s in the closed-loop characteristic polynomial, one can establish an upper limit on the loop gain as follows:

$$K_3 < \frac{0.5\theta_3 + \tau_{p3}}{0.5\theta_3} \tag{8.7}$$

Hence, a stability region for P controller in the tertiary loop is obtained:

$$K_{c3} = r_{p_3}\left(\frac{0.5\theta_3 + \tau_{p3}}{0.5\theta_3 K_{p3}}\right) \ , \ 0 \ < \ r_{p_3} \ < \ 1 \tag{8.8}$$

Note that, r_{p_3} is a dimensionless parameter which can used to tune the P controller. Assuming the deadtime is approximated by the first-order Pade formula, the closed-loop transfer function from C_2 to U is

$$H_{u2}(s) = \frac{K_{c3}(1 + 0.5\theta_3 s)(\tau_{p3}s + 1)}{0.5\tau_{p3}\theta_3 s^2 + (0.5\theta_3 + \tau_{p3} - 0.5K_3\theta_3)s + 1 + K_3} \tag{8.9}$$

Equation 8.9 can be reduced to a general second-order process given by

$$H_{u2}(s) = \frac{(\tau_z s + 1)\exp(-\theta s)}{\tau_{o3}^2 s^2 + 2\zeta_{o3}\tau_{o3}s + 1} \tag{8.10}$$

where τ_{o3} and ζ_{o3} are

$$\tau_{o3} = \sqrt{\frac{0.5\tau_{p3}\theta_3}{1 + K_3}} \tag{8.11}$$

$$\zeta_{o3} = \frac{0.5\theta_3 + \tau_{p3} - 0.5rp_3(\frac{2\tau_{p3}+\theta_3}{\theta_3})}{2\sqrt{0.5\tau_{p3}\theta_3(1 + r_{p_3}(\frac{2\tau_{p3}+\theta_3}{\theta_3}))}} \tag{8.12}$$

The damping factor ζ_{o3} has to be greater than 1 in order to obtain real and distinct roots. Hence, the transfer function H_{u2} can be expressed in the form of:

$$H_{u2}(s) = \frac{K_{c3}(\tau_{p3}s + 1)(1 + 0.5\theta_3 s)}{(\tau_{a3}s + 1)(\tau_{b3}s + 1)} \tag{8.13}$$

where

$$\tau_{a3} = -\frac{1}{\tau_{o3}(-\zeta_{o3+\sqrt{\zeta_{o3}^2+1}})} \quad , \zeta_{o3} > 1 \tag{8.14}$$

$$\tau_{b3} = -\frac{1}{\tau_{o3}(-\zeta_{o3+\sqrt{\zeta_{o3}^2-1}})} \quad , \zeta_{o3} > 1 \tag{8.15}$$

By using the model reduction rules established in Skogestad (2003), the transfer function H_{u2} can be further reduced into:

$$H_{u2} = K_{Hu2}\left(\frac{0.5\theta_3 s + 1}{\tau_{b3}s + 1}\right) \tag{8.16}$$

$$K_{Hu2} = \frac{K_{c3}\tau_{p3}}{\tau_{a3}} \tag{8.17}$$

Here, the Skogestad's rule is applied to reduce the model which will be used to develop tuning relations for the secondary and primary controllers.

8.3.2 Secondary controller design

The closed loop setpoint transfer function from C_1 to U based on Figure 8.3 is given by:

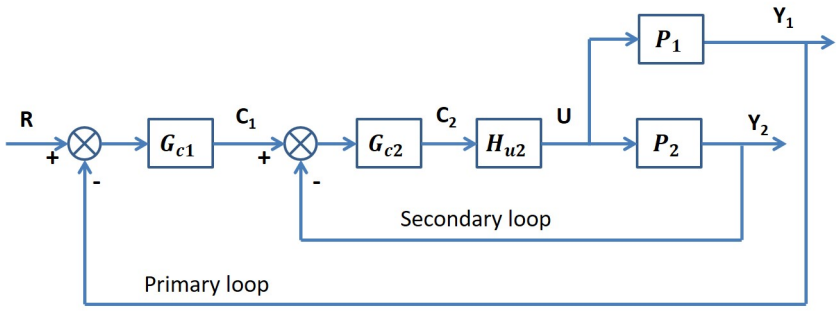

Figure 8.3: Block diagram of parallel cascade control of secondary loop controller.

$$H_{u1}(s) = \frac{G_{c2}(s)H_{u2}(s)}{1 + G_{c2}(s)H_{u2}(s)P_2(s)} \tag{8.18}$$

Again for simplicity, a Proportional (P) controller is used for the secondary loop, i.e., $G_{c2} = K_{c2}$. The characteristic equation for the secondary loop controller $1 + G_{c2}H_{u2}P_2 = 0$.

Assuming the deadtime is approximated via the first-order Pade formula, the closed-loop characteristic equation becomes:

$$1 + K_2 \left(\frac{1 + 0.5\theta_3 s}{\tau_{b3}s + 1}\right)\left(\frac{1 - 0.5\theta_2 s}{1 + 0.5\theta_2 s}\right)\left(\frac{1}{\tau_{p2}s + 1}\right) = 0 \tag{8.19}$$

where the secondary loop gain $K_2 = K_{c2}K_{Hu2}K_{p2}$. A third-order closed-loop characteristic polynomial is obtained:

$$\begin{aligned} &0.5\theta_2\tau_{p2}\tau_{b3}s^3 + (\tau_{p2}\tau_{b3} + 0.5\theta_2\tau_{p2} + 0.5\theta_2\tau_{b3} - 0.25\theta_2\theta_3K_2)s^2 \\ &(\tau_{p2} + \tau_{b3} + 0.5\theta_2 + 0.5\theta_3K_2 - 0.5\theta_2K_2)s + 1 + K_2 = 0 \end{aligned} \tag{8.20}$$

Based on the necessary Routh stability criterion, all of the coefficients of s must be greater than zero. The coefficient of s^3 is definitely greater than

zero because the process deadtime and time constant are always positive, i.e., $0.5\theta_2\tau_{p2}\tau_{b3} > 0$.

As for the coefficient of s^2, for this coefficient to be greater than zero, an upper bound on the loop gain K_2 is required:

$$K_2 < \frac{\tau_{p2}\tau_{b3} + 0.5\theta_2\tau_{p2} + 0.5\theta_2\tau_{b3}}{0.25\theta_2\theta_3} \tag{8.21}$$

Based on the coefficient of s, either an upper or lower bound of the loop gain K_2 can be given depending on the values of secondary and tertiary process deadtimes:

$$K_2 > -\frac{\tau_{p2} + \tau_{b3} + 0.5\theta_2}{0.5(\theta_3 - \theta_2)} \quad , \text{if} \quad \theta_3 > \theta_2 \tag{8.22}$$

$$K_2 < \frac{\tau_{p2} + \tau_{b3} + 0.5\theta_2}{0.5(\theta_2 - \theta_3)} \quad , \text{if} \quad \theta_2 > \theta_3 \tag{8.23}$$

Assuming that $\theta_3 > \theta_2$, equation 8.22 shows that the lower bound of the loop gain is a negative. Hence, the maximum lower bound for the loop gain is zero, i.e., based on the coefficient of s^0. With regard to the second condition where $\theta_2 > \theta_3$ is most likely to occur in a tubular reactor, the upper limit on the loop gain in equation 8.23 shall be obtained.

Considering that $\theta_3 > \theta_2$, the loop gain can be expressed as follows:

$$K_2 = r_{p_2}\left(\frac{\tau_{p2}\tau_{b3} + 0.5\theta_2\tau_{p2} + 0.5\theta_2\tau_{b3}}{0.25\theta_2\theta_3}\right) \ , \ 0 \ < \ r_{p_2} \ < \ 1 \tag{8.24}$$

In the case of $\theta_2 > \theta_3$, there are two upper bounds on loop gain K_2. For a stable tuning, the loop gain must be in between its maximum lower bound and minimum upper bound. Therefore, the loop gain has to be less than the minimum upper bound.

$$K_2 = r_{p_2} \ \min[K_{2a}, K_{2b}] \ , \ 0 \ < \ r_{p_2} \ < \ 1 \tag{8.25}$$

where r_{p_2} is a parameter between 0 and 1, while K_{2a} and K_{2b} are the upper bounds shown in equations 8.21 and 8.23 respectively.

8.3.3 Primary controller design

For the primary control loop, a proportional-integral-derivative (PID) controller is used to control the primary process. Note that, PID-type controller is the most common control scheme used in industries (Åström and Hägglund, 2004).

There are several forms of PID controller that have been reported in literature where one of the forms is known as an ideal PID controller given as:

$$K_{PID}(s) = K_C \left(1 + \frac{1}{\tau_I s} + \tau_D s\right) \tag{8.26}$$

where K_C, τ_I and τ_D denotes the controller gain, integral time, and derivative time respectively. The stability theorems corresponding to the PID comptroller form in equation 8.26 have recently been established by Seer and Nandong (2017). These theorems are adapted and applied to construct the stabilizing region of PID controller used in the primary loop (i.e., in Section 8.3.3).

However, the use of an ideal PID controller in industries is still fairly limited. The reason for this is that an ideal PID controller is susceptible to encountering 'derivative kick' which can lead to a large impulse spike in the controller output. In a long run, the impulse spike can cause damages to the actuators and the equipment. Hence, in order to reduce the impulse spike, first order lag filter is added into the ideal PID controller, i.e.,:

$$K_{PIDF}(s) = K_C \left(1 + \frac{1}{\tau_I s} + \tau_D s\right)\left(\frac{1}{\tau_F s + 1}\right) \tag{8.27}$$

In equation 8.27, there are four tuning parameters to be determined. In most of the existing tuning rules, the filter time constant (τ_F) is often determined in an ad-hoc manner or simply set to a small value. In developing the primary controller design, a new transfer function in equation 8.28 is developed based on the combination of the tertiary and secondary controller loop - see Figure 8.4.

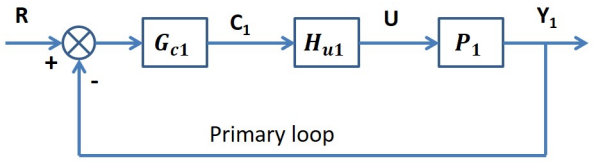

Figure 8.4: Primary controller loop that combine both tertiary and secondary loops.

$$\frac{Y_1}{R} = \frac{G_{c1}H_{u1}P_1}{1 + G_{c1}H_{u1}P_1} \tag{8.28}$$

The transfer function H_{u1} in equation 8.28 is obtained from equation 8.18. However, the denominator of the transfer function is in third order and hence, a reduction rule is applied to simplify the transfer function H_{u1}. By substituting

H_{u2} obtained in equation 8.16 into equation 8.18, the transfer function of H_{u1} simplifies to:

$$H_{u1} = \frac{K_2^o(0.5\theta_3 s + 1)(0.5\theta_2 s + 1)(\tau_{p2} s + 1)}{\tau_{Ts3} s^3 + \tau_{Ts2} s^2 + \tau_{Ts1} s + 1 + K_2} \tag{8.29}$$

where

$$\begin{aligned}
\tau_{Ts3} &= 0.5\theta_2 \tau_{b3} \tau_{p2} \\
\tau_{Ts2} &= 0.5\theta_2 \tau_{p2} + 0.5\theta_2 \tau_{b3} + \tau_{b3} \tau_{p2} - 0.25\theta_2 \theta_3 K_2 \\
\tau_{Ts1} &= 0.5\theta_2 + \tau_{p2} + \tau_{b3} + 0.5\theta_3 K_2 - 0.5\theta_2 K_2 \\
K_2^o &= K_2 K_{Hu2} \\
K_2 &= K_2 K_{Hu2} K_{p2}
\end{aligned} \tag{8.30}$$

Note that, the denominator of equation 8.29 is simplified by factorization, which can lead to either one of the following:

$$H_{u1} = \frac{K_2^o(0.5\theta_3 s + 1)(0.5\theta_2 s + 1)(\tau_{p2} s + 1)}{(\tau_{a2} s + 1)(\tau_{c2}^2 s^2 + 2\zeta_{o2}\tau_{c2} s + 1)} \quad \text{, if} \quad \zeta_{o2} < 1 \tag{8.31}$$

$$H_{u1} = \frac{K_2^o(0.5\theta_3 s + 1)(0.5\theta_2 s + 1)(\tau_{p2} s + 1)}{(\tau_{a2} s + 1)(\tau_{b2} s + 1)(\tau_{c2} s + 1)} \quad \text{, if} \quad \zeta_{o2} > 1 \tag{8.32}$$

By applying Skogestad rule (Skogestad, 2003), the transfer function H_{u1} in equation 8.32 is reduced to

$$H_{u1} = \frac{K_{Hu1}(0.5\theta_2 s + 1)}{(\tau_{sc1} s + 1)(\tau_{b2} s + 1)} \tag{8.33}$$

Equation 8.32 can be further reduced to

$$H_{u1} = \frac{K_{Hu1}}{\tau_{hu1} s + 1} \tag{8.34}$$

where

$$\begin{aligned}
K_{Hu1} &= K_2^o \left(\frac{\tau_{p2}}{\tau_{a2}} \right) \\
\tau_{sc1} &= \tau_{c2} - 0.5\theta_3 \\
\tau_{hu1} &= \frac{\tau_{sc1} \tau_{b2}}{0.5\theta_2}
\end{aligned} \tag{8.35}$$

Here, the closed-loop characteristic equation corresponding to the primary controller tuning is $1 + G_{c1} H_{u1} P_1 = 0$

Let us consider G_{c1} is a PID with filter (PIDF) controller as shown in equation 8.27. In this particular case, in order to reduce the polynomial order of the

characteristic equation, the first-order Taylor series is used to approximate the deadtime.

$$1 + K_{c1}\left(1 + \frac{1}{\tau_{I1}s} + \tau_{D1}s\right)\left(\frac{1}{\tau_{F1}s+1}\right)\left(\frac{K_{Hu1}}{\tau_{hu1}s+1}\right)\left(\frac{K_{p1}(1-\theta_1 s)}{\tau_{p1}s+1}\right) \quad (8.36)$$

The following polynomial is obtained by expanding (8.36),

$$\begin{aligned}&(\tau_{I1}\tau_{F1}\tau_{hu1}\tau_{p1})s^4 + (\tau_{I1}\tau_{F1}\tau_{hu1} + \tau_{I1}\tau_{F1}\tau_{p1} + \tau_{I1}\tau_{hu1}\tau_{p1}\\ &- K_1\theta_1\tau_{I1}\tau_{D1})s^3 + (\tau_{I1}\tau_{F1} + \tau_{I1}\tau_{hu1} + \tau_{I1}\tau_{p1} + K_1\tau_{I1}\tau_{D1}\\ &- K_1\theta_1\tau_{I1})s^2 + (\tau_{I1} + K_1\tau_{I1} - K_1\theta_1)s + K_1 = 0\end{aligned} \quad (8.37)$$

where the primary loop gain $K_1 = K_{c1}K_{Hu1}K_{p1}$

The necessary Routh stability condition for a controller tuning is that all coefficients of s must be greater than zero as a prerequisite for closed-loop stability. Due to this condition, the corresponding ranges for the integral time constant, derivative time constant and primary loop gain can be derived.

In equation 8.37 the coefficient of s^4 is greater than zero as the time constant is always positive. From the coefficient of s^3, for this coefficient to be greater than zero, the primary loop gain has to obey the upper bound as in equation 8.38.

$$K_1 < \frac{\tau_{F1}\tau_{hu1} + \tau_{F1}\tau_{p1} + \tau_{hu1}\tau_{p1}}{\tau_{D1}\theta_1} \quad (8.38)$$

Based on the coefficient of s^2, either a lower or an upper bound is obtained:

$$K_1 > -\frac{(\tau_{F1} + \tau_{hu1} + \tau_{p1})}{(\tau_{D1} - \theta_1)} \quad \text{, if} \quad \tau_{D1} > \theta_1 \quad (8.39)$$

$$K_1 < \frac{(\tau_{F1} + \tau_{hu1} + \tau_{p1})}{(\theta_1 - \tau_{D1})} \quad \text{, if} \quad \tau_{D1} < \theta_1 \quad (8.40)$$

A few cases can occur for which are described as follows.

Case 1

If $\tau_{D1} > \theta_1$, then K_1 has only one upper bound which is given by equation 8.38 and a lower bound equals to zero. Equation 8.39 shows that the lower bound is a negative value, hence, zero is the maximum lower bound.

Case 2

If $\tau_{D1} < \theta_1$, then K_1 has two upper bounds given by equations 8.38 and 8.40. Between these two upper bounds, the smallest value of upper bound will be the new upper limit for the primary loop gain. Here, there are two possibilities, either the limit in equation 8.38 or 8.40 is the new upper limit. Hence, this case can be divided into two sub-cases.

Case 2.1

If the value obtained from equation 8.38 is smaller than the value of equation 8.40, then this leads to:

$$\frac{\tau_{F1}\tau_{hu1} + \tau_{F1}\tau_{p1} + \tau_{hu1}\tau_{p1}}{\tau_{D1}\theta_1} < \frac{(\tau_{F1} + \tau_{hu1} + \tau_{p1})}{(\theta_1 - \tau_{D1})} \tag{8.41}$$

Thus,

$$\tau_{D1} > \frac{\theta_1\tau_{F1}\tau_{hu1} + \theta_1\tau_{F1}\tau_{p1} + \theta_1\tau_{hu1}\tau_{p1}}{\theta_1\tau_{F1} + \theta_1\tau_{hu1} + \theta_1\tau_{p1} + \tau_{F1}\tau_{hu1} + \tau_{F1}\tau_{p1} + \tau_{hu1}\tau_{p1}} \tag{8.42}$$

Note that, equation 8.42 represents a lower bound for derivative time constant which is a result of the upper limit of K_1 in equation 8.38 be smaller than that in equation 8.40. Based on the conditions set in ***Case 2.1*** and in equation 8.42, the derivative time constant is expressed as:

$$\begin{aligned}\tau_{D1} =& r_{D_1}\left(\theta_1 - \frac{\theta_1\tau_{F1}\tau_{hu1} + \theta_1\tau_{F1}\tau_{p1} + \theta_1\tau_{hu1}\tau_{p1}}{\theta_1\tau_{F1} + \theta_1\tau_{hu1} + \theta_1\tau_{p1} + \tau_{F1}\tau_{hu1} + \tau_{F1}\tau_{p1} + \tau_{hu1}\tau_{p1}}\right) \\ &+ \frac{\theta_1\tau_{F1}\tau_{hu1} + \theta_1\tau_{F1}\tau_{p1} + \theta_1\tau_{hu1}\tau_{p1}}{\theta_1\tau_{F1} + \theta_1\tau_{hu1} + \theta_1\tau_{p1} + \tau_{F1}\tau_{hu1} + \tau_{F1}\tau_{p1} + \tau_{hu1}\tau_{p1}}\end{aligned} \tag{8.43}$$

where r_{D_1} is between 0 and 1.

Case 2.2

If the upper limit in equation 8.38 is greater than that in equation 8.40, then K_1 has an upper bound that follows equation 8.40 and this leads to:

$$\tau_{D1} < \frac{\theta_1\tau_{F1}\tau_{hu1} + \theta_1\tau_{F1}\tau_{p1} + \theta_1\tau_{hu1}\tau_{p1}}{\theta_1\tau_{F1} + \theta_1\tau_{hu1} + \theta_1\tau_{p1} + \tau_{F1}\tau_{hu1} + \tau_{F1}\tau_{p1} + \tau_{hu1}\tau_{p1}} \tag{8.44}$$

Now there are two upper bounds for the derivative time constant. A minimum upper bound is chosen to ensure stable tuning, thus, the derivative time constant is then chosen as follows:

$$\tau_{D1} = r_{D_1}\ \text{minimum}[\tau_{D1a}, \theta_1] \quad \text{, where} \quad 0 < r_{D_1} < 1 \tag{8.45}$$

where $\tau_{D1a} = \tau_{D1}$ from equation 8.44.

Based on the values of τ_{D1}, the controller gain is given by either

$$K_1 = r_{p_1}\left(\frac{\tau_{F1}\tau_{hu1} + \tau_{F1}\tau_{p1} + \tau_{hu1}\tau_{p1}}{\tau_{D1}\theta_1}\right) \ , \ 0 \ < \ r_{p_1} \ < \ 1 \tag{8.46}$$

or,

$$K_1 = r_{p_1}\left(\frac{(\tau_{F1} + \tau_{hu1} + \tau_{p1})}{(\theta_1 - \tau_{D1})}\right) \ , \ 0 \ < \ r_{p_1} \ < \ 1 \tag{8.47}$$

From equation 8.37, based on the coefficient of s the loop gain will encounter either a lower limit

$$K_1 > -\frac{\tau_{I1}}{(\tau_{I1} - \theta_1)} \quad , \text{if} \quad \tau_{I1} > \theta_1 \tag{8.48}$$

or an upper limit

$$K_1 < \frac{\tau_{I1}}{(\theta_1 - \tau_{I1})} \quad , \text{if} \quad \tau_{I1} < \theta_1 \tag{8.49}$$

Case 3

If integral time is greater than the primary loop process deadtime i.e., condition shown in equation 8.44, then the loop gain either follows ***Case 2.1*** or ***Case 2.2*** with the same boundary constraints. This is because the loop gain in equation 8.44 needs to be greater than a negative value, hence, the maximum lower bound is still zero.

Case 4

If the integral time is smaller than the primary process deadtime, i.e., as given by equation 8.49 then a new upper limit for the loop gain as a function of the integral time is formed. This then leads to multiple upper bounds with additional possibilities as in the ***Case 2.2***.

For this study, **Case 3** is adopted in the development of the primary loop control tuning. For this case, the limits of the loop gain and derivative time have been established previously by using the necessary criterion of stability. As for the integral time, its limit is determined based on sufficient criterion of stability. Sufficient criterion of stability corresponds to the Routh's array stability of the closed-loop characteristic polynomial. Rouths stability criterion determines the number of closed-loop poles in the right half s-plane.

The algorithm for attaining the sufficient Routh's stability criterion is as follow:

Step 1: The order of denominator of a closed-loop transfer function must be finite.

$$a_n s^n + a_{n-1} s^{n-1} + ... + a_0 = 0 \tag{8.50}$$

where $a_n \neq 0$ and $a_0 > 0$.

Step 2: The coefficients of the polynomial have to be arranged as follows, and subsequently, the values of the coefficients are calculated.

$$
\begin{array}{cccccc}
s^n & a_n & a_{n-2} & a_{n-4} & a_{n-6} & ... \\
s^{n-1} & a_{n-1} & a_{n-3} & a_{n-5} & a_{n-7} & ... \\
s^{n-2} & b_1 & b_2 & b_3 & b_4 & ... \\
s^{n-3} & c_1 & c_2 & c_3 & c_4 & ... \\
. & . & . & & & \\
. & . & . & & & \\
. & . & . & & & \\
s^1 & d_1 & & & & \\
s^0 & e_0 & & & &
\end{array}
\tag{8.51}
$$

where the coefficients b_i are

$$
b_i = \frac{a_{n-1} \times a_{n-2i} - a_n \times a_{n-2i-1}}{a_{n-1}} \tag{8.52}
$$

and so forth, till all subsequent coefficients are zero. Similarly, cross multiplication of the coefficients from the two previous rows to obtain c_i, ect.

$$
c_i = \frac{b_1 \times a_{n-2i-1} - a_{n-1} \times b_{i+1}}{b_1} \tag{8.53}
$$

until the n^{th} row of the array has been completed. Any missing coefficients are to be replaced by zeros (Shamash, 1975). The powers of s act as labels to the array, they are not considered to be a part of the array. The column beginning with a_0 is considered to be the first column of the array.

Step 3: Assuming that the necessary criterion is met (i.e., all coefficients of the closed-loop characteristic polynomial are positive), then for sufficient conditions, all the coefficients of constant b_i, c_i, ect., must be positive.

Based on the case study (**Case 3**), the polynomial coefficients,

$$
\begin{array}{lccc}
s^4: & a_4 & a_2 & a_0 \\
s^3: & a_3 & a_1 & 0 \\
s^2: & b_1 & b_2 & b_3 \\
s^1: & c_1 & c_2 & \\
s^0: & d_1 & &
\end{array}
\tag{8.54}
$$

the coefficients to be identified are b_1, b_2, b_3, c_1, c_2 and d_1; calculations are performed as in the Step 2.

Based on the coefficient of b_1, the bounds on integral or reset time are determined. One can have either a lower or an upper limit on the reset time:

$$\tau_{I1} > \frac{-\alpha_1\lambda_2}{\gamma_{1-5}\beta_{1-4} - \alpha_1\lambda_1} \quad \text{if} \quad \gamma_{1-5}\beta_{1-4} > \alpha_1\lambda_1 \tag{8.55}$$

or an upper limit

$$\tau_{I1} < \frac{\alpha_1\lambda_2}{\alpha_1\lambda_1 - \gamma_{1-5}\beta_{1-4}} \quad \text{if} \quad \gamma_{1-5}\beta_{1-4} < \alpha_1\lambda_1 \tag{8.56}$$

where

$$\begin{aligned}
\alpha_1 &= \tau_{F1}\tau_{hu1}\tau_{p1} \\
\beta_{1-4} &= \tau_{F1}\tau_{hu1} + \tau_{F1}\tau_{p1} + \tau_{hu1}\tau_{p1} - K_1\theta_1\tau_{D1} \\
\gamma_{1-5} &= \tau_{F1} + \tau_{hu1} + \tau(p1) + K_1\tau_{D1} - K_1\theta_1 \\
\lambda_1 &= 1 + K_1 \\
\lambda_2 &= K_1\theta_1
\end{aligned} \tag{8.57}$$

The lower limit shown in equation 8.55 has a negative value. Therefore, the maximum lower limit for the integral time constant is still given by the time-delay of the primary process as stated in **Case 3**. Please note that, the upper limit of the integral time is obtained from equation 8.56.

As for the coefficient of c_1, by combining all the possibilities of the upper and lower limits, the range of the integral time constant is:

$$\tau_{I1} = r_{I_1}\left(\frac{\alpha_1\lambda_2}{\alpha_1\lambda_1 - \gamma_{1-5}\beta_{1-4}} - \tau_{I1,lm}\right) + \tau_{I1,lm} \ , \ 0 \ < \ r_{I_1} \ < \ 1 \tag{8.58}$$

where

$$\tau_{I1,lm} = \text{maximum } [\tau_{I1}, \theta_1] \tag{8.59}$$

It is interesting to summarize that, for all the controller tuning from tertiary to primary loops, one only needs to tune the dimensionless positive parameters given as r_{p_3}, r_{p_2}, r_{p_1}, r_{I_1} and r_{D_1} whose values lie between 0 and 1.

8.3.4 Multi-scale control for primary controller design

Previously in Section 8.3.3, the primary controller design is based on the Routh-Hurwitz stability via the PID stability theorems in Seer and Nandong (2017). Also note that, it has been assumed that Hu_1 is an overdamped second order system. Alternatively, we can also design the primary controller via the Multi-scale Control (MSC) scheme reported in Nandong and Zang (2013a,b). Noteworthy, this MSC scheme has been successfully adopted in a number of control system

designs, e.g., in Nandong and Zang (2014b) and decentralized PID control (Nandong and Zang, 2014a). For details regarding the MSC scheme, please refer to the aforementioned references. The interest to use MSC scheme in this study is motivated by flexibility of the scheme to address both overdamped and underdamped systems. Also the MSC scheme can systematically be used to design first-order lag and lead-lag filters where conventionally they are designed in ad-hoc manners. Considering equation 8.31, where Hu_1 is an underdamped second order system, an augmented plant Pa_1 can be expressed as $Pa_1(s) = Hu_1(s)P_1(s)$, which is

$$Pa_1 = \frac{K_2^o Kp_1(0.5\theta_3 s + 1)(0.5\theta_2 s + 1)(\tau_{p2} s + 1)(1 - 0.5\theta_1 s)}{(\tau_{a2} s + 1)(\tau_{c2}^2 s^2 + 2\zeta_{o2}\tau_{c2} s + 1)(\tau_{p1} s + 1)(1 + 0.5\theta_1 s)} \tag{8.60}$$

Similarly, by applying Skogetad rules to reduce the order of the augmented plant, the following transfer function is produced

$$Pa_1 = \frac{K_1^o(0.5\theta_3 s + 1)(1 - 0.5\theta_1 s)}{(\tau_{c2}^2 s^2 + 2\zeta_{o2}\tau_{c2} s + 1)(1 + 0.5\theta_1 s)} \tag{8.61}$$

where the augmented process gain $K_1^o = K_2^o Kp_1(\tau_{p2}/\tau_{p1})$.

After obtaining equation 8.61, by using partial fraction expansion, the system reduces to a sum of two modes

$$Pa_1 = \frac{k_0(bs + 1)}{\tau_{c2}^2 s^2 + 2\zeta_{o2}\tau_{c2} s + 1} + \frac{k_1}{\beta s + 1}\ , \quad \beta = 0.5\theta_1 \tag{8.62}$$

It is assumed that the settling time of the underdamped second order mode is longer than the first order mode. Due to this assumption, the second-order mode is the outermost (slowest) one and the first-order part is the inner-layer mode. The modes parameters in equation 8.62 are given as follows:

$$k_1 = \frac{2K_{msc}\beta(\beta - 0.5\theta_3)}{\tau_{c2}^2 + 2\zeta_{o2}\tau_{c2}\beta + \beta^2} \tag{8.63}$$

$$K_{msc} = k_0 + k_1 \tag{8.64}$$

$$k_0 = \frac{K_{msc}(\tau_{c2}^2 + 2\zeta_{o2}\tau_{c2}\beta - \beta^2 + \theta_3\beta)}{\tau_{c2}^2 + 2\zeta_{o2}\tau_{c2}\beta + \beta^2} \tag{8.65}$$

$$b = -\frac{K_{msc}0.5\theta_3\beta + k_1\tau_{c2}^2}{k_0\beta} \tag{8.66}$$

In this case, the inner-layer mode is controlled by using a P-only controller with the gain equals to $k_{c,m1}$. The closed loop inner-layer transfer function becomes

$$G_1(s) = \frac{k_{c,m1}}{1 + k_{c,m1} m_1} = \frac{k^o_{c,m1}(\beta s + 1)}{\tau_{c1} s + 1} \tag{8.67}$$

where the overall gain and closed-loop time constant are given as

$$\begin{aligned} k_{c,m1} &= \frac{k_{c,m1}}{1 + k_{c,m1} k_1} \\ \tau_{c1} &= \frac{\beta}{1 + k_{c,m1} k_1} \end{aligned} \tag{8.68}$$

A ratio of open-loop time constant to closed-loop time constant is established

$$\lambda_1 = \frac{\beta}{\tau_{c1}} \tag{8.69}$$

where in practical control applications, the ratio has to be larger than unity for a more aggressive controller action. This means that the closed-loop system is faster than the corresponding open-loop system. Hence from equation 8.69, the sub-controller gain can be expressed as

$$k_{c,m1} = \frac{\lambda_1 - 1}{k_1} \quad \text{where } \lambda_1 > 1 \tag{8.70}$$

Similarly, one can also assume that a P-only controller is used to control the outermost mode, m_0, where the corresponding closed-loop outermost transfer function is

$$G_0 = \frac{k_{c,m0}}{1 + k_{c,m0} m_0} \tag{8.71}$$

which can be expressed as

$$G_0 = \frac{k^o_{c,m0}(\tau^2_{c2} s^2 + 2\zeta_{o2}\tau_{c2} s + 1)}{\tau^2_{c0} s^2 + 2\zeta_{c0}\tau_{c0} s + 1} \tag{8.72}$$

In equation 8.72, the overall gain, closed-loop time constant and damping coefficient are expressed as

$$k^o_{c,m0} = \frac{k_{c,m0}}{1 + k_{c,m0} k_0} \tag{8.73}$$

$$\tau_{c0} = \frac{\tau_{c2}}{\sqrt{1 + k_{c,m0} k_0}} \tag{8.74}$$

$$\zeta_{c0} = \frac{2\zeta_{o2}\tau_{c2} + k_{c,m0} k_0 b}{2\left(\frac{\tau_{c2}}{\sqrt{1 + k_{c,m0} k_0}}\right)} \tag{8.75}$$

As for the outermost mode case, the time constant ratio is

$$\lambda_0 = \frac{\tau_{c2}}{\tau_{c0}} \tag{8.76}$$

Therefore, the outermost sub-controller gain can be written in the form of

$$k_{c,m0} = \frac{\lambda_0^2 - 1}{k_0} \tag{8.77}$$

By substitution of equation 8.77 into equation 8.75, the closed-loop damping coefficient can be expressed in terms of time constant ratio

$$\zeta_{c0} = \frac{2\zeta_{o2}\tau_{c2} + (\lambda_0^2 - 1)b}{2\left(\frac{\tau_{c2}}{\lambda_0}\right)} \tag{8.78}$$

From equation 8.78, one can draw a general conclusion that as λ_0 increases, the system becomes less oscillatory while the time constant becomes larger. This is because the damping coefficient and time constant ratio have opposite trends in response to a change in λ_0. Therefore, there will be an optimum value for λ_0 in yielding a minimum closed-loop settling time.

It is recognized that a P-controller for the outermost-loop will not be efficient enough to remove the upcoming disturbances. Hence, one has to add the integral action to the outermost sub-controller. Furthermore, if the outermost mode is underdamped, it is suggested to add the derivative action to the outermost sub-controller in order to reduce the oscillatory nature of the closed-loop system.

In this work, we consider that the outermost sub-controller takes the following parallel PID form

$$K_0(s) = k_{c0}\left(1 + \frac{1}{\tau_I s} + \frac{\tau_D s}{\alpha\tau_D s + 1}\right) \tag{8.79}$$

The overall multi-scale controller can be shown to be in the form of parallel PID controller augmented with a lead-lag filter:

$$K_{msc} = k_{c0}k_{c,m1}^{o}\left(1 + \frac{1}{\tau_I s} + \frac{\tau_D s}{\alpha\tau_D s + 1}\right)\left(\frac{\beta s + 1}{\tau_{c1} s + 1}\right)\text{sign}(k_{c,m1}) \tag{8.80}$$

Here, the $\text{sign}(k_{c,m1})$ denotes the sign of the inner-layer sub-controller which is included in equation 8.80 in order to obtain the correct overall controller sign. The overall controller gain is obtained by direct comparison between equation 8.80 with the PID controller augmented with a lead-lag filter:

$$K_{msc} = K_C\left(1 + \frac{1}{\tau_I s} + \frac{\tau_D s}{\alpha\tau_D s + 1}\right)\left(\frac{\tau_{fd} s + 1}{\tau_{fg} s + 1}\right) \tag{8.81}$$

where the overall controller gain is

$$K_C = \left(\frac{\lambda_0^2 - 1}{k_0}\right)\left(\frac{k_{c,m1}}{1 + k_{c,m1}k_1}\right)\text{sign}(k_{c,m1}) \tag{8.82}$$

From (8.80), the lead-time is

$$\tau_{fd} = \beta = 0.5\theta_1 \tag{8.83}$$

and the lag-time is

$$\tau_{fg} = \tau_{c1} = \frac{\beta}{\lambda_1} \tag{8.84}$$

The reset or integral time can be specified as a fraction of the open-loop time constant, i.e.,

$$\tau_I = \rho_i \tau_{c2} \tag{8.85}$$

Similarly, the derivative time can be expressed in terms of

$$\tau_D = \frac{\rho_D}{\zeta_{o2}} \tag{8.86}$$

Note that, the value of α may be set to a small value (i.e. $\alpha < 0.1$). In general there are four tuning parameters (i.e. ρ_i, ρ_D, λ_0 and λ_1) for the MSC formula to meet the desired phase margin (PM) and gain margin (GM). The main purpose of using the MSC scheme to derive the tuning formula for the primary loop is to obtain a robust primary controller.

8.4 General Tuning Procedures

Step 1: Linearization of the process models. Manipulated and controlled variables are first identified for a process plant. Once the variables have been identified, a linearization of the process model (i.e., a transfer function) can be obtained. Note that, for simplification, the linearized model is then simplified via a model reduction (reduce high-order model into a first or second-order model).
Step 2: Tertiary controller tuning. Set $r_{p_3} = 0.01$ and gradually increased the values until a desired gain margin (GM) of about 8.0 dB and phase margin (PM) about 60 - 80°. Once r_{p_3} value is obtained, the tertiary controller tuning is calculated by using equation 8.8.
Step 3: Secondary controller tuning. Set $r_{p_2} = 0.01$ and gradually increase the value until GM of about 8.0 dB and PM about 60 - 80°. Once r_{p_2} value is

obtained, the secondary controller tuning is calculated by using either equation 8.24 or 8.25.

Step 4: Primary controller tuning using PIDF controller tuning.

Method 1 - PIDF controller tuning. Initially set τ_F to a small value (i.e.,$\tau_F = 0.1$). Then, set $r_{D_1} = r_{I_1} = r_{p_1} = 0.1$. Gradually increase r_{p_1} until GM is about 8.0dB. Next, moderately increase r_{D_1} and r_{I_1} until PM is about 60 - 80^o. Once all the parameters values are attained, the primary loop controller tuning can be expressed as in equation 8.27.

Method 2 - MSC controller tuning. First, set $\alpha = 0.1$. Second, set $\rho_D = \rho_i = 0.1$ and $\lambda_0 = \lambda_1 = 1.2$. Gradually increase λ_0 and λ_1 until GM = 8.0dB is reached. Then, increase ρ_D and ρ_i until a desired value of PM is achieved. Note that, for a better disturbance rejection, it is often suggested to set $\lambda_0 > \lambda_1$. When all parameters are obtained, the PID controller based on MSC can be expressed via equation 8.81.

Step 5: Evaluate performance and robustness. A triple-loop controller robustness is first compared to a double-loop parallel cascade control design. Then, a triple-loop parallel cascade control scheme using the PIDF controller is then compared with a triple-loop using MSC controller in terms of disturbance rejection, setpoint tracking, and under modelling uncertainties.

8.5 Application

For this study, the newly developed triple-loop parallel cascade control design methodology is applied to a WGSR-MR system. The idea of this implementation is to control the temperature of the membrane reactor when the system is subjected to several disturbances such as flowrate disturbances of ± 30%, temperature disturbances of ± 5% and modelling errors of ± 30%.

Here, the inlet plant feed flow rate is the major disturbance in this process system as feed flow rate keeps varying in response to daily fluctuation (due to product demand and product purity). This fluctuation influences the production of hydrogen and the temperature of the membrane reactor. It should be noted that the temperature is the most important variable in view of its potential influence over catalyst's deactivation. Moreover, runaway reaction may occur due to poor designs of the flowsheet and/or temperature control system. In term of challenge to control design, this WGSR-MR is subjected to long delay in the outlet response time due to the use of long membrane tubes. As mentioned

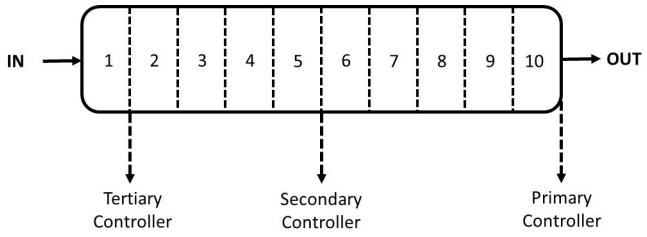

Figure 8.5: Primary, secondary, and tertiary controllers placement in the WGSR-MR.

earlier, a double loop parallel cascade control may be insufficient in handling such a large time-delay system. Therefore, in this work a triple-loop parallel cascade control is developed to counter the effect of long time-delay in the WGSR-MR system. As reported in (Saw and Nandong, 2016), for efficient modelling and simulation purposes, the WGSR-MR is divided into 10 equal sub-sections; the primary, secondary, and tertiary controller measurements are placed at the selected sub-sections - see Figure 8.5. The manipulated variable is the recycled ratio of retentate flow rate which indirectly controlled the inlet temperature of the steam. The objective of the control system is to control the outlet temperature of the membrane reactor against process disturbances. When encountering the process disturbances, the tertiary and secondary controller of this process system will quickly reduce the disturbance effect before it significantly upsets the whole process system.

Upon linearization, the transfer function from manipulated variable to reactor temperature at the tertiary location (see Figure 8.5) P_3(s) is

$$P_3(s) = \frac{(2.127 \times 10^{-5} \exp(-0.03s))}{1.087s + 1} \tag{8.87}$$

while the secondary process P_2(s)

$$P_2(s) = \frac{(2.098 \times 10^{-5} \exp(-1.62s))}{4.061s + 1} \tag{8.88}$$

and the primary process P_1(s)

$$P_1(s) = \frac{(2.830 \times 10^{-5} \exp(-5.68s))}{7.573s + 1} \tag{8.89}$$

A comparative study on performance/robustness is done between the double-loop and triple-loop parallel cascade control (PCC) in terms of disturbance rejection. Here, a decrement of 20 K in inlet temperature at time = 4 hr is set as

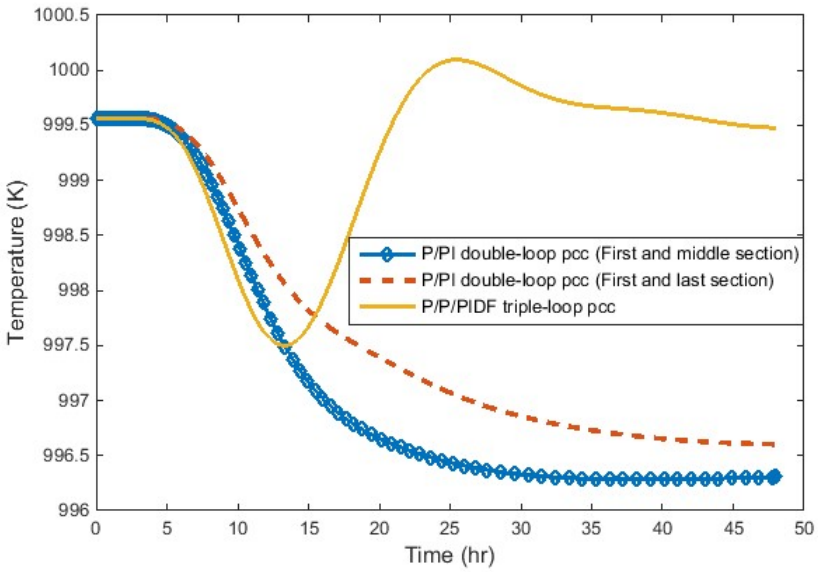

Figure 8.6: Outlet temperature subjected to inlet temperature disturbance.

the disturbance to the WGSR-MR system. Notice in Figure 8.6, there are two different double-loop PCC scheme. The red dashes line represents the double-loop PCC scheme where the controllers are placed at the P_3 and P_1 locations (see Figure 8.5). Meanwhile, the blue dotted line represents the double-loop PCC controller placed at the P_3 and P_2 locations.

As illustrated in Figure 8.6, it can be seen that the double-loop PCC is not able to suppress the inlet temperature disturbance with a decrement of 5%. Both the double-loop PCC are not able to bring the outlet temperature back to its normal operating temperature. On the contrary, the triple-loop PCC is able to reject the inlet temperature disturbance. Hence, the triple-loop PCC is suitable for this WGSR-MR system to function reliably even under harsh conditions. In order to improve the triple-loop PCC, the MSC controller tuning is adopted in the primary controller design. To test the robustness of the triple-loop PCC, both the MSC and conventional P-P-PIDF are subjected to a similar disturbance event, setpoint tracking and modelling uncertainties.

8.5.1 Disturbance rejection

First, let us compare the PCC scheme performances in terms of disturbance rejection. Note that, the fresh inlet flow rate is chosen to be the disturbance source as the flow rate is commonly subjected to fluctuation (i.e., due to varying demand

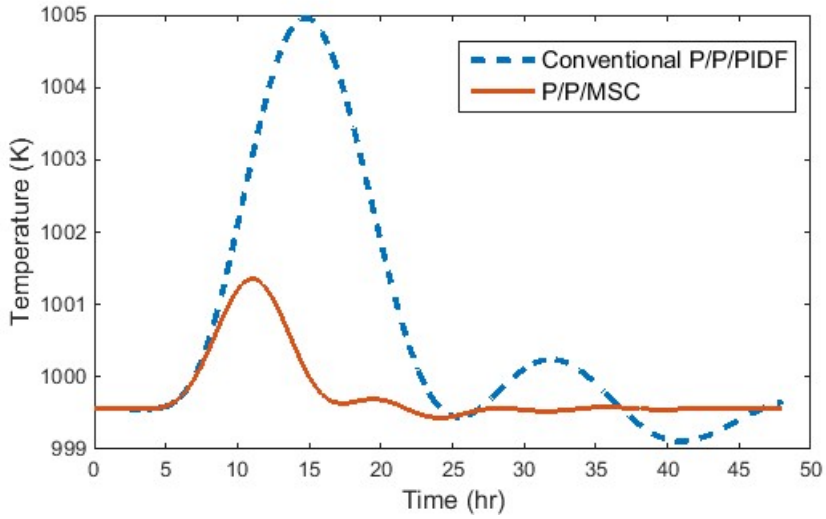

Figure 8.7: Outlet temperature profile towards increment of flowrate disturbance.

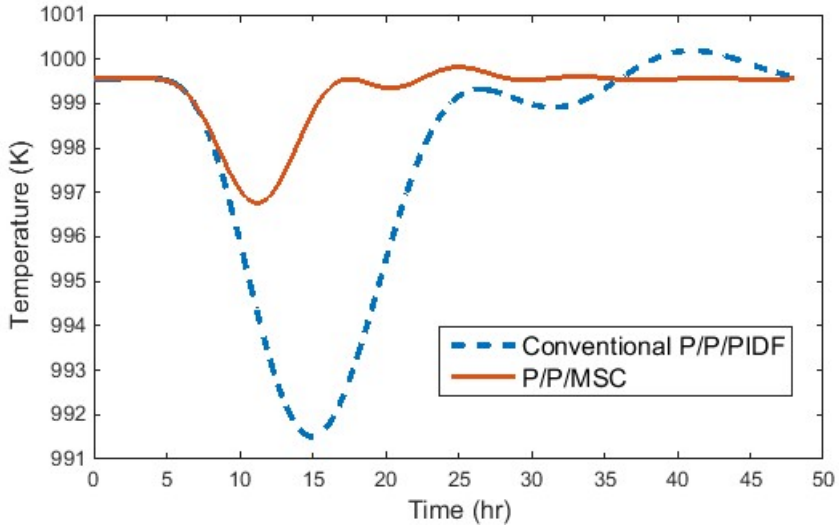

Figure 8.8: Outlet temperature profile towards decrement of flowrate disturbance.

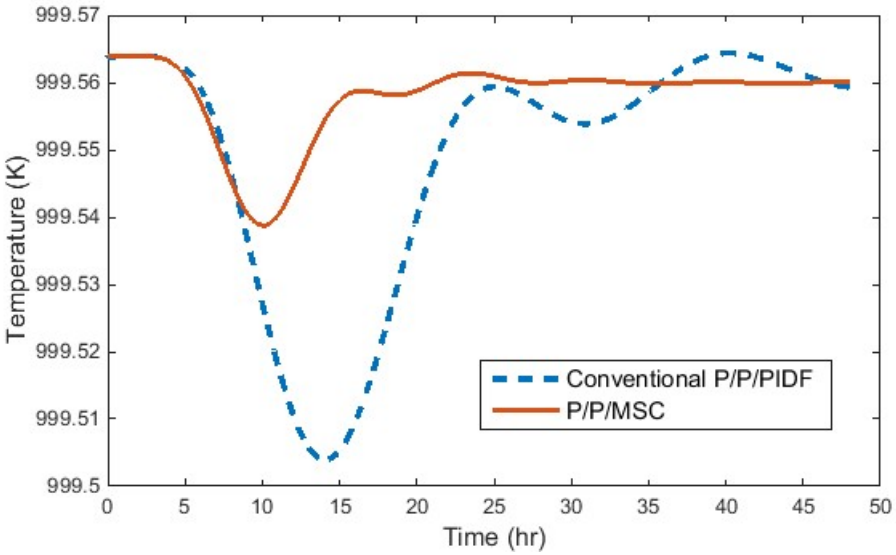

Figure 8.9: Outlet temperature profile under modelling uncertainties.

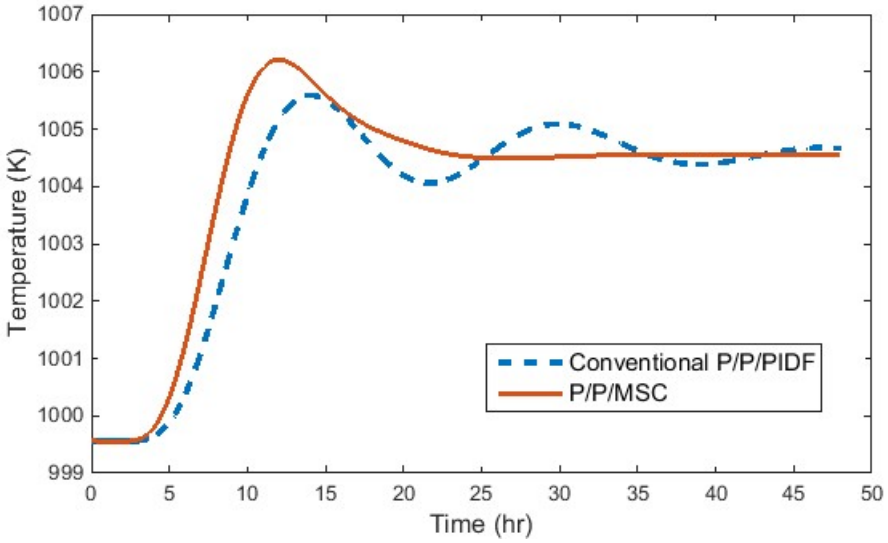

Figure 8.10: Outlet temperature profile towards setpoint tracking.

of hydrogen). Therefore, the inlet flow rate should represent a disturbance in the WGSR-MR system. A 30% increment and decrement of the inlet flow rate at time = 4 hr are introduced into the WGSR-MR.

Figure 8.7 shows both control scheme performances in the presence of 30% increase in the inlet flow rate. The outlet temperature profile shows that when the conventional PIDF is used in the primary loop, the PCC scheme is not able to effectively control the outlet temperature; a higher overshoot (spike) followed by mild oscillation. The conventional P/P/PIDF scheme shows 0.5% higher overshoot compared to the P/P/MSC scheme. Furthermore, the conventional controller has triple longer settling time compared to MSC tuning. This shows that MSC gives a better performance even when the system is subjected to sudden substantial increase in the fresh inlet flow rate. Note that, the outlet temperature profile is chosen to be the primary variable because this variable has great effect on the system performance, i.e., temperature affects the yield of hydrogen. Similar trend is shown for the decrement of 30% in the inlet flowrate - see Figure 8.8.

8.5.2 Modelling uncertainties

Both PCC schemes are subjected to modelling uncertainties in tortuosity, pore diameter of the catalyst pellet and membrane fouling with modelling errors $\pm$ 30% at time, $t = 4$ hr. Note that in this modelling uncertainties, both the PCC schemes are not subjected to any external disturbances.

Figure 8.9 shows the outlet temperature profiles of the WGSR-MR under the uncertainties. It can be seen from this figure that the MSC controller implemented in the primary loop gives better performance under the specified model uncertainties than the conventional PIDF controller. Both of the controllers show fluctuation of less than 1%. Nevertheless, it is very important for a controller to be able to handle model uncertainties, as mathematical models are usually subjected to many uncertainties factor due to the difference in ideal conditions and reality.

8.5.3 Setpoint tracking

The comparison of the control scheme performances based on the setpoint tracking is presented. Figure 8.10 shows the closed-loop temperature profiles under the conventional PIDF tuning and the MSC-PID tuning. Even though the con-

ventional PIDF controller has lower percentage of overshoot, it leads to a longer settling time than that of the MSC controller tuning. In short, the MSC produces a better controller performance overall as the percentage difference of the overshoot is less than 1%, while the settling time for MSC controller is 50% faster than the conventional PIDF controller.

8.6 Summary

The summaries on this chapter are as follows:

- A general procedure of triple-loop parallel cascade control tuning has been developed following rigorous stability analyses based on three first-order plus deadtime (FOPDT) processes arranged in parallel.
- The novel contribution of this study is the development of the three loop control strategy algorithm for a parallel cascade control based on the basic characteristic equation.
- The triple-loop parallel cascade control scheme is useful for controlling systems with large transport delays, for examples in a long tubular reactor, heat exchanger and pipeline carrying liquids or gases.
- For controlling the temperature in a large-scale multi-tubular membrane reactor assisted water-gas shift reaction (WGSR-MR) system, it has been found that the proposed triple-loop scheme demonstrates superior disturbance rejection performance over the commonly reported double-loop parallel cascade scheme.
- It is worth highlighting that Multi-Scale Control (MSC) scheme can be effectively used to design a parallel PID controller augmented with a lead-lag filter. The use of this MSC-based PID form in primary loop can further improve the control performance over the one, in which the primary PIDF controller is tuned via the classical Routh-Hurwitz criteria.
- The key significance in this chapter is the development of an effective control system design of the WGSR membrane reactor process, which can overcome the non-linear dynamic behaviours and also long transport delay.

- The work in this chapter has been submitted to International Journal of Systems Science 2017. [1]

[1]Three-loop parallel cascade control design for Water-Gas Shift Reaction in membrane reactor. Submitted to *IFAC Journal of Systems and Control*.

Chapter 9

Conclusions and Recommendations

9.1 Conclusions

To date, there are limited works relating to the study of system engineering of WGSR-MR particularly with regards to process optimization and control. Current publications on process optimization in WGSR-MR are restricted to single objective optimization (SOO). As for the previous research related to process control in WGSR-MR, single input single output (SISO) controllers were mentioned in literature. Note that, the single objective optimization approach is impractical as optimization of a single objective can result in the system to operate outside feasible operating limits. As for process control, the WGSR-MR system is highly nonlinear and inherently has a long process deadtime (due to membrane reactor length). Hence, SISO process control is inadequate in providing a safe and smooth operation for a process with long time-delay and nonlinear behaviour. In response to these research gaps, this dissertation has presented results of investigation in process optimization and control of a WGSR-MR system.

This dissertation address four important research questions: (1) how to design a water-gas shift membrane reactor process system, (2) how to improve the practicality of the system engineering study (process optimization) of a water-gas shift reaction membrane reactor, (3) how to optimize system design under uncertainties, and (4) how to improve control performance for a long process deadtime and highly nonlinear system. The conclusions are presented as follows:

9.1.1 Design of WGSR-MR process systems

To date, works related to WGSR-MR, were published as a stand-alone unit of membrane reactor. In a stand-alone unit, it is difficult to grasp the effect of interaction of other equipment on the membrane reactor unit. In this study, four possible process system flowsheets are developed based on sequential chemical process design (for details refer to Chapter 5). It should be noted that, there can be more than these four process flowsheets for the WGSR-MR. The detailed economic performances of these four plausible WGSR-MR process systems are evaluated. The best WGSR-MR process system is identified. The proposed WGSR-MR process system is simple and can be implemented in process optimization and control studies.

On top of that, this study also presents the effect of parametric economic assessment on the NPV of the WGSR-MR system. It is discovered that the parameters which are the retentate temperature, permeate and retentate pressures have the most significant effects on the systems economy (for details refer to Chapter 6). It is worth mentioning that, the parametric study is conducted for the identification of the crucial parameters to be included in the optimization process. This scrutinizing approach helps in the reduction of computational effort in the process optimization via the use of a small set of decision variables. It is important to note that, the process optimization is only made possible if there is a reliable mathematical model of the system. In this study, a one-dimensional heterogeneous membrane reactor coupled with macrokinetics model is developed. This model combination is proven to be one of the best reactor-kinetic model based on the accuracy of the model prediction against literature data (for details refer to Chapter 4). To further enhance the accuracy of this model combination, the incorporation of non-ideal properties in the model has been made. The non-ideal properties vary with the changes of state variables. In a membrane reactor, the operating pressure and temperature vary along the reactor. Thus, for practicality the impacts of these variations on properties must modelled, i.e., as a function of temperature and pressure rather than a constant value. Bear in mind that, the 1D model developed in this study not only has a highly comparable accuracy with a 2D model, but it also has the advantage of computational efficiency over a complex 2D model.

9.1.2 Multi-objective optimization of WGSR-MR

There have been limited studies on process optimization of WGSR-MR. The focuses of most previous works were mainly on single objective optimization. In this dissertation, a multi-objective optimization is used to conduct the process optimization for WGSR-MR process system (for details refer to Chapter 7). In this study, we successfully optimize both economic and dynamic operability of the water-gas shift membrane reactor (WGSR-MR) system. The result has revealed that by optimizing with only one objective function (i.e. economic or dynamic performance criterion), the design does not guarantee the desirable controllability. i.e., the design might be profitable but have poor controllability. This is because, while only looking at one objective function, for an example economic objective function, one will only attain the results when the system continuously operates on the systems constraints. However, in reality this operation will face difficulties especially when encountering system fluctuations (which is normal in industries). It is also disadvantageous as once the optimization is done, there will be little room left for improving the control performance because the process design has been fixed. Thus, to counter this disadvantage, integrated process design and control should be used in optimization instead. Therefore, this study opts to optimize the system via a multi-objective function formulated based on (1) steady-state economics and (2) dynamic operability. This leads to cost reductions and secured process safety as the process is optimized under the dynamic constraints. Improved controllability of the design implies less cost is needed to control the whole network of system.

This study also evaluates the optimum performance of the WGSR-MR under uncertainties (i.e., market and cost uncertainties). It is known that process uncertainties can cause deviation in the future values which can result in changes in the optimized results. There are two types of uncertainties, known as internal and external uncertainties (for details refer to Chapter 7). In short, internal uncertainties are the model uncertainties such as efficiency of the column, pore size of the catalyst pellets and many more. External uncertainties are market pricing, electricity cost and demand in product quantity. Internal uncertainties can be addressed through good control strategy, while external uncertainties require extra effort to predict them. In this study, Monte-Carlo Markov Chain (MCMC) with Metropolis-Hastings (MH) algorithm is used to simulate the external uncertainties. From this study, one can predict that uncertainty value and how much it might cause changes to the optimization results. The severity depends on the

future changes of the uncertainties. Unfortunately, one is not able to determine all uncertainties that may have an effect on the system. Thus, in order to address all other possible uncertainties, the possible solution is to design a robust control design that is able to handle daily fluctuation as well as uncertainties due to unknown perturbations.

9.1.3 Triple-loop parallel cascade control strategy

A good control scheme is crucial for safe and reliable operation of any chemical process. This study aims to develop an effective methodology for a process inherently suffering from nonlinearity and long process deadtime. A triple-loop parallel cascade control algorithm has been developed for the WGSR-MR process. It is discovered that with the triple-loop multi-scale control (MSC)-PID parallel cascade control tuning, effective performance of the system can be achieved even under harsh disturbances, such as fluctuation of flowrate up to $\pm$ 30% or even under temperature fluctuation (for details refer to Chapter 8). It is worth mentioning that, a general tuning procedure for the triple-loop cascade control is developed. This tuning procedure contributes to a generic design of a triple-loop cascade control which can be widely applied not only to a nonlinear system and also on a system that is subjected to long transport delay. The triple-loop parallel cascade control scheme is useful for controlling systems such as a long tubular reactor, heat exchanger and pipeline carrying liquids or gases.

9.2 Recommendations

Below are a few recommendations on future research directions:

a) Membrane-assisted reactor.
   It is recommended that different types of membrane reactor should be tested for process system involving water-gas shift reaction. New technology such as spiral membrane tube or hollow fiber membrane can be the key to minimize the reactor size to produce Hydrogen with high purity.

b) Expanding multi-objective optimization of WGSR-MR.
   A multi-objective optimization does not limit to only two objectives. One can consider adding to the objective functions by including other criteria, such as minimization of by-product, minimization of environmental impact

(CO_2 emissions), and many more. Besides, it is also recommended to increase the number of uncertainties in order to address in advanced some uncertain situations.

c) Expanding the developed process control strategy.
It is recommended to combine the proposed triple-loop parallel cascade control into higher order loop parallel cascade control with some other advanced control strategies such as model predictive control (MPC), feedforward control, robust control, adaptive control, and nonlinear control to address the nonlinearity of WGSR-MR process and multiple disturbances/uncertainties.

Bibliography

Abdollahi, M., J. Yu, P. K. Liu, R. Ciora, M. Sahimi, and T. T. Tsotsis (2010). Hydrogen production from coal-derived syngas using a catalytic membrane reactor based process. *Journal of Membrane Science 363*(1), 160–169.

Aboudheir, A., A. Akande, R. Idem, and A. Dalai (2006). Experimental studies and comprehensive reactor modeling of hydrogen production by the catalytic reforming of crude ethanol in a packed bed tubular reactor over a ni/al2o3 catalyst. *International journal of hydrogen energy 31*(6), 752–761.

Adams, T. A. and P. I. Barton (2009). A dynamic two-dimensional heterogeneous model for water gas shift reactors. *International Journal of Hydrogen Energy 34*(21), 8877–8891.

Adrover, M. E., D. Borio, and M. Pedernera (2016). Comparison between wgs membrane reactors operating with and without sweep gas: Limiting conditions for co-current flow. *International Journal of Hydrogen Energy*.

Adrover, M. E., E. López, D. O. Borio, and M. N. Pedernera (2009a). Simulation of a membrane reactor for the wgs reaction: Pressure and thermal effects. *Chemical Engineering Journal 154*(1), 196–202.

Adrover, M. E., E. López, D. O. Borio, and M. N. Pedernera (2009b). Theoretical study of a membrane reactor for the water gas shift reaction under nonisothermal conditions. *AIChE journal 55*(12), 3206–3213.

Ahmed, S. and R. Garcia (2003). Dynamic capacity acquisition and assignment under uncertainty. *Annals of Operations Research 124*(1-4), 267–283.

Albrecht, T., S. Papadokonstantakis, H. Sugiyama, and K. Hungerbühler (2010). Demonstrating multi-objective screening of chemical batch process alternatives during early design phases. *Chemical Engineering Research and Design 88*(5), 529–550.

Alhammadi, H. Y. and J. A. Romagnoli (2004). Incorporating environmental, profitability, heat integration and controllability considerations. *The integration of process design and control 17*, 264.

Amandusson, H., L.-G. Ekedahl, and H. Dannetun (2000). The effect of co and o 2 on hydrogen permeation through a palladium membrane. *Applied surface science 153*(4), 259–267.

Aslan, N. (2008). Multi-objective optimization of some process parameters of a multi-gravity separator for chromite concentration. *Separation and Purification Technology 64*(2), 237–241.

Åström, K. and T. Hägglund (2004). Revisiting the ziegler–nichols step response method for pid control. *Journal of process control 14*(6), 635–650.

Augustine, A. S., Y. H. Ma, and N. K. Kazantzis (2011). High pressure palladium membrane reactor for the high temperature water–gas shift reaction. *International Journal of Hydrogen Energy 36*(9), 5350–5360.

Ayastuy, J., M. Gutierrez-Ortiz, J. González-Marcos, A. Aranzabal, and J. Gonzalez-Velasco (2005). Kinetics of the low-temperature wgs reaction over a cuo/zno/al2o3 catalyst. *Industrial & engineering chemistry research 44*(1), 41–50.

Babita, K., S. Sridhar, and K. Raghavan (2011). Membrane reactors for fuel cell quality hydrogen through wgsr–review of their status, challenges and opportunities. *international journal of hydrogen energy 36*(11), 6671–6688.

Bailey, M. P. (2014). Chemical engineering plant cost index (cepci). *Chemical Engineering 121*(2), 68–69.

Baker, R. (2001). Membrane technology in the chemical industry: future directions. *Membrane Technology: in the Chemical Industry*, 268–295.

Bala Suresh, Ralf Gubler, X. H. and Y. Yamaguchi (2015). Hydrogen. *https://www.ihs.com/products/hydrogen-chemical-economics-handbook.html*.

Baloyi, L. N., B. C. North, H. W. Langmi, B. J. Bladergroen, and T. V. Ojumu (2016). The production of hydrogen through the use of a 77 wt% pd 23 wt% ag membrane water gas shift reactor. *South African Journal of Chemical Engineering 22*, 44–54.

Barbieri, G., A. Brunetti, T. Granato, P. Bernardo, and E. Drioli (2005). Engineering evaluations of a catalytic membrane reactor for the water gas shift reaction. *Industrial & engineering chemistry research 44*(20), 7676–7683.

Basile, A., S. Curcio, G. Bagnato, S. Liguori, S. Jokar, and A. Iulianelli (2015). Water gas shift reaction in membrane reactors: Theoretical investigation by artificial neural networks model and experimental validation. *International Journal of Hydrogen Energy 40*(17), 5897–5906.

Basile, A., F. Gallucci, and S. Tosti (2008). Synthesis, characterization, and applications of palladium membranes. *Membrane science and technology 13*, 255–323.

Basile, A., A. Iulianelli, T. Longo, S. Liguori, and M. De Falco (2011). Pd-based selective membrane state-of-the-art. In *Membrane reactors for hydrogen production processes*, pp. 21–55. Springer.

Basile, A., L. Paturzo, and F. Gallucci (2003). Co-current and counter-current modes for water gas shift membrane reactor. *Catalysis today 82*(1), 275–281.

Battersby, S., B. Ladewig, M. Duke, V. Rudolph, and J. Diniz da Costa (2010). Membrane reactor modelling, validation and simulation for the wgs reaction using metal doped silica membranes. *Asia-Pacific Journal of Chemical Engineering 5*(1), 83–92.

Beale, E. M. (1955). On minimizing a convex function subject to linear inequalities. *Journal of the Royal Statistical Society. Series B (Methodological)*, 173–184.

Bellman, R. and R. E. Kalaba (1965). *Dynamic programming and modern control theory*, Volume 81. Citeseer.

Benninga, S. et al. (2010). Principles of finance with excel. *OUP Catalogue*.

Bequette, B. W. and P. Mahapatra (2010). Model predictive control of integrated gasification combined cycle power plants. Technical report, Rensselaer Polytechnic Institute.

Bhattacharyya, D., R. Turton, and S. E. Zitney (2010). Steady-state simulation and optimization of an integrated gasification combined cycle power plant with co2 capture. *Industrial & Engineering Chemistry Research 50*(3), 1674–1690.

Biegler, L. T. and I. E. Grossmann (2004). Retrospective on optimization. *Computers & Chemical Engineering 28*(8), 1169–1192.

Birge, J. R. and F. Louveaux (2011). *Introduction to stochastic programming*. Springer Science & Business Media.

Bond, G. (1987). *Heterogeneous catalysis principles and applications*. Oxford University Press.

Bond, G. and D. Thompson (1999). Catal rev. *Catal. Rev. 41*, 319.

Boutikos, P. and V. Nikolakis (2010). A simulation study of the effect of operating and design parameters on the performance of a water gas shift membrane reactor. *Journal of Membrane Science 350*(1), 378–386.

Box, G. E. and N. R. Draper (1987). *Empirical model-building and response surfaces*, Volume 424. Wiley New York.

Bradford, M. C. and M. A. Vannice (1996). Catalytic reforming of methane with carbon dioxide over nickel catalysts i. catalyst characterization and activity. *Applied Catalysis A: General 142*(1), 73–96.

Brambilla, A. and D. Semino (1992). Nonlinear filter in cascade control schemes. *Industrial & engineering chemistry research 31*(12), 2694–2699.

Brambilla, A., D. Semino, and C. Scali (1994). Design and control selection of cascade loops in distillation. In *Proc. of IFAC Workshop on Integration of Process Des. & Control, Baltimore, MD*, Volume 171.

Brunetti, A., A. Caravella, G. Barbieri, and E. Drioli (2007). Simulation study of water gas shift reaction in a membrane reactor. *Journal of Membrane Science 306*(1), 329–340.

Brush, S. G. (1962). Theories of liquid viscosity. *Chemical Reviews 62*(6), 513–548.

Bryden, K. J. and J. Y. Ying (2002). Nanostructured palladium–iron membranes for hydrogen separation and membrane hydrogenation reactions. *Journal of Membrane Science 203*(1), 29–42.

Buxbaum, R. E. (1993, June 1). Composite metal membrane for hydrogen extraction. US Patent 5,215,729.

Buxbaum, R. E. (2002, October 8). Hydrogen generator. US Patent 6,461,408.

Callaghan, C., I. Fishtik, R. Datta, M. Carpenter, M. Chmielewski, and A. Lugo (2003). An improved microkinetic model for the water gas shift reaction on copper. *Surface Science 541*(1), 21–30.

Camacho, E. F. and C. B. Alba (2013). *Model predictive control*. Springer Science & Business Media.

Campbell, C. T. and K. Daube (1987). A surface science investigation of the water-gas shift reaction on cu (111). *Journal of Catalysis 104*(1), 109–119.

Caravella, A., L. Melone, Y. Sun, A. Brunetti, E. Drioli, and G. Barbieri (2016). Concentration polarization distribution along pd-based membrane reactors: A modelling approach applied to water-gas shift. *International Journal of Hydrogen Energy 41*(4), 2660–2670.

Chacon-Mondragon, O. and D. Himmelblau (1996). Integration of flexibility and control in process design. *Computers & chemical engineering 20*(4), 447–452.

Chakraborty, A. and A. A. Linninger (2002). Plant-wide waste management. 1. synthesis and multiobjective design. *Industrial & engineering chemistry research 41*(18), 4591–4604.

Chakraborty, A. and A. A. Linninger (2003). Plant-wide waste management. 2. decision making under uncertainty. *Industrial & Engineering Chemistry Research 42*(2), 357–369.

Chein, R., Y. Chen, Y. Chyou, and J. Chung (2014). Three-dimensional numerical modeling on high pressure membrane reactors for high temperature water-gas shift reaction. *International Journal of Hydrogen Energy 39*(28), 15517–15529.

Chein, R., Y.-C. Chen, and J. Chung (2013). Parametric study of membrane reactors for hydrogen production via high-temperature water gas shift reaction. *International Journal of Hydrogen Energy 38*(5), 2292–2305.

Chen, W.-H., C.-W. Tsai, Y.-L. Lin, R.-Y. Chein, and C.-T. Yu (2017). Reaction phenomena of high-temperature water gas shift reaction in a membrane reactor. *Fuel 199*, 358–371.

Cheng, S.-H., H.-J. Chen, H. Chang, C.-K. Chang, and Y.-M. Chen (2008). Multi-objective optimization for two catalytic membrane reactorsmethanol synthesis and hydrogen production. *Chemical Engineering Science 63*(6), 1428–1437.

Cheng, Y., M. Pena, J. Fierro, D. Hui, and K. Yeung (2002). Performance of alumina, zeolite, palladium, pd–ag alloy membranes for hydrogen separation from towngas mixture. *Journal of membrane science 204*(1), 329–340.

Chiappetta, G., G. Clarizia, and E. Drioli (2008). Theoretical analysis of the effect of catalyst mass distribution and operation parameters on the performance of a pd-based membrane reactor for water–gas shift reaction. *Chemical Engineering Journal 136*(2), 373–382.

Chidambaram, M. (1993). Parallel cascade nonlinear control of nonlinear-systems-application to an unstable bioreactor. *Hungarian Journal of Industrial Chemistry 21*(2), 109–116.

Choi, Y. and H. G. Stenger (2003). Water gas shift reaction kinetics and reactor modeling for fuel cell grade hydrogen. *Journal of Power Sources 124*(2), 432–439.

Chueh, P. and J. Prausnitz (1967). Vapor-liquid equilibria at high pressures: Calculation of partial molar volumes in nonpolar liquid mixtures. *AIChE Journal 13*(6), 1099–1107.

Collot, A.-G. (2003). *Prospects for hydrogen from coal*. IEA Clean Coal Centre London.

Cornaglia, C. A., M. E. Adrover, J. F. Múnera, M. N. Pedernera, D. O. Borio, and E. A. Lombardo (2013). Production of ultrapure hydrogen in a pd–ag membrane reactor using noble metals supported on la–si oxides. heterogeneous modeling for the water gas shift reaction. *International Journal of Hydrogen Energy 38*(25), 10485–10493.

Costa, J. L. R., G. S. Marchetti, and M. do Carmo Rangel (2002). A thorium-doped catalyst for the high temperature shift reaction. *Catalysis today 77*(3), 205–213.

Cuéllar-Franca, R. M. and A. Azapagic (2015). Carbon capture, storage and utilisation technologies: A critical analysis and comparison of their life cycle environmental impacts. *Journal of CO2 Utilization 9*, 82–102.

Dantzig, G. B. (1955). Linear programming under uncertainty. *Management science 1*(3-4), 197–206.

Dixon, A. (2014). *Modeling and Simulation of Heterogeneous Catalytic Processes*, Volume 45. Academic Press.

Dong, X., H. Wang, Z. Rui, and Y. Lin (2015). Tubular dual-layer mfi zeolite membrane reactor for hydrogen production via the wgs reaction: Experimental and modeling studies. *Chemical Engineering Journal 268*, 219–229.

Donoso, Y. and R. Fabregat (2016). *Multi-objective optimization in computer networks using metaheuristics*. CRC Press.

Douglas, J. M. (1988). *Conceptual design of chemical processes*, Volume 1110. McGraw-Hill New York.

Dyner, I., B. Lopez, and S. Arango (2003). Modeling uncertainty in electricity markets for learning, policy and strategy. In *International System Dynamics Conference, New York*.

Economou, I. G. and M. D. Donohue (1996). Equations of state for hydrogen bonding systems. *Fluid phase equilibria 116*(1), 518–529.

Edlund, D. J. and W. A. Pledger (1994). Catalytic platinum-based membrane reactor for removal of h 2 s from natural gas streams. *Journal of membrane science 94*(1), 111–119.

Emun, F., M. Gadalla, T. Majozi, and D. Boer (2010). Integrated gasification combined cycle (igcc) process simulation and optimization. *Computers & chemical engineering 34*(3), 331–338.

Farrauto, R., S. Hwang, L. Shore, W. Ruettinger, J. Lampert, T. Giroux, Y. Liu, and O. Ilinich (2003). New material needs for hydrocarbon fuel processing: generating hydrogen for the pem fuel cell. *Annual Review of Materials Research 33*(1), 1–27.

Fernandez, E., J. A. Medrano, J. Melendez, M. Parco, J. L. Viviente, M. van Sint Annaland, F. Gallucci, and D. P. Tanaka (2016). Preparation and characterization of metallic supported thin pd–ag membranes for hydrogen separation. *Chemical Engineering Journal 305*, 182–190.

Ferro-Luzzi, M., M. Bouwhuis, E. Passchier, Z.-L. Zhou, R. Alarcon, M. Anghinolfi, R. Van Bommel, T. Botto, J. Van den Brand, M. Buchholz, et al. (1996). Measurement of tensor analyzing powers for elastic electron scattering from a polarized 2 h target internal to a storage ring. *Physical review letters 77*(13), 2630.

Fishtik, I. and R. Datta (2002). A ubi–qep microkinetic model for the water–gas shift reaction on cu (111). *Surface Science 512*(3), 229–254.

Fogler, H. S. (1999). Elements of chemical reaction engineering.

Francesconi, J. A., M. C. Mussati, and P. A. Aguirre (2007). Analysis of design variables for water-gas-shift reactors by model-based optimization. *Journal of Power Sources 173*(1), 467–477.

Froment, G. F. and K. B. Bischoff (1979). *Chemical reactor analysis and design*. John Wiley and Sons Inc., New York, NY.

Gallucci, F., A. Comite, G. Capannelli, and A. Basile (2006). Steam reforming of methane in a membrane reactor: an industrial case study. *Industrial & engineering chemistry research 45*(9), 2994–3000.

Gallucci, F., E. Fernandez, P. Corengia, and M. van Sint Annaland (2013). Recent advances on membranes and membrane reactors for hydrogen production. *Chemical Engineering Science 92*, 40–66.

Gascon, J. and F. Kapteijn (2010). Metal-organic framework membranes - high potential, bright future? *Angewandte Chemie International Edition 49*(9), 1530–1532.

Gebreslassie, B. H., Y. Yao, and F. You (2012). Design under uncertainty of hydrocarbon biorefinery supply chains: multiobjective stochastic programming models, decomposition algorithm, and a comparison between cvar and downside risk. *AIChE Journal 58*(7), 2155–2179.

Gelfand, A. E. and A. F. Smith (1990). Sampling-based approaches to calculating marginal densities. *Journal of the American statistical association 85*(410), 398–409.

Geman, S. and D. Geman (1984). Stochastic relaxation, gibbs distributions, and the bayesian restoration of images. *IEEE Transactions on pattern analysis and machine intelligence* (6), 721–741.

Geoffrion, A. M. (1972). Generalized benders decomposition. *Journal of optimization theory and applications 10*(4), 237–260.

Georgis, D., F. V. Lima, A. Almansoori, and P. Daoutidis (2012). Modeling and control of a water gas shift membrane reactor for hydrogen production. In *American Control Conference (ACC), 2012*, pp. 4287–4292. IEEE.

Georgis, D., F. V. Lima, A. Almansoori, and P. Daoutidis (2014). Thermal management of a water–gas-shift membrane reactor for high-purity hydrogen production and carbon capture. *Industrial & Engineering Chemistry Research 53*(18), 7461–7469.

Ghasemzadeh, K., R. Zeynali, and A. Basile (2016). Theoretical study of hydrogen production using inorganic membrane reactors during wgs reaction. *International Journal of Hydrogen Energy 41*(20), 8696–8705.

Ghenciu, A. F. (2002). Review of fuel processing catalysts for hydrogen production in pem fuel cell systems. *Current opinion in solid state and materials science 6*(5), 389–399.

Ginés, M., N. Amadeo, M. Laborde, and C. Apesteguia (1995). Activity and structure-sensitivity of the water-gas shift reaction over cu zn al mixed oxide catalysts. *Applied Catalysis A: General 131*(2), 283–296.

Goel, V. and I. E. Grossmann (2006). A class of stochastic programs with decision dependent uncertainty. *Mathematical programming 108*(2-3), 355–394.

Gonzalez, J., M. Gonzalez, M. Laborde, and N. Moreno (1986). Effect of temperature and reduction on the activity of high temperature water gas shift catalysts. *Applied catalysis 20*(1), 3–13.

Gosiewski, K., K. Warmuzinski, and M. Tanczyk (2010). Mathematical simulation of wgs membrane reactor for gas from coal gasification. *Catalysis Today 156*(3), 229–236.

Gottschalk, F. and G. Hutchings (1989). Manganese oxide watergas shift catalysts initial optimization studies. *Applied catalysis 51*(1), 127–139.

Grainger, D. and M.-B. Hägg (2007). Evaluation of cellulose-derived carbon molecular sieve membranes for hydrogen separation from light hydrocarbons. *Journal of Membrane Science 306*(1), 307–317.

Grashoff, G., C. Pilkington, and C. Corti (1983). The purification of hydrogen. *Platinum Metals Review 27*(4), 157–169.

Green, D. W. et al. (2008). *Perry's chemical engineers' handbook*, Volume 796. McGraw-hill New York.

Gruss, H. and H. Schmick (1928). Thermal conductivity of some gas mixtures. *Wiss. Veroffentl. Siemens-Konzern 7*, 202.

Gryaznov, V., V. Polyakova, E. Savitskii, L. Frades, E. Khrapova, E. Khuares, and G. Shkola (1970). Influence of the nature and amount of the second component of binary-palladium alloys on their catalytic activity with respect to the dehydrogenation of cyclohexane. *Bulletin of the Academy of Sciences of the USSR, Division of chemical science 19*(11), 2368–2371.

Gubbins, K. E., K. S. Shing, and W. B. Streett (1983). Fluid phase equilibriums: experiment, computer simulation, and theory. *The Journal of Physical Chemistry 87*(23), 4573–4585.

Guillén-Gosálbez, G. and I. E. Grossmann (2009). Optimal design and planning of sustainable chemical supply chains under uncertainty. *AIChE Journal 55*(1), 99–121.

Harstad, K. G., R. S. Miller, and J. Bellan (1997). Efficient high-pressure state equations. *AIChE journal 43*(6), 1605–1610.

Haruta, M., N. Yamada, T. Kobayashi, and S. Iijima (1989). Gold catalysts prepared by coprecipitation for low-temperature oxidation of hydrogen and of carbon monoxide. *Journal of catalysis 115*(2), 301–309.

Haryanto, A., S. Fernando, N. Murali, and S. Adhikari (2005). Current status of hydrogen production techniques by steam reforming of ethanol: a review. *Energy & Fuels 19*(5), 2098–2106.

Hastings, W. K. (1970). Monte carlo sampling methods using markov chains and their applications. *Biometrika 57*(1), 97–109.

Hla, S., L. Morpeth, M. Dolan, et al. (2015). Modelling and experimental studies of a water-gas shift catalytic membrane reactor. *Chemical Engineering Journal 276*, 289–302.

Holleck, G. L. (1970). Diffusion and solubility of hydrogen in palladium and palladium–silver alloys. *The Journal of Physical Chemistry 74*(3), 503–511.

Hosseini, S. S. and T. S. Chung (2009). Carbon membranes from blends of pbi and polyimides for n 2/ch 4 and co 2/ch 4 separation and hydrogen purification. *Journal of Membrane Science 328*(1), 174–185.

Hsieh, H. (1991). Inorganic membrane reactors. *Catalysis Reviews 33*(1-2), 1–70.

Huang, J., L. El-Azzami, and W. W. Ho (2005). Modeling of co 2-selective water gas shift membrane reactor for fuel cell. *Journal of membrane science 261*(1), 67–75.

Hutchings, G. J., R. G. Copperthwaitet, F. M. Gottschalk, R. Hunter, J. Mellor, S. W. Orchard, and T. Sangiorgio (1992). A comparative evaluation of cobalt chromium oxide, cobalt manganese oxide, and copper manganese oxide as catalysts for the water-gas shift reaction. *Journal of Catalysis 137*(2), 408–422.

Ismail, A. F. and L. David (2001). A review on the latest development of carbon membranes for gas separation. *Journal of membrane science 193*(1), 1–18.

Iyoha, O., R. Enick, R. Killmeyer, B. Howard, M. Ciocco, and B. Morreale (2007). H 2 production from simulated coal syngas containing h 2 s in multi-tubular pd and 80wt% pd–20wt% cu membrane reactors at 1173k. *Journal of Membrane Science 306*(1), 103–115.

Jacobs, G., L. Williams, U. Graham, G. A. Thomas, D. E. Sparks, and B. H. Davis (2003). Low temperature water–gas shift: in situ drifts-reaction study of ceria surface area on the evolution of formates on pt/ceo 2 fuel processing catalysts for fuel cell applications. *Applied Catalysis A: General 252*(1), 107–118.

Kanai, Y., T. Watanabe, T. Fujitani, M. Saito, J. Nakamura, and T. Uchijima (1994). Evidence for the migration of znox in a cu/zno methanol synthesis catalyst. *Catalysis letters 27*(1-2), 67–78.

Kanniche, M. and C. Bouallou (2007). Co 2 capture study in advanced integrated gasification combined cycle. *Applied Thermal Engineering 27*(16), 2693–2702.

Keiski, R. L., T. Salmi, P. Niemistö, J. Ainassaari, and V. J. Pohjola (1996). Stationary and transient kinetics of the high temperature water-gas shift reaction. *Applied Catalysis A: General 137*(2), 349–370.

Kentish, S. E., C. A. Scholes, and G. W. Stevens (2008). Carbon dioxide separation through polymeric membrane systems for flue gas applications. *Recent Patents on Chemical Engineering 1*(1), 52–66.

Kikuchi, E., S. Kawabe, and M. Matsukata (2003). Steam reforming of methanol on ni/al2o3 catalyst in a pd-membrane reactor. *Journal of the Japan Petroleum Institute 46*(2), 93–98.

Koc, R. (2012). *Technical and economic performance assessment of pd/alloy membrane reactor technology options in the presence of uncertainty*. Worcester Polytechnic Institute.

Koc, R., N. K. Kazantzis, and Y. H. Ma (2011). Process safety aspects in water-gas-shift (wgs) membrane reactors used for pure hydrogen production. *Journal of Loss Prevention in the Process Industries 24*(6), 852–869.

Koc, R., N. K. Kazantzis, and Y. H. Ma (2014). Membrane technology embedded into igcc plants with co 2 capture: An economic performance evaluation under uncertainty. *International Journal of Greenhouse Gas Control 26*, 22–38.

Koc, R., N. K. Kazantzis, W. J. Nuttall, and Y. H. Ma (2012). Economic assessment of inherently safe membrane reactor technology options integrated into igcc power plants. *Process Safety and Environmental Protection 90*(5), 436–450.

Kookos, I. K. and J. D. Perkins (2001). An algorithm for simultaneous process design and control. *Industrial & engineering chemistry research 40*(19), 4079–4088.

Koros, W., Y. Ma, and T. Shimidzu (1996). Terminology for membranes and membrane processes. *J. Membr. Sci 120*(2), 149–159.

Koros, W. J. and R. Mahajan (2000). Pushing the limits on possibilities for large scale gas separation: which strategies? *Journal of Membrane Science 175*(2), 181–196.

Kothari, R., D. Buddhi, and R. Sawhney (2008). Comparison of environmental and economic aspects of various hydrogen production methods. *Renewable and Sustainable Energy Reviews 12*(2), 553–563.

Kumar, P., E. Akpan, H. Ibrahim, A. Aboudheir, and R. Idem (2008). Kinetics and reactor modeling of a high temperature water- gas shift reaction (wgsr) for hydrogen production in a packed bed tubular reactor (pbtr). *Industrial & Engineering Chemistry Research 47*(12), 4086–4097.

Kuramochi, T., A. Ramírez, W. Turkenburg, and A. Faaij (2012). Comparative assessment of co 2 capture technologies for carbon-intensive industrial processes. *Progress in energy and combustion science 38*(1), 87–112.

Lai, R. and G. R. Gavalas (2000). Zsm-5 membrane synthesis with organic-free mixtures. *Microporous and mesoporous materials 38*(2), 239–245.

Lang, Y., S. E. Zitney, and L. T. Biegler (2011). Optimization of igcc processes with reduced order cfd models. *Computers & Chemical Engineering 35*(9), 1705–1717.

Lazo, J. G. L., M. A. C. Pacheco, M. Vellasco, and M. A. Dias (2003). Real option decision rules for oil field development under market uncertainty using genetic algorithms and monte carlo simulation. In *Proceedings of the 7th Annual International Conference on Real Options-Theory Meets Practice, Washington DC, USA*.

Lee, S. (2006). *Encyclopedia of chemical processing*, Volume 1. Taylor & Francis US.

Lee, Y., M. Skliar, and M. Lee (2006). Analytical method of pid controller design for parallel cascade control. *Journal of Process Control 16*(8), 809–818.

Li, A., W. Liang, and R. Hughes (2000). The effect of carbon monoxide and steam on the hydrogen permeability of a pd/stainless steel membrane. *Journal of Membrane Science 165*(1), 135–141.

Li, Y., F. Liang, H. Bux, W. Yang, and J. Caro (2010). Zeolitic imidazolate framework zif-7 based molecular sieve membrane for hydrogen separation. *Journal of Membrane Science 354*(1), 48–54.

Li, Z., Q. Tang, and C. A. Floudas (2012). A comparative theoretical and computational study on robust counterpart optimization: Ii. probabilistic guarantees on constraint satisfaction. *Industrial & engineering chemistry research 51*(19), 6769–6788.

Lide, D. (2009). Internet version 2009. *CRC Handbook of Chemistry and Physics. 89th edition. Boca Raton, FL: CRC Press. Web of Science*.

Lima, F. V., R. Amrit, M. Tsapatsis, and P. Daoutidis (2013). Nonlinear model predictive control of igcc plants with membrane reactors for carbon capture. In *American Control Conference (ACC), 2013*, pp. 3747–3752. IEEE.

Lima, F. V., P. Daoutidis, M. Tsapatsis, and J. J. Marano (2012). Modeling and optimization of membrane reactors for carbon capture in integrated gasification combined cycle units. *Industrial & Engineering Chemistry Research 51*(15), 5480–5489.

Lindsay, A. L. and L. A. Bromley (1950). Thermal conductivity of gas mixtures. *Industrial & Engineering Chemistry 42*(8), 1508–1511.

Lloyd, L., D. Ridler, and M. Twigg (1996). The water-gas shift reaction. *Catalyst handbook 2*, 283–338.

Lozowski, D. (2012). Chemical engineering plant cost index (cepci). *Chem Eng 119*, 84.

Lu, G., J. D. da Costa, M. Duke, S. Giessler, R. Socolow, R. Williams, and T. Kreutz (2007). Inorganic membranes for hydrogen production and purification: a critical review and perspective. *Journal of colloid and interface science 314*(2), 589–603.

Lund, C. R. (1996). Effect of adding co to mos2/al2o3 upon the kinetics of the water-gas shift. *Industrial & engineering chemistry research 35*(9), 3067–3073.

Luyben, M. L. and W. L. Luyben (1997). *Essentials of process control*. McGraw-Hill,.

Luyben, W. L. (1973). Parallel cascade control. *Industrial & Engineering Chemistry Fundamentals 12*(4), 463–467.

Luyben, W. L. (1989). *Process modeling, simulation and control for chemical engineers*. McGraw-Hill Higher Education.

Luyben, W. L. (1994). Snowball effects in reactor/separator processes with recycle. *Industrial & engineering chemistry research 33*(2), 299–305.

Ma, D. and C. R. Lund (2003). Assessing high-temperature water-gas shift membrane reactors. *Industrial & engineering chemistry research 42*(4), 711–717.

Ma, L.-C., B. Castro-Dominguez, N. K. Kazantzis, and Y. H. Ma (2015). Integration of membrane technology into hydrogen production plants with co 2 capture: An economic performance assessment study. *International Journal of Greenhouse Gas Control 42*, 424–438.

Majidi, M., S. Nojavan, N. N. Esfetanaj, A. Najafi-Ghalelou, and K. Zare (2017). A multi-objective model for optimal operation of a battery/pv/fuel cell/grid hybrid energy system using weighted sum technique and fuzzy satisfying approach considering responsible load management. *Solar Energy 144*, 79–89.

Marín, P., F. V. Díez, and S. Ordóñez (2012). Fixed bed membrane reactors for wgsr-based hydrogen production: Optimisation of modelling approaches and reactor performance. *International journal of hydrogen energy 37*(6), 4997–5010.

Markatos, N., E. Vogiatzis, M. Koukou, and N. Papayannakos (2005). Membrane reactor modelling: A comparative study to evaluate the role of combined mass and heat dispersion in large-scale adiabatic membrane modules. *Chemical Engineering Research and Design 83*(10), 1171–1178.

Marler, R. T. and J. S. Arora (2010). The weighted sum method for multi-objective optimization: new insights. *Structural and multidisciplinary optimization 41*(6), 853–862.

Marrero, T. and E. A. Mason (1972). Gaseous diffusion coefficients. *Journal of Physical and Chemical Reference Data 1*(1), 3–118.

Martin, J. J. (1979). Cubic equations of state-which? *Industrial & Engineering Chemistry Fundamentals 18*(2), 81–97.

Martín, M. and A. Martínez (2015). Addressing uncertainty in formulated products and process design. *Industrial & Engineering Chemistry Research 54*(22), 5990–6001.

Matsumura, Y. and J. Tong (2008). Methane steam reforming in hydrogen-permeable membrane reactor for pure hydrogen production. *Topics in Catalysis 51*(1-4), 123–132.

Maybeck, P. S. (1982). *Stochastic models, estimation, and control*, Volume 3. Academic press.

McCarthy, M. C., V. Varela-Guerrero, G. V. Barnett, and H.-K. Jeong (2010). Synthesis of zeolitic imidazolate framework films and membranes with controlled microstructures. *Langmuir 26*(18), 14636–14641.

McLeary, E., J. Jansen, and F. Kapteijn (2006). Zeolite based films, membranes and membrane reactors: Progress and prospects. *Microporous and Mesoporous Materials 90*(1), 198–220.

McLellan, B., E. Shoko, A. Dicks, and J. D. Da Costa (2005). Hydrogen production and utilisation opportunities for australia. *International Journal of Hydrogen Energy 30*(6), 669–679.

Mendes, D., V. Chibante, J.-M. Zheng, S. Tosti, F. Borgognoni, A. Mendes, and L. M. Madeira (2010). Enhancing the production of hydrogen via water–gas shift reaction using pd-based membrane reactors. *international journal of hydrogen energy 35*(22), 12596–12608.

Mendes, D., A. Mendes, L. Madeira, A. Iulianelli, J. Sousa, and A. Basile (2010). The water-gas shift reaction: from conventional catalytic systems to pd-based membrane reactorsa review. *Asia-Pacific Journal of Chemical Engineering 5*(1), 111–137.

Mendes, D. M. P. et al. (2012). Use of pd-ag membrane reactors in the water-gas shift reaction for producing ultra-pure hydrogen.

Metropolis, N., A. W. Rosenbluth, M. N. Rosenbluth, A. H. Teller, and E. Teller (1953). Equation of state calculations by fast computing machines. *The journal of chemical physics 21*(6), 1087–1092.

Michalek, J. J., P. Ebbes, F. Adigüzel, F. M. Feinberg, and P. Y. Papalambros (2011). Enhancing marketing with engineering: Optimal product line design for heterogeneous markets. *International Journal of Research in Marketing 28*(1), 1–12.

Mitsos, A., G. M. Oxberry, P. I. Barton, and W. H. Green (2008). Optimal automatic reaction and species elimination in kinetic mechanisms. *Combustion and Flame 155*(1), 118–132.

Mohseni-Bonab, S., A. Rabiee, S. Jalilzadeh, B. Mohammadi-Ivatloo, and S. Nojavan (2015). Probabilistic multi objective optimal reactive power dispatch considering load uncertainties using monte carlo simulations. *Journal of Operation and Automation in Power Engineering 3*(1), 83–93.

Mond, L. and C. Langer (1888). Improvements in obtaining hydrogen. *British Patent 12608*(7).

Montazer-Rahmati, M. M. and R. Binaee (2010). Multi-objective optimization of an industrial hydrogen plant consisting of a co 2 absorber using dga and a methanator. *Computers & Chemical Engineering 34*(11), 1813–1821.

Montgomery, D. C. (2008). *Design and analysis of experiments*. John Wiley & Sons.

Montgomery, D. C. and R. H. Myers (1995). Response surface methodology: process and product optimization using designed experiments. *Raymond H. Meyers and Douglas C. Montgomery. A Wiley-Interscience Publications*.

Mori, T. (2005). Rd&d for launching the initial market by hydrogen from natural gas. In *Proceedings of the international hydrogen energy congress and exhibition IHEC*.

Morpeth, L. D., M. D. Dolan, et al. (2015). Modelling and experimental studies of a water–gas shift catalytic membrane reactor. *Chemical Engineering Journal 276*, 289–302.

Mukherjee, R. et al. (1998). Effectively design shell-and-tube heat exchangers. *Chemical Engineering Progress 94*(2), 21–37.

Nakamura, J., J. M. Campbell, and C. T. Campbell (1990). Kinetics and mechanism of the water-gas shift reaction catalysed by the clean and cs-promoted cu (110) surface: A comparison with cu (111). *J. Chem. Soc., Faraday Trans. 86*(15), 2725–2734.

Nandong, J. and Z. Zang (2013a). High-performance multi-scale control scheme for stable, integrating and unstable time-delay processes. *Journal of Process Control 23*(10), 1333–1343.

Nandong, J. and Z. Zang (2013b). Novel multiscale control scheme for nonminimum-phase processes. *Industrial & Engineering Chemistry Research 52*(24), 8248–8259.

Nandong, J. and Z. Zang (2014a). Generalized multi-scale control scheme for cascade processes with time-delays. *Journal of Process Control 24*(7), 1057–1067.

Nandong, J. and Z. Zang (2014b). Multi-loop design of multi-scale controllers for multivariable processes. *Journal of Process Control 24*(5), 600–612.

Nandong, J. and Z. Zang (2014c). Pid controller tuning via multi-scale control scheme for parallel cascade processes. In *Industrial Electronics and Applications (ICIEA), 2014 IEEE 9th Conference on*, pp. 684–689. IEEE.

Natesakhawat, S., X. Wang, L. Zhang, and U. S. Ozkan (2006). Development of chromium-free iron-based catalysts for high-temperature water-gas shift reaction. *Journal of Molecular Catalysis A: Chemical 260*(1), 82–94.

Newsome, D. S. (1980). The water-gas shift reaction. *Catalysis Reviews Science and Engineering 21*(2), 275–318.

Nixon, J. (2016). Designing and optimising anaerobic digestion systems: A multi-objective non-linear goal programming approach. *Energy 114*, 814–822.

Ockwig, N. W. and T. M. Nenoff (2007). Membranes for hydrogen separation. *Chemical Reviews 107*(10), 4078–4110.

Ogunnaike, B. A. and W. H. Ray (1994). *Process dynamics, modeling, and control*, Volume 1. Oxford University Press New York.

Outlook, A. E. et al. (2016). Energy information administration. *Department of Energy*.

Ovesen, C., B. Clausen, B. Hammershøi, G. Steffensen, T. Askgaard, I. Chorkendorff, J. K. Nørskov, P. Rasmussen, P. Stoltze, and P. Taylor (1996). A microkinetic analysis of the water–gas shift reaction under industrial conditions. *Journal of catalysis 158*(1), 170–180.

Oyama, S. T., P. Hacarlioglu, Y. Gu, and D. Lee (2012). Dry reforming of methane has no future for hydrogen production: comparison with steam reforming at high pressure in standard and membrane reactors. *International journal of hydrogen energy 37*(13), 10444–10450.

Pabby, A. K., S. S. Rizvi, and A. M. S. Requena (2015). *Handbook of membrane separations: chemical, pharmaceutical, food, and biotechnological applications*. CRC press.

Pacheco Tanaka, D. A., L. Tanco, T. Nagase, J. Okazaki, Y. Wakui, F. Mizukami, and T. M. Suzuki (2006). Fabrication of hydrogen-permeable composite membranes packed with palladium nanoparticles. *Advanced Materials 18*(5), 630–632.

Padhan, D. G. and S. Majhi (2012a). An improved parallel cascade control structure for processes with time delay. *Journal of Process Control 22*(5), 884–898.

Padhan, D. G. and S. Majhi (2012b). Synthesis of pid tuning for a new parallel cascade control structure. *IFAC Proceedings Volumes 45*(3), 566–571.

Park, D., G. Duffy, J. Edwards, D. Roberts, A. Ilyushechkin, L. Morpeth, T. Nguyen, et al. (2009). Kinetics of high-temperature water-gas shift reaction over two iron-based commercial catalysts using simulated coal-derived syngases. *Chemical Engineering Journal 146*(1), 148–154.

Parpas, P., B. Ustun, M. Webster, and Q. K. Tran (2015). Importance sampling in stochastic programming: A markov chain monte carlo approach. *INFORMS Journal on Computing 27*(2), 358–377.

Pedersen, K. S., P. L. Christensen, and J. A. Shaikh (2014). *Phase behavior of petroleum reservoir fluids*. CRC Press.

Pen, M., J. Gomez, J. G. Fierro, et al. (1996). New catalytic routes for syngas and hydrogen production. *Applied Catalysis A: General 144*(1), 7–57.

Peng, D.-Y. and D. B. Robinson (1976). A new two-constant equation of state. *Industrial & Engineering Chemistry Fundamentals 15*(1), 59–64.

Pennanen, T. and M. Koivu (2005). Epi-convergent discretizations of stochastic programs via integration quadratures. *Numerische mathematik 100*(1), 141–163.

Perry, R. H. and D. W. Green (1984). Perry chemical engineerings handbook. *Mc. Graw-Hill, Japan*.

Piemonte, V., M. De Falco, B. Favetta, and A. Basile (2010). Counter-current membrane reactor for wgs process: membrane design. *international journal of hydrogen energy 35*(22), 12609–12617.

Podolski, W. F. and Y. G. Kim (1974). Modeling the water-gas shift reaction. *Industrial & Engineering Chemistry Process Design and Development 13*(4), 415–421.

Poling, B. E., J. M. Prausnitz, J. P. O'connell, et al. (2001). *The properties of gases and liquids*, Volume 5. McGraw-Hill New York.

Pottmann, M., M. A. Henson, B. A. Ogunnaike, and J. S. Schwaber (1996). A parallel control strategy abstracted from the baroreceptor reflex. *Chemical engineering science 51*(6), 931–945.

Qi, X. and M. Flytzani-Stephanopoulos (2004). Activity and stability of cu-ceo2 catalysts in high-temperature water-gas shift for fuel-cell applications. *Industrial & engineering chemistry research 43*(12), 3055–3062.

Qiao, A., K. Zhang, Y. Tian, L. Xie, H. Luo, Y. Lin, and Y. Li (2010). Hydrogen separation through palladium–copper membranes on porous stainless steel with sol–gel derived ceria as diffusion barrier. *Fuel 89*(6), 1274–1279.

Quddus, M. R., Y. Zhang, and A. K. Ray (2010). Multiobjective optimization of a porous ceramic membrane reactor for oxidative coupling of methane. *Industrial & Engineering Chemistry Research 49*(14), 6469–6481.

Raja, G. L. and A. Ali (2015). Modified parallel cascade control structure for integrating processes. In *Recent Developments in Control, Automation and Power Engineering (RDCAPE), 2015 International Conference on*, pp. 90–95. IEEE.

Raja, G. L. and A. Ali (2017). Smith predictor based parallel cascade control strategy for unstable and integrating processes with large time delay. *Journal of Process Control 52*, 57–65.

Rangaiah, G. P. (2009). *Multi-objective optimization: techniques and applications in chemical engineering*, Volume 1. World Scientific.

Rankin, D. W. (2009). Crc handbook of chemistry and physics, edited by david r. lide.

Rao, A. S., S. Seethaladevi, S. Uma, and M. Chidambaram (2009). Enhancing the performance of parallel cascade control using smith predictor. *ISA transactions 48*(2), 220–227.

Rase, H. F. (2000). *Handbook of commercial catalysts: heterogeneous catalysts*. CRC press.

Rautenbach, R. and R. Albrecht (1989). *Membrane separation processes*. John Wiley and Sons Inc., New York, NY.

Rhodes, C., G. Hutchings, and A. Ward (1995). Water-gas shift reaction: finding the mechanistic boundary. *Catalysis Today 23*(1), 43–58.

Rhodes, C., B. P. Williams, F. King, and G. J. Hutchings (2002). Promotion of fe 3 o 4/cr 2 o 3 high temperature water gas shift catalyst. *catalysis communications 3*(8), 381–384.

Roy, D. and G. Thodos (1968). Thermal conductivity of gases. hydrocarbons at normal pressures. *Industrial & Engineering Chemistry Fundamentals 7*(4), 529–534.

Roy, D. and G. Thodos (1970). Thermal conductivity of gases. organic compounds at atmospheric pressure. *Industrial & Engineering Chemistry Fundamentals 9*(1), 71–79.

Saaty, T. L. (2003). Decision-making with the ahp: Why is the principal eigenvector necessary. *European journal of operational research 145*(1), 85–91.

Salcedo, R., E. Antipova, D. Boer, L. Jiménez, and G. Guillén-Gosálbez (2012). Multi-objective optimization of solar rankine cycles coupled with reverse osmosis desalination considering economic and life cycle environmental concerns. *Desalination 286*, 358–371.

San Shwe, H., D. Park, G. Duffy, J. Edwards, D. Roberts, A. Iltushechkin, L. Morpeth, and T. Nguyen (2009). Kinetics of high-temperature water-gas shift reaction over two iron-based commercial catalysts using simulated coal-derived syngases. *Chemical engineering journal 146*(1), 148–154.

Santosh, S. and M. Chidambaram (2016). A simple method of tuning parallel cascade controllers for unstable foptd systems. *ISA transactions 65*, 475–486.

Sanz, R., J. Calles, D. Alique, L. Furones, S. Ordóñez, and P. Marín (2015). Hydrogen production in a pore-plated pd-membrane reactor: Experimental analysis and model validation for the water gas shift reaction. *International Journal of Hydrogen Energy 40*(8), 3472–3484.

Saracco, G. and V. Specchia (1994). Catalytic inorganic-membrane reactors: present experience and future opportunities. *Catalysis Reviews Science and Engineering 36*(2), 305–384.

Satterfield, C. N. (1991). Heterogeneous catalysis in industrial practice.

Saw, S. Z. and J. Nandong (2016). Optimization of economic and operability performances of water-gas shift membrane reactor. In *26th European Symposium on Computer Aided Process Engineering*, Volume 38 of *Computer Aided Chemical Engineering*, pp. 847 – 852. Elsevier.

Saw, S. Z., J. Nandong, and U. K. Ghosh (2015). Dynamic simulation of adiabatic packed bed tubular reactor for wgsr under cascade temperature control strategies-effect of secondary temperature measurement location. In *Asia Pacific Confederation of Chemical Engineering Congress 2015: APCChE 2015, incorporating CHEMECA 2015*. Engineers Australia.

Schoofs, A., F. Van Asperen, P. Maas, and A. Lehr (1987). I. computation of bell profiles using structural optimization. *Music Perception: An Interdisciplinary Journal 4*(3), 245–254.

Seborg, D., T. F. Edgar, and D. Mellichamp (2006). *Process dynamics & control*. John Wiley & Sons.

Seborg, D. E., D. A. Mellichamp, T. F. Edgar, and F. J. Doyle III (2010). *Process dynamics and control*. John Wiley & Sons.

Sedigh, M. G., M. Jahangiri, P. K. Liu, M. Sahimi, and T. T. Tsotsis (2000). Structural characterization of polyetherimide-based carbon molecular sieve membranes. *AIChE journal 46*(11), 2245–2255.

Seer, Q. H. and J. Nandong (2017). Stabilization and pid tuning algorithms for second-order unstable processes with time-delays. *ISA transactions 67*, 233–245.

Seferlis, P. and M. Georgiadis (2004). The need for simultaneous design education. *The integration of process design and control 17*, 10.

Sengers, J. V., R. Kayser, C. Peters, and H. White (2000). *Equations of state for fluids and fluid mixtures*. Elsevier.

Shah, M., M. C. McCarthy, S. Sachdeva, A. K. Lee, and H.-K. Jeong (2012). Current status of metal–organic framework membranes for gas separations: promises and challenges. *Industrial & Engineering Chemistry Research 51*(5), 2179–2199.

Shah, R. K. and D. P. Sekulic (2003). *Fundamentals of heat exchanger design*. John Wiley & Sons.

Shahhosseini, H. R., M. Farsi, and S. Eini (2016). Multi-objective optimization of industrial membrane smr to produce syngas for fischer-tropsch production using nsga-ii and decision makings. *Journal of Natural Gas Science and Engineering 32*, 222–238.

Shahrokhi, M. and G. Baghmisheh (2005). Modeling, simulation and control of a methanol synthesis fixed-bed reactor. *Chemical Engineering Science 60*(15), 4275–4286.

Shamash, Y. (1975). Model reduction using the routh stability criterion and the padé approximation technique. *International Journal of Control 21*(3), 475–484.

Shapiro, A., D. Dentcheva, et al. (2014). *Lectures on stochastic programming: modeling and theory*, Volume 16. SIAM.

Sharifzadeh, M. (2013). Integration of process design and control: A review. *Chemical Engineering Research and Design 91*(12), 2515–2549.

Sharma, S. and G. P. Rangaiah (2013). Multi-objective optimization applications in chemical engineering.

Shoko, E., B. McLellan, A. Dicks, and J. D. da Costa (2006). Hydrogen from coal: production and utilisation technologies. *International Journal of Coal Geology 65*(3), 213–222.

Sigfusson, T. I. (2007). Pathways to hydrogen as an energy carrier. *Philosophical Transactions of the Royal Society of London A: Mathematical, Physical and Engineering Sciences 365*(1853), 1025–1042.

Simpson, T. W., J. Peplinski, P. N. Koch, and J. K. Allen (1997). On the use of statistics in design and the implications for deterministic computer experiments. *Design Theory and Methodology-DTM'97*, 14–17.

Skogestad, S. (2003). Simple analytic rules for model reduction and pid controller tuning. *Journal of process control 13*(4), 291–309.

Smith, R., M. Loganathan, M. S. Shantha, et al. (2010). A review of the water gas shift reaction kinetics. *International Journal of Chemical Reactor Engineering 8*(1).

Smith, R. B., L. Muruganandam, and S. M. Shekhar (2011). Cfd analysis of water gas shift membrane reactor. *Chemical Engineering Research and Design 89*(11), 2448–2456.

Steward, D., G. Saur, M. Penev, and T. Ramsden (2009). Lifecycle cost analysis of hydrogen versus other technologies for electrical energy storage. *US National Renewable Energy Laboratory (NREL)*.

Stiel, L. I. and G. Thodos (1964). The thermal conductivity of nonpolar substances in the dense gaseous and liquid regions. *AIChE Journal 10*(1), 26–30.

Tan, J. C. and A. K. Cheetham (2011). Mechanical properties of hybrid inorganic–organic framework materials: establishing fundamental structure–property relationships. *Chemical Society Reviews 40*(2), 1059–1080.

Tanaka, Y., T. Utaka, R. Kikuchi, T. Takeguchi, K. Sasaki, and K. Eguchi (2003). Water gas shift reaction for the reformed fuels over cu/mno catalysts prepared via spinel-type oxide. *Journal of Catalysis 215*(2), 271–278.

Tanksale, A., J. N. Beltramini, and G. M. Lu (2010). A review of catalytic hydrogen production processes from biomass. *Renewable and Sustainable Energy Reviews 14*(1), 166–182.

Topsøe, H. and M. Boudart (1973). Mössbauer spectroscopy of co shift catalysts promoted with lead. *Journal of Catalysis 31*(3), 346–359.

Tosti, S., A. Basile, L. Bettinali, F. Borgognoni, F. Gallucci, and C. Rizzello (2008). Design and process study of pd membrane reactors. *International Journal of Hydrogen Energy 33*(19), 5098–5105.

Tosti, S., A. Basile, R. Borelli, F. Borgognoni, S. Castelli, M. Fabbricino, F. Gallucci, and C. Licusati (2009). Ethanol steam reforming kinetics of a pd–ag membrane reactor. *international journal of hydrogen energy 34*(11), 4747–4754.

Tosti, S., A. Basile, G. Chiappetta, C. Rizzello, and V. Violante (2003). Pd–ag membrane reactors for water gas shift reaction. *Chemical Engineering Journal 93*(1), 23–30.

Towler, G. and R. K. Sinnott (2012). *Chemical engineering design: principles, practice and economics of plant and process design*. Elsevier.

Turner, J. A. (1999). A realizable renewable energy future. *Science 285*(5428), 687–689.

Turton, R., R. C. Bailie, W. B. Whiting, and J. A. Shaeiwitz (2008). *Analysis, synthesis and design of chemical processes*. Pearson Education.

Turton, R., R. C. Bailie, W. B. Whiting, J. A. Shaeiwitz, and D. Bhattacharyya (2012). *Analysis, synthesis and design of chemical processes*. Pearson Education.

Twigg, M. V. and M. S. Spencer (2001). Deactivation of supported copper metal catalysts for hydrogenation reactions. *Applied Catalysis A: General 212*(1), 161–174.

Twigg, M. V. and M. Twigg (1989). *Catalyst handbook*. CSIRO.

Uemiya, S., T. Endo, R. Yoshiie, W. Katoh, and T. Kojima (2007). Fabrication of thin palladium-silver alloy film by using electroplating technique. *Materials transactions 48*(5), 1119–1123.

Uemiya, S., N. Sato, H. Ando, and E. Kikuchi (1991). The water gas shift reaction assisted by a palladium membrane reactor. *Industrial & Engineering Chemistry Research 30*(3), 585–589.

Vielstich, W., A. Lamm, and H. Gasteiger (2003). Handbook of fuel cells, vol 3: Fuel cell technology and applications: Part 1.

Vinnicombe, G. (2000). *Uncertainty and Feedback: H loop-shaping and the ν-gap metric*. World Scientific.

Vitart, X., P. Carles, and P. Anzieu (2008). A general survey of the potential and the main issues associated with the sulfur–iodine thermochemical cycle for hydrogen production using nuclear heat. *Progress in Nuclear Energy 50*(2), 402–410.

Vlysidis, A., M. Binns, C. Webb, and C. Theodoropoulos (2011). A techno-economic analysis of biodiesel biorefineries: assessment of integrated designs for the co-production of fuels and chemicals. *Energy 36*(8), 4671–4683.

Wei, Y. S. and R. J. Sadus (2000). Equations of state for the calculation of fluid-phase equilibria. *AIChE Journal 46*(1), 169–196.

Welk, M., T. Nenoff, and F. Bonhomme (2004). Defect-free zeolite thin film membranes for h 2 purification and co 2 separation. *Studies in surface science and catalysis 154*, 690–694.

Wilkes, J. O. (2006). *Fluid Mechanics for Chemical Engineers with Microfluidics and CFD.* Pearson Education.

Williams, R. H. (2002). Toward zero emissions for transportation using fossil fuels. *Transportation Research Board, Washington, DC*.

Yeragi, D. C., N. C. Pradhan, and A. K. Dalai (2006). Low-temperature water-gas shift reaction over mn-promoted cu/al2o3 catalysts. *Catalysis letters 112*(3-4), 139–148.

Yin, C., J. Gao, and L. Zhang (2011). Multiple degrees of freedom control for cascade processes with time delay. *Procedia Engineering 15*, 3–7.

Yoon, K. P. and C.-L. Hwang (1995). *Multiple attribute decision making: an introduction*, Volume 104. Sage publications.

Yu, C.-C. (1988). Design of parallel cascade control for disturbance-rejection. *AIChE journal 34*(11), 1833–1838.

Yu, W., T. Ohmori, T. Yamamoto, A. Endo, M. Nakaiwa, and N. Itoh (2007). Optimal design and operation of methane steam reforming in a porous ceramic membrane reactor for hydrogen production. *Chemical Engineering Science 62*(18), 5627–5631.

Yun, S. and S. T. Oyama (2011). Correlations in palladium membranes for hydrogen separation: a review. *Journal of Membrane Science 375*(1), 28–45.

Yunqiang, J., S. Hongye, L. Zuwei, and H. Weifeng (2011). Modeling and multi-objective optimization of refinery hydrogen network. *Chinese Journal of Chemical Engineering 19*(6), 990–998.

Yurieva, T. and T. Minyukova (1985). State of copper in cu- zn- al oxide catalysts for methanol synthesis. *Reaction Kinetics and Catalysis Letters 29*(1), 55–61.

Zadeh, L. (1963). Optimality and non-scalar-valued performance criteria. *IEEE transactions on Automatic Control 8*(1), 59–60.

Zhang, Y., Z. Wu, Z. Hong, X. Gu, and N. Xu (2012). Hydrogen-selective zeolite membrane reactor for low temperature water gas shift reaction. *Chemical Engineering Journal 197*, 314–321.

Zhao, J. and S. V. Olesik (1999). Phase diagram studies of methanol–chf 3 and methanol–h 2 o–chf 3 mixtures. *Fluid phase equilibria 154*(2), 261–284.

Every reasonable effort has been made to acknowledge the owners of copyright material. I would be pleased to hear from any copyright owner who has been omitted or incorrectly acknowledged.

Appendix A

Basic Constants

Table A.1: Constants for each species needed in calculation

Species	**Molecular weight**	T_b	T_{cr}	P_{cr}	V_{cr}	ω
CO	28.01	81.66	132.85	34.94	93.10	0.045
H_2O	18.02	373.15	647.14	220.64	55.95	0.344
CO_2	44.01	194.65	304.12	73.74	94.07	0.225
H_2	2.02	20.38	33.25	12.97	65.00	-0.216

Note: Molecular weight is in (g/gmol), T_b is in (K), T_{cr} is in (K), P_{cr} is in (bar) and V_{cr} is in (cm^3/mol). Values adapted from Perry and Green (1984).

Table A.2: Binary gas diffusivity for component pairs

Pair	A_{dif}	B_{dif}	C_{dif}	D_{dif}	E_{dif}	F_{dif}	**Eqn.**
CO-H_2O	0.187×10^{-5}	2.072	-	0	0	0	a
CO-CO_2	3.15×10^{-5}	1.57	-	0	113.6	0	a
CO-H_2	15.39×10^{-3}	1.548	0.316×10^{8}	1	-2.80	1067	a
H_2O-CO_2	9.24×10^{-5}	1.5	-	0	307.9	0	a
H_2O-H_2	-	1.020	-	-	-	-	b
CO_2-H_2	3.14×10^{-5}	1.75	-	0	11.7	0	a

Note: $D_{12} = D_{21}$. Eqn. a - $D_{iI} = (A_{dif}T_{dif}^{B}/P)[\ln(C_{dif}/T)]^{-2D_{dif}}\exp(-E_{dif}/T - F_{dif}/T^2)$ (Marrero and Mason, 1972) and Eqn. b - $D_{iI} = (B_{dif}/P)$ (Satterfield, 1991). Here T is in (K), P is in (atm) and D_{iI} is in (cm^2/s). Values adapted from Perry and Green (1984).

Table A.3: Specific heat capacity constants for selected species

Species	A_{cp}	B_{cp}	C_{cp}	D_{cp}
CO	6.60	1.20×10^{-3}	0	0
H_2O	8.22	0.15×10^{-3}	1.34×10^{-6}	0
CO_2	10.34	2.74×10^{-3}	0	-1.955×10^{5}
H_2	6.62	0.81×10^{-3}	0	0

Note: T is in (K), P is in (atm) and $C_{p,i}$ is in (cal/mol.K). Values adapted from Perry and Green (1984).

Table A.4: Gas phase viscosity constants for selected species

Species	A_{vis}	B_{vis}	C_{vis}	D_{vis}
CO	1.1127×10^{-6}	0.5338	94.7	0
H_2O	1.7096×10^{-8}	1.1146	0	0
CO_2	2.148×10^{-6}	0.46	290.0	0
H_2	1.797×10^{-7}	0.685	-0.59	140

Note: T is in (K) and μ is in (N.s/m^2). Values adapted from Perry and Green (1984).

Table A.5: Thermal conductivity constants for each species

Species	A_{lam}	B_{lam}	C_{lam}	D_{lam}
CO	5.1489×10^{-4}	0.6863	57.13	501.92
H_2O	5.3345×10^{-6}	1.3973	0	0
CO_2	3.1728	-0.3838	964.0	1.86×10^{6}
H_2	2.2811×10^{-3}	0.7452	12.0	0

Note: T is in (K) and λ is in (kcal/h.m.K). Values adapted from Perry and Green (1984).

Appendix B

Carbon Capture

B.1 Carbon Capture and Reuse Proposed Design

This study proposed a new technology of carbon capture reuse design by employing a membrane reactor with H_2 selective membrane with the incorporation of dry methanation reaction. This reaction not only consumed CO_2 but also produces high-purity H_2 and also carbon monoxide (CO). This technology is able to reduce CO_2 emission which thereby reduce carbon taxes, it can also produce valuable H_2 as well as CO, which are necessary reactants for many petrochemical reactions. In this case CO is one of the main reactants in the process industries that we chose and hence it can be recycled back to the process and thereby decreases the cost of purchasing raw materials.

B.1.1 Main equipment and characteristics

The main equipment used in this proposed solution is a membrane reactor (MR). The characteristic of this reactor is the combination of reaction and separation in one single unit. This technology is not only able to reduce the cost of separation but also able to increase the purity of the separation due to high selectivity of the membrane. The reaction (i.e., dry methanation) as described in equation B.1 occurs inside the membrane reactor.

$$CH_4 + CO_2 \rightleftharpoons 2H_2 + 2CO \tag{B.1}$$

Carbon dioxide and methane gas are the main reactant to produce hydrogen and carbon monoxide gases. In this case, the methane gas is obtained from the

waste product of other industrial plants. This proposed solution does not only solve carbon emission, it also solves the waste product of methane emission from other industries.

With incorporation of H_2 selective membrane in the proposed membrane reactor, high purity of H_2 is obtained and through the removal of hydrogen gas, the reaction shown in equation B.1 is shifted towards the right and thereby able to increase the conversion of carbon dioxide. The remaining product is then recycled back towards the feed of the main reaction. Figure B.1 depicts the axial cross-sectional of the membrane reactor. Note that, the proposed membrane reactor is made up of a number of tubes. As for Figure B.2, it shows the radial cross-sectional area of the membrane reactor. Note that, 30^0 tube pitch is chosen due to high heat and mass transfer rates Mukherjee et al. (1998).

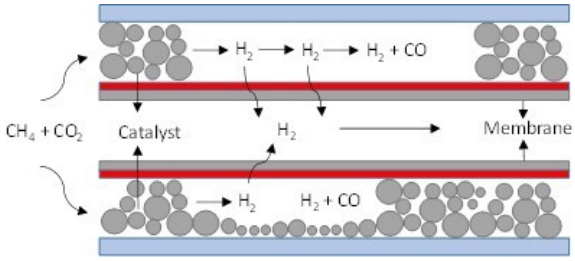

Figure B.1: Axial cross-sectional area of proposed membrane reactor.

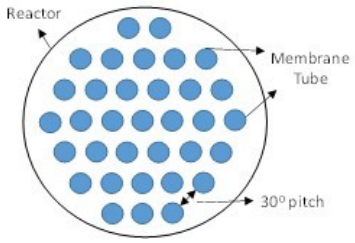

Figure B.2: Radial cross-sectional area of proposed membrane reactor.

B.1.2 Carbon capture and reuse (CCR) MR models

Dry methanation reaction kinetics

Catalyst of Ni/TiO_2 is used for the dry methanation reaction as described in Equation B.1. All the values are obtained from Bradford and Vannice (1996). The kinetics for this reaction is defined as;

$$r_A = \frac{\hat{k_1} P_{CH_4} P_{CO_2}}{\frac{\hat{k_{-1}}\bar{K}}{\hat{k_7}} P_{CO} P{H_2}^{(4-x)/2} + \left(1 + \frac{\hat{k_1}}{\hat{k_7}} P_{CH_4}\right) P_{CO_2}} \tag{B.2}$$

Membrane reactor models

In order to estimate the outlet concentration of the reactor, a theoretical numerical model is used for modelling the membrane reactor. This model consists of mass and energy balance equations with the incorporation of intra-particle mass and heat transfers. The assumptions that governs these equations are: (1) the model assumes a tubular reactor with multiple small tubes in which the catalysts is packed outside of the tubes, (2) only the axial temperature change is taken into account, (3) radial temperature change is neglected due to the fact that the diameter of the membrane reactor is small and adiabatic (no heat loss from the surface of the reactor) Aboudheir et al. (2006) see Figure 5.1, (4) gas properties, permeance and kinetics are assumed to be under non-isothermal conditions which means dependence upon temperature change.

Steady-state mass balance of species, i is given as follows;

$$F_{in,i} - F_{out,i} \pm r_A V - Q_i = 0 \tag{B.3}$$

Q_i as defined in equation B.4 is the permeance of H_2 where by $Q_i = 0$ for species other than H_2. Take note that there is a plus and minus sign in front of rate of reaction r_A; reactant uses minus sign due to consumption and vice versa for the product.

$$Q_i = A_{surf} V \frac{Q_m}{\delta_m} \exp\left(\frac{-E_d}{RT_r}\right) (P_r^{0.5} - P_p^{0.5}) \tag{B.4}$$

Steady-state energy balance is given by;

$$\frac{F_{in} C_{p,g,in} T_{r,in} - F_{out} C_{p,g,out} T_r + \Delta H_{rx} r_A - Q_i C_{p,i} T_r - T_p - U_0 A_{surf} (T_r - T_p)}{(F_{out} C_{p,g})} = 0 \tag{B.5}$$

The system equations involved in this membrane reactor is solved using *fsolve* function available *Matlab 2014b*; the system is highly nonlinear.

Appendix C

Economic Evaluation

C.1 Capital Costs Estimation

The purpose of this appendix is to present the equations and data that are used to calculate the purchased cost equipment and utilities costs that has been introduced in Chapter 6. Data for the purchased cost of equipment, at ambient operating pressure and using carbon steel construction, C_p^0, were fitted to the following equation:

$$\log_{10} C_p^0 = K_1 + K_2 \log_{10}(A) + K_3 [\log_{10}(A)]^2 \tag{C.1}$$

where A is the capacity or size parameter for the equipment. The data for K_1, K_2, and K_3, along with maximum and minimum values used in the correlation, are given in Table C.1.

Table C.1: Equipment cost data to be used in equation C.1

Equipment type	**Equipment description**	K_1	K_2	K_3
Compressors	Centrifugal	2.2897	1.3604	-0.1027
	Rotary	5.0355	-1.8002	0.8253
Heat exchangers	Fixed tube	4.3247	-0.3030	0.1634
	U-tube	4.1884	-0.2503	0.1974
Reactors	Jacketed non-agitated	3.3496	0.7235	0.0025

Note: All data were obtained in 2001 with CECPI of 397. Values from Turton et al. (2012).

Table C.2: Equipment cost data to be used in equation C.1 (continued)

Capacity, Units	**Min size**	**Max size**
Fluid power, kW	450	3000
Fluid power, kW	18	950
Area, m^2	10	1000
Area, m^2	10	1000
Volume, m^3	5	55

Note: All data were obtained in 2001 with CECPI of 397. Values from Turton et al. (2012).

The purposed of having two types of compressor is due to the fact of different compressor capacity requirement in specific locations. Once the capacity of the compressor is more than 450 kW, centrifugal compressor is chosen rather than rotary compressor because of lower capital cost. As for two types of heat exchangers, fixed tube heat exchanger can only be used when there is a smaller differential temperature between tubes and shell. However, if there is large temperature differential, U-tube design is more suitable as it allows for differential thermal expansion between the shell and the tube bundle as well as for individual tubes Shah and Sekulic (2003).

Equation C.1 represent purchased cost for base conditions. In order to calculate bare module equipment cost, including specific materials of construction and operating pressure, a bare module cost factor has to be implemented and form new a equation as follows:

$$C_{BM} = C_p^0 F_{BM} \tag{C.2}$$

where C_{BM} is bare module equipment cost: direct and indirect costs for each unit and F_{BM} is a bare module cost factor: multiplication factor to account for the items with specific materials and operating pressure.

There is an algorithm developed by Shah and Sekulic (2003) which is used for calculating bare module cost factor. First is to calculate the purchased cost for base condition C_p^0 for every desired piece of equipment. This can be done through calculation shown in Equation C.1. This step is then followed by finding

the correct relationship for the F_{BM}. For heat exchangers, pump and vessels, equation C.3.

$$C_{BM} = C_p^0 F_{BM} = C_p^0(B_1 + B_2 F_M F_P) \tag{C.3}$$

where B_1 and B_2 are constants given value of 1.63 and 1.66 respectively for fixed tube and U-tube types of heat exchanger. F_M is the material factors for heat exchanger which in this case the value is 1.4 for fixed tube while 1.7 for U-tube heat exchangers. As for F_P it is the pressure factor given by:

$$\log_{10} F_P = C_1 + C_2 \log_{10}(P) + C_3[\log_{10}(P)]^2 \tag{C.4}$$

where P is the pressure capacity (barg) of the equipments. The constant values of C_1, C_2, and C_3 are 0.03881, -0.11272 and 0.08183 respectively for both fixed tube and U-tube heat exchangers.

As for other equipment such as compressors, the bare module cost is calculated using equation C.2 with own F_{BM} value of 2.6 for centrifugal compressor and 2.4 for rotary compressor. With all the newly calculated bare module equipment cost C_{BM}, the total equipment costs is then updated from 2001 (CECPI - 397) to 2013 (CEPCI - 567.3) Bailey (2014) by using equation C.5,

$$C_2 = C_1 \left(\frac{I_2}{I_1} \right) \tag{C.5}$$

where C refers to purchased cost and I refers to cost index. Subscripts of 1 and 2 refers to base time when cost is known and time when cost is desired respectively.

C.2 Manufacturing Costs Estimation

This manufacturing costs associated with day-to-day operation of a chemical plant. The primary components of the cost of manufacture are raw materials, utilities, and waste treatment. Manufacturing costs are expressed in units of dollars per unit time (commonly per year). Table C.3 below presents the costs for utilities provided by off-sites plants.

Membrane reactor is susceptible to membrane lifespan as well as catalyst degradation. With the cost of membrane reactor are highly dependent on the type of membrane and catalyst; the maintenance fee for changing new membrane and catalyst has to be incorporated in the annualized manufacturing cost. Table C.4 show the cost breakdown of the membrane reactor.

Table C.3: Utilities cost charges

Utility	**Description**	**Cost $/ GJ**	**Cost $/ Common unit**
Steam from Boilers	Low pressure (5 barg, 160^0C)		
	from HP steam	13.28	\$27.70/ 1000 kg
Cooling Tower Water*	Process cooling water:		
	30^0C to 40^0C or 45^0C	0.354	\$14.8/ 1000 m^3
Other Water	High-purity water for		
	process use		\$0.067/ 1000 kg
Electricity cost**	Industrial price		\$0.106/ kWh

Note: *Cooling water return temperatures should not exceed 45^0C due to excess scaling at high temperature. Values from Turton et al. (2012). **Value based from U.S. Energy Information Administration 2016. Outlook et al. (2016)

Table C.4: Membrane reactor cost breakdown

Equipment type	**Cost $/ Common unit**	**Lifespan / years**
Pd price	14.2/g	3
Ag price	1.43/g	3
Shift catalyst price	6.8/kg	10

Note: All price data obtained from Koc et al. (2014)

The maintenance costs in this study include membrane replacement costs as a variable operating cost. This cost is calculated by dividing the membrane bundle equipment cost by the membrane lifetime. Similar concept applies to the shift catalyst replacement costs.